*Electron spin resonance in zinc selenide*

F. Zanich-Khah

ELECTRON SPIN RESONANCE IN ZINC SELENIDE

by

F. ZANICH-KHAH B.Sc.,M.Sc.

Presented in Candidature for the Degree of

Doctor of Philosophy in the University of Durham

December 1974

## ACKNOWLEDGEMENTS

## ABSTRACT

Electron spin resonance techniques were applied to study crystals of ZnSe both doped and undoped. Crystals grown by sublimation at $1300^{\circ}C$ were found to have a mixed cubic-hexagonal structure. Annealing these crystals at $1050^{\circ}C$ increased the hexagonal component. This is the opposite of what is usually observed in crystals produced by the flow process. ZnSe crystals produced at $850^{\circ}C$ by the iodine transport method were found to have a cubic structure. No cubic $\longrightarrow$ hexagonal phase transition could be achieved in these crystals. From the experimental data it is concluded that the hexagonal phase in crystals grown at $1300^{\circ}C$ occurred as a result of the presence of an impurity, probably oxygen.

Electron spin resonance of Mn was studied in detail in cubic, in twinned and in cubic-hexagonal ZnSe crystals. Comparing the Mn concentration and distribution in crystals produced at $1300^{\circ}C$ and at $850^{\circ}C$, it was found that the solubility of Mn was larger in crystals grown at $1300^{\circ}C$. Attempts were made to dope ZnSe with Mn by diffusion, but results indicated that Mn does not diffuse into ZnSe. However, spin resonance results showed that annealing ZnSe:Mn crystals in molten Zn at $850^{\circ}C$ removes some of the Mn impurity.

Electron spin resonance investigations were also carried out in ZnSe crystals doped with I, Cl, Al and In. In these crystals spin resonance signals characteristic of mobile donor electron were detected. These signals were all found to be affected by annealing in molten Zn, and furthermore they were all photosensitive.

Addition of 0.01% Cr to ZnSe was found to prevent charge transport. Spin resonance of a sintered sample containing Cr indicated a trapping level associated with Cr at 0.51 eV below the conduction band.

Luminescence investigations were carried out to identify the characteristic Mn emission band in ZnSe.  In Zn(S,Se):Mn solid solution samples replacement of S by Se was found to quench the Mn emission band of ZnS.  Undoped crystals with emission bands at 6500 A and 6250 A (under UV excitation) were subjected to spin resonance investigations to identify centres responsible.  No evidence could be detected for the presence of the class A centre.

# CONTENTS

## CHAPTER   1

## INTRODUCTION

ZnSe with a band gap of 2.7 eV at room temperature has been of scientific and technological interest in the last few years because of the possibility of fabricating low-cost, low-voltage electro-luminescent devices.  Compared with some other II-VI compounds such as ZnS or CdS, the properties of ZnSe, however, have not been extensively studied.

The purpose of the research work described in this thesis has been to apply electron spin resonance techniques to study crystals of ZnSe, both doped and undoped, bearing in mind the interest mentioned above.  To this end, crystals of ZnSe were produced at $1300^{\circ}$C by a sublimation method.  Spin resonance of the $Mn^{2+}$ ion in these crystals indicated that they had a cubic-hexagonal structure.  A comprehensive programme of annealing was undertaken in an attempt to convert the hexagonal component to cubic, as is usually achieved in crystals produced by the flow process.  However, no hexagonal $\longrightarrow$ cubic phase transition took place.  Instead annealing the samples at $1050^{\circ}$C increased the hexagonal proportion, i.e. a cubic $\longrightarrow$ hexagonal transition occurred. To study this further, ZnSe crystals were produced at $850^{\circ}$C using the iodine transport method.  Spin resonance of the $Mn^{2+}$ ion in these crystals indicated that they had a cubic structure.  Annealing them at $1050^{\circ}$C did not produce any cubic $\longrightarrow$ hexagonal phase transition.  From the experimental data it is concluded that the hexagonal phase in crystals produced at $1300^{\circ}$C had not occurred for thermodynamic reasons, but was attributable to the presence of an impurity in the starting ZnSe material.  This impurity is probably oxygen.

The electron spin resonance of the $Mn^{++}$ ion in cubic, in twinned, and in cubic-hexagonal ZnSe crystals is discussed in Chapter 5 .

From the resonance of the $Mn^{2+}$ ion in crystals produced at different temperatures it was found that Mn has a much smaller solubility in crystals grown at $850^{\circ}C$ than in those produced at $1300^{\circ}C$. Experiments carried out to dope ZnSe with Mn by diffusion showed that Mn does not diffuse into ZnSe. However, spin resonance results indicate that annealing ZnSe:Mn in molten Zn at $850^{\circ}C$ removes some of the Mn impurity.

The results of investigations to identify the characteristic Mn luminescence emission band in ZnSe are presented in Chapter 7 . In solid solution samples of Zn(S,Se) containing Mn, the Mn emission band which has its peak in ZnS at 5800 $\overset{o}{A}$ at room temperature was found to be quenched as Se replaced S in Zn(S,Se):Mn. Two explanations are suggested; one assumes interactions between the Mn and impurity killer centres and the other one assumes interactions between the Mn and the free carriers created by the U.V. excitation. Spin resonance investigations carried out in a number of ZnSe (doped and undoped) crystals which luminesced with emission bands in the 6500 and 6250 A regions gave no indication of the so called class-A centres associated with self-activated emission. It is concluded that some of the emission bands observed were probably due to copper impurity in the starting material.

Spin resonance investigations were also carried out in samples doped with donor impurities (Al, I, Cl, In). In these samples spin response signals due to donor (mobile) electrons were detected. The signals were all photosensitive.

Attempts were made to produce ZnSe:Cr single crystals by sublimation and by the iodine transport method, but addition of 0.01% Cr to the charge prevented charge transport. Spin resonance measurements on a sintered ZnSe:Cr sample indicated the presence of a photosensitive trapping level associated with Cr which lay 0.51 eV below the conduction band.

CHAPTER 2

METHODS OF PRODUCING ZnSe CRYSTALS

There are basically three methods of producing crystals of ZnSe. Two of these utilise growth from the vapour phase and can be described as the flow and sublimation methods. Under a sufficiently high applied pressure ZnSe can be melted and this forms the basis of the third method of growth from the melt.

### The Flow Method

The flow method, and variations on it, are derived from the early work of Frerichs (1) which provided considerable impetus to the development of successful crystal growth of the II-VI compounds. The method which Frerichs originally used to grow CdS crystals consisted of passing $H_2S$ gas to the hot zone of a quartz tube where it reacted with Cd vapour brought to that zone by a carrier gas ($H_2$) which had passed over a boat containing molten Cd. The CdS produced by the reaction of Cd and $S_2$ was deposited on a cooler region of the tube.

Many variations of this method have been reported; notably that due to Stanley (2) who used an inert gas flowing over CdS power held at $1000^{\circ}C$ to carry CdS vapour to a cooler region of the tube (held at $900^{\circ}C$) where CdS crystals grew.

Several workers have used the flow method to grow ZnSe crystals. Park and Chan (3) passed argon over ZnSe powder held at $1300^{\circ}C$ to carry ZnSe vapour to a region of a quartz tube where crystal growth could occur. In the higher temperature regions of the growth zone ($T > 1000^{\circ}C$) the crystals formed were reported to have been mostly small prisms and plates. In the low temperature region ($T < 1000^{\circ}C$) only small needles grew. From X-ray investigations it was concluded that the plate-like crystals were cubic with some having a twinned structure, while the needles were hexagonal.

Similarly Fitzgerald et al (4) using the same method produced hexagonal platelets and rods with the sublimation temperature at $1200^\circ$C and the growth temperature at $1000^\circ$C. On lowering the sublimation temperature to $1100^\circ$C - $1150^\circ$C thin ribbons which were either entirely hexagonal or of a mixed cubic-hexagonal structure grew at a temperature of $900^\circ$C-$950^\circ$C. Dean et al (5) obtained hexagonal needle-like crystals and rods when the sublimation temperature was at about $1200^\circ$C and the growth region at $1100^\circ$C.

Pashinkin et al (6) produced ZnSe crystals from the elements using the flow-method. They report that with the reaction zone of the tube at $1050^\circ$C-$1080^\circ$C some of the needle-like and prismatic crystals grew with an entirely hexagonal structure while others showed mixed cubic-hexagonal phases. When the temperature of the reaction zone was increased to $1120^\circ$C-$1200^\circ$C small cubic crystals were formed. Apparently the hexagonal phase was entirely absent at that reaction temperature. Similarly Hartmann (7) in his experiments sublimed ZnSe in a flow of $N_2$, $N_2$-$H_2$ or $N_2$-$H_2$-HCl gases and found that cubic platelets grew in the area of the tube where the temperature was above $1050^\circ$C, whereas hexagonal needles and disordered crystals occurred in the area where the temperature was between 800-$1050^\circ$C. From his observations Hartmann concluded that hexagonal and disordered crystals occurred in the area of high supersaturation, i.e. in the regions where the nucleation and growth rates were high.

With the flow method generally it is very difficult to achieve stoichiometric proportions during the flow process. Indeed it may be difficult to maintain constant growth conditions. As a result the crystals produced often do not have reproducible properties. However, this is the only method so far by which hexagonal ZnSe crystals in the

form of needles and rods have been produced.

### The Sublimation Method

This method was used originally by Reynolds et al (8) to grow CdS crystals. A charge of CdS powder was placed in a sealed quartz tube containing an atmosphere of $H_2S$. The charge was then fired at $1150^{O}C$ for a few days and as a result of vaporization and local crystallization small prism-shaped crystals grew on the sintered charge. This method was modified by a number of workers, notably Piper and Polich (9), who pulled the charge through a temperature gradient and obtained large single crystals of CdS. Clark and Woods (10) modified the method reported by Piper and Polich, and later in an attempt to bring the stoichiometric conditions under control, designed an arrangement whereby a known partial pressure of S or Cd could be maintained during the sublimation-growth cycle. Using this arrangement Clark and Woods (11) were able to produce CdS crystals with 1 cm diameter and a few cm long. The sublimation method has been used to grow ZnSe crystals (see for instance Aven et al (12)). A paper that describes two sublimation methods of growing ZnSe crystals is that of Burr and Woods (13). These two methods are described on pages 7 and 8.

The advantages of growing ZnSe crystals by this method are that large single crystals can be obtained, and that a certain degree of control over the stoichiometry may be exercised. This results in crystals with more reproducible properties than those of the flow crystals.

Another method of growing ZnSe crystals from the vapour phase utilises chemical (iodine or chlorine) to transport the vapour down a temperature gradient to a region where crystal growth occurs. This method is discussed on page 10.

## Crystals grown from the melt

The growth of large single crystals of ZnSe from the melt has been reported by Tswyinsoto et al (14). Their method consisted of heating ZnSe powder in a graphite crucible under a pressure of 120 atms. of argon. The temperature of the crucible was $1550^{\circ}$C at the bottom and $1700^{\circ}$C at the top (ZnSe has a melting point of $1515 \pm 10^{\circ}$C at a dissociation pressure of 1.8 atms.). The crucible was then cooled at a rate of between $1^{\circ}$C and $2^{\circ}$C per minute from the bottom thus producing single crystals. The crystals obtained are reported to have been n-type with a resisitivity of $10^{8}-10^{9}$ ohm-cm. Their structure was cubic.

Though large single crystals may be obtained by this method, the inherent problem of impurity contamination must be taken into account. For instance Title (15) reports that his melt-grown ZnSe crystals contained chromium which originated from the graphite crucible used. Another problem with this method is that the crucible is very complicated and expensive.

## Growth of Crystals for the present research

For the research work reported in this thesis ZnSe crystals were produced by four methods, i.e. two different sublimation methods (at 1350 and $1150^{\circ}$C), a chemical transport method using iodine, and the flow process using argon as the carrier gas. It is important to state at the outset that the starting material used was ZnSe powder supplied by Derby Luminescents Ltd. (Electronic Grade) and that X-ray powder photographs of this powder indicated that it contained a measurable quantity of ZnO. ESR investigation of a sample made from the powder showed traces of manganese impurity. No other information was available about the impurity content of this material.

(a)    ZnSe crystals produced by sublimation at 1350°C

ZnSe crystals produced at high  temperatures were grown using

the technique described by Clark and Woods (10) for growing large crystals

of CdS.  To grow  ZnSe crystals a powder charge was placed in a silica

tube of 1 cm bore and 15 cm in length (one end was attached to a long

length of silica rod).  After the powder had been degassed by heating in

vacuum, the tube was filled with high-purity argon at a pressure of one

atms. and then (approximately) sealed with a silica plug.  Next the tube

was placed in a horizontal furnace with a uniform but symmetrical tem-

perature gradient about its middle.  The temperature of this middle point

was set at 1350°C and the end of the tube where crystals were to grow

was pulled through the region of maximum temperature first in order to

clean its surface area.  With continued pulling the temperature of this

part of the tube began to fall while that of the charge began to rise

to 1350°C.  Thus the charge was sublimed and transported to the cooler

part of the tube where crystal growth occurred at about 1300°C.  The

tube was pulled at a rate of about 1 cm per 24 hours for about 12 days,

after which the furnace was switched off and allowed to cool very slowly.

In general with this technique more than 80% of the charge was transported.

The resultant boule obtained consisted of a number of single crystals of

varying size, with linear dimensions ranging from 2 to about 7 millimetres.

All these crystals had a very deep red body colour and were luminescent

under U.V. excitation with the emission lying in a band at 6500 $\overset{o}{A}$   at

room temperature.  Their resistivity was of the order of $10^{12}$-$10^{14}$ ohm cm.

To produce doped crystals the required impurity, e.g. Mn, Al, Cr

etc. was added to the charge.  Addition of metallic Mn or Al was found

to have no detectable effect either on charge transport or  the size of

the crystals obtained.  However, addition of 0.01% of Cr inhibited

transport of the charge and sintered material only was obtained.  This

sintered material was pulled through the temperature gradient a second time, but with no effect. Careful examination of the material revealed some extremely small and fine crystals on the surface of the sintered ZnSe. These very fine crystals and the sintered material had a dark brown body colour.

Electron spin resonance of the $Mn^{2+}$ ion in crystals grown as described above indicated that they had a mixed cubic-hexagonal structure. As is explained in Section 5.17, no correlation was found between the size and the hexagonal admixture in any of these crystals. Nor was there any relationship between the hexagonal admixture and the position of the crystal in the boule.

(b)     ZnSe crystals produced by sublimation at 1150$^{o}$C

The other method of producing ZnSe crystals by sublimation (used in the department, though not by the author) was based on the technique developed and reported by Clark and Woods for growing good quality CdS crystals. For a report on this method as applied to ZnSe the reader should consult the paper by Burr and Woods (13). In this method in which a vertical furnace arrangement is used, an ampoule containing the ZnSe charge is provided with a reservoir containing Zn or Se, the temperature of which can be maintained constant during the sublimation-growth cycle. (The reservoir is in communication with the ampoule containing the charge via a narrow orifice). Use of a reservoir allows predetermined partial pressures to be maintained in the ampoule during sublimation-growth processes. To grow ZnSe crystals, a charge of ZnSe is sublimed at a temperature of 1150$^{o}$C to the top of the ampoule which is held at a temperature of about 1100$^{o}$C. The partial pressure of Zn or Se in the growth tube is controlled by maintaining the reservoir at a constant temperature. For instance, using pre-sublimed (Derby) ZnSe

powder it was found that transport of the charge could be best obtained with an atmosphere provided by an excess of Zn in the reservoir held at 550°C. At this temperature the excess Zn partial pressure provides conditions for the vapour to assume stoichiometric proportions (the starting material used to grow ZnSe crystals was ZnSe powder outgassed and sublimed in vacuum to reduce the oxide content). The ampoule was then pulled through the temperature gradient at a rate of 17 or 35 mms per 24 hours to yield a boule some 3-4 cm long and 1 cm in diameter. The polycrystalline boules obtained by this method had a pale yellow body colour. On the whole the high temperature sublimation method yielded very much larger poly-crystals of better quality. Also the incorporation of impurities seemed to be very much more difficult with the lower temperature method. For instance, attempts were made to incorporate Mn, added as metallic Mn and as MnSe, to the charge. ESR of a number of samples cut from the boules indicated that on the whole Mn had not been incorporated; in some samples the Mn concentration was comparable to that of the ZnSe powder (Derby), while in others a small amount of Mn had been incorporated which concentrated in a few points in the samples. However, when Mn was added as $MnCl_2$ to the reservoir containing Zn, the resultant boule contained uniformly distributed Mn.

(c)    Crystals produced by the flow process

ZnSe crystals were also produced in the department by the flow process. In this method a charge of pre-sublimed ZnSe contained in a silica boat was placed inside a silica tube. The temperature of the charge was maintained at about 1150°C and a stream of high-purity argon was used to carry the vapour to a cooler part of the tube (at about 1050°C) where crystal growth took place on a silica liner. The crystals obtained by this method were in the form of platelets, rods and fine

needles, and had a pale yellow body colour. Examination of their

structure under the polarizing microscope indicated that on the whole

the platelets were cubic, whereas the fine rods and needles appeared

to be hexagonal. To produce doped samples the desired impurity was

placed in a separate silica boat maintained at an appropriate temperature.

However, producing doped samples by the flow process can be very

uncertain. For instance an attempt was made to incorporate Mn in the

flow crystals, but the ESR of the $Mn^{2+}$ ion in the resultant crystals

indicated that in most samples Mn had not been incorporated while in

others the small amount of Mn that had been incorporated was found to

have been extremely non-uniformly distributed. The Mn concentration

in the fine hexagonal needles was found to be so small that it was not

possible to carry out ESR investigation of the $Mn^{2+}$ ion in hexagonal

ZnSe, even when a number of needles were tied together to form a bigger

sample.

(d)    Crystals produced by iodine transport method

As mentioned in Section 5,9 the crystals produced at $1300^{\circ}C$

by sublimation were found to have a mixed cubic-hexagonal structure. It

then became desirable to determine whether this admixture was dependent

on the temperature at which crystal growth occurred, or whether other

parameters were involved. As a result it was decided to attempt to

grow some ZnSe crystals at low temperatures using the iodine transport

method. The essence of this technique, first reported by Nische (16),

is believed to be as follows. Iodine is added to the charge in an

ampoule, the air is then removed and the ampoule sealed. The ampoule

is then placed in a uniform temperature gradient with the charge (at

one end of the ampoule) at a point of maximum temperature. The iodine

interacts with the charge in the high temperature region of the ampoule

according to the following reaction

$$ZnSe + I_2(g) = ZnI_2(g) + \frac{1}{2} Se_2(g) \cdot - \cdot - \cdot \cdot - \cdot - \cdot (1)$$
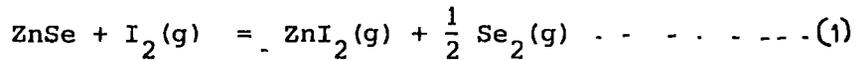
where (g) indicates the material to be in a gaseous state. The
gaseous constituents of the reaction (1) then diffuse to the cooler
part of the ampoule where reverse reaction takes place, i.e.

$$ZnI_2(g) + \frac{1}{2} Se_2(g) = ZnSe + I_2(g)$$
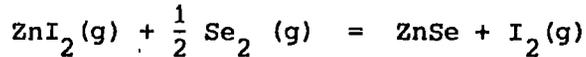
The ZnSe is condensed and the iodine diffuses back to the high temperature
region of the ampoule to participate in the reaction (1) again.

To produce ZnSe crystals by this method the charge and about
5 mgm/cc of iodine were placed in a silica ampoule of 1 cm bore and
about 10 cm length. The air was pumped out, the ampoule sealed and
placed in a furnace. In order to determine the conditions for maximum
transport and optimum crystal growth, a number of runs were carried
out with the maximum temperature ranging from 800 to 930°C. A maximum
temperature of 900°C at the hot end of the ampoule dropping to 850°C
where crystals grew, was found to give the best results. With such
an arrangement more than 90% of the charge was transported to the cooler
end of the ampoule in 10-11 days. The resultant boule obtained con-
sisted of a number of single crystals of millimeter dimensions with
some well formed (111) faces. They had an orange-red body colour (very
much lighter than crystals produced by the high temperature sublimation
method). The starting material used was ZnSe (Derby) powder baked and
sublimed to reduce the oxide content. This treatment was found to be
essential as no charge transport took place if untreated ZnSe powder
was used.

To produce doped crystals, the desired impurity was added to
the charge. Addition of 0.01% Cr to the charge again prevented charge

transport, as it had done with the high temperature sublimation method. However, whereas in the resultant sintered material produced at $1350^{\circ}$C, Cr (from its ESR) was found to have been uniformly incorporated, in the iodine transport method, Cr was found only in a small "patch" of the resultant material which was in the form of a rough powder. Addition of Mn was also found to retard charge transport by about 10-15%.

The structure of the crystals obtained by this method was examined using back reflection X-ray techniques and the polarizing microscope. The ESR spectrum of the $Mn^{2+}$ ion incorporated was also used for this purpose. Over thirty crystals were investigated and in none could the structure be described as anything but cubic. Nor was it possible to convert this structure into hexagonal by annealing (see Section 5.17 ). However, the solubility of Mn in these crystals was found to be smaller than in the crystals produced by sublimation at $1300^{\circ}$C, (see Section 5,12 ).

CHAPTER 3

SOME PROPERTIES OF ZnSe

3.1. Chemical Binding in ZnSe

There is considerable interest in the chemical binding of solids. This arises because an exact knowledge of the chemical binding in solids should lead to a better understanding of their physical and chemical properties.

In the II-VI compounds the chemical binding is a mixture of ionic and covalent, but there is no general agreement as to the extent of the ionic component. This stems essentially from the difficulties and uncertainties that are encountered when trying to determine experimentally the exact contribution of a type of binding in a solid with mixed ionic-covalent bonds.

Attempts to clarify the chemical binding were first made by Pauling in 1932 (1). Pauling defined a concept of electronegativity of atoms from which it was hoped to determine the type of binding involved. Using Pauling's concept, Bube (2) gives the following table of ionicity for some of the II-VI compounds.

| | % ionicity |
|---|---|
| ZnS | 22 |
| ZnSe | 19 |
| CdS | 22 |
| CdSe | 19 |
| PbS | 19 |
| PbSe | 17 |

Thus on the basis of Pauling's original concept, one may expect the above II-VI compounds to be mainly covalent. But theoretical and experimental investigations (mentioned below) disagree with this.

Reviewing theoretical calculations of Segall ( 3 ), Birman ( 4 ), Williams ( 5 ) and Balkanski ( 6 ), and the experimental data obtained from the measurements of the dielectric constants and the piezoelectric constants, Curie ( 7 ) in 1963 concluded that the percentage of the ionic binding in ZnS and CdS was about 75%. Furthermore, using the Pauling's table of electronegativity of 1945 ( 8 ), Curie anticipated the ionic binding to decrease when S is replaced by Se. Saksena ( 9 ) calculated the ionicity of ZnS and CdS from the measured piezoelectric constants and suggested that in these compounds the ionicity is in excess of 60%.

Table 1 illustrates some values of ionicity of a number of compounds predicted by the theories of Pauling, Coulson and Phillips (10,11,12). For a review of the modern theories of ionicity the reader should consult Phillips (12). There is a good deal of recent experimental evidence in support of the ionicity values calculated by Phillips in Table 1. Thus Martin (13) investigated the elastic constants of a large number of crystalline compounds with the sphalerite structure and found that the experimental results could be readily explained in terms involving the ionicity theory defined by Phillips. Martin (14) also investigated theoretically the relationship between the interatomic forces and electronic properties of a number of compounds with the zinc-blende structure and found results in agreement with ionicity as defined by Phillips. Camphaussen et al (15) investigated the positions of the energy bands of ZnSe as a function of pressure and found very good agreement with the theoretical results which had been calculated assuming an ionicity of 0.676. Walter et al (16) investigated theoretically the electronic charge density as a function of position in the unit cell for several semiconductors with the zinc-blende structure and found very good agreement with Phillips' scale of ionicity. It

| Compound | Ionicity | | |
|---|---|---|---|
| | Phillips [12] | Pauling [10] | Coulson [11] |
| CaS | 0.902 | 0.81 | ..... |
| LiF | 0.915 | 0.93 | ..... |
| SiC | 0.177 | 0.11 | 0.06 |
| MgO | 0.241 | 0.88 | .... |
| NaF | 0.946 | 0.98 | .... |
| MgS | 0.786 | 0.67 | ..... |
| ZnO | 0.616 | 0.80 | 0.65 |
| KF | o.955 | 0.99 | ..... |
| ZnS | 0.623 | 0.59 | 0.61 |
| MgSe | 0.790 | 0.65 | .... |
| CdO | 0.785 | o.85 | .... |
| CuCl | 0.746 | 0.82 | 0.25 |
| GaAs | 0.310 | 0.26 | 0.37 |
| InP | 0.421 | 0.26 | 0.37 |
| ZnSe | 0.676 | 0.57 | 0.64 |
| ZnTe | 0.546 | 0.53 | 0.66 |
| CdSe | 0.699 | 0.58 | 0.61 |
| CdTe | 0.675 | 0.52 | 0.61 |

Table 1

is, however, important to point out that in this ionicity scale the selenides are calculated to be more ionic than the sulphides. This should be contrasted with Pauling's scale which predicts the reverse.

Data obtained from ESR measurements have also yielded information on the relative ionicity of a large number of compounds. Van Wieringen [17] investigated the spin resonance of the $Mn^{2+}$ ion and found that the hyperfine coefficient (A) depended on the host lattice. (A) was found to be larger in ionic compounds than in covalent ones. Matamura [18] plotted (A) against ionicity as defined by Pauling (1938) and found a linear relationship. Also the spin resonance results indicate that the g-value of the $Mn^{2+}$ ion varies with ionicity in a manner opposite to that of (A). Fidone and Stevens [19] have shown theoretically that covalency in the bonding leads to a positive contribution to the g-value of an s-state ion. For a discussion of the way in which the spin resonance parameters of the s-state ions vary with ionicity the reader should consult Section 5.9 . Here it is important to point out that from the variation of the hyperfine coefficient (A) with ionicity, ZnSe appears to be less ionic than ZnS, whereas the calculations of Phillips and Coulson (see Table 1) predict the reverse.

## 3.2    Energy Band Structure of ZnSe

Attempts to calculate the band structure of solids which crystallise with the zinc-blende lattice were first made by Herman [20], who developed a semi-empirical perturbation scheme to relate the band structures of solids with the zinc-blende lattice to those with the diamond structure. Crystallographically the two types of solids are identical apart from the fact that whereas in the diamond structure

all the atomic sites are occupied by atoms of the same kind, in material of the zinc-blende type, such as ZnSe, the sites are alternately occupied by Zn and Se atoms. This results in absence of inversion symmetry in the zinc-blende solids. This absence of symmetry provides the principal difference in the band structures of the two types of crystals. Herman's work was extended by Parmenter (21) and Dresselhaus (22) who derived group theoretical character tables from which all the symmetry properties of a zinc-blende band structure could be deduced. Furthermore they took into account the spin-orbit inter-action which can have a profound effect by removing the degeneracy of the valence band. (23-27).

More recently an extensive amount of theoretical work has been carried out and there now appears to be very good agreement between the theory and experimental data obtained from reflectivity, dispersion and absorption measurements.

All the evidence obtained so far indicates that ZnSe has a relatively simple band structure with the minimum vertical energy separation of the conduction and the valence bands which occurs at the centre of the Brillouin Zone. Thus Aven et al (28) found very intense and narrow exciton absorption bands just below the absorption edge which occurred without any phonon participation thus indicating a direct band gap. The edge emission results obtained by Reynolds et al (29) were explained by Aven and Segall (30) in terms of a direct band gap. Hite et al (31) in their study of excitons and the absorption edge in cubic ZnSe could find no evidence for any indirect excitonic transition or any evidence indicating that the band gap in any other part of the Brillouin Zone is smaller than that at the centre of the zone. Reflectivity measurements carried out by Cardona (32), and an

investigation of the Faraday rotation by Balkanski (33) also lead to the same conclusion. Hall mobility data obtained by Aven and Segall (30) could best be explained by taking the value of the electron mass calculated by Marple (34) assuming a direct band gap with extrema at $K = 0, 0, 0$.

Figure (3.1) illustrates schematically the band structure of cubic ZnSe at $K = 0$. The valence band which has a symmetry $\Gamma_4$ in the absence of spin-orbit interaction is split into two sub-bands by spin-orbit interaction. The separation of these two bands at room temperature is $0.45 \pm 0.04$ eV (28).

ZnSe may also crystallize with a wurtzite structure. Considering the geometrical similarity and symmetry of the hexagonal and the cubic structures Birman (35) suggested that the band structure of a wurtzite type of solid at points in K-space along the C-axis can be derived from that of the zinc-blende along [111] direction by applying a small hexagonal crystal field as a perturbation to the zinc-blende lattice. Birman's suggestion has been investigated experimentally and theoretically and found valid and very useful (36,37).

The inclusion of the hexagonal crystal field considered by Birman lifts the degeneracy of the top cubic valence band so that in the hexagonal structure the valence band consists of three sub-bands. The relationship between the cubic and the hexagonal band structure is illustrated in Figure (3.2.).

In hexagonal ZnSe, just as in cubic ZnSe, the minimum separation of the conduction and the valence bands is believed to occur at the centre of the Brillouin zone. Liang et al ( 38) investigated the exciton structure and the absorption edge of hexagonal ZnSe and found the absorption process to be a direct one with the minimum separation of

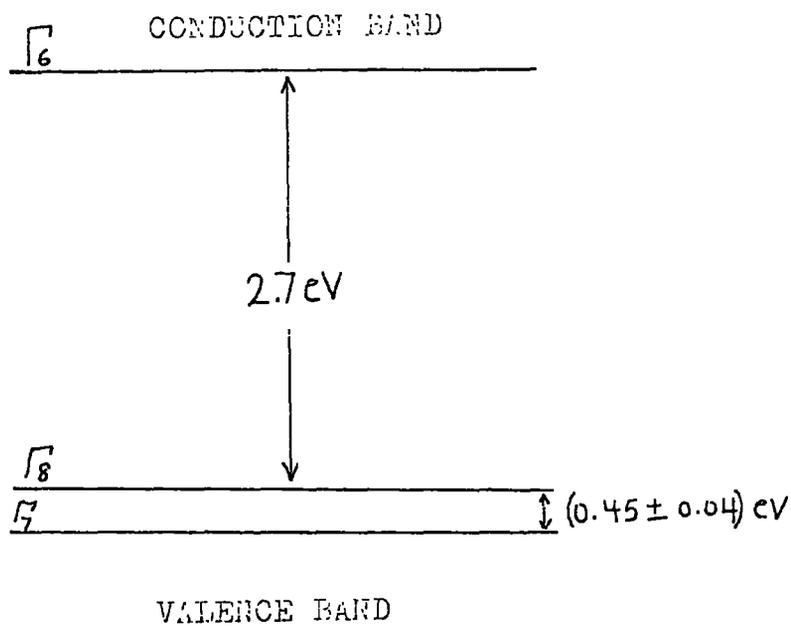Fig.( 3.1 ) Energy bands for ZnSe ( cubic ) at
K=0,0,0, at 300 K  (28).
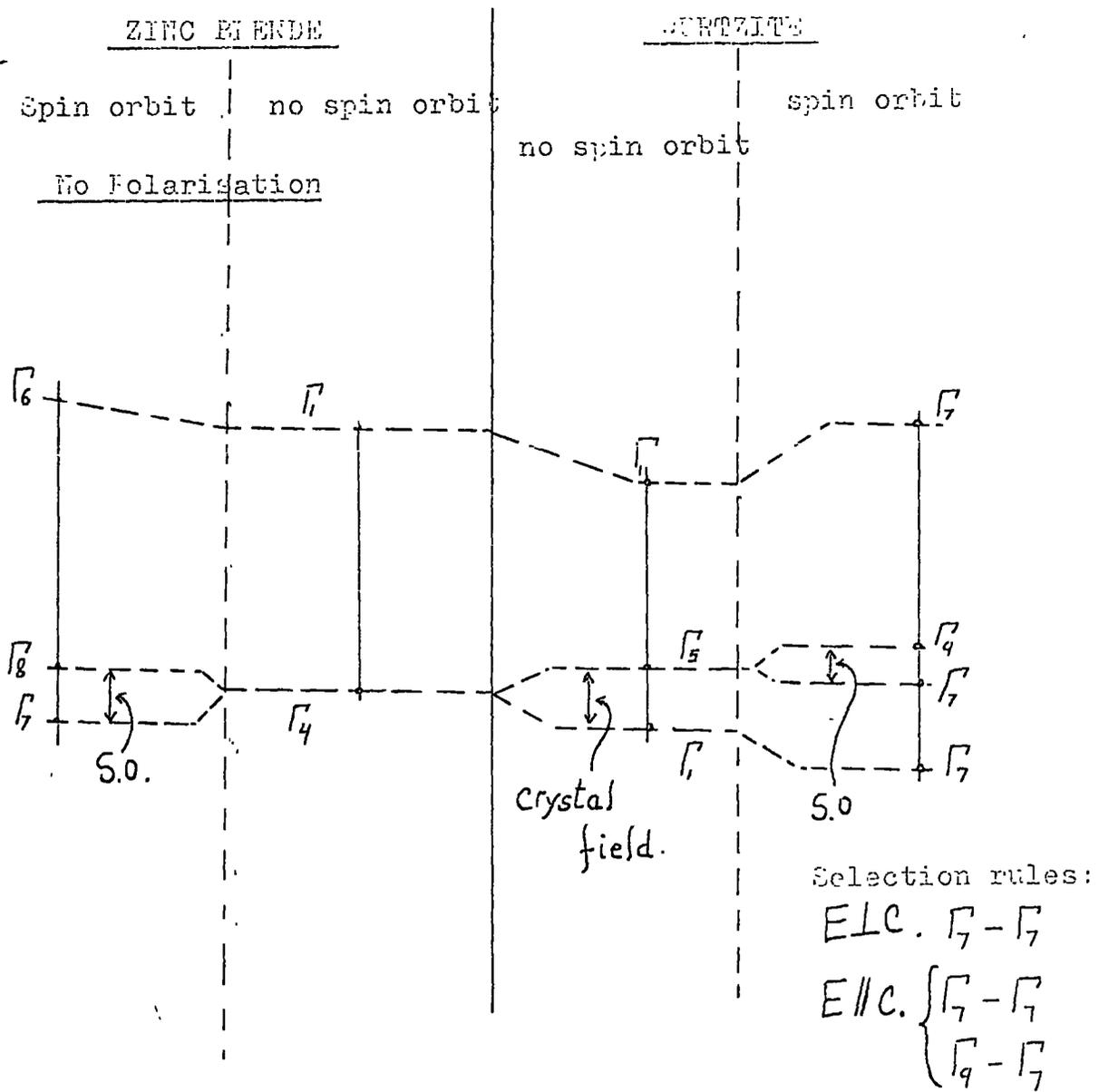
Fig.( 3.2 ) Band structure and selection rules for the Zinc blende and wurtzite structures at K=0,0,0. The crystal field and spin orbit splittings are indicated schematically. Transitions which are allowed for the photon electric vector parallel and perpendicular to the c-axis are indicated. The selection rules are due to Dresselhaus( 22 ).

the bands at K = 0. Also, in agreement with the selection rules proposed
by Dresshaus (22), optical transition to the conduction band from the
top valence band occurs only for light polarized with its E-vector ⊥ to
the C-axis. Transitions from the other two valence bands occur for
light polarized with E||C and E⊥C.

Figure (3.3) illustrates the hexagonal band structure of ZnSe
proposed by Liang et al (38), while Figure (3.4) illustrates the photo-
conductivity peaks for cubic and hexagonal ZnSe at room temperature
as measured by Park et al (39).

## 3.3    Effective Carrier Masses in ZnSe

Aven et al (40) calculated the effective electron and hole masses
from their study of excitons in cubic ZnSe. They assumed hydrogenic
excitons in ZnSe and determined a value for the exciton effective mass

$$\mu = \frac{m_e^* \, m_h^*}{m_e^* + m_h^*}$$

Using the relation

$$\frac{m_h^*}{m_e^*} = \left(\frac{\mu_c}{\mu_h}\right)^{2/3}$$

and substituting known values of electron and hole mobilities they found
values of $0.1 \, m_e$ and $0.6 \, m_e$ for the electron and hole effective masses.
Marple (34) from his study of infra-red reflectivity and Faraday
rotation in ZnSe, obtained an electron effective mass of $(0.17 \pm 0.025)m_e$
and found that the temperature dependence of the Hall mobility data
obtained by Aven and Segall (30) could be explained better with this
slightly larger value. Bower et al (41) calculated the effective electron
mass in ZnSe theoretically (from the band structure calculations at
K = 0) and found a value of $0.91 \, m_e$. The reason for such a large

Conduction Band

$\Gamma_7$ ──────────────────────

$2.874\,eV$

$\Gamma_9$ ──────────────────────
$\Gamma_7$ ────────────────────── $\updownarrow$ $0.065\,eV$

$\Gamma_7$ ────────────────────── $\updownarrow$ $0.465\,eV$

Valence Band

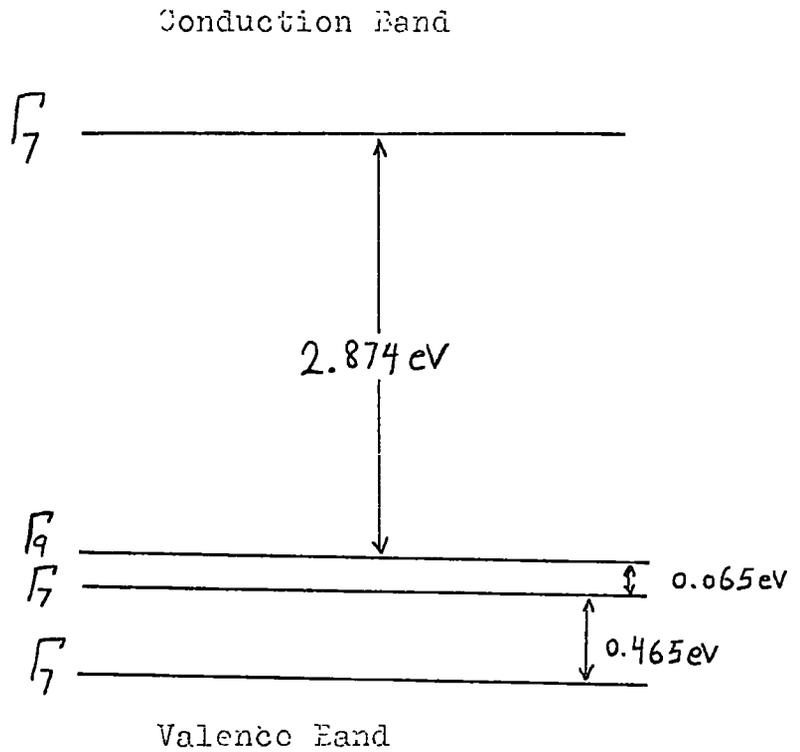Fig.(3.3) Schematic band structure of hexagonal ZnSe
at K=0,0,0, at 15K. Transitions to the conduction band ($\Gamma_7$)
are allowed for light polarized with E⊥C ($\Gamma_9 \rightarrow \Gamma_7$) only,
while transitions for the other two valence sub-bands
are allowed for E⊥C and ∥C .
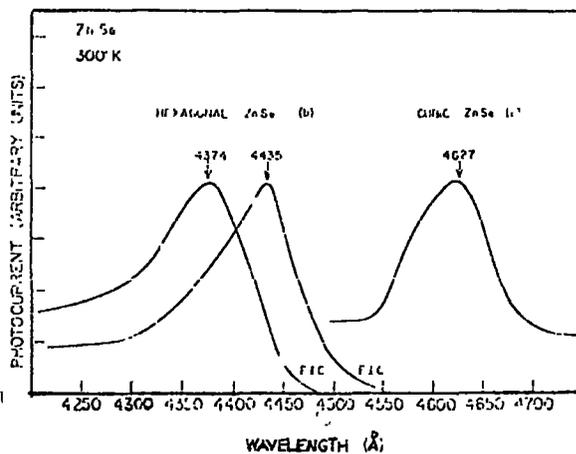
Fig.(3.4) Photoconductivity spectra of ZnSe at 300K.

(a) Cubic ZnSe in unpolarized light.

(b) Hexagonal ZnSe in polarized light (39).

discrepancy with the experimentally determined values seems to lie in

the unsuitable mathematical functions used in the calculations.

The value of 0.6 $m_e$ obtained by Aven et al (40) for the effective

hole mass in cubic ZnSe must be considered an average value, since the

top valence band is degenerate and probably consists of a light and a

heavy hole band.


## 3.4    Electrical Properties of ZnSe

The properties of ZnSe have not been investigated as extensively

as those of some other members of the II-VI compounds.  One reason for

this has been the unavailability of suitable samples.  But, in recent

years considerable progress has been made in producing single crystals

of ZnSe and before long, much more experimental evidence should become

available.

The data available so far indicates that ZnSe can be made both

n- and p-type when doped with suitable impurities.  Deviation from

stoichiometry in the form of excess zinc also produces n-type conduc-

tivity, but no p-type conductivity due to excess of Se has been observed.

In common  with other II-VI compounds ZnSe exhibits a very strong

tendency towards self-compensation.  As a result, samples made without

any special treatment may have very low electrical conductivity.  For

n-type samples it has been found possible to increase the conductivity

by reducing the concentration of the compensating acceptors by annealing,

but for p-type samples no way of reducing the concentration of the donor-

type centres has been found.  The conductivity of the p-type samples

is usually about $10^{-10}$ $\Omega^{-1}$ $cm^{-1}$ and as a result p-type ZnSe has not

attracted any technological attention.

Generally what is hoped to occur when, for instance, ZnSe is

doped with an impurity such as Cu (which has one fewer valence electrons than Zn), is for Cu atoms to replace Zn ions and produce free holes when sufficient ionization energy is supplied. Instead it appears that the incorporation of Cu is accompanied with the formation of donor-type native defects which combine with the impurity atoms to form something similar to donor-acceptor pairs. The net result of this is that the majority of the Cu atoms are prevented from producing free holes. In p-type ZnSe containing Cu, transport measurements show a donor density almost the same as that of Cu acceptors (30 ).

In ZnSe, impurities such as Cl, Br and I replacing Se ions, and Ga, Al and In replacing Zn ions act as donors. Experimental data indicates that the halogens have a relatively large ionization energy in ZnSe. Aven et al (30) obtained a value of 0.19 eV in a Cl-doped samples, and Bube (42) found a value of 0.21 eV in Br-doped samples. These values are comparable with those found in ZnS, but differ greatly from those in CdS and CdSe (where the average halogen ionization energy is about 0.03 eV).

The solubility of some metallic donors (Al, Ga and In) seems to be very large in ZnSe. Aven and Segall (30, 43) doped a ZnSe sample with Al by diffusion and from their transport measurements found a degenerate donor band coinciding with the bottom of the conduction band.

Though the ionization energy of the halogens in ZnSe is rather large, shallow donor centres do exist. Aven et al (30) annealed an undoped ZnSe sample in molten zinc and from transport measurements found a donor level 0.008 eV below the conduction band. Nothing, however, is known about the identity of this centre.

The ionization energy of the acceptor centres in ZnSe seems to be very close to those in CdSe. Thus Stringfellow et al (44) found

an ionization energy of 0.72 eV for Cu in p-type ZnSe, and Bube [42] obtained an activation energy of about 0.6 eV for the acceptor-type sensitizing centres (class II centres) from photoconductivity experiments. Though not enough data is available to draw any firm conclusions, nevertheless it appears as if in the donor ionization energy in II-VI compounds is determined mainly by the cations while the acceptor ionization energy is determined mainly by the anions.

## 3.5    Charge Carrier Mobility in ZnSe

The charge carrier mobility in ZnSe was first investigated by Aven and Segall [28] who found electron mobility values of 80 $cm^2$/v sec and 260 $cm^2$/v sec at 300 K in a Ga-doped sample and an undoped sample which had been annealed in molten zinc. These preliminary measurements were later on extended to Cl-doped and Al-doped samples [30] in a wider temperature range. At temperatures above 100 K the mobility in three samples ZnSe:Cl, ZnSe:Al and ZnSe undoped was found to be almost the same thus indicating a scattering process common in the three samples. Theoretical investigation of the possible scattering processes indicated that in ZnSe in common with other II-VI compounds, the polar optical mode lattice vibrations were responsible at high temperatures. At temperatures below 100 K ionized impurity scattering was suggested. The highest mobility value obtained was 700 $cm^2$/v sec at 200 K.

Since this early work, other investigators have confirmed that the mobility at high temperatures is controlled by optical mode lattice vibrations and what is more significant they have reported consistently higher mobility values. Thus Woodbury et al [45] in 1964 reported a mobility value of 2700 $cm^2$/v sec at 80 K, Fukua et al [46] in 1967 reported a value of 3000 $cm^2$/v sec at 90 K and more recently (1970) Aven [47] obtained a value of 12000 cm/v sec at 50 K in a high purity

sample which had been annealed in molten zinc.

The improvement in mobility since 1963 has been to a large extent the result of improvements in the purity of the ZnSe starting material and samples made. Also annealing in molten zinc (the zinc extraction technique as it is sometimes called) has played a very important double-role in this respect. Experiments show that using this technique it is possible to reduce the concentration of acceptor like metallic impurities such as Cu in ZnSe quite considerably. This is made possible by the fact that some metallic impurities are more soluble in molten zinc than in ZnSe and hence diffuse out of ZnSe at high temperatures. The annealing process seems also to be very effective in reducing the concentration of compensating (acceptor-type) native defects. The result is that both the conductivity and the mobility improve. The experimental work of Aven (47) demonstrates this very effectively.

Recently Aven in the course of his transport measurements on high purity ZnSe crystals has found a double acceptor centre that could affect the conductivity and mobility considerably. Such a centre was first observed in high purity CdTe following heat treatment in Cd atmosphere by Lorenz et al (48,49). Briefly, it was found that when a high purity sample was irradiated with light at low temperatures the conductivity and the mobility increased sharply and persisted when the light was turned off. On warming the sample a decrease in conductivity and mobility was observed at a critical temperature.

It appears that on irradiating the sample at low temperature, the free holes created are captured by the doubly ionized acceptor centres which become singly charged. The kinetic energy of the free electrons is not, however, sufficiently large to surmount the repulsive field of these singly charged centres. As a result the electrons

created remain free even when the light is turned off. The mobility increases since the scattering power of the charged centres is decreased (scattering by ionized centres is proportional to the square of the charge they carry).

On increasing the temperature of the sample, the kinetic energy of the free electrons increases, so that at a critical temperature they can surmount the potential barrier of the singly charged centres and convert them into doubly charged ones. The conductivity and mobility now decrease to their dark values.

Aven carried out annealing treatment of ZnSe samples containing double acceptors. His results show that whereas before annealing the sample had mobility values of 3960 $cm^2$/v sec in the dark at 55.6 K, and the mobilities changed to 12000 $cm^2$/v sec and 13600 $cm^2$/v sec after annealing for approximately 300 hours, thus indicating that the concentration of the double acceptors had been reduced very considerably.

The identity of these double acceptors is at the moment unknown. Furthermore, it is not definitely clear whether they are native defects (such as vacancies, interstitials etc.), impurities or complex centres consisting of native defects and impurities.


## 3.6    P-type Mobility in ZnSe

Very few transport measurements have been carried out in p-type ZnSe because of the extremely low conductivity of such samples. Aven et al (28) found a mobility value of 11 $cm^2$/v sec at 473 K in a Cu-doped sample. Stringfellow et al (44) found a value of 30 $cm^2$/v sec at 296 K in a similar sample.

## CHAPTER 4

## ELECTRON SPIN RESONANCE

### 4.1    Quantum Numbers

The energy state of an electron in an atom can be specified by four quantum numbers. These are n, the principal quantum number, 1, the orbital angular momentum quantum number, $m_\ell$ the magnetic quantum number and s, the spin quantum number.

n, the principal quantum number of a single electron in an atom, can take up values that are integral and non-zero and are from unity upwards.

The orbital motion of an electron around the nucleus produces an angular momentum. Classically the orbital angular momentum could take up any value, but in a quantum mechanical treatment of the atom the angular momentum is quantized and this is reflected in the allowed values of 1 which are integral and range from 0 to (n-1) for an electron with principal quantum number n.

An electron also carries a charge and as a result a magnetic moment is associated with its orbital angular momentum. In the presence of a magnetic field the dipole moment represented by a vector precesses at a constant angle about the direction of the applied field. This means that the component of the orbital angular momentum along the direction of the applied field is constant and is given by $m_\ell \left(\frac{h}{2\pi}\right)$ where $m_\ell$ is defined as the magnetic quantum number. For a given value of 1, $m_\ell$ may have (21+1) possible values from 1, 1-1, .... to -1. The significance of the quantum number $m_\ell$ is that it gives the possible orientation of the angular momentum vector with respect to an external magnetic field. Since only certain orientations are allowed there is a space quantization, where the component of the angular momentum along the field direction is equal to $m_\ell \left(\frac{h}{2\pi}\right)$ .

· An electron can also be thought of as spinning about an internal axis and therfore possessing an intrinsic angular momentum. The value of this intrinsic angular momentum is $\sqrt{s(s+1)}\,\frac{h}{2\pi}$ where s is the spin quantum number with a value of 1/2. In analogy with the definition of $m_\ell$ a spin magnetic quantum number $m_s$ is associated with the spin angular momentum; $m_s$ has values of ±1/2. The two values of $m_s$ represent the two possible orientations of the spin magnetic dipole with respect to an applied magnetic field.

## 4.2    Resultant Angular Momentum

For a complex atom with a large number of electrons the overriding condition that determines the distribution of electrons in the various energy states, is the Pauli exclusion principle. This states that no two electrons in an atom may have identical sets of quantum numbers. As a result there is a limit of $2n^2$ to the number of electrons permitted in any given shell with principal quantum number n. When all the possible states for a given value of n are taken up the result is a closed or filled shell. In such a system it can be shown that the resultant electronic angular momentum is zero. Paramagnetism which is the basis of electron spin resonance, occurs in atoms or ions that have a resultant angular momentum, i.e. mainly in atoms or ions that have an odd number of electrons.

To find the resultant angular momentum of all the electrons one has to consider how the angular momenta associated with the orbital and spin motions of the electrons are coupled together. Basically two types of interactions must be considered. One is the mutual repulsion between the electrons due to their charge, and the other is the magnetic coupling interaction between the magnetic dipole moments of the orbital and spin motions of the individual electrons.

Wave mechanical treatment of the mutual repulsion of a number

of electrons in an atom shows that there are electrostatic exchange

forces which tend to couple strongly the electron spin angular momenta

on the one hand and the orbital angular momenta on the other. Thus on

the basis of these exchange forces vectors representing the spin angular

momenta of electrons combine to form a resultant total spin momentum S,

and independently all the orbital angular momentum vectors combine to

form a resultant orbital angular moment L. The resultant total electronic

angular momentum of the atom is then given by $\underline{J} = \underline{L} + \underline{S}$ where $\underline{J}$ can have

the following possible values

$$J = (L+S), \quad (L+S-1), \quad \ldots \quad \ldots \quad \ldots \quad (L-S) \quad \ldots (2)$$

The group of levels given by the above equation is usually referred to

in spectroscopy as a multiplet, the multiplicity of the system being

(2S+1) by definition. The multiplet spacing is determined by the spin-

orbit coupling constant $\lambda$ defined via the spin-orbit interaction energy,

i.e. $\lambda \, \underline{L} \cdot \underline{S}$ .

This type of coupling (Russell-Saunders coupling as it is

usually called) occurs mainly in light atoms. The essence of it is that

the forces which couple the spin angular momenta together and the forces

that couple the orbital angular momenta together are very strong, but

the forces coupling the orbital to the spin system are relatively weak.

Throughout this thesis this is the type of spin-orbit coupling that is

assumed to be relevant.

In heavy elements the interaction between the orbital angular

momentum and the spin of the individual electrons is large. This comes

about as a result of a magnetic coupling between the spin and the orbital

magnetic dipole moments of the individual electrons. In such a system

the spin and the orbital angular momenta of the individual electrons

combine to form a resultant angular momentum. These resultants are then added together to form the total electronic angular momentum $\underline{J}$ of the atom.

In analogy with the definition of $m_\ell$ and $m_s$, three more quantum numbers $M_J$, $M_L$ and $M_S$ are defined for the atom. These quantum numbers denote the components of $\underline{J}$, $\underline{L}$ and $\underline{S}$ along the direction of the applied magnetic field.

## 4.3     Spin Resonance

When an atom with a resultant electronic angular momentum $\underline{J}$ is placed in a magnetic field, the vector can take up (2J+1) orientations. These orientations correspond to a (2J+1)-fold splitting of the degenerate energy level by the magnetic field. If the magnetic moment of the electrons is derived from spin angular momentum only, i.e. if $\underline{L}$ = 0 then the separation of the energy levels is g$\beta$H and the energy levels are given by $E_{Ms}$ = g$\beta$HM$_s$ where the constant g is known as the splitting factor (or the g-factor) and in the case of a free electron has a value of     2.0023.

If on the other hand orbital angular momentum only is involved, i.e. if $\underline{S}$ = $\underline{O}$ , then the separation of the energy levels is $\beta$H and the energy levels are given by   $E_{M_L}$ = $\beta$HM$_L$ .

When $\underline{L}$ and $\underline{S}$ are coupled (as in the case of Russell-Saunders coupling) forming a resultant $\underline{J}$, the energy levels are given by $E_{M_J}$ = g$_J$$\beta$HM$_J$ , where g$_J$ is the Lande splitting factor.

$$g_J = 1 + \frac{S(S+1) + J(J+1) - L(L+1)}{2J(J+1)} \qquad \text{-----(3)}$$

Notice that in the three different cases the magnitude of the splitting of the energy level is essentially exhibited in the g-factor.

In the simplest case when $M_J = M_S = \pm 1/2$ only two energy levels are obtained in a magnetic field and they diverge linearly with increasing applied field. Transitions between these two levels can be induced by introducing electromagnetic radiation of frequency $\nu$ polarized with its H-vector perpendicular to the static field H. Transition from the ground state $M_S = -1/2$ to the upper state $M_S = +1/2$ can occur when the resonance condition $h\nu = g\beta H$ is satisfied. The interaction which causes the transition is between the spin magnetic dipole and the oscillating magnetic field of the microwave radiation in accordance with the selection rule $\Delta M_S = \pm 1$.

If in contrast to the above case, S had a value of, for example, 3/2, again the application of a magnetic field would split the (2S+1)-fold degenerate ground state into (2S+1) = 4 levels. Then when the resonance condition is satisfied, transitions between adjacent levels can occur in accordance with the selection rule $\Delta M_S = \pm 1$. Since the energy levels are split equally by the applied magnetic field, only a single absorption line would be observed, even though three different transitions are involved. This situation should be contrasted with the result that would be obtained if the atom were placed in a solid thus experiencing a crystal field (see below).

## 4.4    Crystal Field

A paramagnetic ion in a solid is subjected to two types of inter-action. One is an interaction between the magnetic dipoles arising from the magnetic ions themselves, and the other an interaction between the paramagnetic ion and the neighbouring diamagnetic ions. The magnetic dipole interaction can be reduced to a negligible level by having a small concentration of paramagnetic ions present. Nothing can however

be done to eliminate the interaction of the paramagnetic ion with the electric field set up within the solid by the charged diamagnetic ions. If this electric field (referred to as the crystal field) is sufficiently strong some of the degeneracy of the electronic energy levels may be lifted to give rise to a splitting in the absence of an applied magnetic field (this is known as zero-field splitting). Figure (4.1) illustrates the case for an atom with $S = 3/2$ (a) in free space, and (b) in a solid. Whereas in (a) the spectrum consists of a single absorption line, even though three transitions are involved, in (b) as a result of the zero-field splitting the spectrum consists of three lines the separation of which may depend critically on the crystal field strength and its symmetry. One result of this is that the g-factor is no longer given by (3) but is best defined experimentally from the resonance condition $h\nu = g\beta H$. Its magnitude may also depend now on the orientation of the symmetry axes of the solid with respect to the external magnetic field.

The fundamental idea of crystal field theory as proposed originally by Bequerel (1) in 1929 is that a metal ion placed in a solid is subjected to an electric field. This was formalised into a theory by Bethe (2) who investigated by means of symmetry concepts how the strength and symmetry of crystal fields affected the electronic energy levels of free ions. In 1930 Kramer (3) established a basic theorem concerned with the effect of crystal fields on the ground state of paramagnetic ions. This theorem states that in a paramagnetic ion containing an odd number of electrons no electric field can remove all the degeneracy of the ground state, i.e. the ground state must remain at least two-fold degenerate. This two-fold degeneracy can be removed by applying a magnetic field to give rise to Kramer's doublets in ESR.

The first notable application of the new theory was made by Van Vleck (4) in 1932. He investigated the magnetic properties of the
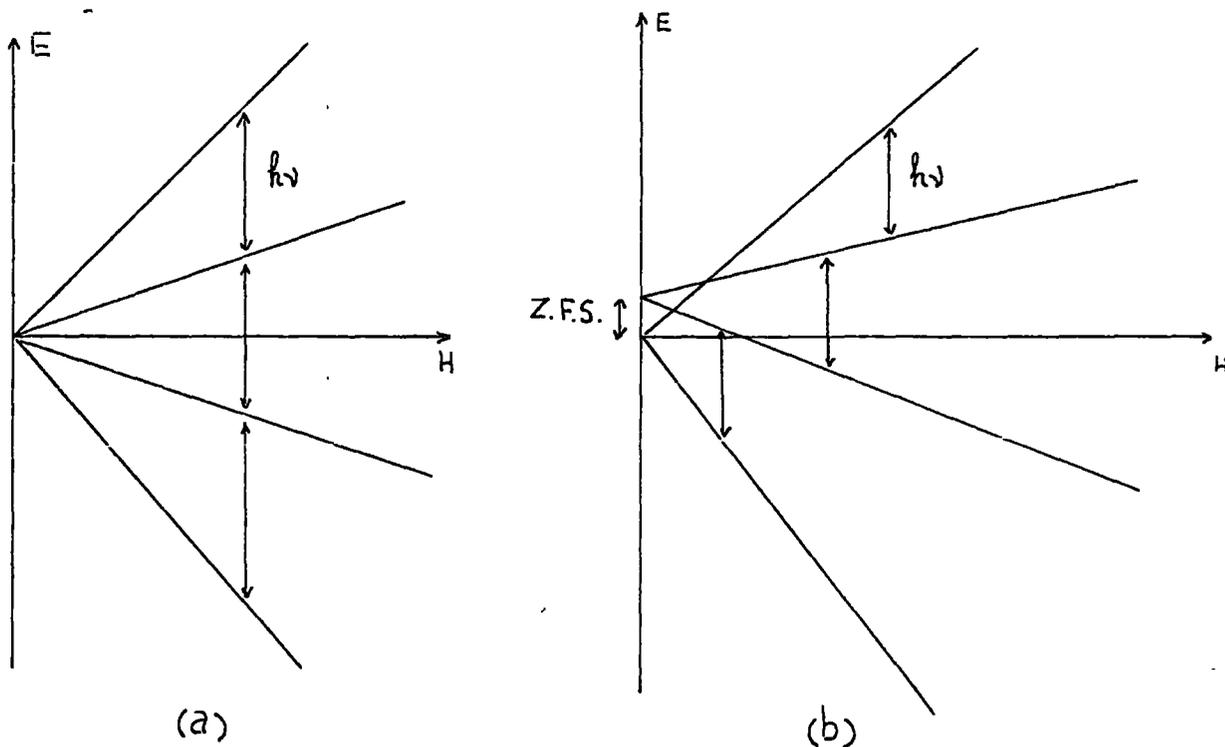
Fig.(4.1).
(a) Energy levels with no zero-field splitting.


(b) Energy levels with zero-field splitting due to a
    crystal field.


In (a) the system gives one spin resonance absorption line
while in (b) three lines which may not be equal in spacing
and intensity may be observed.

ions of the iron series of transition elements and was able to show

why the susceptibility of these ions corresponded (very nearly) to

spin-only values as a consequence of quenching of their orbital angular

momentum by crystal fields. His model was also able to predict in which

cases there would be a small deviation. Later on (5) he investigated

the processes by which the optical absorption bands occur when ions are

placed in crystal fields of octahedral symmetry. It was shown that the

vibration of the co-ordinating ligands had to be taken into account in

order to obtain transition probabilities different from zero, i.e. the

transitions involved are normally forbidden. Van Vleck (6) also investi-

gated the Jahn-Teller theorem as applied to ions in an octahedral

crystal field. This theorem states that no non-linear molecule can be

stable in a degenerate state apart from the cases covered by the Kramer's

theorem (here a molecule means the combined system of metal ion and its

nearest neighbours). In such a case the system distorts via nuclear

displacements to lower the symmetry so that the degeneracy is removed.

In essence the crystal field acting on a paramagnetic ion is

composed of contributions from all the charged diamagnetic ions and

defects present in the solid. The calculation of the crystal field on

such a basis is an almost impossible task. Instead as a first approxima-

tion the effect of the surrounding nearest neighbour ligands only is

considered. This is done by assuming that the electric field can be

simulated by a group of point charges or dipoles completely external

to the paramagnetic ion. This means that the solid is assumed to be

entirely ionic and because of this care has to be exercised in extending

the results of crystal field calculations to solids with any degree of

covalency in their bonding.

The splitting of degenerate electronic energy levels by a crystal field can be readily understood from the following qualitative example in which a 3d' ion is assumed to be surrounded by six negative charges in an octahedral arrangement (the ion is assumed to be at the centre of the co-ordinate system and the negative charges at distances of $\pm$ a on each of the positive and negative co-ordinate axes). An electron in the $n = 3$, $l = 2$ level can occupy any one of the five degenerate d orbitals (these orbitals, as was pointed out on page 2q correspond to $2l + 1$ possible values of $m_l$ , and are degenerate in the absence of a magnetic or electric field). Figure (4.2) illustrates the five d orbitals situated at a site of octahedral symmetry in relation to six equivalent point charges. From this it can be seen that the x, y and z axes of the octahedron are equivalent and that the xy yz and zx orbitals (called d$\varepsilon$ orbitals) all have the same electrostatic interaction with the array of negative charges. Similarly the two remaining orbitals $d(x^2 - y^2)$ and $dz^2$ (called d$\gamma$ orbitals) have the same interaction energy, though this is less obvious. Since the two d$\gamma$ orbitals extend to regions of high charge density, i.e. they point directly towards the negative charges, their interaction energy is higher than that of d$\varepsilon$ orbitals. It follows that the degeneracy of the orbitals is partially lifted and the free ion energy level is split into two levels one doubly and the other triply degenerate. The order of the splitting is as illustrated in Figure (4.3), in which the lower level is triply degenerate and the upper level doubly so. Group theoretical work of Gorter (7) shows that this order of splitting would be reversed if instead of an octahedral environment the ion were placed in a tetrahedral one.
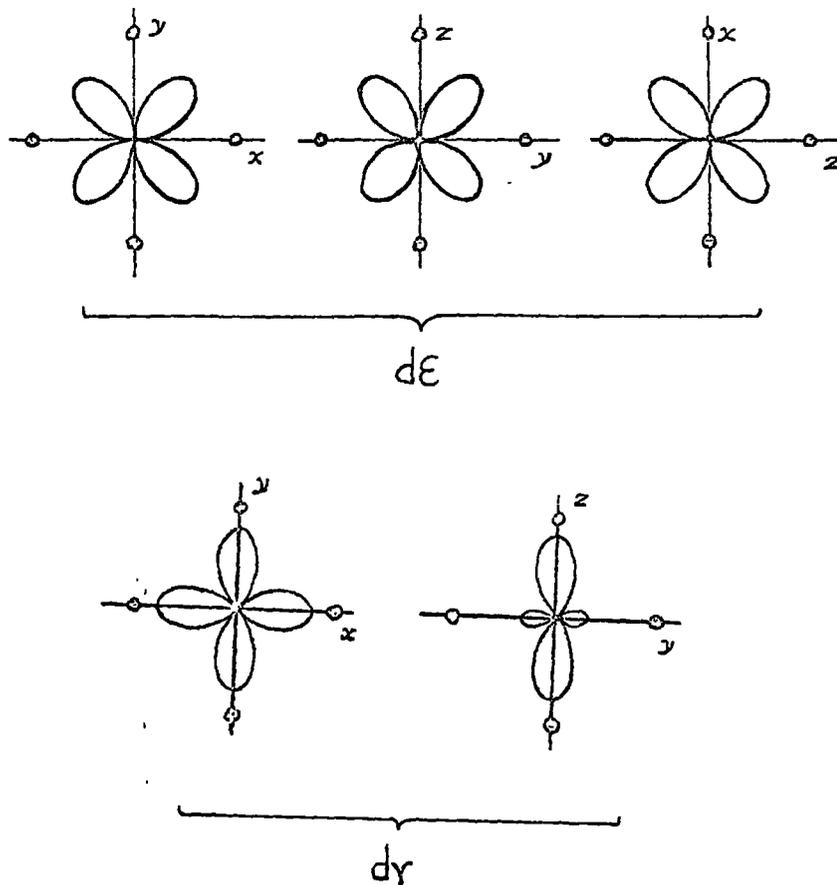
Fig.(4.2) Diagrams of d-electron orbitals situated in a site of octahedral symmetry in relation to six equivalent point charges , shown as large dots.
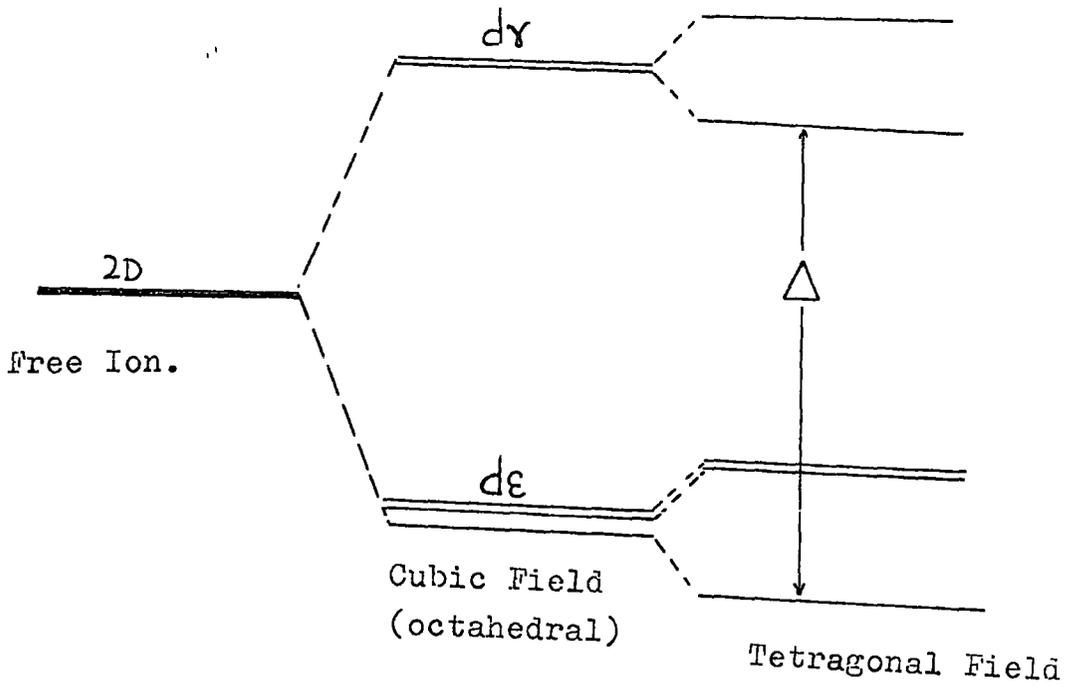
Fig.(4.3) Splitting of the 2D energy level by an octahedral ( cubic ) field (dγ is two-fold degenerate and dε is three-fold degenerate). In a tetragonal field there are three singlets and one level which is two-fold degenerate.

By extending the above argument it is easy to see what would happen if a tetragonal distortion, for example a small symmetrical displacement of the charges at $\pm a$ on the z-axis, were introduced in the octahedral environment. Two of the orbitals, xy and yz or $d\epsilon$ will be equally affected in their energy while the third, xy, experiences an interaction energy of a different magnitude (8). Similarly the two $d\gamma$ orbitals now have different interaction energies since the octahedral symmetry has been lowered. The result is that a tetragonal distortion leads to further splittings, resulting in three singlets and one doubly degenerate level, as shown in Figure (4.3).

So far no mention has been made of the spin which doubles the degeneracy of each orbital level. In particular for ESR one is interested in the degeneracy of the ground state, i.e. the lowest level in Figure (4.3). Spin-orbit coupling has now to be taken into account, and considered as a perturbation of this ground state. Applying first order perturbation theory, calculations show that the effect of spin-orbit coupling of the type $\lambda L.S$ is to mix some of the higher states into the ground state with the result that while in the absence of spin-orbit coupling the tetragonal field had quenched out the orbital angular momentum, spin-orbit coupling reinstates a small amount of angular momentum(9). This is of the order of $\lambda/\Delta$ where $\Delta$ is the crystal field splitting.

Essentially two different methods have been employed to calculate the splitting of energy levels by the crystal field. One method employs group theory and makes full use of the symmetry properties of the ligands. This method can be accurate but in order to obtain the magnitude of the splitting and the order of the levels specific knowledge of the crystal field and the ion under consideration is required. For a review of this method see (10,11,12).

The alternative method is to employ perturbation theory, which however, gives a more approximate and semi-quantitative result. With this technique the zero-field splitting and the additional splitting produced when a magnetic field is applied (as in ESR), can be handled very effectively via the Spin Hamiltonian.

Generally whatever method of calculation is employed, the first step is to derive an expression for the crystal field potential $V$ $(x,y,z)$ in the vicinity of the paramagnetic ion. This potential is usually assumed to obey Laplace's equation $\Delta^2 V = 0$, the solution of which may be expanded in spherical harmonics in the form

$$V = \sum_n \sum_m A_n^m \, r^n \, Y_n^m \, (\theta, \phi) \qquad \qquad ----(4)$$

Considerable simplification is introduced when account is taken of the symmetry of the crystal field and the type of electron orbitals involved. For instance, in the case of the crystal field of a regular octahedron with OZ as the polar axis and d-orbitals electrons, terms with $n > 4$ are discarded and the expansion can be written as

$$V = A_4^o \, r^4 \left[ Y_4^o \, (\theta, \phi) + \left( \frac{5}{14} \right)^{\frac{1}{2}} \left\{ Y_4^4 \, (\theta, \phi) + Y_4^{-4} \, (\theta, \phi) \right\} \right] \qquad ---(5)$$

When the octahedron is tetragonally distorted (as in the case considered earlier) the tetragonal field is represented as

$$V = A_2^o \, r^2 \, Y_2^o \, (\theta, \phi) + A_4^o \, r^4 \, Y_4^o \, (\theta, \phi) + A_4^4 \, r^4 \, Y_4^4 \, (\theta, \phi) + A_4^{-4} \, r^4 \, Y_4^{-4} \qquad ---(6)$$

this is basically the sum of a cubic (octahedral) field and an axial field.

Crystal field potentials represented in the above forms can now be used in the perturbation method to calculate the matrix elements of the energy of the electrons in the crystal field. These matrix

elements are in the form of

$$\int \psi' \ \Sigma \ -eV \ (x,y,z) \ \psi \, d \, \tau \qquad \qquad \text{---(7)}$$

where $\Sigma$ -eV (x,y,z) is the energy of the electrons in the crystal

field. The summation is taken over all the electrons involved. The

wave functions are in spherical co-ordinates and because of this there

are advantages in representing the crystal potential in harmonic

functions, i.e. it is now easier to calculate the matrix elements.

The crystal field potential may also be represented in Cartesian

co-ordinates, when the above equation becomes

$$V \ = \ C_4 \ (x^4 + y^4 + z^4 - 3/5 \ r^4) \qquad \qquad \text{---(8)}$$

The advantages of this form of representation is that the operator

equivalent of Stevens (13) can now be used to simplify the calculation

of the matrix elements. In this method one replaces the potential

function operators x, y and z by $J_x$, $J_y$ and $J_z$ respectively as these

are equivalent operators and have the same transformation properties.

However, in contrast to x, y and z the operators $J_x$, $J_y$ and $J_z$ do not

commute and this has to be taken into account when finding the equivalent

operators.


## 4.5   Hyperfine Structure

The nucleus of a paramagnetic ion may also have a spin and hence

a magnetic moment. The spinning electrons orbiting the nucleus would

then interact with this magnetic moment and as a result the spin energy

level may split by a small amount giving rise to hyperfine structure in

the ESR spectra.

In the simplest case, that of the hydrogen atom with a nuclear

spin of 1/2, the nuclear spin will align itself either parallel or

anti-parallel to the applied magnetic field and the electron spins.
As a result each of the electron spin levels of +1/2 and -1/2 will be
split two-fold.  Generally if the nuclear spin is I, then each spin
level would split into (2I+1) levels in the presence of a magnetic
field, this corresponds to (2I+1) different possible orientations of
the nucleus.  The allowed transitions between the nucleus levels are
given by the selection rule  $\Delta M_I = 0$.

## 4.6    Super-Hyperfine Structure

The unpaired electrons of a paramagnetic ion in a solid may
also interact with the nuclear spin of a neighbouring diamagnetic ion
if the diamagnetic ion has a nuclear magnetic moment.  The result of
this interaction is an additional splitting of the spin level giving
rise to super-hyperfine structure in the ESR spectrum.  The appearance
of SHF structure indicates that the paramagnetic electron cannot be
considered to spend the whole of its time on the paramagnetic ion, but
that its wave function embraces one or more of the surrounding diamag-
netic  ions.

## 4.7    Spin Hamiltonian

Apart from the effect of the crystal field on the orbital levels,
there are other perturbations which must also be considered.  To see
the relative significance of these it is necessary to consider the
general Hamiltonian of the ion which may be taken as being the sum of
all energy contributions.  Thus the general Hamiltonian H can be
written as

$$H = H_1 + H_2 + H_3 + H_4 + H_5 + H_6 \qquad ---(9)$$

$H_1$ represents the sum of the total kinetic energy of the electrons, the

Coulomb interaction between the electrons and nuclei of charge Ze,

and the repulsive energy between the electrons.  It is given by

$$H_1 = \sum_i (P_i^2/2_m - Ze^2/r_i) + \sum_{i>J-1} e^2/r_{iJ} \qquad ---(10)$$

where $P_i$ is the momentum of the ith electron, and $r_i$ is its distance

from the nucleus.  $r_{iJ}$ is the distance between electron i and electron

J.  The whole expression is summed over all electrons and gives the

unperturbed electronic energy levels.  This is obviously the most

dominant term in the general Hamiltonian though it plays no part in

the Spin Hamiltonian.

$H_2$ represents the magnetic interaction between the spin of the

electrons and their orbital angular momentum.

$$H_2 = \sum_{iJ} a_{iJ} \ell_i \cdot s_J + b_{iJ} \ell_i \cdot \ell_J + c_{iJ} s_J \cdot s_i \qquad ---(11)$$

In the case of Russell-Saunders spin-orbit coupling this term can be

written as $\lambda L.S$, where $\lambda$ is the spin-orbit coupling constant of the ion.

$H_3$ represents the interaction between the magnetic moment of the

nucleus and the magnetic field set up by the orbital and spin moments

of the electrons.  It can be written as

$$H_3 = 2\gamma\beta\beta_r \left[ \sum \left\{ \frac{(\ell_i - s_i) \cdot I}{r_i^3} + \frac{3(r_i \cdot s_i)(r_i \cdot I)}{r_i^5} \right\} + \frac{8\pi\delta}{3} \left( r_i \right)\left( s_i \cdot I \right) \right] \qquad ---(12)$$

The last term of this expression containing the $\delta$ function represents

the interaction of S-state electrons with the nuclear spin I.  It is

always zero unless there are S-state electrons present, in which case

the other two terms are zero.  $H_4$ represents the electrostatic inter-

action between the quadrupole moment Q of the nucleus and the electrons

and is given by

$$H_4 = \frac{e^2 Q}{2I(2I-1)} \left[ \sum \frac{I(I+1)}{r_i^3} - \frac{3(r_i \cdot I)^2}{r_i^5} \right] \qquad ---(13)$$

This interaction is usually very small.

$H_5$ represents the interaction of the free ion with an external magnetic field H and can be written as

$$H_5 = \sum_i \beta (\ell_i + 2s_i).H \qquad \qquad ---(14)$$

(there is also a direct interaction between the magnetic moment of the nucleus and the applied field. This is, however, very small and is neglected in ESR).

So far only those interactions have been considered which would be expected for a free ion in a magnetic field. The last term in the Hamiltonian is the crystal field interaction which allows for the effect of placing the free ion in a crystalline environment. This term can be written as

$$H_6 = \sum_i -eV (x,y,z) \qquad \qquad ---(15)$$

In treating the effect of the crystal field by the perturbation method, it is necessary to know how its magnitude of the interaction compares with other terms (spin-orbit coupling for instance) in the Hamiltonian. This is required in order to know at what point in the calculations the crystal field effect should be introduced as a perturbation. For this purpose three distinct cases can be considered.

(a)     Strong Fields  -  This situation prevails in substances in which there is a considerable amount of covalent bonding between the paramagnetic ion and the surrounding diamagnetic ions (e.g. iron group cyanides etc.). In such cases there is a considerable overlap of the electrons orbitals and as a result the basic assumption of the crystal field calculation is not valid. Crystal field theory then has to give way to more sophisticated molecular orbital theories.

(b)     Medium Fields - This situation applies for example to the iron
group of transition elements in which the unpaired electrons are exposed
to the crystal field.  In such cases the crystal field interaction is
stronger than the spin-orbit coupling, and can lead to a reduction or
even elimination of the orbital angular momentum.

(c)     Weak Fields - The weak field is appropriate to the ions of the
rare earths in which the unpaired 4f electrons are shielded by electrons
in the outer orbitals.  In these ions the crystal field interaction is
very much weaker than spin-orbit coupling.

Generally the total Hamiltonian $(q)$ is very complicated and
useful information cannot be derived from it easily and quickly.  More-
over, in most experimental cases one is not interested in all the energy
levels of the paramagnetic ion under consideration.  For instance, in
ESR interest is centred on the lowest energy level (or levels) in which
transitions take place.  Thus what is required is a method of treating
the levels between which transitions take place in isolation, bearing
in mind the fact that the higher lying levels may have some influence
on the lowest level.  This is done by using the spin Hamiltonian which is
a particular form of the general Hamiltonian of $(q)$ .  The main feature
of the spin Hamiltonian is the use of a fictitious effective spin operator
S' which may be defined as follows.  If a system in an external magnetic
field exhibits $(2S'+1)$ levels (apart from any hyperfine splitting), then
S' is defined as the effective spin of the system.  The $(2S'+1)$ energy
levels are then treated as if they originated from a fictitious state S'
for which the magnetic dipole has $(2S'+1)$ possible orientations.  The
interactions that the paramagnetic ion undergoes are then described in
terms consisting of the products of various components of S' raised to
appropriate powers and a number of coefficients.  For a full mathematical

discussion of the way in which this is achieved the reader is referred

to the following (14,15,16). Here, suffice it to say that the spin

Hamiltonian of a system must reflect the symmetry of the environment

of the paramagnetic ion and that it must give a complete description

of the observed ESR spectrum. For an example of an ion with $S'=5/2$ in

a cubic crystal field the spin Hamiltonian may be written as

$$H_S = g\beta H.S' + \frac{1}{6}a\left['S_x^4 + 'S_y^4 + 'S_z^4 - \frac{1}{5}S'('S+1)(3S'^2+3S'-1)\right] + AI.S' + \sum I.A_n.S' \quad ---(16)$$

where the first term describes the Zeeman interaction, the second term

the interaction of the paramagnetic ion with the cubic crystal field,

the third term the hyperfine interaction and the last term the super-

hyperfine interaction. The coefficients g, a, A and $A_n$ are the

quantities which are determined experimentally from the ESR spectrum.

## 4.8    Experimental Techniques

The electron spin resonance spectrometer used in the investigations

reported in this thesis, had been originally built in the department to

investigate the possibility of using ESR techniques to identify defects

and other centres in CdS. For a detailed discussion of the spectro-

meter the interested reader should consult (17). Generally a conven-

tional spin resonance spectrometer can be divided into five basic

parts;  a source of microwave power, a specimen holder, a detecting

system, a magnetic system and a recording system. The source of micro-

wave power used was a reflex Kylstron (type 2K25) with an output of

about 25 mW and a lifetime of approximately 600 hrs. The specimen

holder was a gold-plated rectangular (microwave) cavity into which the

microwave energy was directed. The cavity had a variable iris coupling

which could be set for 100%. The microwave power absorbed in the

cavity could be monitored on an oscilloscope (from the monitor point

in Figure (4.4) by modulating the Klystron with a frequency of 50 Hz.
The detection system consisted of a microwave bridge followed by a
microwave superhetᵉrodyne receiver (Ex. U.S.A.F.) with a balanced mixer
input.  The output was then either monitored on an oscilloscope or
amplified in a phase sensitive detector for recording.  The magnet used
was a Newport Instrument Ltd. type A water-cooled electromagnet with a
power supply type D104 (Newport Instruments Ltd.).  This stabilized
power supply allowed the magnetic field to be set accurately anywhere
within the range 0-6 kilogauss for measurement.  The magnetic field
was measured using a proton resonance magnetometer type P MK 2 (Newport
Instruments Ltd.) with its dial scale calibrated accurately in kilogauss.
The electromagnet was fitted with auxiliary  modulation coils so that
the field could be modulated.  By using a sinusoidally modulated magnetic
field (with the amplitude of modulation smaller than the spin resonance
absorption linewidth) it is possible to sweep across an absorption line
successively thus obtaining a display on an oscilloscope.  This permits
direct photographic recording of the spin resonance absorption.  Further-
more if the magnetic field is modulated the signal can be amplified
using a phase sensitive amplifier fed from the output of the super-
hetᵉrodyne receiver.  In this case the phase sensitive amplifier would
work by sampling the variation in the magnitude of the absorption as
the spin resonance line is magnetically scanned (by the modulation coils)
and by comparing the phase of the absorption with that of the field
modulation.  Finally the amplifier output was fed to a chart recorder
to produce a trace of the derivative of the absorption line.  Figure (4.5)
illustrates the absorption line, the output phase variation as the
magnetic field is modulated when the line peak is passed.  Also
illustrated in Figure (4.5)  is the resultant first derivative.
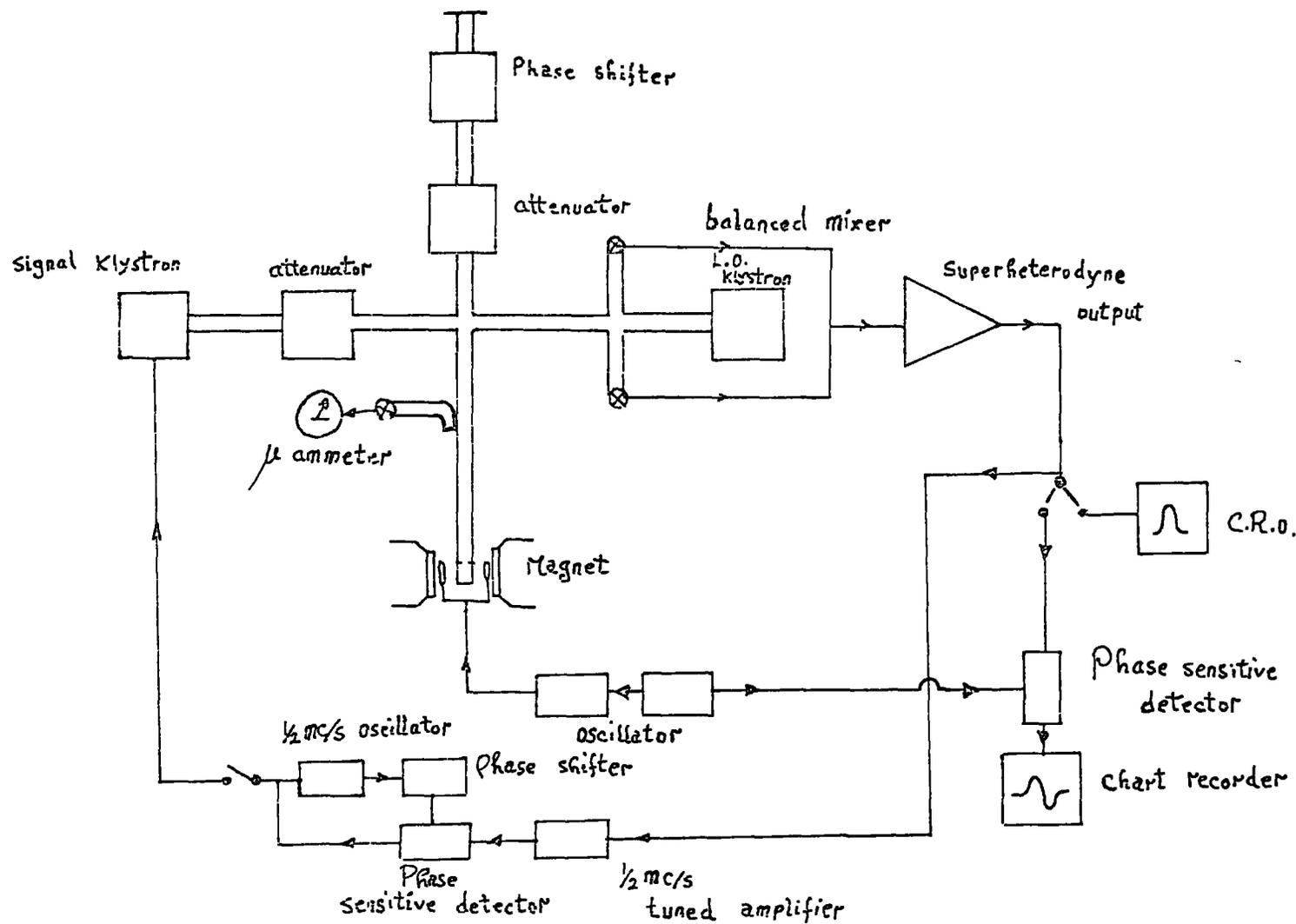
Fig.(4.4) Block diagram of the 3-cm microwave spectrometer.

Absorption

Output in
Phase

Output
antiphase

H

Magnetic
field

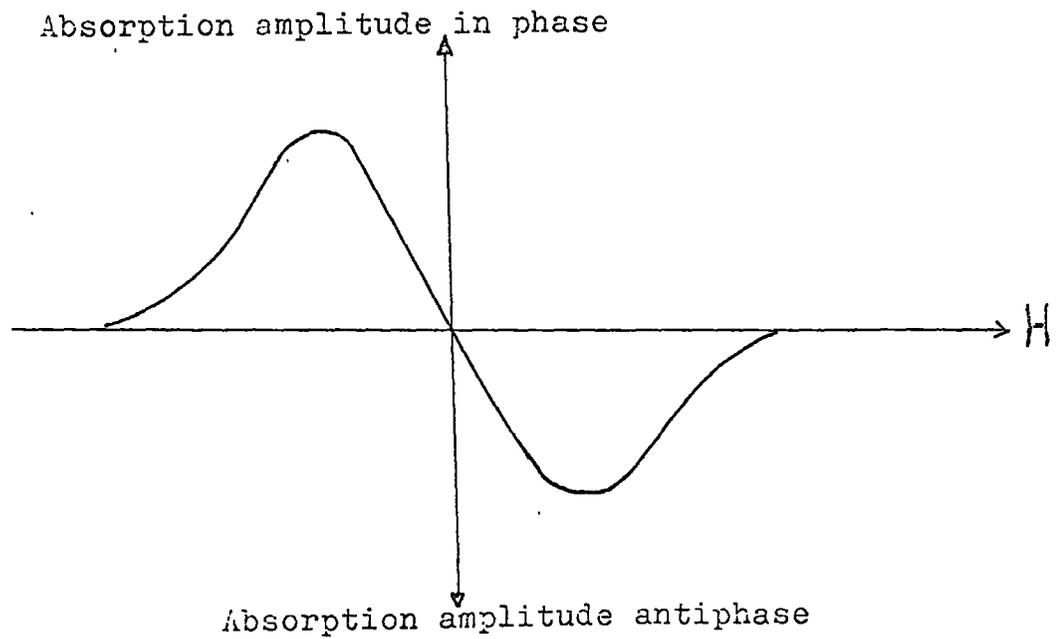Absorption amplitude in phase

H

Absorption amplitude antiphase
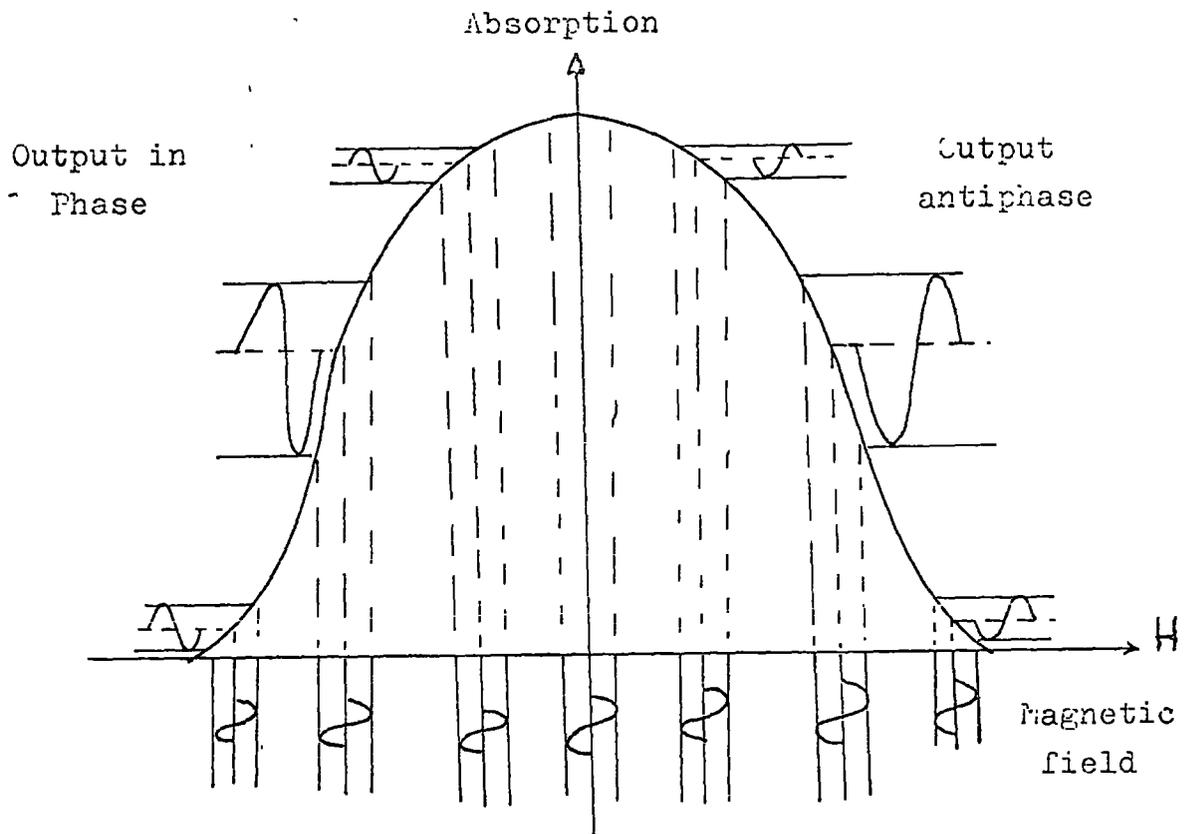
Fig.(4.5) The differentiated absorption line.

To conduct low temperature measurements a cryostat system consisting of two double concentric glass dewars was used. With liquid helium in the inner dewar and liquid nitrogen in the other, investigations could be carried out at temperatures down to 4.2 K. The temperature was measured using a copper-constantan thermocouple. To prevent liquid coolant from entering the cavity, a brass sealing can was used to surround and seal the cavity. This was screwed into the waveguide as shown in Figure (4.6).

Preliminaty ESR results indicated that the performance of the spectrometer left a great deal to be desired. Thus to improve the performance two new power supplies were made for the klystrons. It is important to note that monochromatic microwave power is required for spin resonance investigations and that with a klystron valve the reflector voltage determines the frequency of the output. Instabilities in the voltages applied to the reflector, resonator and the heater of the valve would broaden the spin resonance absorption line. In the two power supplies made the minimum specifications were as follows:

Reflector voltage       -85 to -200       stability 250:1

Resonator voltage       230 to  330       stability 200:1

Heater voltage          -6.3 v.  D.C.     stability  75:1

Apart from the klystron power supplies, the home-made phase sensitive detector built into the spectrometer was replaced with a Brookdeal Phase Sensitive Detector type PDB1. to achieve improved sensitivity and resolving power.

Since most of the centres (defects, impurities etc.) in the 2-6 compounds are affected by optical radiation, it is essential to have facilities which allow the spin resonance spectrum to be investi-gated while the sample is receiving optical radiation. In the original

QUARTZ ROD

←stainless steel waveguide

←Stainless steel tube

Microwave Cavity
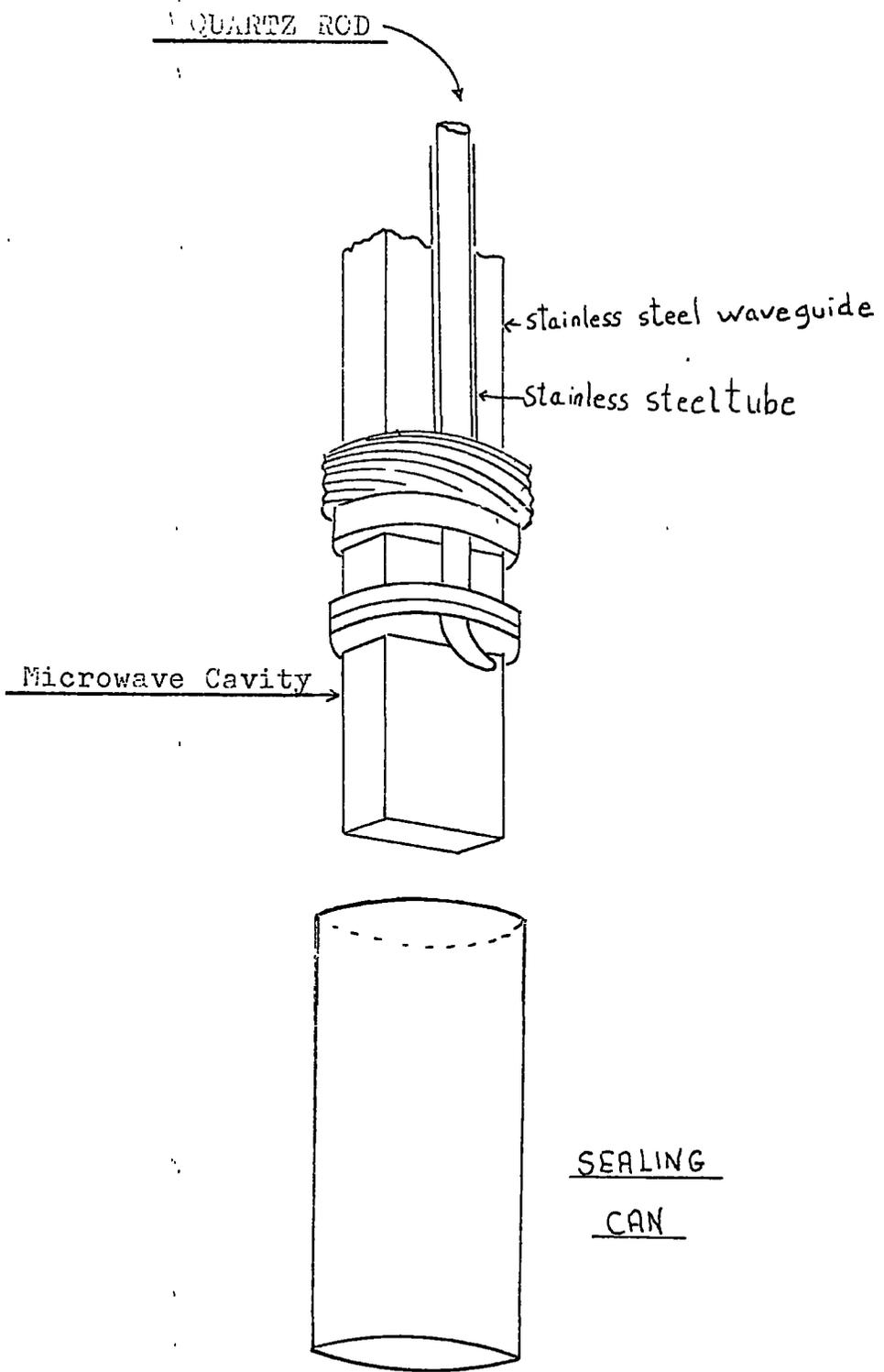
SEALING
CAN

Fig.(4.6).

spectrometer the existing facility for this purpose consisted of a
slit in the narrow face of the cavity (where the sample was mounted)
together with clearances in the glass sealing can and the two dewars
at regions corresponding to the slit in the cavity. This system was
found to be unsatisfactory. The slit in the narrow face of the cavity
lay at a region of maximum magnetic field and was found to reduce the
Q-value of the cavity resulting in loss of sensistivity. Also microwave
power escaping from the slit in the cavity was reflected back from
the pole-pieces after it had passed through the bubbling coolant. This
produced additional noise in the microwave signal. Furthermore, the
clearance between the outer dewars and the pole pieces was about 1 mm
on either side, so that optical radiation could be effectively
directed into the cavity only for certain orientations of the magnetic
field. To overcome these deficiencies, studies were carried out to
determine the best method of irradiating samples in the microwave
cavity. Commercially available flexible fibre-optic light guides
were considered, but none could be found to suit the geometry of the
microwave cavity-sealing-can without introducing adverse effects.
Figure (4.6) illustrates the best solution obtained; namely a length
of quartz rod (7 mm diameter) carrying optical radiation into the cavity.
The end was cut and polished at an angle to direct maximum optical
energy on to the sample. Experiments carried out to ascertain what
effect the small aperture in the broad side of the cavity had (where
the tapered quartz rod enters the cavity) indicated that the reduction
of the Q-value of the cavity was small. The top end of the quartz rod
was also polished to improve the efficiency of the system to allow the
maximum possible transmission of optical radiation.

With this arrangement it was possible, for instance, to study
the spin resonance of donors in ZnSe under U.V. excitation. However,
as is explained in section 5.10 no change could be detected in the
spin resonance of the $Mn^{2+}$ ion in ZnSe under U.V. excitation.

To study the photoluminescence of ZnSe, a Barr and Stroud
double-prism spectrometer equipped with an E.M.I. photomultiplier type
9684B was used. Figure (4.7) illustrates diagrammatically the arrange-
ment employed. U.V. radiation from a high pressure Hg lamp excited
luminescence in the sample mounted on the sample block of an all-metal
cryostat. Using liquid nitrogen in the cryostat the lowest sample
temperature recorded was 85 K. The emission from the sample was
chopped mechanically at a frequency consistent with the frequency
band of the plug-in filters used on the Barr and Stroud lock-in
amplifier type EL 7921 The output of the photomultiplier was amplified
and displayed on a Honeywell chart recorder type Electronic 15. The result
was then corrected for the spectral sensitivity of the photomultiplier
and the dispersion produced by the prism material in the spectrometer.

## 4.9    Electron Spin Resonance in the II-VI Compounds

Most of the technologically important properties of the II-VI
compounds are either associated with or are affected by native point
defects. These defects come about mainly as a result of deviation
from stoichiometry, since it is extremely difficult, if not impossible,
to control the partial pressures (of say Zn and Se) during the firing
process to produce a crystalline compound with exact stoichiometric
proportions. At the same time it is important to bear in mind that
thermodynamical considerations of the free energy of crystalline solids
indicate that at temperatures above absolute zero, all solids deviate

HIGH PRESSURE MERCURY LAMP

COPPER SULPHATE
SOLUTION

FILTER

ROTARY PUMP

CRYOSTAT

SAMPLE

CHOPPER

WAVELENGTH
DRIVE

CHART
RECORDER

BARR AND
STROUD
AMPLIFER

BRANDENBURG
H.T. SUPPLY

E.M.I.
PHOTOMULTIPLIER

-ve
H.T.
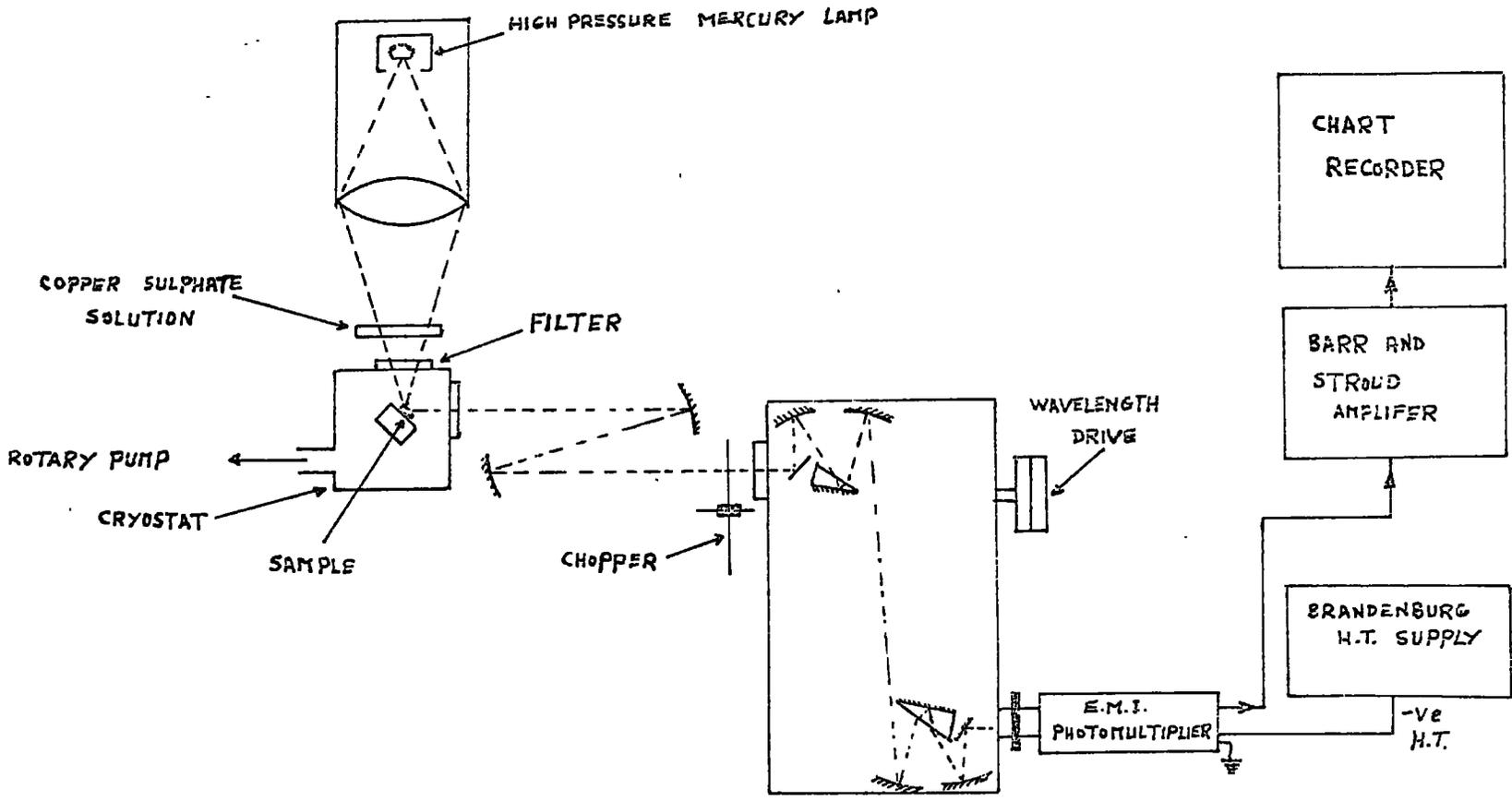
Fig.(4.7) Arrangement for measuring the photoluminescent
emission.

from the ideal crystalline solid and must contain defects. In general these defects may be in the form of vacancies and interstitials. In the II-VI compounds vacancies, cations and anions, act as acceptors and donors, and as a result the deviation from stoichiometry is to some extent exploited to control the electrical conductivity. As far as interstitials are concerned, very little is known about their electrical or optical properties in the II-VI compounds.

However, when native defects occur in a solid, certain chemical and electrical requirements must be satisfied. For instance the crystal as a whole must remain electrically neutral. Charge compensation in the presence of charged native defects can be satisfied in a number of ways. One way is that for each positively charged defect, there should also be a negatively charged one. Thus in an ionic compound (where an anion vacancy has an effective charge equal but opposite to that of the missing ion) in the presence of an anion vacancy, charge neutrality can be satisfied by having an equal number of cation vacancies or an equal number of anion interstitials (or some of both). A second way in which charge neutrality can be satisfied is by a process in which the valency state, i.e. the charge state, or one or more of the ions surrounding a charged defect can change. This method of charge compensation (i.e. controlled valency) is not, however, particularly common.

Another way in which charge compensation may occur is by free carrier compensation. In this process which occurs in semiconductors, charge neutrality is achieved by the introduction or removal of free carriers. Thus in ZnSe when an anion vacancy occurs, the vacancy can trap two electrons and become neutral. These electrons may be released by thermal excitation resulting in n-type conductivity. A similar process in the presence of cation vacancies may produce free holes. This method

of fulfilling charge neutrality with its potential to provide free carriers is very important in wide-band-gap semiconductors of the ZnSe-type, as it allows a range of conductivities to be achieved if sufficient control over the stoichiometry can be exercised.

The results mentioned in Section 3.1 indicate that ZnSe is about 65% ionic. Hence Schottky defects, i.e. cation and anion vacancies, occurring in equal numbers to provide charge compensation, can be regarded as the most probable defects. These vacancies would be on the whole randomly distributed in the solid, but there is a definite probability that some of the cation and anion vacancies will be close enough to attract each other, to form pairs of neutral double-vacancies or even larger vacancy clusters.

Another possibility is for an anion which has left its proper lattice site to take up interstitial position. This interstitial may be so far away from the vacancy that there is no coulomb interaction between them. On the other hand, they may be close enough to form an associated interstitial-vacancy pair. The occurrence of this type of defect (i.e. a Frankel defect) in a compound solid depends, apart from other factors, on the ionic radius of the potential interstitital and the lattice parameters.

Generally the concentration of defects in a crystalline solid is found to be very much higher than that predicted from thermodynamical considerations. The main reason for this is that the concentration of defects encountered in practice is not the thermal equilibrium concentration. Usually a crystal is produced at higher temperatures and cooled rather rapidly. This rapid cooling greatly reduces the mobility of the defects to migrate to the surface or grain boundary etc. As a result a high concentration of defects is frozen into the solid. Also

in a compound such as ZnSe it is important to bear in mind the effect of unavoidable (and the deliberately added) impurities. For again, through the requirements of charge compensation, impurities may produce native (point) defects. Some of these native defects may actually become associated with the impurities to form impurity-vacancy defect pairs (as in the self-activated centre for instance).

From the above very short discussion it may appear that since most defect centres in the II-VI compounds are charged, spin resonance techniques should be able to identify them very readily, but such a conclusion would be very premature and optimistic. In fact the contribution made by spin resonance techniques towards identifying native defects associated with electrical, photoconductive and optical phenomena in the II-VI compounds (with the exception of two associated centres) has not as yet been very great. The reason for this probably is that most charged native defects tend to be compensated with other native defects (e.g. vacancy-vacancy pairs or clusters) or impurities in such a way that they are not paramagnetic. Reviewing the spin resonance results reported up to 1967, Title ( 18 ) concluded that there was no definite evidence to suggest that isolated vacancies exist in the II-VI compounds. This conclusion still stands if one considers the reported results. There is, however, one exception. In a very brief note Watkin ( 19 ) reports that after irrradiating a ZnSe sample with 1.5 MeV electrons at 40 K he observed a spin resonance signal that he interpreted as being due to an isolated Zn vacancy. No information was given about the electrical or optical properties of the sample before or after the irradiation. Watkin's observation (and interpretation) has not, however, been confirmed.

Where spin resonance techniques have made a significant contribution has been in connection with vacancy-impurity associated centres.

Basically two types of vacancy-impurity complexes have been conclusively identified so far. One is an association of a cation vacancy and a donor impurity (the so called self-activated A-centre), and the other an anion vacancy associated with an acceptor impurity. To explain the self-activated luminescence in ZnS, various models have been proposed [20] which proved to be inconsistent with experimental results [21]. In 1956 Prener and Williams [22] suggested that the self-activated centre consisted of a doubly ionized Zn vacancy with which was associated an ionized donor impurity at a nearest neighbour site. Such a complex centre has a negative effective charge and is diamagnetic in the dark. This model was shown to be in agreement with luminescence results [23], which also showed that the wavelength of the self-activated emission peak depended on whether a halide or a trivalent metal impurity was used as co-activator. Although these results were in agreement with the proposed model, it could not however, be taken as proving the existence of class A-centre. This had to be done using ESR techniques.

The ESR of a class A-centre was first reported by Kasi et al [24] in 1961 in ZnS:NaCl polycrystals at 77 K under U.V. excitation. However in the absence of any hyperfine structure, the result could not be considered conclusive. In 1965 the ESR results obtained by Schneider et al [25] in Ga, Br and I-doped ZnS contained recognisable hyperfine structures which proved without doubt the existence of the class A-centre.

Generally there are two kinds of class A-centre, depending on whether a group VII impurity or a group VII metal impurity is used as co-activator. The difference between the two arises from the fact that the group VII impurity replaces an S ion adjacent to the Zn vacancy whereas the group III impurity replaces a Zn ion in the second nearest neighbour shell of the Zn vacancy. The group VII donor impurity is

therefore very much closer to the vacancy than a group III donor impurity.

The ESR results show that under optical excitation the centre becomes paramagnetic by capturing a free hole. This hole is subjected to an electric field arising from the Zn vacancy and the associated donor impurity. In Cl-doped ZnS at 1.3 K the captured hole is fixed at an S ion furthest from the donor impurity. At 77 K the hole, however, hops rapidly amongst the three equivalent S ions adjacent to the vacancy. The hopping motion becomes negligible at temperatures below 60 K. No hopping motion occurs in Al or Ga-doped ZnS at 77 K. In this case it is believed that the thermal energy of the captured hole is not sufficient to surmount the repulsive electric field due to ionized Ga or Al. Again the hole is localized at an S ion furthest from the impurity donor. This implies that the group III metal donors have a larger effective charge than the group VII impurity donors.

The other type of vacancy-impurity complex which has been identified by ESR is a centre consisting of an anion vacancy in association with an acceptor impurity in a nearest neighbour site. This complex centre was proposed by Shinoya (16) to be responsible for the orange-red luminescence in ZnS doped with Cu. According to this model the vacancy is doubly ionized and the associated acceptor has captured an electron and has therefore a filled shell. The vacancy-impurity complex has as a result a positive effective charge in the dark and is non-paramagnetic. ESR results show that under U.V. excitation at 77 K the complex centre captures an electron and becomes paramagnetic. Thus the ESR spectrum is characteristic of a trapped electron interacting with the nucleus of the acceptor and also with the $Zn^{67}$ nucleus. These interactions provide the super-hyperfine structure in the spectrum (27) which enable the centre to be identified unambiguously.

A similar centre has also been found in ZnS:Ag and ZnS:Au (28 ). In ZnSe the centre has been detected in samples doped with P, As and Sb (29 ).

Up to date the conclusive identification of the above two classes of vacancy-impurity centres has been the only universally accepted significant contribution of spin resonance techniques to the identification of the native defects in the II-VI compounds. Spin resonance investigations of (deliberately added) impurities have however been more successful.

Copper is the most widely used acceptor and activator in the II-VI compounds. Although such phenomena as luminescence, photoconductivity, absorption and quenching of luminescence and photoconductivity which are associated with copper, have been investigated extensively, as yet there is no clear understanding of the nature of the copper centre or centres. In the most extensive spin resonance study of copper impurity in ZnS Holten et al ( 30 ) found ten distinct ESR spectra indicating ten unrelated copper centres in ZnS crystals. Seven of these centres were found to be photo-sensitive and in some crystals usually more than one of them could be detected.

All the resonance spectra contained a considerable hyperfine structure arising from the magnetic moments of the various copper isotopes and this helped to identify the ESR lines associated with copper centres in the complex ESR spectra. Some of the observed centres were found to have such small relaxation times that they could only be detected at 1.3 K. At 4.2 K the ESR lines had broadened so much that they could no longer be observed.

Holton et al found that none of the ten spectra could be attributed to isolated substitutional $Cu^{2+}$. Such a centre is frequently

invoked to explain, for instance, the so called copper-red infra-red

spectrum of ZnS (31,32). As yet, however, there is no ESR evidence of

its existence in ZnS, although such evidence has been found in ZnO (15).

Holten et al found that the data could not be explained in terms of

Cu ($3d^9$) in a tetrahedral or octahedral crystal field with any degree

of certainty. Nor could any of the centres found be correlated with

the observed physical properties of the crystals (the luminescence for

instance).

An impurity which has an electronic configuration similar to

that of Cu ($3d^9$) is $Ni^+$. ESR investigations carried out by Watts (33)

indicate that nickel exists in ZnSe in three difference valence states

($Ni^+$, $Ni^{2+}$, $Ni^{3+}$) all of which are stable in 1.3 K.

Impurities can also associate together to form complex centres.

Electron spin resonance of associated impurities in a II-VI compound was

first reported by Morigaki et al (34) in CdSe:Fe:Cu. The ESR spectrum

showed that Fe occupied a Cd site while an ion with an effective negative

charge, i.e. a $Cu^{+1}$ ion occupying a Cd site was associated with it.

Since then Fe-Cu associated pairs have been reported in ZnS, ZnSe, ZnO,

ZnTe, CdTe and CdS (30,35). In addition an Fe-Li associate has been

reported in CdS (36) and Fe-Ag associate in ZnS (35) and an Fe-As

associate in ZnSe (37).

Electron spin resonance data indicate that all the impurities

in Fe-Cu, Fe-Li and Fe-Ag associates take up substitutional cation sites

with Cu, Li and Ag at the nearest possible sites to Fe in each associate.

In this way there is a local charge compensation between Fe and the

associated impurity. It must be pointed out that, for instance, a $Cu^{+1}$

ion taking up a Zn site has a negative effective charge.

In the case of the Fe-As associate in ZnSe, arsenic takes up a

Se site which is the nearest neighbour site to $Fe^{3+}$. The most likely

charge state of the arsenic seems to be triply negative, since in this state it is diamagnetic (as indicated by ESR data) and provides charge compensation for $Fe^{3+}$.

Since iron appears to be a common contaminant in the II-VI compounds and is a well known killer of luminescence, Kemp (35) investigated its relationship with copper which is an activator in CdS. Kemp's electron spin resonance data show that Fe and Cu are bound together very strongly in an associated form. Kemp suggests that this strong bonding increases the ionization energy of Cu to such an extent that it does not function as a luminescent centre.

So far Fe is the only one of the well known killer impurities for which ESR in the presence of an activator has been investigated in several of the II-VI compounds. It would be extremely rewarding to carry out similar ESR investigations of the other killer impurities in an attempt to see if a strong association of impurities is generally responsible for the killing of luminescence, and if so whether it also applies when the luminescence is due to an internal transition as in the case of Mn.

Electron spin resonance has also been used to elucidate the basic role of some impurities in the II-VI compounds. Originally it was believed that Si, Ge and Sn in ZnS and ZnSe formed double donors (38). Subsequent ESR investigations showed that the group IV impurities act as hole traps. Suto et al (39) studied ESR of Ge and Pb in ZnSe crystals and from the hyperfine and the super-hyperfine structures of the resonance spectra showed that $Ge^{2+}$ and $Pb^{2+}$ form hole traps. The variation of the photo-sensitive ESR signal with optical excitation shows that the energy level of the hole trap in the band gap is a deep one.

Apart from the investigations outlined above, spin resonance has also been used to monitor structural phase changes. Thus Van Wieringen (40) used the spin resonance of the $Mn^{2+}$ ion in ZnS to observe changes in the structure as the sample was subjected to high pressures. The spin resonance of the $Mn^{2+}$ ion in ZnS was also used by Aven et al (41) to investigate the effect of such impurities as Cu, Ag and Al on cubic $\longrightarrow$ hexagonal and hexagonal $\longrightarrow$ cubic phase transitions in ZnS (see Section 5.17). While Schneider et al (42) in their spin resonance investigations showed that the $Mn^{2+}$ ion can be used as a sensitive probe to study the stacking faults and cubic-hexagonal admixture in ZnS. For an outline of the donor spin resonance in II-VI compounds, the reader should consult Section 6.2.

CHAPTER   5

ELECTRON SPIN RESONANCE OF Mn in ZnSe,

PHASE TRANSITION IN ZnSe:Mn

## 5.1   The $Mn^{2+}$ ion

Mn with an electronic configuration of $1s^2....3d^5 \ 4s^2$ is a member of the iron series of the transition elements.  It has been the subject of scientific interest for many years for two main reasons.  One is that many compounds containing Mn as an activator luminesce   in the visible part of the spectrum (see Chapter 7); the other is connected with the paramagnetic properties of the $Mn^{2+}$ ion which has a half-filled 3d electron shell.  In accordance with Hund's rules the five electrons of this shell all have spins which are aligned in the same direction resulting in a ground state which is an orbital singlet but six-fold spin degenerate.  Basically an ion with such a ground state $\left( ^6S_{5/2} \right)$ will produce a single ESR absorption line with a g-value corresponding to that of the free electron of 2.0023.  In practice, however, the spectrum of the $Mn^{2+}$ ion in different substances consists of many fine, hyperfine and in some cases super-hyperfine, structure lines with g-values which are different from 2.0023.

As the ground state of $Mn^{2+}$ is an S-state, it cannot be split by a crystal field alone, because it possesses no orbital degeneracy. Nor can spin-orbit coupling by itself remove the six-fold spin degeneracy.  It follows that Bethe's symmetry arguments involved in crystal field theory cannot be applied to explain the observed zero-field splitting.

To explain the zero-field splitting Van Vleck and Penny (1) assumed that the effect of crystal field and spin-orbit interaction

can be treated by perturbation theory. Their calculations confirmed

that neither perturbation acting alone can produce any splitting of

the S-state ground level but both acting together can. It was also

found that the perturbation had to be carried to a high order before

any splitting was indicated. Van Vleck and Penny's idea was that

spin-orbit coupling mixes the 4P excited state into the 6S ground

state to a small extent leading to a splitting of the ground level •

Abragam and Pryce (2), and Pryce (3) showed however, that the processes

suggested by Van Vleck and Penny were inadequate to explain the

splittings observed. They therefore considered an additional spin-

spin interaction and argued that this mechanism could be the dominant

one. Physically their idea was that in the crystal field there will

be some distortion of the orbits even though the ion is in an S-state.

Suppose, therefore that instead of the charge cloud being a perfect

sphere it is slightly ellipsoidal. Then the dipole-dipole energy of

the spins varies with their orientation with respect to the axes of

the ellipsoid and thus the energy eigenvalues depend on the spin

orientation. From their arguments they showed that this type of

mechanism is a second order effect whereas the type of mechanism

envisaged by Van Vleck and Penny is of fourth order. The zero-field

splitting on the basis of the spin-spin interaction has been calculated

by Watanabe (4) who also considered some other possible mechanisms

involving admixtures of the higher states with the ground level. His

calculated values for the splitting were, however, smaller than those

obtained experimentally (5,6). Powell et al (7) and Gabriel et al (8)

performed more elaborate calculations and found that omitting the spin-

doublet state of the $3d^5$ configuration as Watanabe had done, resulted

in a very much smaller calculated splitting value. They pointed out

that the contribution of this state to the ground level via spin-orbit

coupling was of major importance. However, in order to obtain a correct value for the ground state splitting of the $Mn^{2+}$ ion in the cubic crystal field of MgO using their model, they had to choose relatively large values for the crystal field parameter and the spin-orbit coupling constant.

Up to this stage all the calculations had been based on a common model which considered the magnetic ion to be separate (i.e. unattached) from the host lattice in accordance with the basic assumption of crystal field theory. In 1960 however, Kondo (9) in order to explain the discrepancy between the measured and the calculated splitting considered covalent contributions which may result from overlap effects between the $Mn^{2+}$ ion and the surrounding ions. He computed the covalent contributions to the axial field splitting of $Mn^{2+}$ in strained MgO and fitted his calculations to the experimental results in a phenomenological manner. In view of the adjustable parameters involved in Kondo's calculations it is rather difficult to determine the extent of the covalent contribution to the zero-field splitting. It must, however, be borne in mind that in most substances (e.g. II-VI compounds) there is definitely some covalent contribution to the chemical binding and therefore that the basic idea of the crystal field theory which considers the magnetic ion to be completely separate from the host lattice is strictly speaking somewhat unrealistic.

Apart from Kondo's work, there have in recent years been a number of theoretical papers on the zero-field splitting of the S-state ion (10,11,12). But, as yet, in spite of the elaborate models and mathematical techniques which are being employed, there exists no exact explanation of the mechanisms involved in producing zero-field splitting in S-state ions.

The available data, however, indicate that in a crystal field

of cubic symmetry the six-fold spin degenerate ground state of the

$Mn^{2+}$ ion splits into a quartet $\Gamma_8$ and a doublet $\Gamma_7$ (7,13). Whereas

the doublet lies energetically lowest in the crystal field of octa-

hedral symmetry, it is the quartet $\Gamma_8$ which is the lowest in the

tetrahedral symmetry. When the crystal field has a trigonal component

(as in hexagonal ZnSe for instance) the quartet $\Gamma_8$ splits further into

two Kramers doublets.

Generally the ESR results show that there exists a relatively

large variation in the ground state splitting of the $Mn^{2+}$ ion in

different substances. Furthermore, this variation appears to be

dependent to some extent on the ionicity of the host lattice. Usually

the splitting is found to increase as the ionicity of the host lattice

increases. The variation, in contrast with that of hyperfine splitting

is not, however, a linear one.

Another point of interest in the $Mn^{2+}$ ion concerns its hyperfine

splitting. Since the magnetic field at the centre of the S-state charge

distribution is zero, no magnetic interaction leading to hyperfine

splitting should occur. In practice, however, extensive hyperfine

structure is observed in the ESR spectrum. To explain this Abragam (14)

suggested that configurational interaction in which a 3s electron is

raised to a 4s level without changing the spin was responsible (i.e.

configurational interaction of the form $3s\ 3d^5\ 4s$ with $3s^2\ 3d^5$). Cal-

culations, however, showed that this mechanism was inadequate to account

for the relatively large hyperfine splitting observed. Instead Wood

and Prat (15), and Heine (16) proposed that a large splitting may

occur as a result of interactions between the 3d, and $3s^2$, $2s^2$ and $1s^2$

electrons. This can be seen from the fact that the orbital wave

functions of the s-electrons are different depending on whether the

s-electrons have spins parallel or anti-parallel to the d-electrons. In the parallel case there is an exchange interaction which is absent in the anti-parallel case. The result is that the s-electrons are not exactly paired but "polarized." This polarization of the core electrons produces a magnetic field at the nucleus. In a series of papers Freeman and Watson in 1961 and 1965 (17) and in 1967 (18) have adequately demonstrated the validity of this mechanism and have obtained good agreement between the calculated and measured hyperfine splitting in ionic compounds. The agreement is less good in compounds with some degree of covalency because the theoretical calculations use a model involving free S-state ions. This is to some extent a reasonable approximation in ionic compounds where there is no overlap of the orbitals (i.e. the paramagnetic electrons are localized close to their nuclei), but not in covalent or semi-covalent compounds where there is overlapping of the orbitals with the paramagnetic electrons located somewhat further from the nuclei.

Even though the mechanism responsible for hyperfine interaction did not become clear until the work of Freeman and Watson in 1961 and later, experimentally the existence of a relationship between hyperfin- splitting and covalency had been evaluated much earlier. In 1955 Van Wieringen (19) was able to show from the ESR of a number of $Mn^{2+}$- doped compounds that there existed a regular relationship between hyper- fine splitting and covalency. It was found that the more ionic a compound, the larger was the hyperfine splitting coefficient, A, of the spin Hamiltonian. This work was extended by Matamura (20) who plotted the hyperfine splitting coefficient A against the ionicity of the bond in a number of compounds and obtained a straight line thus indicating a linear relationship.

## 5.2    Structure of ZnSe

ZnSe, like ZnS, may crystallize with two different structures; zincblende and wurtzite. The zincblende modification can be regarded as composed of two interpenetrating close-packed cubic sub-lattices of Zn and Se ions, displaced with respect to each other by 1/4 of the body diagonal. Similarly, the wurtzite modification can be regarded as composed of two hexagonal sub-lattices of Zn and Se ions displaced from each other by a distance of 3/8C along the C-axis. In both structures there is a tetrahedral arrangement of Zn and Se ions, i.e. each Zn ion is surrounded tetrahedrally by four Se ions and similarly each Se ion is surrounded by four Zn ions. The separation of the nearest Zn-Se ions in the ideal zincblende structure is $3/4 \, a_{cubic}$, and that in the wurtzite structure is $3/8 \, a_{hex.}$, where $a_{cubic}$, $a_{hex}$ and C are the lattice parameters. In the ideal zincblende and wurtzite structures the parameters are related as follows:-

$$a_{hex.} \quad = \quad 1/2 \, \sqrt{2} \;\; a_{cubic}$$

$$C \quad = \quad 2/3 \, \sqrt{3} \;\; a_{cubic}$$

From the point of view of a Zn (or Se) ion, the geometrical arrangement of the nearest neighbouring shell of ions is the same in both structures. This similarity also extends to the second shell of nearest ions. However, significant geometrical differences appear in the third more remote shells of surrounding ions.

In most of the II-VI compounds, the actual wurtzite structure deviates slightly from the ideal structure. This deviation is usually reflected in the value of the ratio C/a which is 1.6330 in an ideally perfect wurtzite structure. For instance, if the values of C and a reported by Chan and Park (21) are used, then for ZnSe C/a = 1.6308.

The consequence of this deviation from an ideally perfect structure is that each Zn (or Se) ion can no longer be considered to lie at the centre of a tetrahedron, and that the bond lengths and the bond angles are slightly different from what they would have been in an ideal structure. Although this distortion may be geometrically very small, its effect on the crystal field, for instance, could be significant. For a discussion of the way in which this distortion may affect the trapping levels in ZnS, the reader is referred to (22). The distortion of the wurtzite structure in the II-VI compounds has been discussed by Keffer and Portis (23) who suggest that the reason for the distortion lies in the partially ionic nature of bonding in these compounds. By assuming an effective charge of ± fe per ion, Keffer and Portis have shown that as a result of the long range polar interactions the parameter C/a could take values different from 1.63330. According to this possible explanation the II-VI compound with constituent ions that shows the greatest electronegativity difference, would be expected to have the wurtzite structure exhibiting the greatest distortion.

Looking along the Zn-Se bonds in cubic ZnSe, there are three different double layers that repeat themselves in the sequence:

$$ABCABCABC \longrightarrow [111]$$

In the wurtzite structure there are, however, only two layers, A and B, which repeat themselves as

$$ABABAB \longrightarrow \text{C-axis} .$$

A frequency one-dimensional disorder in most of the II-VI compounds is due to stacking faults which destroy the periodicity of the stacking layers along a [111] growth direction. An example of such a stacking disorder is

$$\begin{array}{c} \overset{II}{\overbrace{\phantom{xxxx}}} \\ ABCABCABCBACBACBA \\ \underset{I}{\underbrace{\phantom{xxxx}}} \end{array}$$
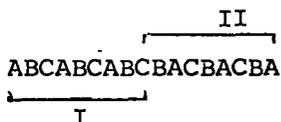
i.e., as the result of the stacking fault, the cubic section II has a stacking sequence which is the reverse of that in cubic section I, so that the two sections together form a twin with the interposing stacking layers, BCB, having a hexagonal packing. The hexagonal section, however, need not necessarily stop after three layers. For example, in a similar sample the hexagonal packing could continue for many layers to form a very much thicker hexagonal section.

### 5.3    ZnSe Crystal Field and the $Mn^{2+}$ ion

In cubic ZnSe each Zn ion is surrounded by four equidistant Se ions at the vertices of a tetrahedron with a Zn-Se separation that can be denoted by d. If the Zn ion is replaced by a paramagnetic ion (say Mn), the four Se ions, each with an effective charge of q, produce a potential, V, at the site of the paramagnetic ion which can be written as

$$V = \frac{4q}{d} - \frac{35q}{9d^2} \left( x^4 + y^4 + z^4 - 3/5 \, \rho^4 \right) + \frac{20q}{\sqrt{3} \, d^4} \, x \, y \, z + \dots \qquad -(17)$$

where $\rho^2 = x^2 + y^2 + z^2$ in a rectangular co-ordinate system x, y, and z. In the next shell, there are twelve Zn ions surrounding the paramagnetic ion. These are at a distance of $b = 2 \sqrt{2/3} \, d$, and produce a potential V, where

$$V' = \frac{12q}{b} + \frac{35}{8b^5} \left( x^4 + y^4 + z^4 - 3/5 \, \rho^4 \right) + \dots \qquad ---(18)$$

This contribution from the second nearest neighbours, is only about 9% of that from the first nearest neighbour ions. It follows that the contribution of the third nearest neighbour ions is a fraction of V', and that considering the complexity of the calculations, the effects of the third nearest neighbours, and beyond, can be neglected as a first approximation. The potential V + V' can then be expanded in terms of

spherical functions $Y_n^m$ , to be used, as was explained in Section 4.4

in the perturbation calculations to find the matrix elements of the

energy of the paramagnetic electrons in the crystal field. However,

in the case of the $Mn^{2+}$ ion (an S-state ion), as was pointed out in

Section 5.1, no perturbation calculation has ever given satisfactory

results. It appears that the processes responsible for its zero-field

splitting are more complex than hitherto realised.

In wurtzite ZnSe (assuming a perfect structure) the potentials

V and V' still occur. But, superimposed on the fields of the first

and second nearest neighbour ions is a long range axial field (along

the c-axis), the origin of which can be understood as follows. Because

of the positively and negatively charged ions in ZnSe, the Zn and Se

ions form a network of permanent dipoles which cancel each other out

in the zincblende configuration. In the wurtzite structure, however,

the dipoles produce a resultant electric field along the c-axis. The

calculation of this axial field is usually very difficult as it involves

a summation over all the ions of the wurtzite lattice.

## 5.4 Spin Hamiltonian for the $Mn^{2+}$ ion in Hexagonal ZnSe

The Spin Hamiltonian which best describes the fine structure

spectrum of the $Mn^{2+}$ ion in hexagonal ZnSe can be written as

$$H = g\beta \underline{H} \cdot \underline{S} + \frac{a}{6} \left( S_\xi^4 + S_\eta^4 + S_\zeta^4 - \frac{707}{16} \right)$$

$$+ D \left( S_z^2 - \frac{35}{12} \right)$$

$$+ \left( \frac{7F}{36} \right) \left( S_z^4 - \frac{95}{14} S_z^2 + \frac{81}{16} \right) \quad .. \quad .. \quad .. \quad .. \quad .. \quad (19)$$

where $g\beta \underline{H} \cdot \underline{S}$ represents the Zeeman interaction of the five unpaired 3d

electrons in the magnetic field H, the terms containing the coefficient

a/6 represent the interaction of the paramagnetic electrons with the cubic component of the crystal field in the co-ordinate systems $\xi$, $\eta$, $\zeta$, and the terms with coefficients D and 7F/36 represent the interaction of the paramagnetic electrons with the axial (hexagonal) component of the crystal field. In the case of Mn in cubic ZnSe, $D = F = 0$ so that the interaction with the cubic crystal field is represented by the terms containing the coefficient $\frac{a}{6}$ only.

For hexagonal ZnSe the above Spin Hamiltonian has an exact solution only for the orientation $H||C$. For all other orientations only approximate solutions can be obtained (24). For the orientation $H||C$ the fine structure energy levels are (25)

$$W_{\pm\,5/2} = \pm\, g\beta H + \frac{D}{3} - \frac{(a-F)}{2} \pm \sqrt{\left[3D + \frac{(a-F)}{6} - (3/2)\,g\beta H\right]^2 + \frac{20}{9}\,a^2}$$

$$W_{\pm\,3/2} = \pm\, 3/2\; g\beta H - \frac{2D}{3} + (a-F)$$

$$W_{\pm\,1/2} = \mp\, g\beta H + \frac{D}{3} - \frac{(a-F)}{3} \pm \sqrt{\left[3D + \frac{(a-F)}{6} \mp (3/2)\,g\beta H\right]^2 + \frac{20}{9}\,a^2}$$

Where the indices of the energy levels refer to the electronic magnetic quantum number M. Generally the coefficient a of the cubic component of the crystal field is very small compared with the Zeeman term and the coefficient D, so that as a first approximation the term 20/9 $a^2$ may be neglected. With this approximation, and bearing in mind the resonance condition $\Delta M = \pm 1$, the field position of the fine-structure lines of the $Mn^{2+}$ ion in hexagonal ZnSe are:

$$H_{+\,5/2} = H_o - 4D' + (4/3)\,(a'-F')$$

$$H_{+\,3/2} = H_o - 2D' - (5/3)\,(a'-F')$$

$$H_{+\,1/2} = H_o$$

$$H_{-\,1/2} = H_o + 2D' + (5/3)\,(a'-F')$$

$$H_{-\,3/2} = H_o + 4D' - (4/3)\,(a'-F')$$

where $H_o$ is defined from $h\nu = H_o$ , and $D' = \dfrac{D}{g\beta}$

$$(a'-F') \quad = \quad \dfrac{(a-F)}{g\beta}$$

from these equations, and the experimental spectrum obtained, the parameters g, D and (a-F) can be determined. It must, however, be noted that F and the cubic crystal field parameter, a, cannot be determined separately for the orientations H||C or H⊥C. A value for (a) in a wurtzite crystal may be obtained, if it is borne in mind that the wurtzite structure contains two inequivalent lattice sites for the group II element that Mn replaces. These two sites are displaced with respect to each other by a $60^o$ - rotation about the C-axis. It follows from the analysis of Schneider et al. (26) that when a wurtzite crystal has an orientation different from H||C and H⊥C, the cubic component of the crystal field has different orientations (with respect to the applied magnetic field) at the two sites, and as a result the fine structure lines may split up into doublets. The magnitude of the splitting is directly related to a. In practice, however, the splitting may not be observed with low-sensitivity ESR spectrometers and in ESR spectra which are broad and complex with overlapping. It must be noted that the splitting of the fine structure disappears for orientations H||C and H⊥C, as the two sites are not distinguishable in these orientations.

## 5.5 The Hyperfine Structure Term

The nucleus of the $Mn^{55}$ atom has a nuclear spin of I = 5/2. The five unpaired 3d electrons (of the $Mn^{2+}$ ion) interact with the nucleus and as a result their spin energy levels split further from six to (2S+1)(2I+1) = 36 levels. This interaction can be represented in the Spin Hamiltonian by the term A $\underline{I}.\underline{S}$ (where A is the hyperfine

interaction coefficient), so that the Spin Hamiltonian of the system
becomes

$$H = g\beta\underline{H}.\underline{S} + \frac{a}{6}\left(S_\xi^4 + S_\eta^4 + S_\zeta^4 - \frac{707}{16}\right) + D\left(S_z^2 - \frac{35}{12}\right)$$

$$+ \left(\frac{7F}{36}\right)\left(S_z^4 - \frac{95}{14}S_z^2 + \frac{81}{16}\right) + A\,\underline{I}.\underline{S} \qquad ----(20)$$

The solution of the above Hamiltonian for the orientation $H||C$ as
worked out by Schneider and Sircas (25) up to the terms of third order,
is of the form

$$h\nu = g\beta H_o = g\beta H + (2M-1) + K(a-F) + Am$$

$$+ \left[A^2/(2g\beta H)\right]\left[I(I+1) - m^2 + m(2M-1)\right]$$

$$+ \left[A^3/(2g^2\beta^2H^2)\right]\left[(2I(I+1)-3m^2)(2M-1)-m(S(S+1)+I(I+1)-3M^2+3M-m^2-2)\right]$$

$$- \left[A^2D/(2g^2\beta^2H^2)\right]\left[(3I(I+1)-3m^2)(2M-1)-m(2S(S+1)-6M^2+6M-3)\right] \qquad ----(21)$$

where

$$K = -4/3 \qquad \text{for} \quad M = +5/2$$

$$K = +5/3 \qquad \text{for} \quad M = +3/2$$

$$K = 0 \qquad \text{for} \quad M = +1/2$$

$$K = -5/3 \qquad \text{for} \quad M = -1/2$$

$$K = +4/3 \qquad \text{for} \quad M = -3/2$$

In obtaining the above solution, A is assumed to be isotropic. This
assumption strictly speaking is not valid. However, in the II-VI com-
pounds the anisotropy of A is sufficiently small to be neglected in
obtaining complex mathematical solutions. The expression (21)
is an equation of third degree in H and as such cannot be solved to
find the magnetic field position of the various transitions. An
approximate solution can, however, be obtained if the terms of the
2nd and the 3rd order in A, which are very small compared with the
remaining terms, are neglected. Thus, in the first approximation the

field positions of the ESR transition lines are

$$H_{M,m} = H_o - (2M-1)D' - K(a'-F') - A'm \qquad ----(21A)$$

This approximate equation, however, predicts ESR absorption lines of

equal spacings for a group of M $\longleftrightarrow$ (M-1), m transitions. In practice,

the spacings of such a group are found to be unequal (by a few gauss),

thus indicating that the terms of the 2nd and the 3rd order in A are

essential. Consequently Schneider and Sircar (25) using successive

approximations have obtained the following solution for the

equation

$$H_{M,m} = H_o - (2M-1)(D' - K(a'-F')) - Am$$

$$- \left[A^2/(2H_o)\right]\left[I(I+1) - m^2 + m(2M-1)\right]$$

$$- \left[A^3/(2H_o^2)\right]\left[2(I^2+I-m^2)(2M-1)-m(S^2+S-3M^2+3M-2)\right]$$

$$+ \left(A^2D'/H_o^2\right)\left[(I^2+I-m^2)(2M-1)-m(S^2+S-M^2+M-1)\right] . \qquad ---(22)$$

## 5.6 Spin Hamiltonian for the $Mn^{2+}$ ion in Cubic ZnSe

For the $Mn^{2+}$ ion in cubic ZnSe, the Spin Hamiltonian of (19)

reduces to

$$H = g\beta\underline{H}.\underline{S} + \frac{a}{6}\left(.S_\xi^4 + S_\eta^4 + S_\zeta - \frac{707}{16}\right) + A\,\underline{I}.\underline{S}$$

The energy eigenvalues of this system which were first worked out

by Mataress and Kikuchi (26) using perturbation theory, give the

magnetic field positions of the ESR lines (in accordance with the

conditions $\Delta M = \pm 1$ and $\Delta m = 0$) as

$$H_{M,m} = H_o - A'm - \frac{A'^2}{2H_o}\left[\frac{35}{4} - m^2 + m(2M - 1)\right]$$

$$+ \left(\frac{9'}{64x6}\right)\left(35\cos^4\theta - 30\cos^2\theta + 3 + 5\sin^4\theta\cos4\psi\right) \qquad ---(23)$$

$$x \left(56M^3 - 84M^2 - 134M + 81\right)$$

$$A' = \frac{A}{g\beta}$$

$$a' = \frac{a}{g\beta}$$

where $\theta$ and $\psi$ are the Eulerian angles of the direction of the magnetic field relative to the cubic co-ordinate system. For the orientation $H\|[001]$, $\theta = 0$ and $\psi = 45°$ so that the expression reduces to

$$H_{M,m} = H_o - A'm - \left(\frac{a}{48}\right)\left(56M^3 - 84M^2 - 134M + 81\right)$$

$$- \left(A'^2/2H_o\right)\left[35/4 - m^2 + m(2M - 1)\right] \qquad ----(24)$$

## 5.7   ESR Absorption Spectrum of Cubic ZnSe:Mn

Figure (5.1) illustrates the ESR spectrum of a ZnSe:Mn crystal grown at 850°C for the orientation $H\|[001]$ at 77 K. Neglecting any superhyperfine interaction that may occur, the ESR spectrum is expected to consist of 30 lines arising from the $(2S+1)(2I+1)$ energy levels. In Figure (5.1), however, not all the expected 30 lines can be seen, as there is some overlapping of the components arising from their finite widths and the lack of resolution of the spectrometer. Identification of the lines with the predicted transitions was done by noting the relative intensities of the lines and the signs of the coefficients a and A and their resultant effects in the expression (24).

In general theoretical considerations indicate that the intensity of an absorption line representing a transition M $\longleftrightarrow$ (M-1) is
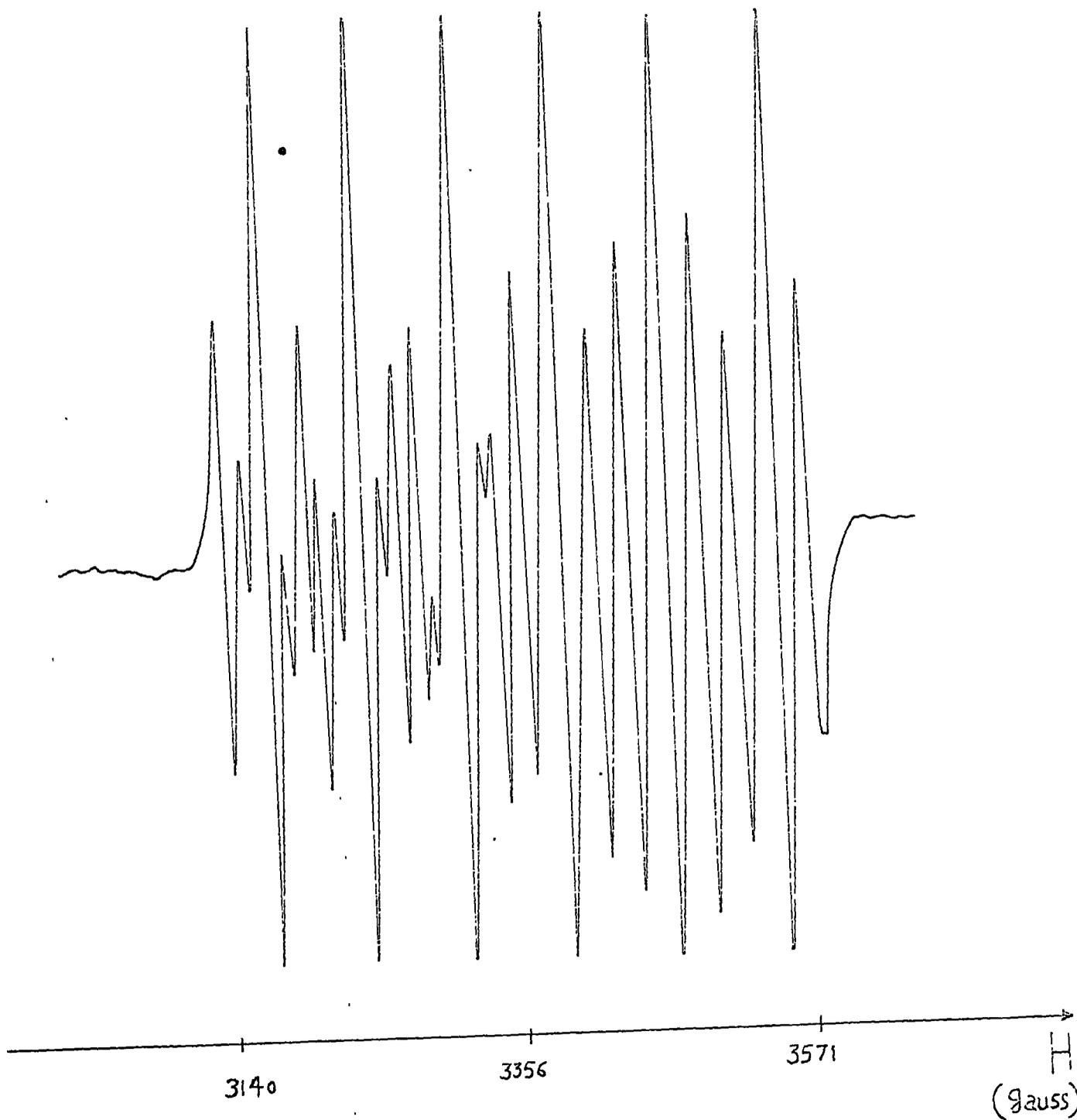
Fig.( 5.1 ) Electron spin resonance absorption spectrum of a ZnSe:Mn crystal (cubic) at 77K for the orientation H||[001] .

proportional to S(S+1)-M(M+1). In essence this corresponds to the projection of the magnetic moment in the direction of the oscillatory magnetic field (due to the microwaves) which is larger for smaller values of $|M|$ than for larger values, i.e. an ESR absorption line due to a transition with a small $|M|$ value has a greater absorption intensity than one due to a transition with a larger $|M|$ value. It follows, therfore, that for the $Mn^{2+}$ ion with $|M|$ values of 1/2, 3/2 and 5/2, the ESR fine-structure absorption lines should have a relative intensity ratio of 9:8:5.

The sign of the cubic crystal field coefficient, a, is known to be positive from experiments on other compounds with a similar structure containing the $Mn^{2+}$ ion (27). Therefore, if the hyperfine terms in the expression ( 24 ) are neglected, an examination of the remaining terms with different quantum numbers M, would give the sequence of the fine-structure transitions with the applied magnetic field. Similarly the sign of the hyperfine coupling coefficient, A, has been found to be negative (27) , so that from the expression (24) it follows that the sequence of increasing m corresponds to increasing the magnetic field. These considerations lead to a complete identification of the ESR absorption lines.

From the recorded spectrum illustrated in Figure (5.1) and the expression (24) , the following values were determined for the parameters involed

$$A = (-61.3 \pm 0.5) \times 10^{-4} \text{ cm}^{-1}$$
$$a = (19.1 \pm 0.5) \times 10^{-4} \text{ cm}^{-1}$$
$$g = 2.0049 \pm 0.0005$$

The value of A is an averaged value calculated from the $M_{\frac{1}{2}} \longleftrightarrow M_{-\frac{1}{2}}$, m = 5/2, 3/2, 1/2 etc. (central) transitions, the separations and sequence of which are illustrated in Figure (5.2).

$m = -\frac{5}{2}$    $m = -\frac{3}{2}$    $m = -\frac{1}{2}$    $m = \frac{1}{2}$    $m = \frac{3}{2}$    $m = \frac{5}{2}$

$\leftarrow A - \frac{2A^2}{H_o} \rightarrow$ $\leftarrow A - \frac{A^2}{H_o} \rightarrow$ $\leftarrow A \rightarrow$ $\leftarrow A + \frac{A^2}{H_o} \rightarrow$ $\leftarrow A + \frac{2A^2}{H_o} \rightarrow$

$H \longrightarrow$
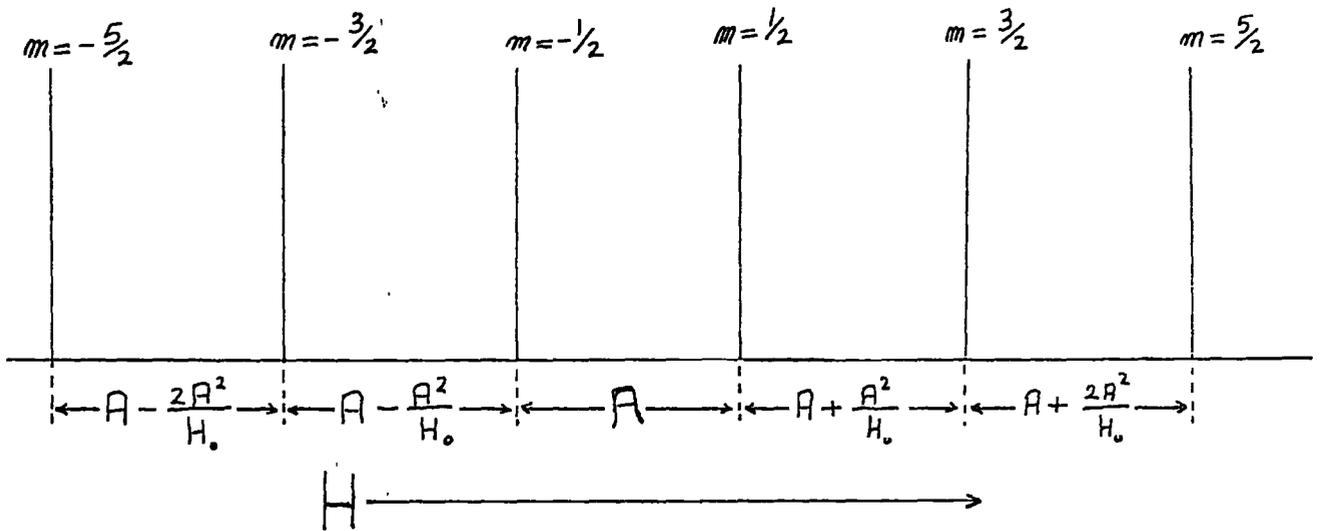
Fig.( 5.2 ) Schematic representation of the central hyperfine transitions $M_{\frac{1}{2}} \longleftrightarrow M_{-\frac{1}{2}}$ , m .Notice the sequence of these transitions as the magnetic field is increased , and how the equal spacing is altered by second order terms. These transitions are not angularly dependent so that in a polycrystalline sample they appear as sharp lines in the spin resonance absorption spectrum.

Notice how the equal spacings of these lines are altered by the second

order correction terms $2A^2/H_o$ first calculated for the ZnS:Mn system

(26). Similarly, the value of (a) given above is an averaged value,

calculated from transition lines, the sequence and separations of which

are indicated in Figure (5.3). These values of the parameters are

consistent with the following reported values for ZnSe:Mn (28);

$$A = -61.7 \ 10^{-4} \ cm^{-1}$$

$$a = 19.7 \times 10^{-4} \ cm^{-1}$$

$$g = 2.005$$

Using the values determined for the various parameters, the ESR

spectrum of the $Mn^{2+}$ ion in cubic ZnSe has been calculated and is

shown in Figure (5.4). Basically the spectrum can be looked upon as

consisting of six groups of five lines, with each group corresponding

to a particular m value. The five lines in each group correspond to

the five permitted M $\longleftrightarrow$ (M-1) transitions and have a relative

intensity ratio of 8:5:9:5:8. In each group notice the symmetrical

arrangement of four lines about a central transition line $M_{\frac{1}{2}}$ $\longleftrightarrow$ $M_{-\frac{1}{2}}$,

as illustrated in Figure (5.3).

The ESR spectrum illustrated in Figure (5.1) is very similar to

that obtained for cubic ZnS:Mn by Mattarese and Kikuchi (27) using a

Varian spectrometer. However, unlike that in Figure (5.1), that of

Mattarese and Kikuchi is well resolved so that all the expected 30

lines can be distinguished clearly. The sequence of transitions as

given by Mattarese and Kikuchi is, however, incorrect.

## 5.8   ESR of Twinned Cubic ZnS:Mn

As mentioned earlier in Section (5.2), a one-dimensional disorder

that may occur in the II-VI compounds, is a stacking fault. Represen-

ting the stacking sequence of cubic ZnSe as ABC, a crystal containing

$M = -\frac{1}{2}$

$M = \frac{1}{2}$

$M = \frac{3}{2}$

$M = \frac{5}{2}$

$M = -\frac{3}{2}$

$$\longleftarrow 4|a| - \frac{2A^2 m}{H_o} \longrightarrow$$

$$\longleftarrow 5|a| - \frac{2A^2 m}{H_o} \longrightarrow$$

$H \longrightarrow$
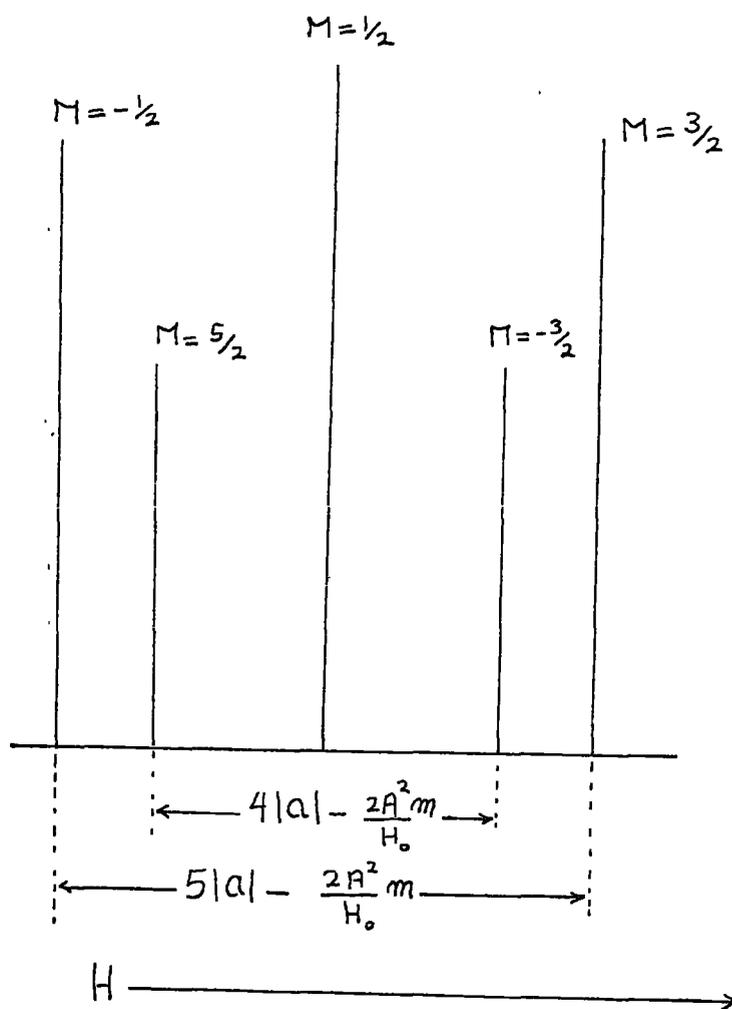
**Fig.( 5.3 )** Schematic representation of fine structure of the spin resonance spectrum of $Mn^{2+}$ in cubic ZnSe for $H \parallel [001]$ . Notice the symmetry and the relative intensity of the transitions indicated.
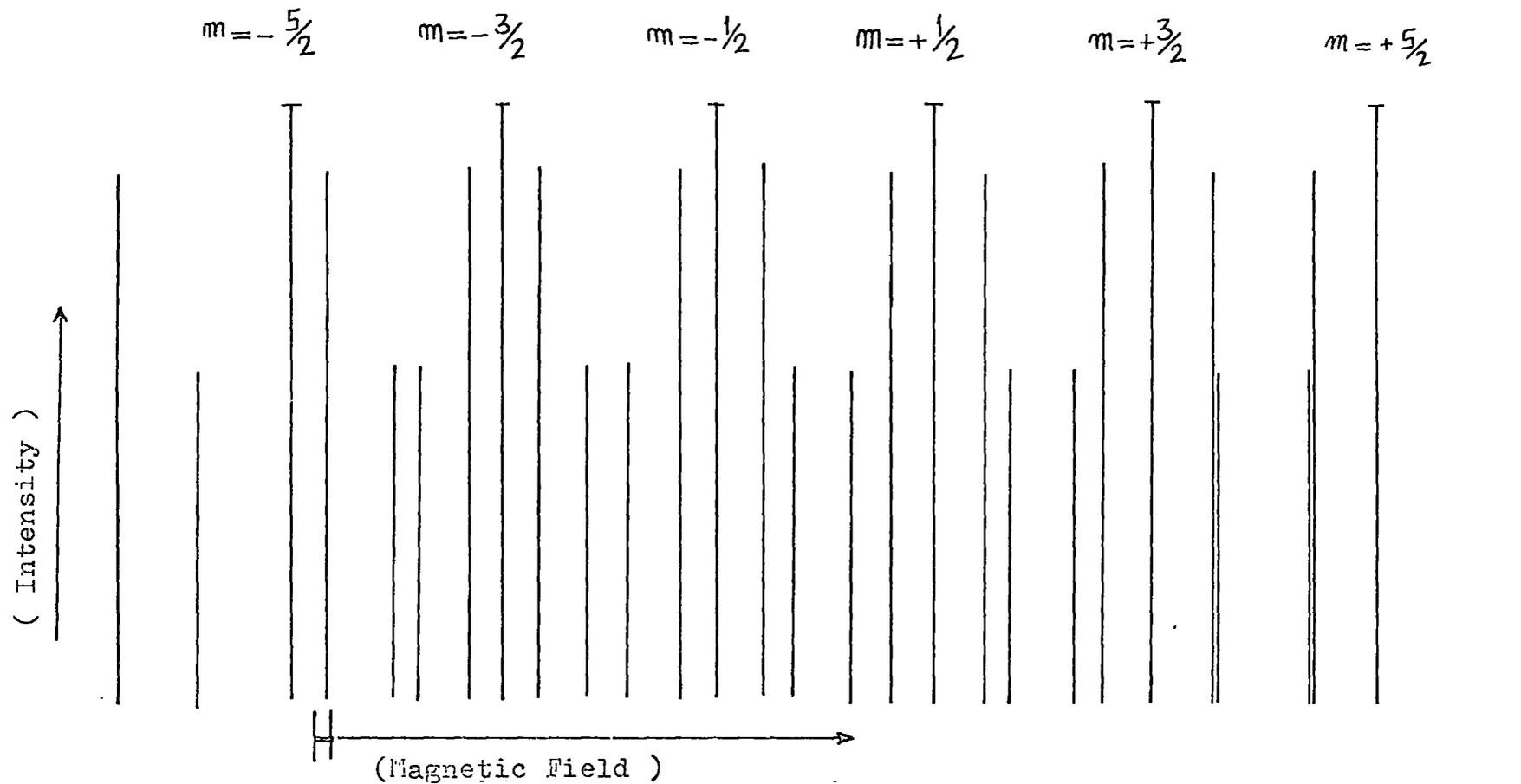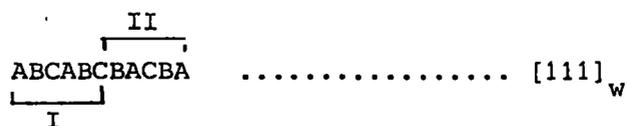
Fig.(5.4 ) Schematic representation of spin resonance absorption spectrum of Mn$^{2+}$ in cubic ZnSe for H$||$[001] based on the parameters determined experimentally.

a stacking fault may have a stacking sequence of

$$\overbrace{\phantom{ABCAB}}^{\text{II}}$$
$$\text{ABCABCBACBA} \quad \ldots\ldots\ldots\ldots\ldots \quad [111]_w$$
$$\underbrace{\phantom{ABCABC}}_{\text{I}}$$

The two cubic parts I and II, form a rotational twin (as one part is

rotated $180^{\circ}$ about the [111] axis) with the transitional layers BCB

having a hexagonal packing. The formation of such a rotational twin in

the structure can lead to a doubling of the number of the angular

dependent ESR absorption lines of the paramagnetic ions in the host

lattices, as the cubic parts may have different orientations with respect

to an applied magnetic field. Also, the axial crystal field produced

by the transitional layers, i.e. the stacking fault, can lead to a shift

in the position of the angularly dependent lines. Depending on the

axial field and the orientation of the crystal, this may cause line

broadening.

Figure (5.5) illustrates the spectrum of a twinned ZnSe:Mn crystal

which was grown at approximately $1100^{\circ}$C. Contrasting this spectrum

with that illustrated in Figure (5.1), it can be seen that Figure (5.5)

consists of two superimposed spectra; one due to a cubic part with

its [001] axis parallel to the applied magnetic field, and the other

due to a second cubic part, say II, making an angle of $70^{\circ}$ 32 with the

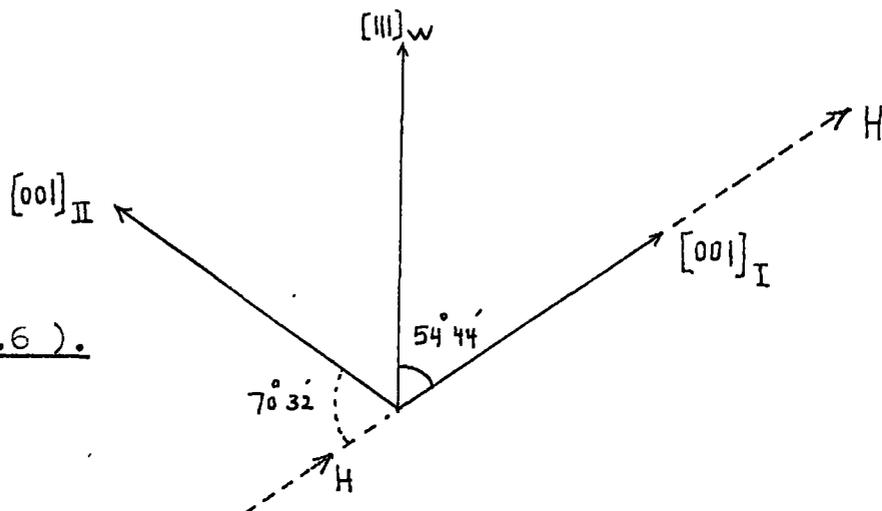applied field (this is illustrated diagrammatically in Figure (5.6).



Fig.( 5.6 ).

Fig.( 5.5 ) Electron spin resonance absorption spectrum of Mn$^{2+}$ in a twinned (cubic) ZnSe crystal at 77K.

Theoretically, the spectrum of such a twinned crystal should consist

of 54 ESR absorption lines (noting that the six central hyperfine

transition lines $M_{\frac{1}{2}} \longleftrightarrow M_{-\frac{1}{2}}$, are not angularly dependent, and that

they therefore coincide). However, in practice a great deal of over-

lapping occurs and not all the 54 lines can be resolved.

Because of severe overlapping in the spectrum it was not possible

to investigate the effect of the stacking fault on the field position

of the angularly dependent lines. Generally, the stacking fault produces

a crystal field along the [111] axis of the cubic crystal, and as a

result the expression $(24)$ giving the field position of the angularly

dependent ESR absorption lines, is no longer valid. Considerable

deviation may occur in a crystal with a high density of stacking faults,

with the deviation obviously being greatest in the orientation $H \parallel [111]$,

as observed in ZnS:Mn crystals containing a high density of stacking

faults (26).

To take account of the stacking faults, the Spin Hamiltonian of

$(23)$ can best be modified by the addition of a small axial field term

of $\Delta(S_z^2 - \frac{35}{12})$. This leads to a correction term of $\Delta(3 \cos^2 v - 1)(2M-1)$

for the angularly dependent lines. Of great interest is the axial field

parameter $\Delta$ which can be found experimentally, and which would vary from

sample to sample depending on the extent of the stacking disorder. It

must, however, be borne in mind that in a cubic crystal with stacking

faults, the axial field experienced by the individual $Mn^{2+}$ ions depends

on their distance from the disordered layers, whereas in hexagonal

ZnSe:Mn for instance, the axial field experienced by the individual

$Mn^{2+}$ ions would be the same. Nevertheless, there is a great temptation

to compare $\Delta$ with the axial field parameter (D) of the $Mn^{2+}$ ion in the

hexagonal crystal, and thus obtain a measure of the density of the

stacking faults. However, nothing is known of the quantitative

relationship between these parameters and the actual crystal fields

they represent, so that any conclusion drawn from the ratio $\Delta/D$ con-

cerning the density of the stacking faults might be correct, or on the

other hand, it might be way out. Very little work has been done on the

stacking faults in the II-VI compounds. It could be that ESR can provide

quantitative information, the only critical requirement being a high-

sensitivity spectrometer.

## 5.9    ESR of the $Mn^{2+}$ ions in Mixed Cubic-Hexagonal ZnSe Crystals
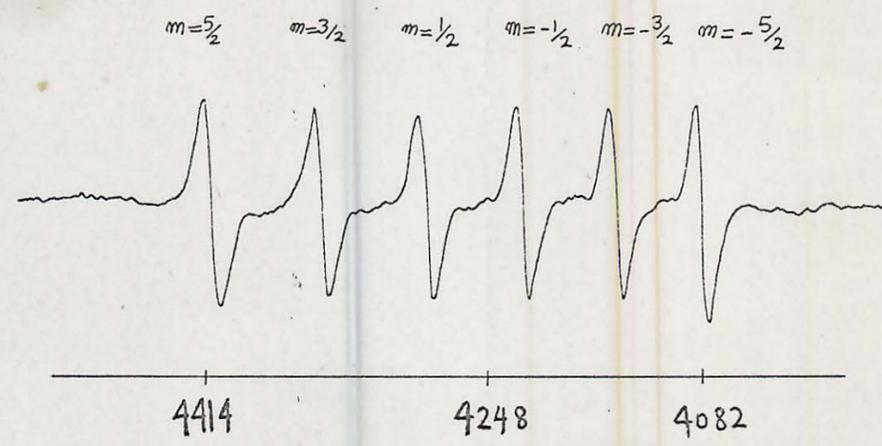
ZnSe:Mn crystals produced at $1300^{\circ}C$ by the sublimation method

were examined by the X-ray back-reflection technique. The X-ray patterns

obtained indicated a symmetry characteristic of a cubic (zincblende)

structure. The ESR absorption spectra were, however, found not to be

characteristic of the $Mn^{2+}$ ion in cubic ZnSe. These spectra were

analysed and shown to be due to the $Mn^{2+}$ ions in ZnSe crystals which

had mixed cubic-hexagonal structures.

Figure (5.7) illustrates a typical ESR absorption spectrum for

such a ZnSe:Mn crystal with the orientation $H \parallel [111]$ cuvic and $H \parallel C$

hexagonal. In contrast with the spectrum of the $Mn^{2+}$ ion in cubic ZnSe,

because of the strong axial crystal field of hexagonal ZnSe, this spectrum

is spread over a considerable range of applied magnetic field. Basically,

it consists of two spectra; one due to the $Mn^{2+}$ ion in hexagonal ZnSe

in the applied magnetic field range of from 1343 to 5351 gauss, and

the other due to the $Mn^{2+}$ ion in cubic ZnSe in a magnetic field that

ranges from approximately 3140 to 3571 gauss in the recording illustrated.

Thus in the applied magnetic field of about 3140 to 3571 gauss, there

is overlapping between the ESR absorption lines of the cubic structure and

the six central hyperfine transition lines $M_{\frac{1}{2}} \longleftrightarrow M_{-\frac{1}{2}}$,

$m = 5/2, 3/2, 1/2, -1/2, -3/2, -5/2$, of the $Mn^{2+}$ ion in the hexagonal

$$M = \tfrac{5}{2}$$

$m=\tfrac{5}{2}$  $m=\tfrac{3}{2}$  $m=\tfrac{1}{2}$  $m=-\tfrac{1}{2}$  $m=-\tfrac{3}{2}$  $m=-\tfrac{5}{2}$

5351         5190         5029

. 69.0 , 66.3 , 64.2 , 62.9 , 59.1 .

$$M = \tfrac{3}{2}$$

$m=\tfrac{5}{2}$  $m=\tfrac{3}{2}$  $m=\tfrac{1}{2}$  $m=-\tfrac{1}{2}$  $m=-\tfrac{3}{2}$  $m=-\tfrac{5}{2}$

4414         4248         4082

. 69.4 , 67.7 , 65.9 , 64.3 , 63.5 .

$$M = \tfrac{1}{2}$$

×11

3571         3356         3140  (gauss)

$$M = -\tfrac{3}{2}$$

$m=\tfrac{5}{2}$ $m=\tfrac{3}{2}$ $m=\tfrac{1}{2}$ $m=-\tfrac{1}{2}$ $m=-\tfrac{3}{2}$ $m=-\tfrac{5}{2}$

1693         1518         1343

. 71.4 , 70.6 , 69.39 , 69.3 , 68.9 .

$$M = -\tfrac{1}{2}$$

$m=\tfrac{5}{2}$  $m=\tfrac{3}{2}$  $m=\tfrac{1}{2}$  $m=-\tfrac{1}{2}$  $m=-\tfrac{3}{2}$  $m=-\tfrac{5}{2}$

2635         2464         2292

. 70.7, 69.0 , 68.6, 67.9, 67.9 .
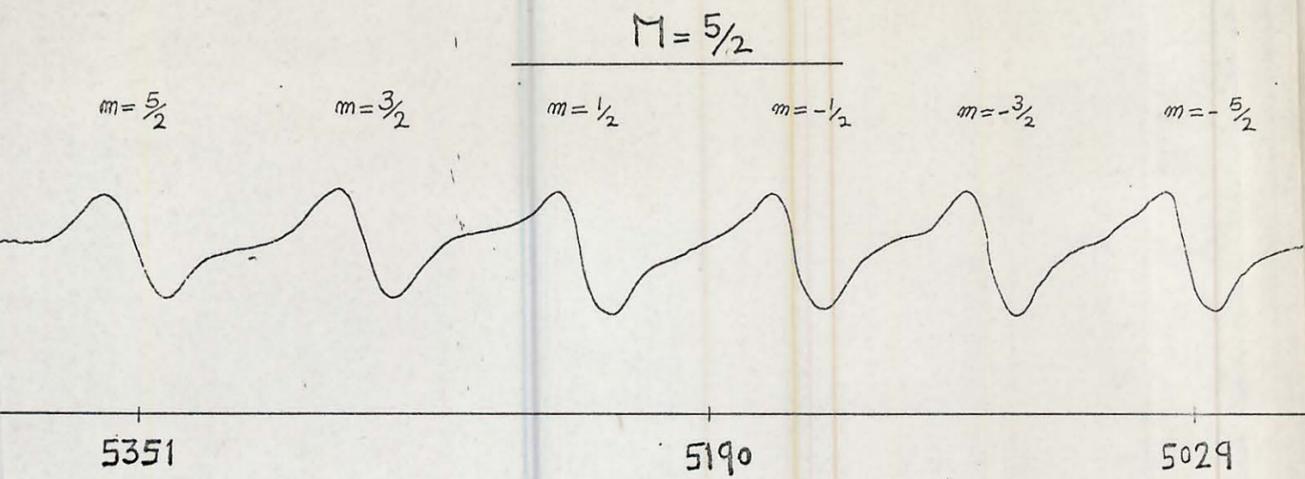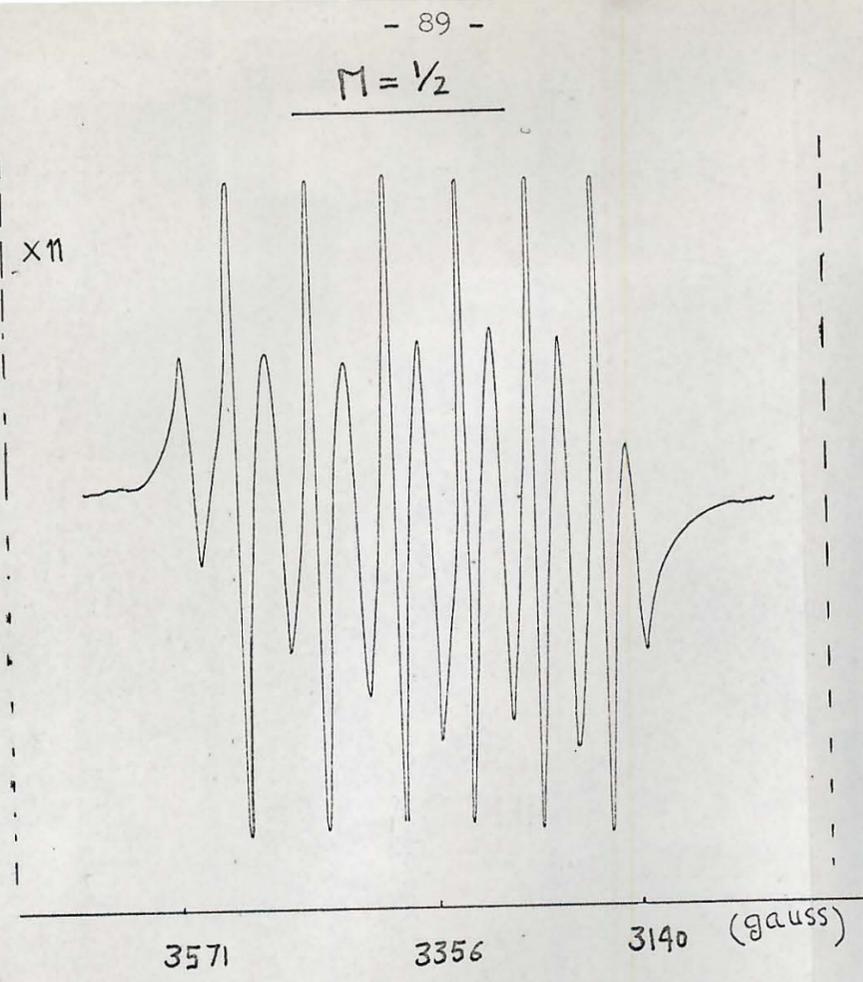
Fig.(5.7) Electron spin resonance of $Mn^{2+}$ in cubic-hexagonal crystal at 77K for the orientation H∥[111] and H∥C. Because of the strong axial field the spin resonance of Mn in hexagonal ZnSe is spread from approximately 1343 to 5351 gauss. This should be contrasted with the spin resonance of $Mn^{2+}$ in cubic ZnSe which is from approximately 3140 to 3571 gauss. Illustrated is also the separation of the hyperfine lines(in hexagonal ZnSe) in four of the five sets, notice how the separation increases as the magnetic field is increased.
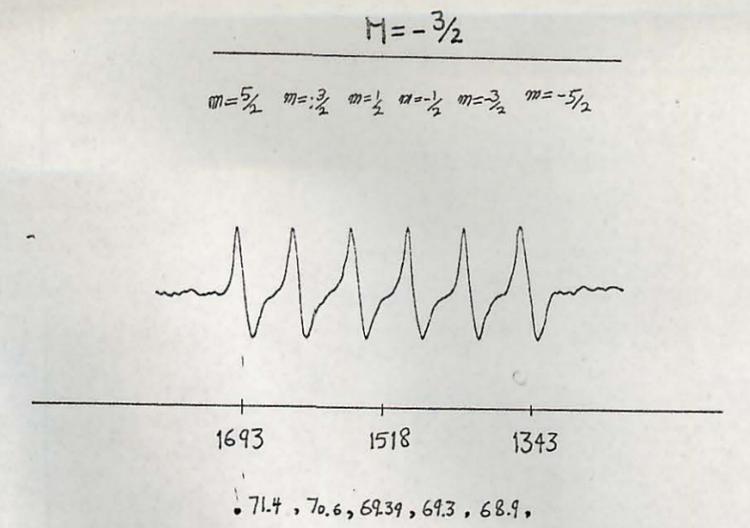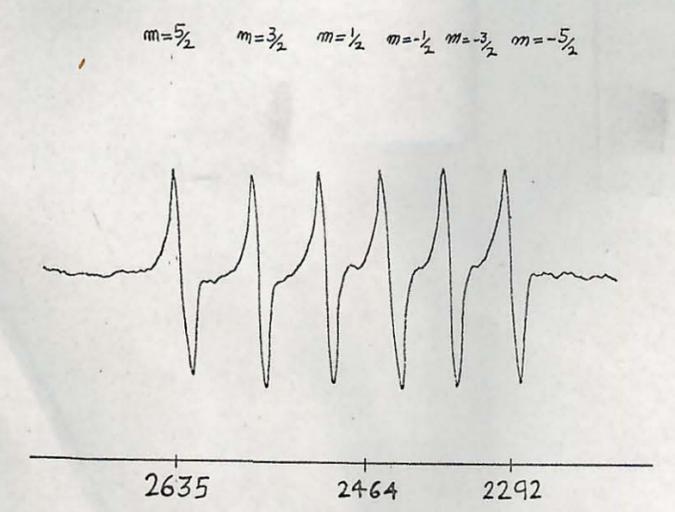
structure. These six lines, however, fall extremely close to the six

central hyperfine transition lines of the cubic structure as the spin

resonance of the $Mn^{2+}$ ion in cubic and hexagonal ZnSe has g-values which

differ very slightly. Between the central hyperfine transitions in the

cubic spectrum there is, however, a great deal of overlapping of the

cubic hyperfine lines. This is partly due to the fact that some of the

$Mn^{2+}$ ions in the cubic part of the crystal experience a variable axial

crystal field, the magnitude of which depends on the separation of the

individual $Mn^{2+}$ ions from the hexagonal layers. Notice that in the

cubic (zincblende) as well as the hexagonal (wurtzite) structure, the

central hyperfine transition lines are not angularly dependent and thus

in the ESR spectrum of a ZnSe:Mn powder sample they would appear as

sharp lines.

Identification of the absorption lines in the hexagonal spectrum

of Figure (5.7) with the transitions involved was carried out by noting

the relative intensity of the lines, together with the signs of the

coefficients A, D and (a-F) and their effects in the equations.

Generally, as was pointed out earlier on, in a multi-level spin system

the intensity of the transition M ⟷ (M-1) is proportional to

S(S+1)-M(M-1). In contrast, the hyperfine transition lines, with

$\Delta m = 0$, which correspond to different nuclear orientations have the

same intensity.

The $Mn^{2+}$ ion in ZnSe has (2S+1) = 6 fine-structure energy levels

which are associated with the transitions $M_{5/2}$, $M_{3/2}$, $M_{1/2}$, $M_{-1/2}$

and $M_{-3/2}$ (here the quantum states of the upper states involved in the

transitions are denoted, i.e. $M_{5/2}$ ⟷ $M_{3/2}$ is denoted as $M_{5/2}$). Each

of these transitions would have an intensity proportional to S(S+1) -

M(M-1), so that the relative intensities of the above five transitions

would be in the ratio of

$$5 : 8 : 9 : 8 : 5$$

But, as a result of the interaction of the five 3d electrons with the nucleus of $(Mn^{55})^{2+}$ ion, each of the six fine-structure energy levels is itself split into six, so that with the condition $\Delta m = 0$, now six hyperfine transitions occur for each M $\longleftrightarrow$ (M-1) transition. However, the relative intensity ratio

$$5 : 8 : 9 : 8 : 5$$

is preserved, so that the ESR absorption spectrum of the $Mn^{2+}$ ion may consist of five groups of six lines with the six lines in each group (of M $\longleftrightarrow$ (M-1)) having the same intensity, but the five groups as a whole having the relative intensity ratio of

$$5 : 8 : 9 : 8 : 5$$

This is exactly what is observed in the spectrum of Figure (5.7 ) if the cubic hyperfine transitions in between the central hyperfine transitions are neglected, and if it is recognised that the intensities of the central transition lines are high because these lines are due (more or less) to the super-imposition of the central transition lines in the hexagonal and the cubic structure.

Though intensity considerations can in principle establish the general shape of an ESR absorption spectrum, as in this case, it cannot, however, establish the sequence of the transitions involved. Thus in the hexagonal part of the spectrum of Figure (5.7 ), the sequence of M $\longleftrightarrow$ (M-1) transitions with increasing applied magnetic field may be $M_{5/2}$, $M_{3/2}$, $M_{1/2}$, $M_{-1/2}$, $M_{-3/2}$, or the sequence may be the other way round. The signs of the coefficients (a-F) and D are, however, known from observations of the $Mn^{2+}$ ions in other compounds (27 ), and it is by making use of these signs in the expressions (22 ), that unequivocal

information as to the order of the transitions involved can be obtained. Inserting the negative sign of D and the positive sign of (a-F) in the expression ( 22 ) and considering various M ←——→ (M-1) transitions, it becomes clear that as the magnetic field is increased, the fine-structure transitions sequence of $M_{-3/2}$, $M_{-1/2}$, $M_{1/2}$, $M_{3/2}$, $M_{5/2}$ occurs. Similarly, the sign of the hyperfine interaction coefficient is known to be negative so that the sequence of increasing m corresponds to increasing the magnetic field. This leads to a complete identification of the observed ESR absorption lines with the transitions involved. This is illustrated in Figure (5.7).

Figure (5.8 ) illustrates the separation of the centres of the five hyperfine groups. Notice the symmetrical positioning of four of the groups about the central transition $M_{1/2}$ ←——→ $M_{-1/2}$ . For the direction H ∥ C, the separation of the groups was found to be a maximum. This is in accordance with crystal field interactions involving an axial field with the $Mn^{2+}$ ion occupying a substitutional site. Indeed the symmetry behaviour of the groups was used in the first place to establish whether the ESR absorption spectrum was that of the $Mn^{2+}$ ions in hexagonal ZnSe or not, and if so, whether the $Mn^{2+}$ ions were incorporated substitutionally. The perturbation calculations of Abraham and Bleaney ( 29A) show that in the case of an axial field the interaction coefficient D has an angular variation of the form $(3\cos^2 \theta -1)$, where in this case θ is the angle between the applied magnetic field and the C-axis. Thus maximum separation of the groups is expected for H∥ C, and minimum for $\theta = 54° 44'$, which corresponds to H ∥ [001] axis of the cubic part. For the orientation H⊥C, the separation obtained was approximately half of that in the orientation H∥C, with the difference that in this orientation the transitions occurred in the reverse order in accordance with the sign change in $(3 \cos^2 \theta-1)$. The angular
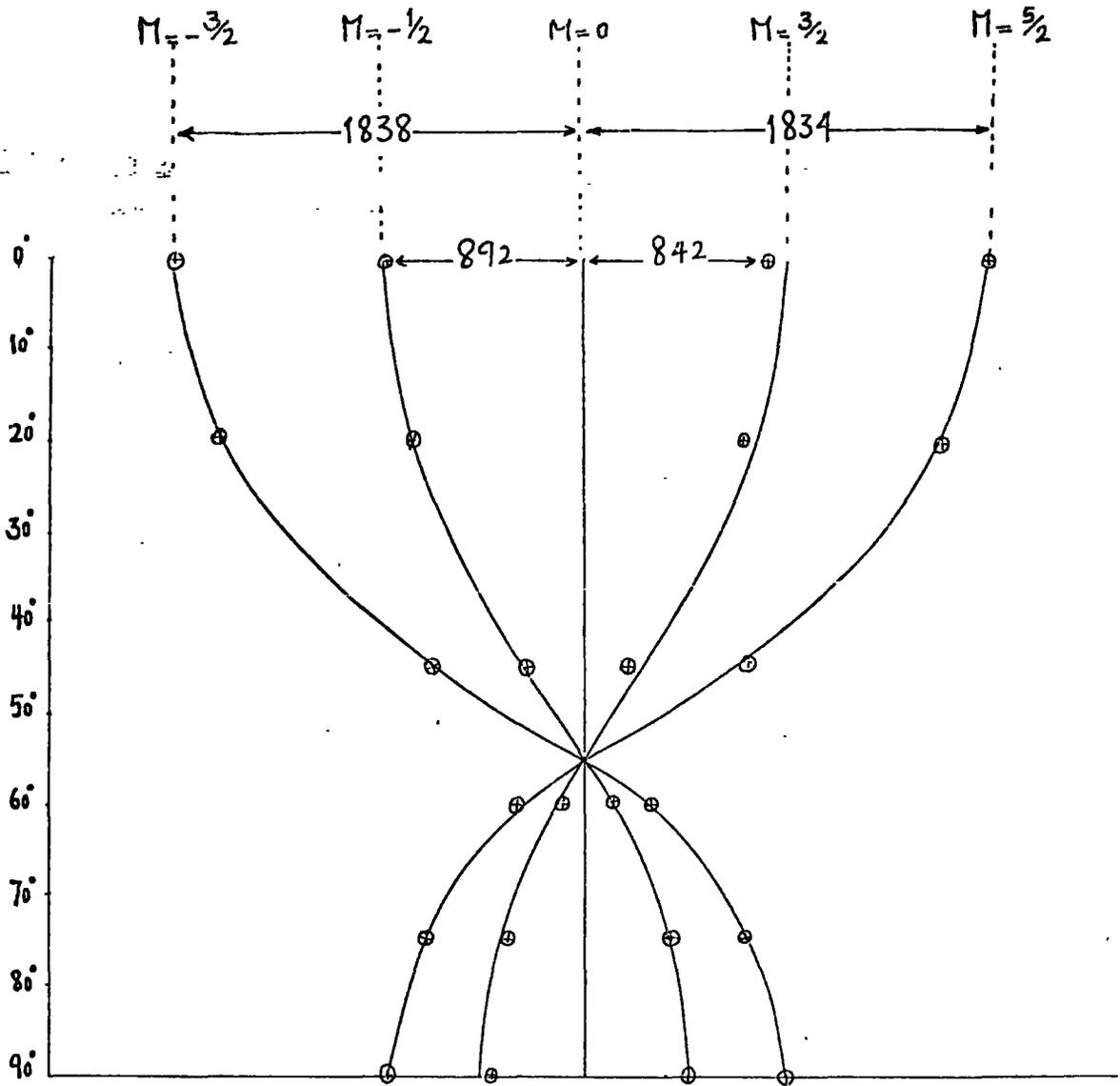
Fig.(5.8) The angular dependence of the the centres of the
five sets of hyperfine lines according to $(3\cos^2\theta-1)$
variation ( solid lines ) and the experimental
results ( circles ) obtained for six orientations.
$\theta = 0$ corresponds to H∥C
$\theta = 54.44$ corresponds to H∥[CO1]
$\theta = 90$ corresponds to H⊥C

variation of the centres of the hyperfine groups is diagramatically illustrated in Figure (5.8).

Figure (5.7) also illustrates the measured separation of the hyperfine lines in each of the four groups $M_{5/2}$, $M_{3/2}$, $M_{-1/2}$ and $M_{-3/2}$. Because of the second and third order terms in the expression the lines in each group are not equally spaced, but their separation increases with increasing magnetic field. In Figure (5.7) the smallest separation is 59.15 gauss for the transition $M_{5/2}$, m = -3/2 and the largest separation is 71.45 gauss for $M_{-3/2}$, m = 5/2. To determine the parameters D, (a-F) and A, use was made initially of the expression (2|A). The values obtained were then corrected with second and third order terms as indicated in Section 5.4. The following values were obtained:

$$A = ( - 62.2 \pm 0.5 ) \times 10^{-4} \, cm^{-1}$$
$$(a - F) = ( 10.4 \pm 0.5 ) \times 10^{-4} \, cm^{-1}$$
$$D = ( 426.5 \pm 0.5 ) \times 10^{-1} \, cm^{-1}$$

These values should be contrasted with the following obtained by Azarbayejani (248) for hexagonal ZnSe at 300 K.

$$A = ( -61.2 ) \times 10^{-4} \, cm^{-1}$$
$$(a - F) = ( 11.05 ) \times 10^{-4} \, cm^{-1}$$
$$D = ( 425.1 ) \times 10^{-4} \, cm^{-1}$$

Notice that because of overlapping between the central hyperfine group $M_{1/2}$ with the cubic spectrum it was not possible to determine the g-value of the $Mn^{2+}$ ion in hexagonal ZnSe.

The spin resonance parameters given above (and those in Section vary from compound to compound depending on the ionicity of the compound containing Mn (this dependence applies also to other s-state ions such as $Cr^{+1}$, $Fe^{3+}$ etc.). Such a dependence was first observed by

Van Weiringen (19 ) in his spin resonance study of the $Mn^{2+}$ ion in a large number of compounds. For instance the g-values in ZnSe and CdTe were found to be larger than the free spin g-value of 2.0023. At the time this was rather surprising since it was believed then that only the spin contributed to the magnetic moment of the $Mn^{++}$ ion. In 1957 Watanabe (29C) predicted theoretically that the admixture of the quartets of the $d^5$ configuration into the $6S_{5/2}$ ground state might lead to a negative deviation from the free spin value. This obviously could not explain Van Weiringen's observations. Fidone and Stevens (29D) considered the effect of covalency in the bonding of the ion to the lattice and showed theoretically that this may lead to a positive contribution to the g-value. Figure (5.9a ) illustrates the variation of the g-value of the $Mn^{2+}$ ion in a number of II-VI compounds with the ionicity in the bonding (with the ionicity calculated from the electronegativity difference formula and table given by Pauling in 1959 (29E)). From Figure (5.9a) it can be seen that the g-value increases with decreasing ionicity.

Van Weiringen also observed that the hyperfine coefficient (A) depended on the ionicity of the host lattice, i.e. the more covalent the bonding, the smaller the hyperfine coefficient. Matamura (20 ) extended this by plotting the hyperfine coefficient against the ionicity of the bond and obtained a linear relationship (the ionicity of the bond was calculated from the electronegativity difference between the substitutional Mn and the anions surrounding Mn in the immediate shell). For a theoretical discussion of ionicity and the hyperfine coefficient of the s-state ion the reader should consult (29F). Figure (5.9b) illustrates the variation of (A) with the ionicity of the bonding.
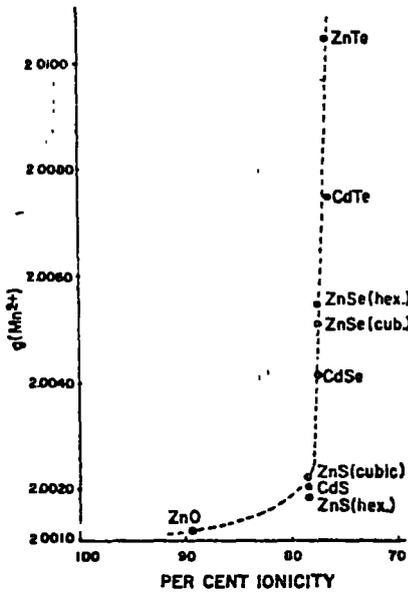
(a)
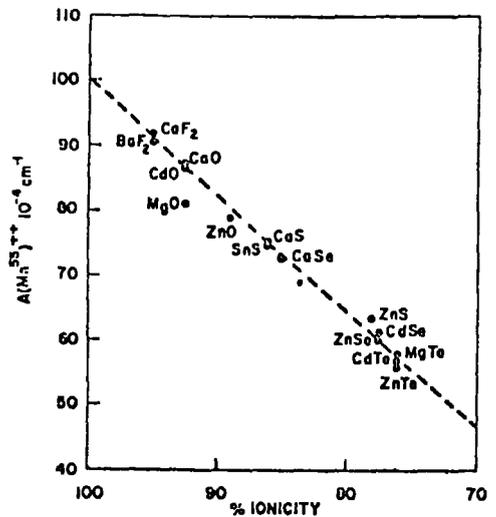
(b)
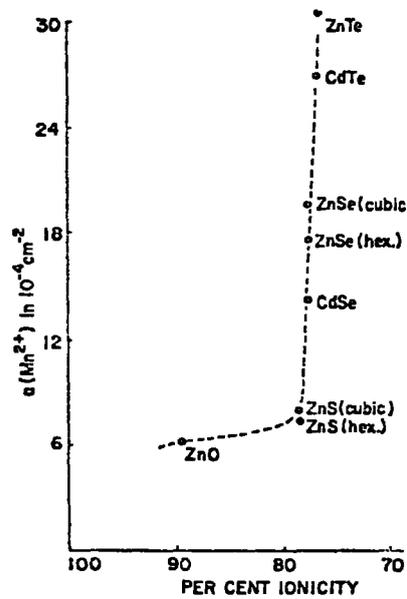
(c)

Fig.( 5.9 )

(a). Variation of the g-value of $Mn^{2+}$ with ionicity in the bonding.

(b). Variation of the hyperfine coefficient A with ionicity in the bonding.

(c). Variation of the cubic crystal field parameter, (a), with ionicity.

Spin resonance investigations of the s-state ions indicate that the cubic crystal field parameter (a) also varies with ionicity of the lattice. Figure (5.9c) illustrates the variation found for the $Mn^{2+}$ ion in a number of II-VI compounds. It is instructive to notice that the calculations of Gabriel et al ( 8 ) predict a value of $0.3 \times 10^{-4}$ $cm^{-1}$ for the cubic crystal field parameter of $Mn^{2+}$ ion in ZnS. The measured value is $7.97 \times 10^{-4}$ $cm^{-1}$, a difference of more than one order of magnitude. This discrepancy is to some extent attributed to the fact that ZnS is not 100% ionic. According to the calculations of Gabriel et al, the cubic crystal field parameter (a) is proportional to $\lambda^4 (Dq)^n$ where $\lambda$ is the spin orbit coupling constant, $(Dq)$ is a measure of the crystal field strength and n a constant varying between 3.5 and 6.

Though reference has been made here to the spin resonance parameters of the $Mn^{2+}$ ion only, in practice the parameters of other s-state ions (Cr, Fe etc.) are found to vary with ionicity in a manner similar to the variations indicated in Figures (5.9a,5.9b,5.9c). From Figures (5.9a,5.9b,5.9c) it can be seen that the magnitude of the resonance parameters of the $Mn^{2+}$ ion suggest that the selenides of Zn and Cd are more covalent than the sulphides.

## 5.10   Variation of the ESR Spectrum of the $Mn^{2+}$ ion with Optical Excitation

Because of the ability of Mn as an activator to produce luminescence in a large variety of compounds, the luminescence was long ago attributed to an internal transition. As a free ion the $Mn^{2+}$ has a spherically symmetrical ground state $^6S$ in which all the five 3d electrons have parallel spins. The first excited state $^4G$ differs energetically from the ground state by 3.3 eV, and in contrast with the $^6S$ state has four electrons which have parallel spins, as in the ground state, and one with reversed spin, i.e. the difference between the two states is due to a spin reversal. With the $Mn^{2+}$ ion in a crystal field, say, of cubic symmetry, some of the degeneracy of the energy levels is removed so that the excited state $^4G$ splits into $^4T_1$, $^4T_2$, $^4A_1$ and $^4E$. The ground state energy level $^6S$ also splits but to a very much lesser extent, so that the state $^6A_1$ derived from it, is usually taken as coinciding with it. Of great important is the transition $^6A_1 \left(^6S\right) \longleftrightarrow ^4T_1 \left(^4G\right)$ which is generally believed to be responsible for the Mn luminescence. This transition is, however, basically forbidden by parity and spin considerations, but occurs because of spin orbit coupling and lattice interactions. It follows then that because of the nature of the $^6A_2 \left(^6S\right) \longleftrightarrow ^4T_1 \left(^4G\right)$ transition there should be a decrease in the population of the ground state $^6A_2 \left(^6S\right)$ during luminescence. This should lead to an attenuation of the $Mn^{2+}$ ESR signal together with the emergence of a new signal originating from the metastable state $^4T_1 \left(^4G\right)$. Observation and investigation of this new signal would be of great help in clarifying the nature of the metastable state responsible for luminescence.

With this aim in mind, the ESR signals of a large number of ZnSe:Mn crystals were monitored while the samples in the microwave

cavity were in darkness and under U.V. excitation of $\lambda$ = 3650 A at room temperature and at 77 K. However, within the sensitivity of our ESR spectrometer and the light energy that could be directed on to the samples in the microwave cavity, no change could be detected. This is presumably because the optical energy directed on to the samples was insufficient.

## 5.11 Electron Spin Resonance Linewidth Broadening Processes

Generally the resolution of fine and hyperfine lines in an ESR absorption spectrum, is limited by the width of the lines which in turn are affected by interactions between paramagnetic ions and their surroundings and by interactions between the paramagnetic ions themselves. These interactions can be briefly discussed under the following headings:

a.      Spin-lattice Interaction

b.      Inhomogeneities in the Lattice

c.      Spin-Spin Interaction.

a.      Spin-Lattice Interaction

In a simple two-level spin system resonance occurs when energy is absorbed from the radiation field to produce spin transitions from the lower energy state to the higher one. The time taken by the electrons to return to their original state is called the relaxation time $\tau$. This relaxation time comprises two terms, $\tau_1$ and $\tau_2$. $\tau_1$ is a relaxation time associated with spin-lattice interaction, while $\tau_2$ is associated with dipole-dipole (spin-spin) interaction. $\tau$, $\tau_1$ and $\tau_2$ are related approximately by the expression

$$\frac{1}{\tau} = \frac{1}{\tau_1} + \frac{1}{\tau_2}$$

with $\tau$ itself related to the absorption line by

$$\tau = \pi 8 \left( \omega - \omega_o \right)_{max} \qquad \text{---(25)}$$

where $\pi 8 \left( \omega - \omega_o \right)_{max}$ is usually referred to as the line-shape function in terms of frequency $\omega$.

The term spin-lattice interaction should cover all the possible processes by which the electrons (spins) transfer their extra energy to the solid. For instance, experimental observations indicate that free carriers are quite effective in removing the extra spin energy (26). However, in all the theoretical treatments because of mathematical difficulties the only process usually considered is the dominant spin-lattice interaction. Basically, strong spin-lattice interaction gives rise to a short $\tau_1$ and broad ESR absorption line. In a case when $\tau_1$ is very short at a given temperature, the greatly broadened line may not be detectable at all. Generally there exists a strong correlation between $\tau_1$ and spin-orbit coupling; a strong spin-orbit coupling produces rapid relaxation and broad lines and vice versa.

In thermodynamical treatments of spin-lattice interaction usually an effective spin temperature is defined in terms of the instantaneous populations of the states. If in a two-level system the thermal equilibrium populations of the two levels are $N_a$ and $N_b$ (where $N_a$ is the population of the lower state and $N_b$ that of the higher state), then $N_a$ and $N_b$ are related through the Boltzman distribution as

$$N_b = N_a \exp \left( - \frac{h\nu}{kT} \right) \qquad \text{---(26)}$$

where
$$h\nu = E_b - E_a$$

If this system is disturbed, as in ESR, the non-equilibrium population $N_a'$ and $N_b'$ are then related as

$$N_b' = N_a' \exp \left( - \frac{h\nu}{kT_s} \right) \qquad \text{----(27)}$$

where $T_s$ is defined as the effective spin temperature. During this time the lattice is assumed to remain at constant ambient temperature T where T is smaller than $T_s$. This line of treatment is, however, justified if the magnetic dipoles are sufficiently strongly coupled together to establish a common spin temperature in a time much shorter than that require to establish thermal equilibrium with the lattice. During the ESR process energy is absorbed and $T_s$ rises steadily as the population difference between the two states decreases. (Equal populations in the two states implies an infinite spin temperature). In the reverse direction, spin-lattice interaction tends to reduce the spin temperature by removing the excess energy and dissipating it in the solid. Soon a state of dynamic equilibrium may be reached when the interaction process removes energy at a rate equivalent to that absorbed by the spins. However, if the incident microwave power is so intense that the relaxation process cannot restore thermal equilibrium, the intensity of the ESR signal would decrease and the absorption line would broaden. This is usually referred to as power saturation broadening.

To explain the way in which excess spin energy is transferred to the lattice Waller in 1932 (30) suggested that spin-lattice inter-action was essentially through the modulation of the magnetic dipole interactions, i.e. he suggested that lattice vibrations influenced the spins through the modulation of the spin-spin interaction. Waller's predicted relaxation times were very much longer than those observed experimentally, but his predicted variation of $\tau_1$ with temperature was similar to the behaviour observed experimentally. In 1939 Kronig (31) suggested that during lattice vibrations the orbital motions undergo periodic modulations as the result of the crystal field itself being
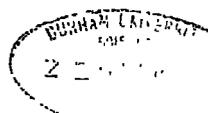
modulated by the lattice vibrations. These changes then react upon the spins causing them to alter their orientations with respect to the constant applied field. (The modulation of the crystal field by the lattice vibrations occurs as a result of the interatomic spacings of the ions altering in a time-dependent manner). The effect of this modulation is to smear out the spin energy levels which may then broaden the ESR absorption lines. Thus in Kronig's theory spin-lattice interaction is via the crystal field whereas in Waller's theory the interaction is via the magnetic dipole interaction. Kronig's theory is the basis of present day spin-lattice interaction even though it is not entirely satisfactory. One reason for this is the crystal field theory itself which with parameters that cannot be calculated, has been found to be too restrictive (32).

b.  Inhomogeneities in the Lattice

Inhomogeneities in the lattice, for example vacancies, interstitials, impurities, stacking faults etc., may alter the symmetry (and the strength) of crystal fields in the vicinity of a paramagnetic ion. For example, in the case of cubic ZnSe:Mn each $Mn^{2+}$ ion is surrounded equidistantly by four $Se^{2-}$ ions. Should one of the four $Se^{2-}$ ions disappear then the crystal field experienced by the $Mn^{2+}$ ion would have a different symmetry than before, thus leading to a different ESR absorption spectrum. Similarly a substitutional impurity ion, usually having a different effective charge, ionic radius and electronegativity from, say, a $Se^{2-}$ ion, would not be exactly at the site of the replaced $Se^{2-}$ ion. This again would disturb the symmetry of the local crystal field. On the whole, any inhomogeneity in the lattice which disturbs the symmetry of the crystal field locally or otherwise, can be expected to have some effect on the ESR absorption spectrum. If inhomogeneities occur randomly, as in the case of a crystal with vacancies and impurities, then the ESR absorption

spectrum would be also affected in a random fashion thus resulting in broadened lines.

c.    Spin-Spin Interaction

Dipole-dipole interaction (or spin-spin interaction) arises from the mutual action of the paramagnetic ions on one another.  Generally each such ion can be regarded as a magnetic dipole which will be precessing in an applied magnetic field $H_z$.  The magnetic field due to such a dipole at the site of another paramagnetic ion in a compound can be resolved into a steady field component $\bar{H}_i$ along $H_z$, and a rotating component perpendicular to $H_z$.  It hence follows that the total field experienced by a paramagnetic ion A is the vectorial sum of $H_z$ and $H_i$. In general, paramagnetic ions due to, say, impurities in a compound, are randomly distributed, so that the extra magnetic field experienced by the paramagnetic ions is liable to vary randomly from zero to a maximum value, from site to site, depending on the number of neighbouring paramagnetic ions, their separations and the orientation of their magnetic moments.  This extra magnetic field would shift randomly the spin energy levels of the ions thereby displacing their ESR absorption lines.  The observed ESR absorption line may thus be considered as an envelope of much narrower lines each corresponding to a particular value of $H_z + H_i$.  Since the variation of $H_i$ in a random system is gaussian, the observed envelope in the absence of any other interaction may be also gaussian.

The effect of spin-spin interaction may vary significantly with the angle of the applied field.  Basically the contribution of each neighbouring dipole has an angular distribution of the form $(1 - 3 \cos^2 \theta)$ where $\theta$ is the angle between the line joining the dipoles and the direction of the applied magnetic field.

Spin-spin interaction was first theoretically investigated by Van Vleck (33) who derived an expression for the mean-square width of the ESR absorption line. This work was extended by Kittle and Abrahams (34) who obtained an expression for the line shape as a function of concentration of paramagnetic ions in the lattice. Thus for similar paramagnetic ions the mean line width is given as

$$h^2 < (\Delta v^2) \quad = \quad 3 \; S'(S'+1) \sum \frac{g^4 \beta^4}{r_{iJ}} \; f \left( \frac{1-3 \; \cos^2 \theta_{iJ}}{2} \right)^2 \quad ----(28)$$

where f is the probability that the lattice site is occupied by a magnetic ion, $r_{iJ}$ is the separation of the i and $J^{th}$ ions.

The rotating component of the precessing dipole may also cause line broadening as it interacts with other dipoles. This rotating or oscillating component of the magnetic field of the dipole is at the right frequency to cause magnetic resonance transitions at the neighbouring paramagnetic ions. This mutual interaction between identical paramagnetic ions shortens the lifetime of the individual ions in a given quantum state and causes line broadening.

### Exchange Interaction

If paramagnetic ions are sufficiently close to one another apart from the interactions mentioned above, there is also an additional effect which may alter the line shape. This effect called exchange interaction, results from overlap of the orbitals of the unpaired electrons, and may narrow the absorption line in a rather complicated manner. For a discussion of this effect the interested reader should consult the published work of Van Vleck (33) and others (35,36). Here suffice it to say that if the paramagnetic ions are similar, exchange interaction may narrow the ESR line at the centre and broaden it in the wings. On the other hand if exchange interaction

is taking place between dissimilar ions, the interaction will tend
to bring the two ESR lines together thus producing a single broad
line.


5.12  Variation of the ZnSe:Mn ESR Spectra with Mn Concentration

Mn Distribution in Different ZnSe Crystals

In ZnSe:Mn an ion, such as $Mn^{2+}$, has 12 equivalent nearest
cation neighbours.  As the Mn concentration is increased from a low
level, the probability of one of the 12 nearest neighbours being also
a $Mn^{2+}$ ion increases.  These nearest-like cations perturb each
other mutually and the result may be detected in the ESR and the
optical absorption spectra.  In the ESR process the mutual perturba-
tion of the $Mn^{2+}$ ions as they approach each other produces dipole-
dipole broadening, while the exchange forces that tend to narrow the
ESR absorption lines become important at small separations.  Studying
the optical absorption spectra of a number of ZnSe:Mn crystals with
different Mn concentrations, McClure (37) found the spectra varying
significantly with Mn concentration and he identified some absorption
bands as being due to $Mn^{2+}$ ions in nearest-neighbour cation sites.
In zinc silicate containing Mn, two luminescence emission bands have
been associated with $Mn^{2+}$.  One of these in the green, occurs at high
Mn concentrations only, and has been attributed by Kroger et al (38)
to clusters of $Mn^{2+}$ ions.  Thus according to Kroger et al the variation
in the relative intensities of the emission bands in willemite is due
to interactions between the $Mn^{2+}$ ions affecting the lifetimes of the
various excited states.  However, it must be stated that this explan-
ation is not universally accepted, and that another school of thought
has put forward an explanation within the concept of the co-ordination
theory (39).

In ZnSe:Mn very little is known about the behaviour of Mn at high concentrations. Figures (5.10) and (5.11) illustrate the ESR spectra for the orientations $H \parallel (111)$ and $H \perp (111)$ of a ZnSe:Mn sample with a Mn concentration of 0.1%. This sample and others, the ESR spectra of which are illustrated in Figures (5.12, 5.13, 5.14, 5.15, 5.16), were produced at $850^{\circ}C$ by the iodine transport method. To determine whether the manganese was distributed uniformly in each crystal growth run, the ESR spectra of at least six samples from different parts of the growth tube were investigated. No variation in the Mn concentration could be found in the samples of any particular crystal growth run when the iodine transport method was used. Of significant interest in the spectra of Figures (5.10) and (5.11) is the indication that at Mn concentrations of up to 0.1% the dipole-dipole interaction broadens the individual lines without affecting the overall shape of the spectrum. However, at a concentration of 0.1%, the $Mn^{2+}$ ions aggregate sufficiently close to one another to enhance the interactions to such an extent that the overall shape of the spectrum begins to distort. Notice that the interaction is stronger for the orientation $H \perp (111)$ than for the orientation $H \parallel (111)$ in all the spectra illustrated, up to a concentration when a single ESR absorption line only emerges for the two directions. Figures(5.12, 5.13, 5.14, 5.15) illustrate the ESR spectra for Mn concentrations of 0.2% and 0.35% which show the dramatic build up in the overall distortion as the concentration is increased. Also, comparing spectra of Figures(5.12, 5.13) with those of Figures(5.14, 5.15) line narrowing can be clearly seen which indicates that at a concentration of between 0.2-0.35% the $Mn^{2+}$ ions approach one another sufficiently closely for the exchange interactions to become significant. As the Mn concentration is increased further the distortion becomes complete so that at

Fig.(5.10) Electron spin resonance of $Mn^{2+}$ in a cubic ZnSe crystal ( with a Mn concentration of 0.1% )at 77K for the orientation H||[111]. Apart from broadened lines due to dipole-dipole interaction notice the onset of distortion in the spectrum.

Fig.(5.11) Electron spin resonance of Mn^{2+} in a cubic ZnSe crystal ( as in Fig.(5.10)) at 77K for the orientation H⊥[111].

Fig.(5.12) Electron spin resonance of $Mn^{2+}$ in a cubic ZnSe crystal ( with a Mn concentration of 0.2% ) at 77K for the orientation $H \parallel [111]$ .

Fig.(5.13)  Electron spin resonance of Mn²⁺ in a cubic crystal [ as in Fig. (5.12)] at 77K for the orientation H⊥[111] .
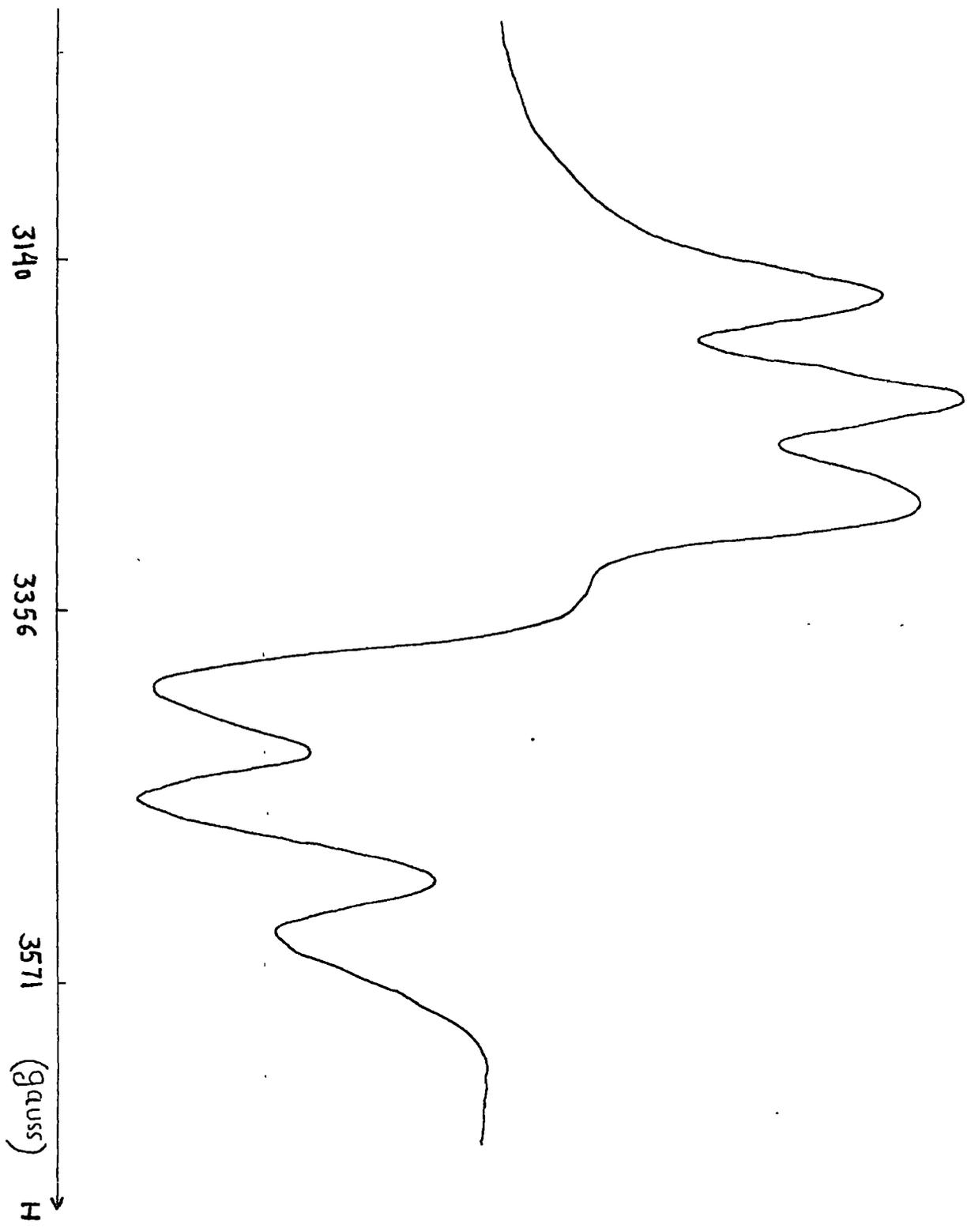
Fig.(5.14)   Electron spin resonance of Mn²⁺ in a cubic ZnSe crystal ( with a Mn concentration of 0.35%) at 77K for the orientation H‖[111] .
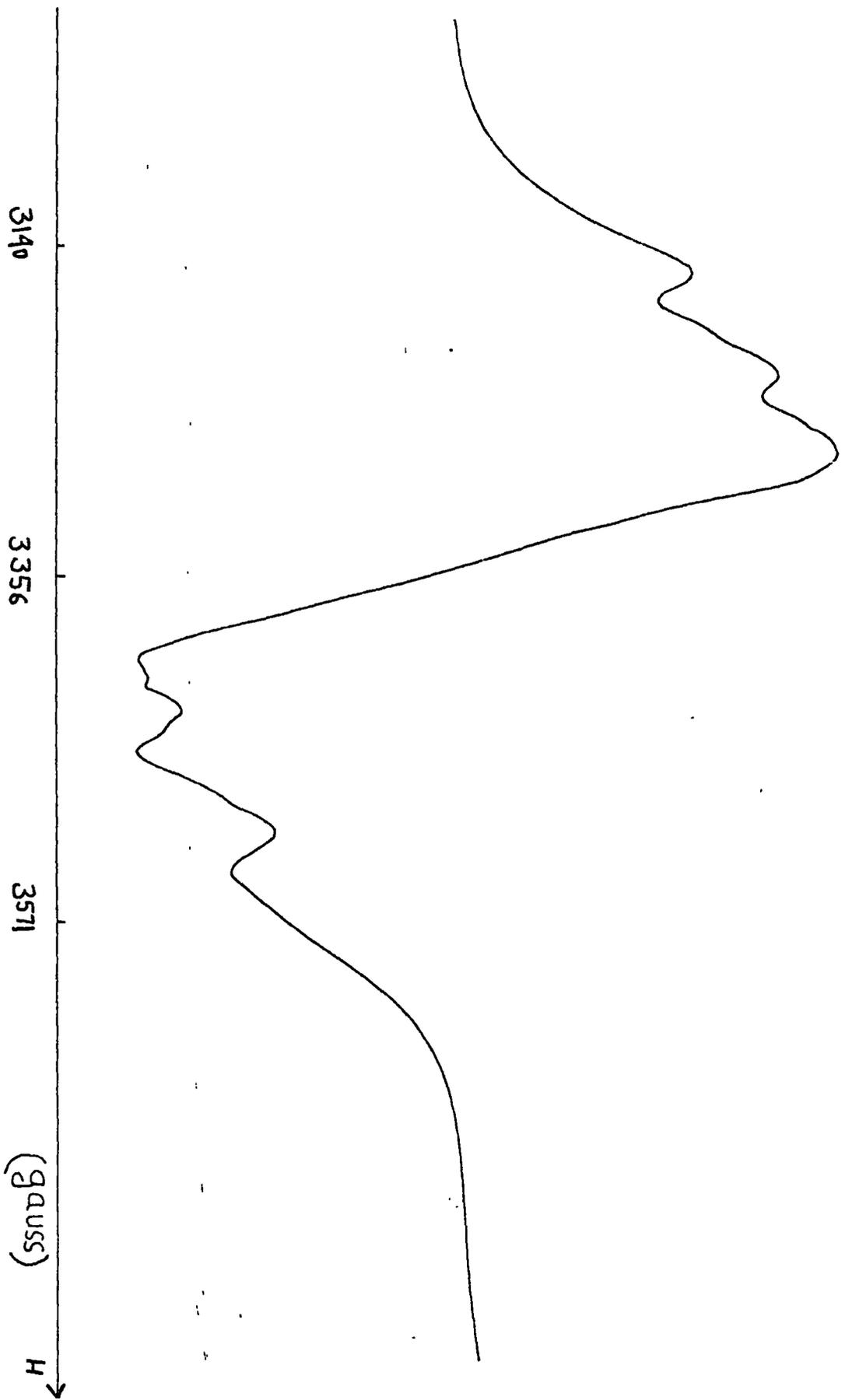
Fig.(5.15) Electron spin resonance of $Mn^{2+}$ in a cubic ZnSe crystal [as in Fig.(5.14)] at 77K for the orientation $H \perp [111]$
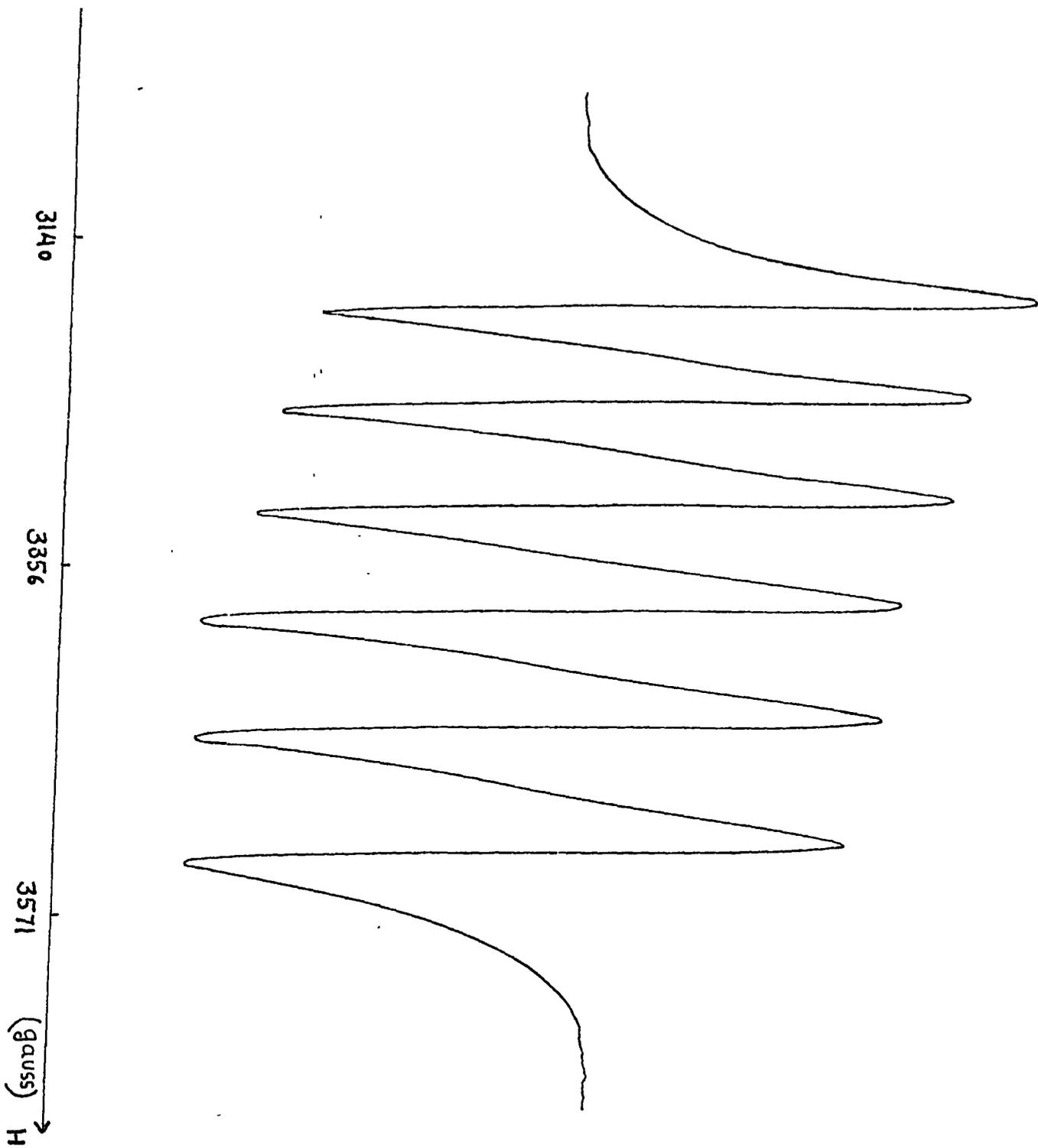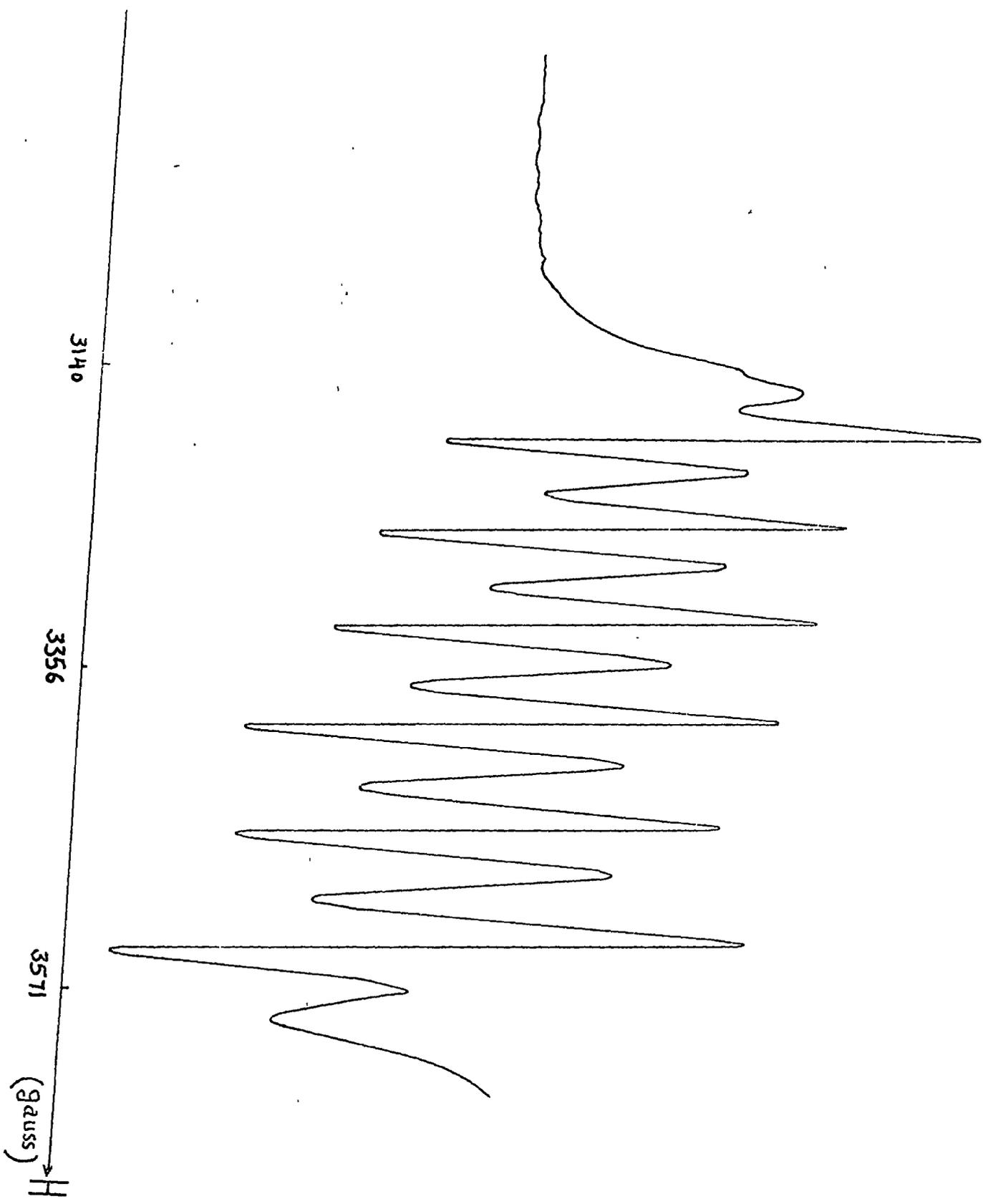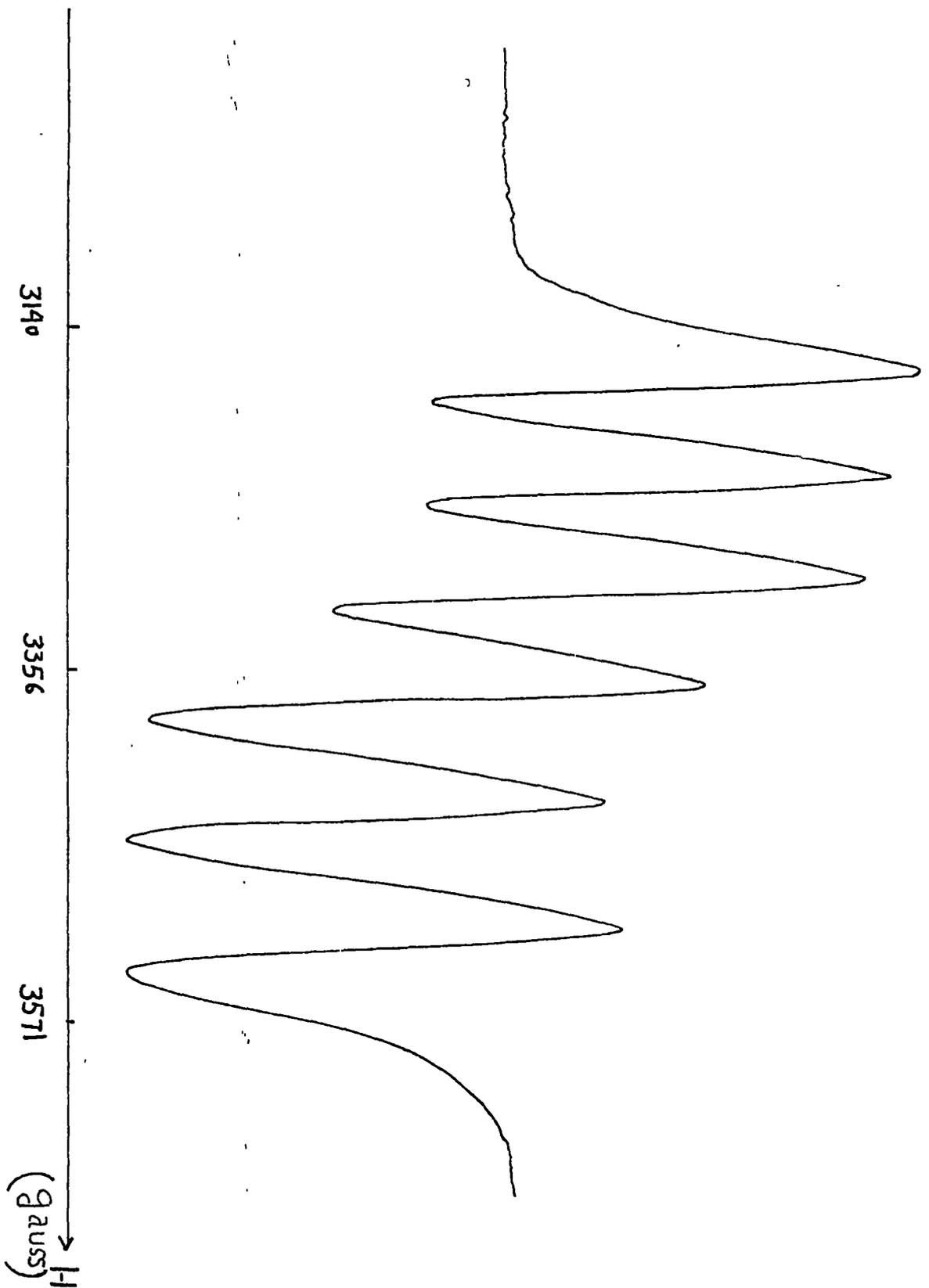
Fig.(5.16) Electron spin resonance of $Mn^{2+}$ in a cubic ZnSe crystal ( with a Mn concentration of 0.55% ) at 77K for the orientation $H//[111]$ .

concentrations of 0.55% a single broad line only can be observed.
However, because of exchange interactions, the line shape no longer
approximates to a Gaussian, but if the asymmetrical distortion from
the base line is neglected, it can be regarded as approximately
Lorentzian.

Of great significance is the question as to whether the above
results apply to ZnSe:Mn crystals produced at all (possible) temperatures,
or whether they are characteristic of crystals produced by the iodine
transport method at $850^{\circ}C$. An investigation of ZnSe:Mn crystals produced
at $1300^{\circ}C$ shows the latter to be the case. For example, ZnSe:Mn
crystals grown at $1300^{\circ}C$ with Mn concentrations of 0.4% and 0.2%
(their spectra are illustrated in Figures (5.17, 5.18)) show no sign
of any distortion of the line shape similar to that observed in com-
parable samples produced by the low-temperature iodine-transport
technique.

Setting aside the possibility that the high concentration of
iodine may be the cause of the $Mn^{2+}$ ions aggregating at low concentra-
tions in crystals produced at $850^{\circ}C$, one has to consider the basic
mechanism of crystal growth in order to find a satisfactory explanation.

According to the present-day theory of crystal growth involving
screw dislocations, a screw dislocation emerges on the face of a
crystal thus providing it with a self-perpetuating step. This step
is envisaged to have a number of kinks. In addition the actual process
of growth on a crystal face from the vapour phase is believed to
involve three steps. First, transport of ions from the vapour phase
to the crystal surface form an adsorbed layer. Second, diffusion of
the adsorbed ions on the crystal surface to a step, and third further
diffusion along the step to kinks where the ions are bound to become
part of the crystal. Considerable surface diffusion is required to
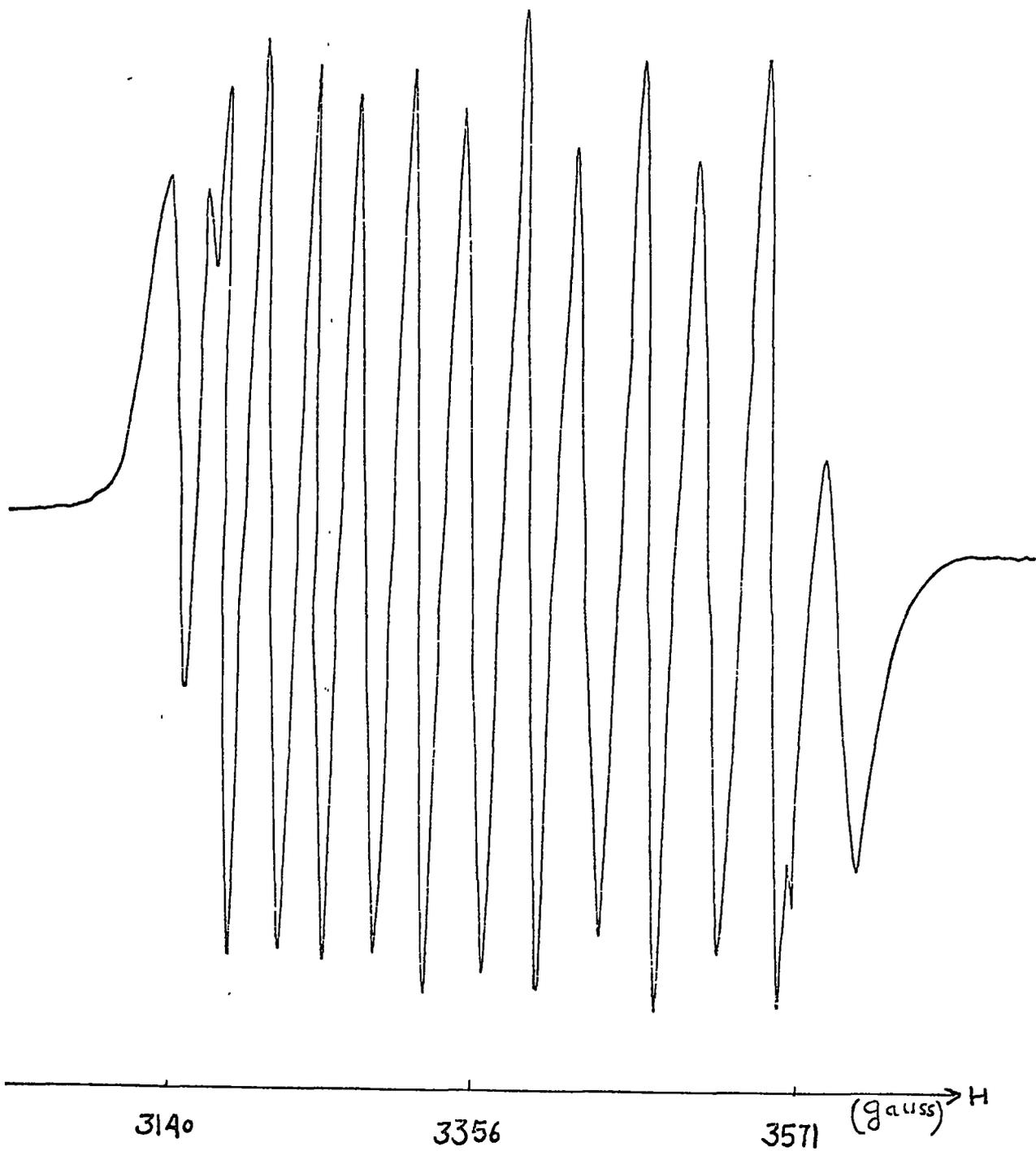
Fig.(5.17) Electron spin resonance of Mn^{2+} in a cubic ZnSe crystal ( produced at 1300C with a Mn concentration of 0.4% ) at 77K for the orientation H∥[111] .
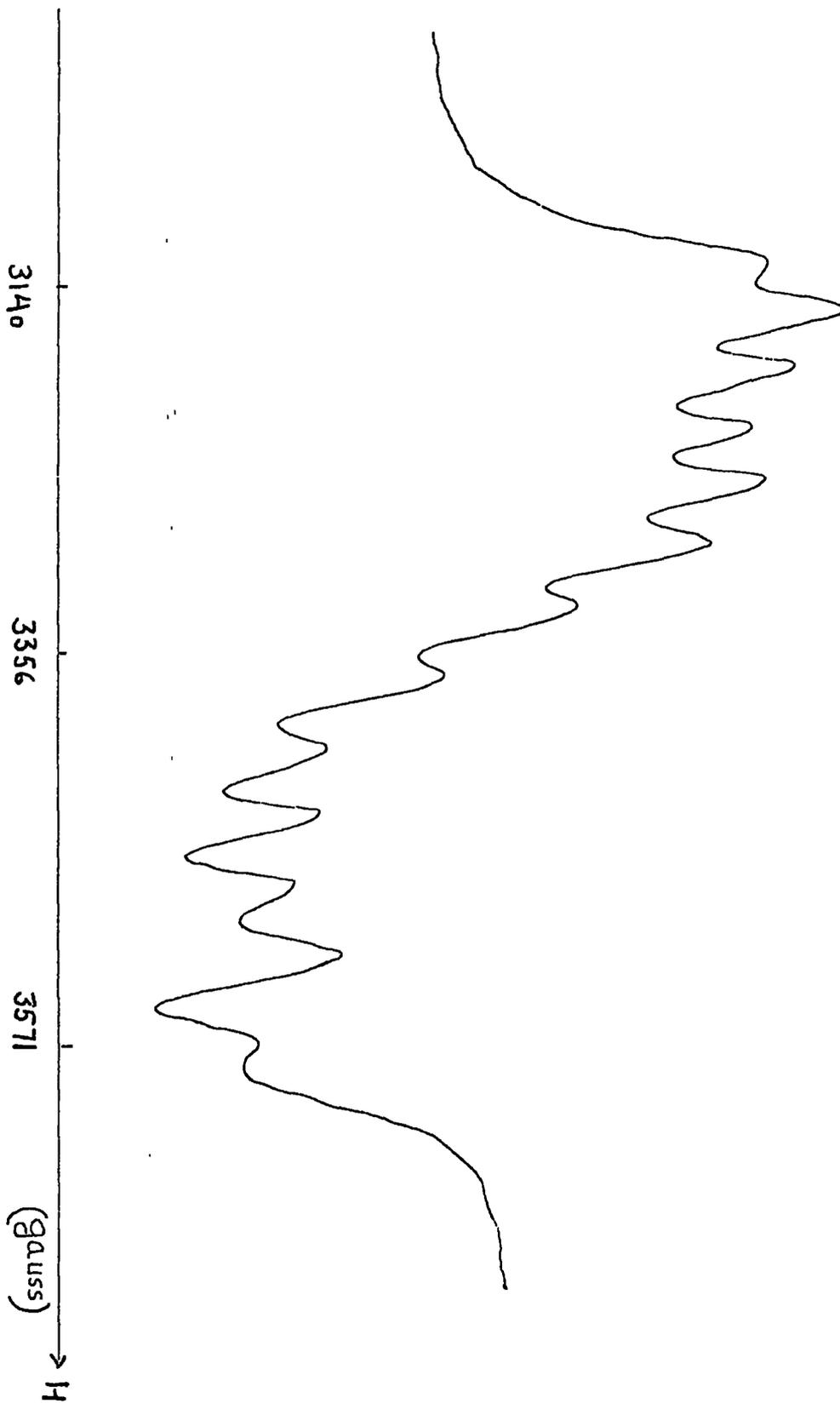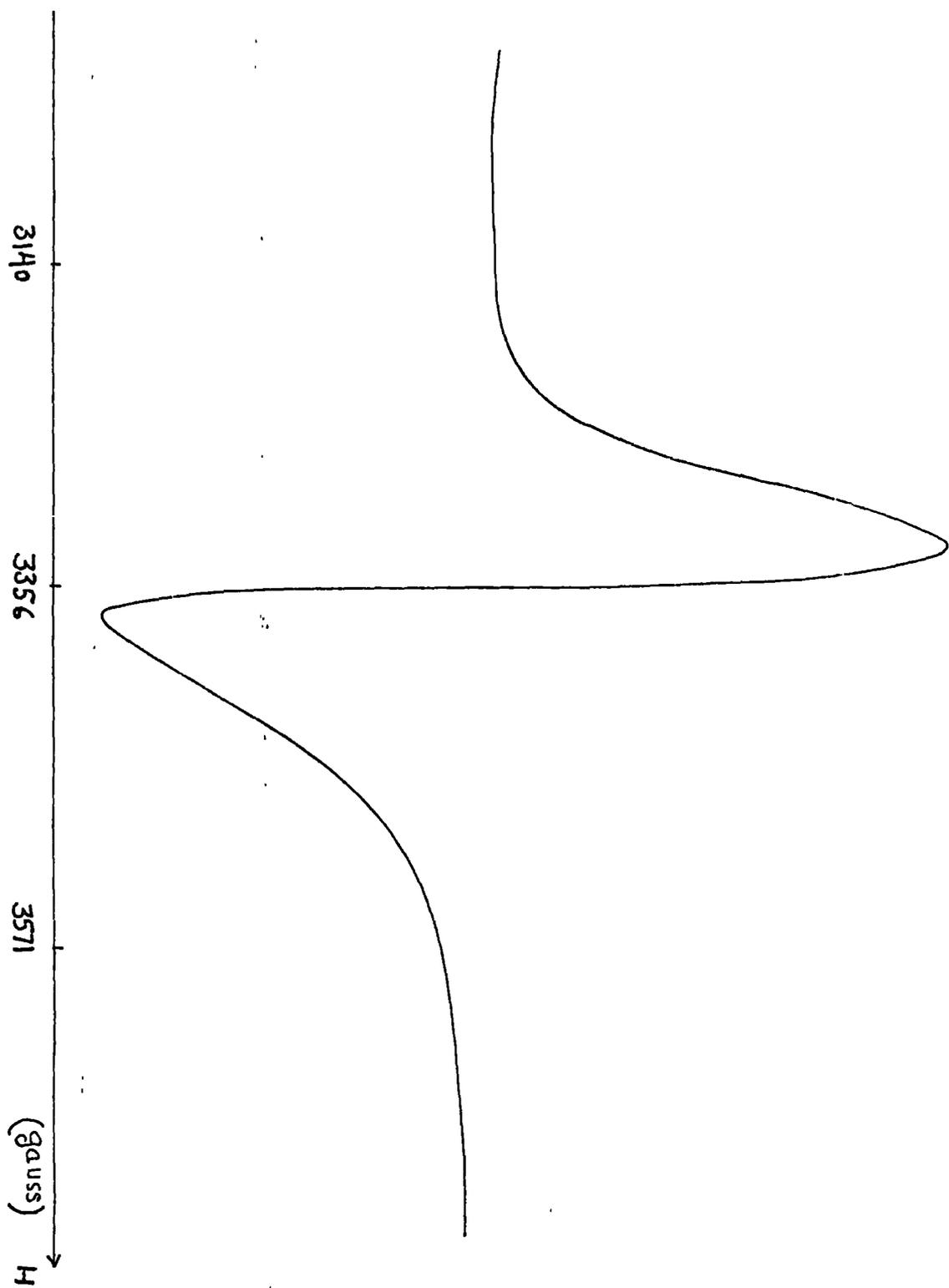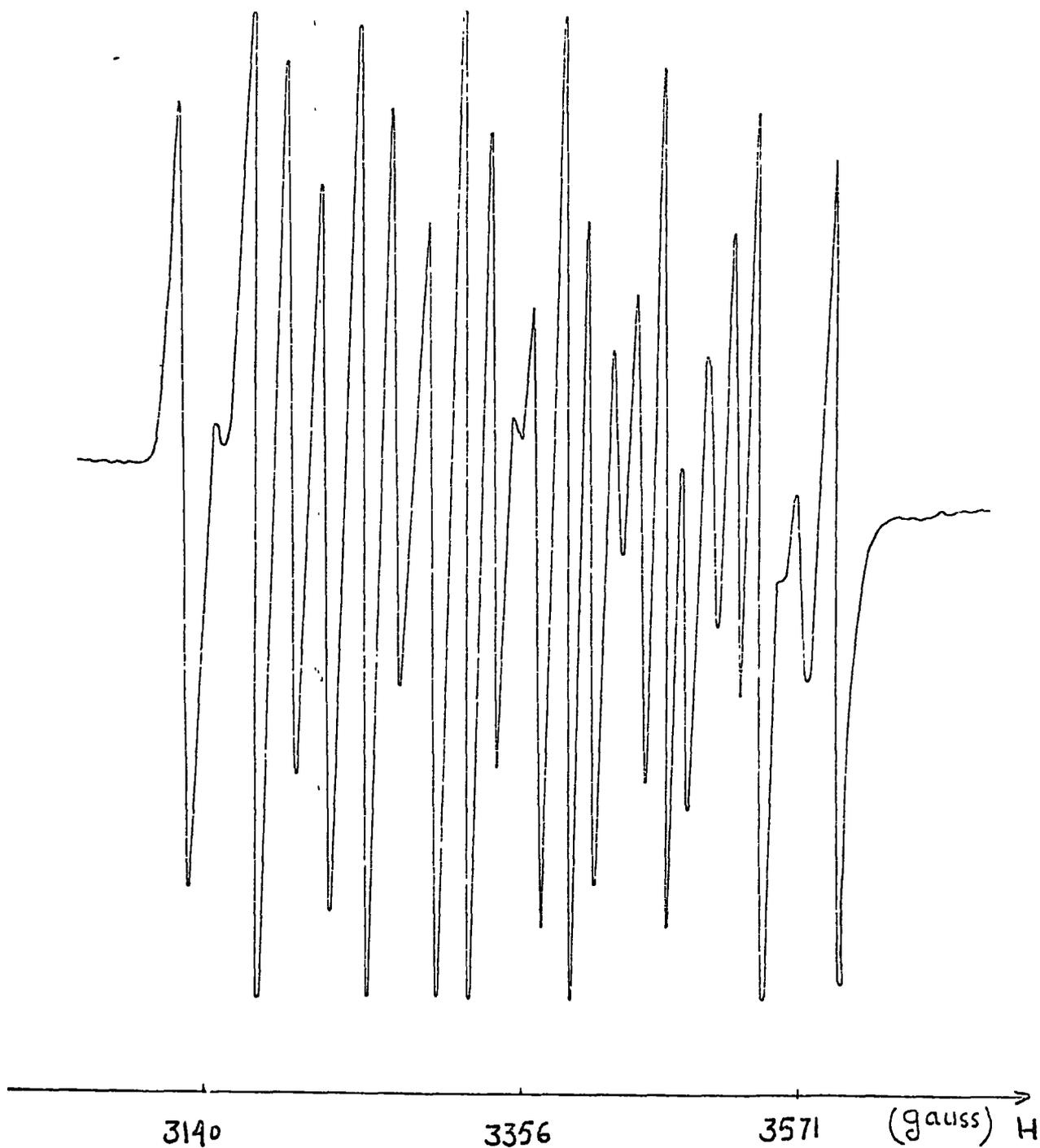
Fig.(5.18)  Electron spin resonance of $Mn^{2+}$ in a twinned ( cubic) ZnSe crystal ( produced at 1300C with a Mn concentration of 0.2% ) at 77K. This spectrum is similar to that illustrated in Fig. (5.5) .

be an essential element if the crystal growth rate is to be explained. Moreover, in crystal growth from the vapour phase the rate of direct arrival of an ion at a particular growth point is believed to be very small compared with the rate of indirect arrival by diffusion. Diffusion is, however, very much temperature dependent and there will be very significant differences in the diffusion rates at two very different temperatures. From this it follows that the possibility exists of $Mn^{2+}$ ions taking up different distributions (for the same concentration) in ZnSe crystals produced at $850^{\circ}C$ and at $1300^{\circ}C$. Thus at $1300^{\circ}C$ the $Mn^{2+}$ ions with their very much greater thermal energies and mobilities can ensure a much more uniform distribution in a crystal than, say, at $850^{\circ}C$. Thus on the basis of this reasoning, up to a point, it is the growth temperature which determines whether the $Mn^{2+}$ ions aggregate or not. It follows, therefore, that more Mn can be incorporated in ZnSe crystals produced at high temperatures without the ions interacting with one another than in crystals produced at $850^{\circ}C$. It would be of great interest to extend these results by finding the critical Mn concentrations (i.e. concentrations at which various interactions begin) in ZnSe crystals produced at $1300^{\circ}C$.

## 5.13    The Effect of Annealing on ZnSe:Mn Electron Spin Resonance Absorption Spectrum

In the ZnSe:Mn samples investigated, it was found that at room temperature not a great deal of hyperfine structure could be resolved in the ESR spectra. Reducing the temperature to 77 K narrowed the lines considerably so that spectra similar to that in Fig.$(5.1)$ could be observed. However, at no temperature was it possible to resolve the spectrum to such an extent that all the expected lines could be observed clearly.

In the previous section the possible processes responsible for line broadening in ESR were briefly discussed. In the light of that discussion, it is useful to consider briefly the possible causes of line broadening in our samples. Of the possible processes mentioned, dipole-dipole interaction can be neglected here as this interaction is important only in the presence of a high Mn concentration or when the $Mn^{2+}$ ions in a sample with a relatively low overall Mn concentration, aggregate close to one another to produce dipole-dipole interaction. Spin-lattice interaction, however, should be looked at in more detail, as this term covers all the possible processes by which the spins lose their extra energy to the lattice. One such process is the interaction of the free carriers with the paramagnetic ions. Briefly, the free carriers are scattered by the paramagnetic ions and in the process the extra spin energy is removed. Thus Schnieder et al (26) in their investigation of the relaxation time in ZnS:Mn found that the relaxation time decreased sharply as free electrons were created by irradiating the sample with U.V. light. Similarly, Lamb et al (40) found that in low resistivity CdS:Mn crystals the relaxation time at room temperature was so short that the hyperfine structure of the spectra could not be resolved. To obtain a well-resolved spectrum comparable to that of a high-resistivity sample at room temperature, the temperature of the low-resistivity sample had to be reduced to about 4 K in order to freeze out the free electrons.

In the case of our ZnSe:Mn samples, a shortened relaxation time as a result of interactions between free carriers and the $Mn^{2+}$ ion must be ruled out as all the "as-grown" samples investigated were of high resistivity (with a resistivity of approximately $10^{12} - 10^{14}$ ohm.cm.)

It is, however, known that these samples contained acceptor-type impurities and native defects (as annealing such a sample in molten Zn at 850°C decreased the resistivity to approximately $10^3$ ohm.cm). As was mentioned before impurities and native defects can broaden the ESR lines by affecting the crystal field symmetry in the vicinity of some paramagnetic ions. That very probably this was the case in our sample can be concluded from the fact that reducing the temperature of a sample from 77 K to 4.2 K produced only very marginal narrowing in the width of the ESR lines of the $Mn^{2+}$ ion. Yet the effect of reducing the temperature from 300 K to 77 K on the line-width was very significant. This clearly indicated that native defects and impurities were responsible for the broadness of the ESR lines in our samples. Furthermore, it can be concluded that the relaxation time $\tau_1$ in ZnSe:Mn at room temperature is not very long, but at 77 K it becomes sufficiently long for the hyperfine lines to be resolved in a good-quality, high-resistivity crystal. This means that the relaxation time in ZnSe:Mn is probably comparable to that in CdTe:Mn, but shorter than that in ZnS:Mn or CdS:Mn. Since spin-lattice interaction is responsible for the relaxation time, it follows that in CdTe:Mn and ZnSe:Mn spin-lattice interaction is much stronger than in ZnS:Mn or CdS:Mn.

To investigate the effect of free carriers on the ESR absorption lines of ZnSe:Mn, and the effect of annealing in general, a number of samples (ZnSe:Mn) were annealed in Se and Zn. Of the two samples annealed in Se at 650°C for four days each, apart from a negligible decrease in the Mn concentration, no change in the ESR spectra could be seen at 300 K or 77 K. However, the four samples annealed in Zn at 850°C each for seven days, all showed significant decreases in their Mn concentrations. Furthermore, definite line broadening could be seen

in all the samples at 300 K and 77 K.  (It is important to note that
as the result of annealing in molten Zn the resistivity of these
samples decreased from approximately $10^{12}$ ohm.cm. to about $10^{2}$ ohm.cm.
Figure (5.19) and Figure (5.20) illustrate the ESR spectra of a sample
before and after annealing.  Basically the two ESR spectra are rather
complex as the sample had a twinned structure similar to that mentioned
in Section  5.8 .  Two of the four annealed samples were then annealed
for a second time.  Again the ESR results in both samples indicated
significant decreases in the Mn concentrations of the two samples.
Figures (5.21) and (5.22) illustrate the ESR spectra of a sample for
the orientation $H \parallel$ [110] at 77 K obtained after the first and second
annealing run.  From these spectra notice the definite narrowing of
the lines as a result of annealing for a second time (a similar
improvement was also observed in the other sample).  However, it must
be noted that though  the spectrum of Figure (5.22) is better resolved
than that in Figure (5.21), it is slightly broader than the spectrum
obtained for the same sample before it was annealed.  Obviously this
is due to a decrease in the Mn relaxation time brought about by an
increase in the density of the free carriers with annealing.

To explain the narrowing of the ESR lines after the second
annealing (compared with the spectrum obtained after the first annealing)
the following suggestion should be considered.  As shown, annealing
ZnSe:Mn in molten Zn removes some of the Mn impurity, i.e. in the
presence of molten Zn at $850^{\circ}$C, Mn appears to have a tendency to
diffuse out of ZnSe.  During the annealing process when the overall
Mn concentration is relatively high, there is a possibility that some
of the Mn ions may approach one another (while diffusing out) to produce
dipole-dipole interactions.  This coupled with the increased free
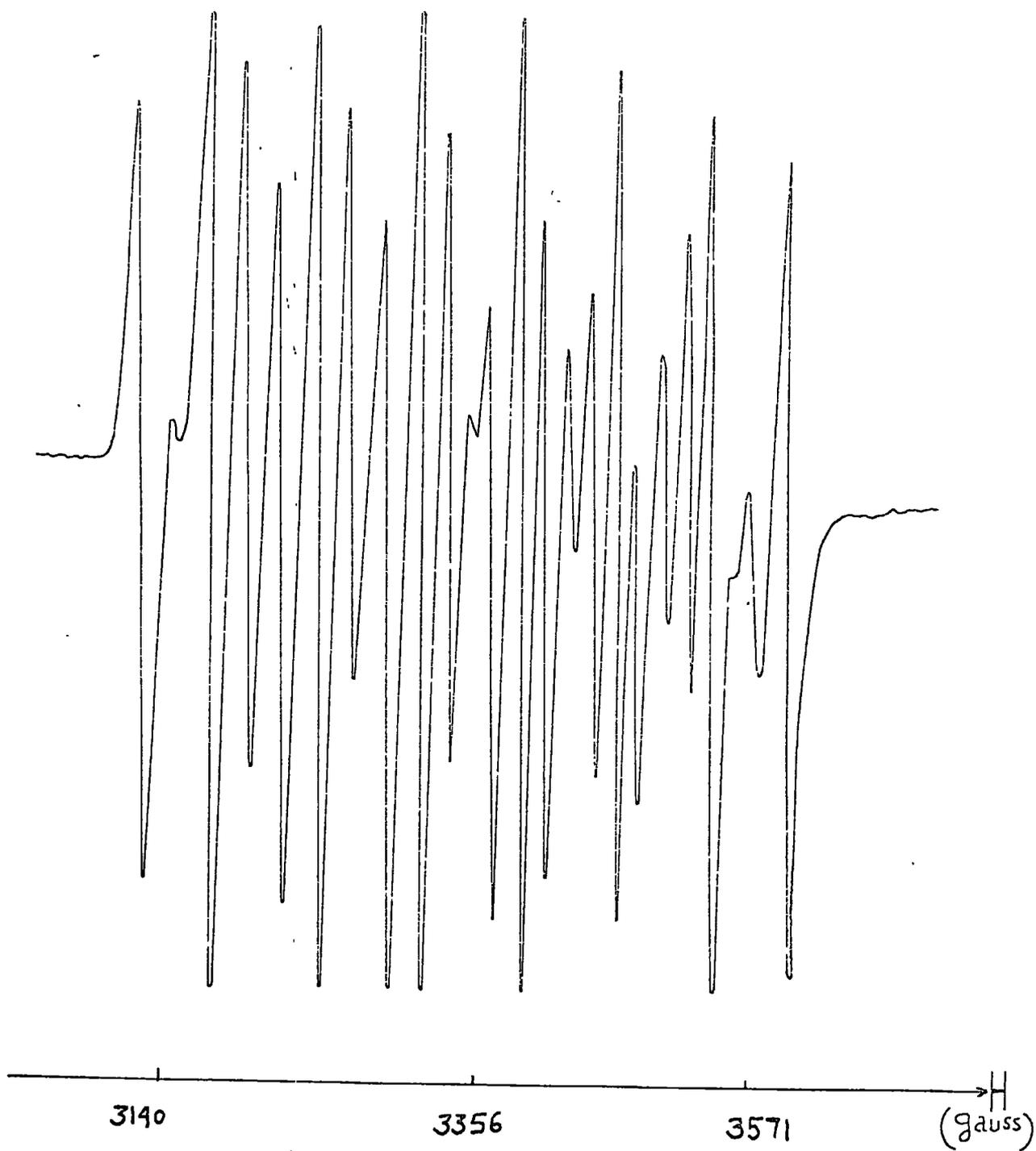
Fig. (5.19)  Electron spin resonance of $Mn^{2+}$ in a twinned (cubic) ZnSe crystal  before annealing.
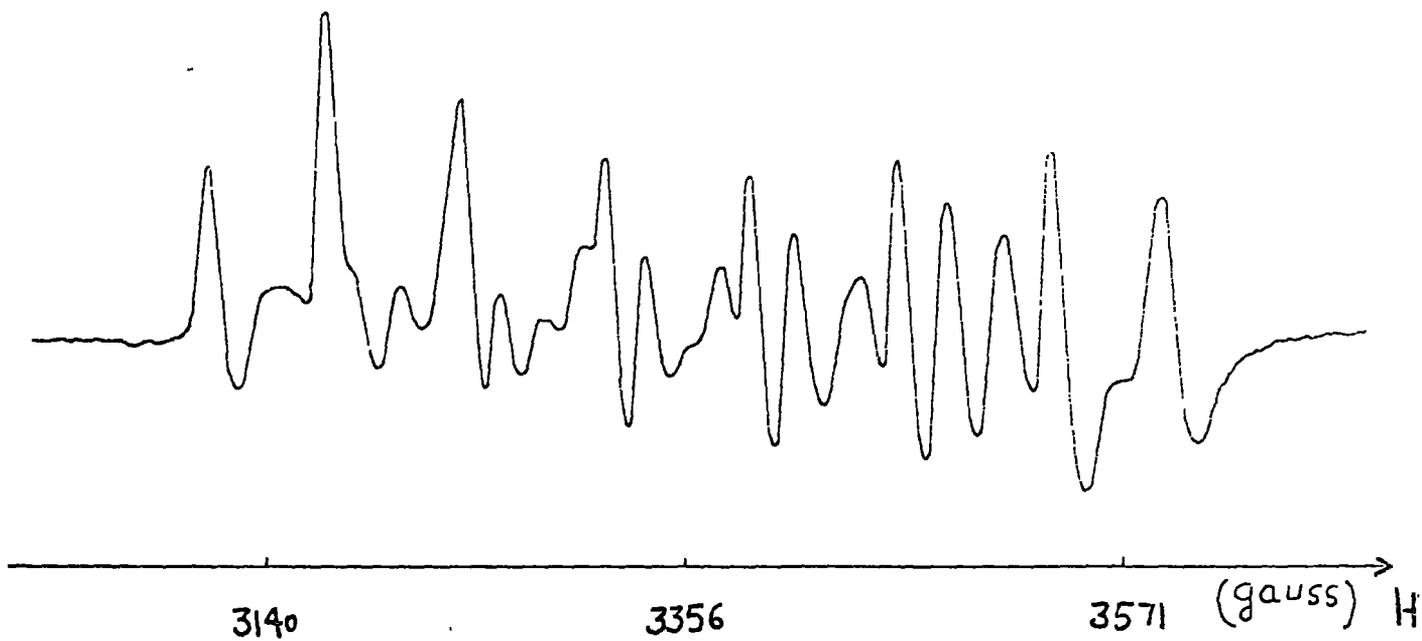
Fig.(5.20) Electron spin resonance of $Mn^{2+}$ in a ZnSe crystal [ as in Fig.(5.19) for the same orientation and amplification ] after annealing in molten zinc. As a result of dipole-dipole interaction the lines are broadened and the overall shape of the spectrum is distorted .
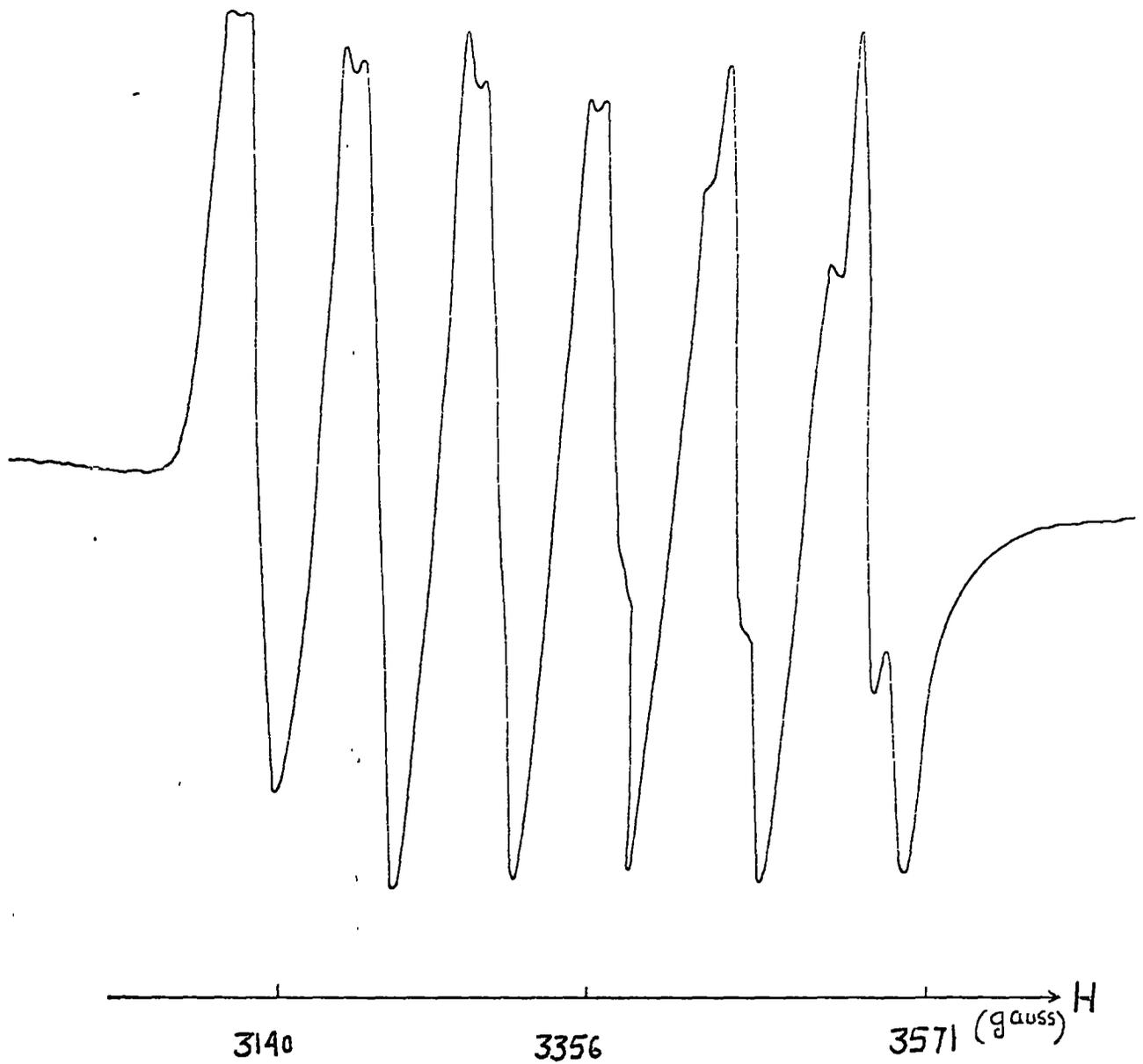
Fig.(5.21) Electron spin resonance of Mn$^{2+}$ in a ZnSe crystal [ as in Fig.(5.20)] at 77K for the orientation H∥[110] .
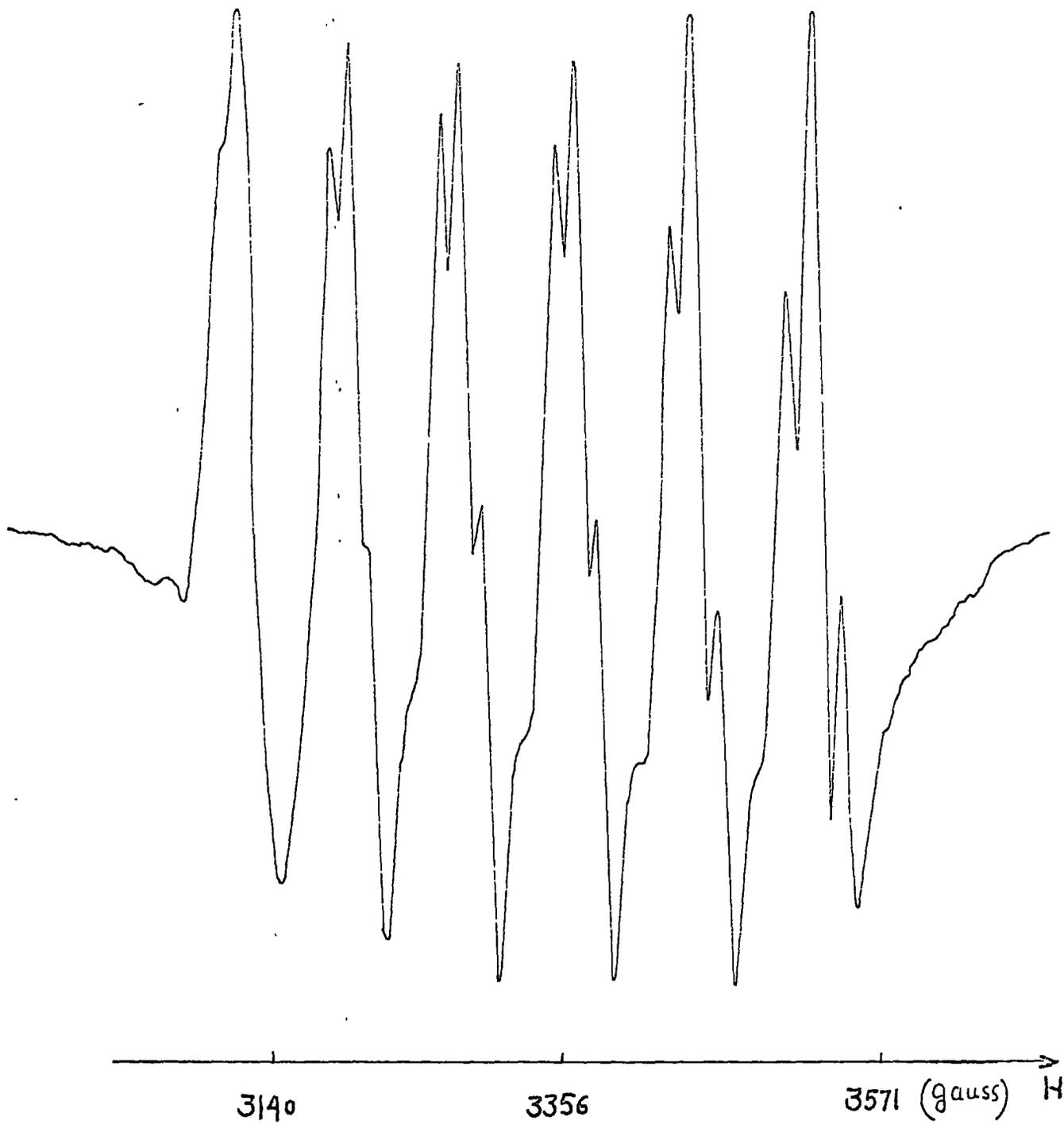
Fig.(5.22) Electron spin resonance of $Mn^{2+}$ in a ZnSe crystal [as in Fig.(5.21) but five times more amplification] after annealing in molten zinc for the second time.

carrier concentration, produces a slight broadening of the ESR lines as can be seen in Figure (5.20). When the sample is annealed for the second time, at the start the overall Mn concentration is lower than the original concentration before annealing. Again, during the annealing process Mn diffuses out of the sample, but this time because the overall concentration is relatively low and is being reduced all the time, not only Mn aggregates do not occur, but also any such collection existing would gradually break up, thus removing the small amount of dipole-dipole interaction present. The ESR absorption spectrum would now be more detailed, i.e. it would be better resolved as can be seen in Figure (5.22). Thus whether Mn aggregates or not in a ZnSe:Mn sample as it is annealed, depends firstly on the Mn concentration and secondly on the length of time the sample is annealed.

In the context of the above discussion it is important to note that Mn cannot be incorporated in ZnSe by diffusion. Thus in a number of experiments attempts were made to incorporate Mn in ZnSe by diffusion at $950^{\circ}C$ but with no success. Similarly no diffusion of Mn into ZnSe took place when Mn was added to Zn in which the ZnSe sample was annealed for five days at $850^{\circ}C$.

## 5.14   Polymorphism

ZnSe:Mn crystals produced at $1300^{\circ}C$ were found to have a mixed cubic-hexagonal structure. A comprehensive programme of annealing was undertaken to see if the hexagonal phase could be eliminated, as is usually achieved in flow crystals. It was found, however, that the hexagonal phase could not be annealed out, instead its proportion increased when the samples were annealed at $1050^{\circ}C$. This is the first report of the cubic $\longrightarrow$ hexagonal phase transition in ZnSe.

In this section polymorphism is briefly considered, followed by a short discussion of reported phase transitions in some of the II-VI compounds. In Section 5.17 observations of the cubic $\longrightarrow$ hexagonal phase transition in ZnSe are reported and an explanation offered.

Several elements and many compounds can exist with more than one crystalline structure because of changes in the arrangement of their atoms. In principle, just as any substance can exist in the solid, liquid or gaseous state depending on the pressure and temperature prevailing, so also a solid formed from the melt or vapour phase may crystallize in more than one possible structure depending on the temperature-pressure conditions.

Polymorphism in compounds (an allotropy in elements) was originally thought to be rather rare. Most of the investigations were carried out at atmospheric pressure, and it was found that transition from one structure to another took place at a definite temperature $T_t$, called the transition point. The structure A, stable at temperatures below $T_t$, was called the low-temperature modification, and structure B, stable at temperatures above $T_t$, was called the high-temperature modification. Furthermore, it was found that whereas A could not exist at temperatures above $T_t$, structure B could exist at temperatures below $T_t$, in a metastable state. Also, two types of polymorphic transitions were differentiated; one reversible, and the other irreversible. In some compounds it was found that structure A changed to B when heated, with the reverse occurring on cooling. Whereas, in some other substances, the transition from one modification to another was found to be irreversible; one modification was thought to be unstable in the entire temperature range.

However, all these observations did not take into account sufficiently the effect of pressure. For instance, a modification which is unstable in the entire solid-state temperature range of a compound at atmospheric pressure, may turn out to be quite stable at high pressures. As in processes involving changes of state, polymorphic transitions must also be considered in the context of a temperature-pressure framework. This became obvious as soon as thermodynamics was applied. Later on, with the advent of sophisticated X-ray techniques with which the structure of a sample could be investigated at different pressures, polymorphism was recognised to be a quite general phenomenon.

Experimentally, polymorphic phase transitions bear a very close resemblance to changes of state, for instance, to the phase transition of a solid to the liquid state (melting). In both kinds of transition there is a discontinuous change in the volume, with evolution or absorption of heat at the transition point.

Thermodynamically, the use of two concepts, Gibb's phase rule, and Gibb's free energy, can clarify the basis of polymorphic phase transition very readily.

Since two polymorphic modifications can under certain conditions of temperature and pressure establish equilibrium with each other, they must therefore obey Gibb's phase rule,

$$F = C - P + 2$$

where F represents the degrees of freedom of the system (i.e. the number of the parameters of the system that can be varied arbitrarily, consistent with the maintenance of equilibrium), C is the number of components of the system and P is the number of phases in the system. For a polymorphic transition $P = 2$ and $C = 1$ so that $F = 1$, that is there is only one degree of freedom in the system. In other words,

if the pressure is kept constant, the transition must set in at a definite temperature, and conversely, if the temperature is kept constant the transition must set in at a definite pressure. Moreover, according to thermodynamics the state of stable equilibrium in a system is characterized by a minimum in the Gibb's free energy G which is given by

$$G = E - TS + PV \qquad \qquad ---(29)$$

where E is the internal energy, T the temperature, S the entropy, P the pressure and V the volume. This means that when a substance under a given set of temperature-pressure conditions, has a number of polymorphic modifications (or phases), the modification with the least amount of free energy will be the most stable phase. All other modifications will tend to transfer into it, i.e. the other modifications are metastable. As the temperature of the substance is changed, the free energies of the possible phases of the substance also change so that at a certain pressure, two phases may establish equilibrium with one another when they have the same free energy, i.e. when

$$G_1 - G_2 = 0 = (E - TS + PV)_1 - (E - TS + PV)_2 \qquad ---(30)$$

Generally when the temperature of a solid is altered under constant pressure, the change in the volume is negligibly small so that (30) can be written as

$$0 = (E - TS)_1 - (E - TS)_2 \qquad \qquad ---(31)$$

At absolute zero, (31) simplifies to

$$E_1 = E_2$$

where E = the internal energy, at T = 0 is given by

$$E = \tfrac{1}{2}h\nu - U$$

where U is the lattice binding energy and $\tfrac{1}{2}h\nu$ is the zero-point energy.

Thus at absolute zero, the polymorphic form which has the greatest lattice energy, also has the lowest free energy and is the stable phase. As the temperature is increased, the internal energy increases. In addition the term TS becomes more and more significant so that the minimum free energy becomes dependent on the difference between these two terms. Generally, however, the free energy (E - TS) decreases as the temperature is increased, as can be seen by differentiating

(E - TS) = N as    dN = dE - TdS - SdT

but    dE = TdS - PdV in a reversible change in which heat is absorbed, and since dv = 0, then dN = -SdT, i.e.

$$\frac{dN}{dT} = -S \qquad\qquad ----(32)$$

i.e. the free energy decreases at a rate which is equal to the entropy.

The significance of (32) can be seen more fully by considering a substance which can exist in two different crystalline forms, a low-temperature structure, and a high-temperature structure which has a high entropy, and at absolute zero a higher internal energy. As the temperature is increased the free energy of the low-temperature phase decreases at a rate of

$$\left(\frac{dN}{dT}\right)_L = -S_L \qquad\qquad ---(33)$$

and that of the high-temperature phase at a rate of

$$\left(\frac{dN}{dT}\right)_H = -S_H \qquad\qquad ----(34)$$

Since $S_H > S_L$, the free energy of the high-temperature phase decreases at a faster rate, so that at a critical temperature $T_t$, the high-temperature phase would have a lower free energy than the low-temperature phase, and therefore becomes the stable phase. At this temperature an abrupt increase in the internal energy of the substance occurs. This

increase corresponds to the latent heat of transformation and is given by

$$\Delta E = T_t (S_H - S_L)$$

$$= T_t \Delta S$$

$$- --(35)$$

Experimentally, the free energy of a solid is reflected in its vapour pressure which depends on the escape of atoms (or ions) from the solid. In a crystal with two phases present, the stable phase having the smaller free energy would have a lower vapour pressure than the less stable phase.

Phase transitions of the type considered above which involve sudden changes in the crystal structure and discontinuous changes in the internal energy and other thermodynamical properties, are usually referred to as phase transitions of the first order. In contrast, there is another kind of phase transition which does not involve a sudden change in the structure and discontinuous change in internal energy. In these, the transition is spread over a temperature interval, and occurs at an increasing rate up to some limiting temperature T, when the transition stops. Generally, this kind of transition is one of order-disorder. At absolute zero, there is complete order in the structure, but as the temperature is increased the structure is gradually disturbed and becomes disordered. The disorder increases with temperature at an increasing rate up to a critical temperature when complete randomness in the structure is achieved.

Thermodynamically, the polymorphic form of a compound which has a minimum Gibbs free energy is the most stable one. In the case of a temperature-dependent transformation under a negligible pressure, an increase in temperature produces a new polymorphic form with a higher internal energy and entropy. Generally, for a given compound there are a large number of ways in which its atoms can be arranged with crystalline regularity. Each such arrangement is a possible polymorphic

modification of the compound, with each having its own potential

energy of configuration. At absolute zero, of all the possible

structures, the one with minimum configurational energy (which is most

stable) can be expected. Then, on this basis as the temperature is

increased one may expect the compound to take up a series of possible

intermediate structures with each having a configurational energy

corresponding to the temperature. In practice, however, not all the

possible structures are realized for the following reasons.

Basically a crystalline compound consists of a large number of

continuously linked atoms (or ions) in which the coupling (bonding)

between the nearest neighbours is very strong, i.e. the crystal can be

looked upon as a system of coupled oscillators in which each atom has

three degrees of freedom. Moreover, the atoms in the system may couple

in different ways to produce various modes of vibrations for the system

as a whole. Thus a crystalline system with m atoms may have (3m-6)

possible modes of inner vibrations (excluding three degrees of trans-

latory freedom and three degrees of rotation freedom of the crystal

system as a whole), with each mode of vibration having a different

thermal energy depending on the symmetry of the crystalline system.

However, not all the (3m-6) modes of vibrations are permissible in

every possible structure. In short, if this were not the case, there

would not be polymorphism, because otherwise, at any temperature the

crystalline system would be able to set up vibrational modes of maximum

(thermal) energy corresponding to the temperature. The structure as

a whole would then be one of minimum Gibbs free energy at each and

every temperature. However, the vibrational modes of a crystalline

system are controlled by the symmetry of the structure and only certain

definite modes are possible in any given structure. If the structure

of a compound is of lowest configuration energy and its symmetry is

such that it permits vibrational modes of maximum energy corresponding

to a temperature range, then in that temperature range there would be

an absence of polymorphism, since the system as a whole is one of

minimum Gibbs free energy.  The temperature range may be a wide one,

i.e. from O K up to melting point, in which case the compound would

have only one stable configuration, although metastable configurations

are possible and may occur, for instance, when the compound is produced

from the melt or vapour phase.  In such a case the process of annealing

would be irreversible, i.e. as the temperature is increased the meta-

stable phase disappears without its reappearance on cooling.

Similarly, if a compound is characterized with a dominant mode

of vibrations of large energy in a temperature range, then the structures

which are not of appropriate symmetry necessary for that mode of vibra-

tion, would be excluded.  This accounts for the absence of possible

structures of increasing configuration energy as the temperature is

increased from absolute zero.  The structure of a compound, as was

mentioned before, at absolute zero is one of lowest configuration energy,

and the symmetry is such that as the temperature is increased, the

structure remains consistent with the dominant mode of vibrations.

As the temperature is increased, the amplitudes of thermal vibrations

increase, resulting more and more in strained bonds.  Before this could

cause total disruption of the bonds, another situation may develop.

If there is another structure whose symmetry is such that it permits

modes of thermal vibrations of higher energy with less strain in the

bonds, then the old structure would tend to transfer itself into it.

This new structure would have a greater entropy than the low-temperature

form, and it would tend to have more open spaces available for the

enhanced vibrations of the atoms (or ions). One of the ways by which this may occur is for the high-temperature modification to take up a structure of lower co-ordination than that of the low-temperature; since a configuration of lower co-ordination gives a greater freedom of movement to the atoms. This obviously would result in the high-temperature modification having a smaller density.

In general, when atoms can assume several possible co-ordinations, there would be a tendency for them to display low co-ordination in crystals formed at high temperatures and high co-ordination for crystals formed at low temperatures. In practice, however, there are many exceptions to this, notably in Fe and Na, in which the high-temperature forms appear to favour high co-ordination. In principle, a structure of high co-ordination is one of lower internal energy and entropy, and is thereby stable at low temperatures, whereas a structure of lower co-ordination is of higher internal energy and entropy.

The rate at which a structure transforms into a new one, depends on many factors and appears to be rather complex. Experimentally different polymorphic transitions have been found to occur with different speeds ranging all the way from transformations which are instantaneous to those which are extremely slow. Apart from temperature and pressure, impurities, crystal size, and structural defects are amongst the factors which have to be considered. Temperature is obviously the most important factor, as basically the mobility of atoms in a solid depend on it. Generally in polymorphic transitions one can consider an energy barrier opposing the transition. Then the rate of a polymorphic transition would depend on the number of atoms that temperature endows with energy in excess of this energy barrier. In other words, a certain activation energy $\gamma$ is required to cause the transformation to proceed, and the

speed of the transformation would then depend on a factor of the form $e^{-\gamma/kT}$.

From the above qualitative reasoning, it is now clear that a modification which is metastable in a certain temperature and pressure range, would continue to exist under those conditions, if the activation energy supplied is not sufficient to cause the structure to transform, i.e. the modification continues to exist beyond its stability region as long as the rate of transformation is negligibly low. The rate of transformation would obviously depend on the energy barrier and is thus liable to vary considerably from one transformation to another. In compounds with large energy barriers, metastable states would tend to occur regularly, whereas in configurations with a relatively low energy barrier, metastable states may be absent.

Theoretically not a great deal can be done to calculate $\gamma$. However, theories have been advanced to determine the probability of nucleation of one crystal phase $\alpha$ with another $\beta$, and the rate of advancement of the $\alpha-\beta$ interface (41,42,43). But, these theories assume ideal (perfect) crystals and structures, whereas it is established that nucleation of the $\alpha$ phase is very sensitive to structural defects and impurities (44), so that the theoretical calculations hardly apply to real crystals (45,46,47).

Often the existence (or addition) of the desired phase accelerates (sometimes quite considerably) a polymorphic transition by providing the necessary nuclei for the formation of the new phase. Also it is well known that in many cases the velocity of transformation depends on the crystal size. For instance, certain transformations proceed faster when the material is a fine powder, and in certain other cases the transformation is more rapid when the material is a single crystal (41,47).

Furthermore, there is a considerable amount of experimental evidence
indicating that traces of some impurities affect the velocity of phase
transformation quite considerably (48,49). In some cases the impurities
appear to stabilize the unstable phase by retarding the velocity of
phase transformation, whereas in others, they appear to act as catalysts
and accelerate the change. For instance, the cubic form of ferric
oxide ($Fe_2O_3$) which when pure transforms into the rhombohedral form at
$300^{\circ}C$, can be made stable up to $800^{\circ}C$ by adding traces of sodium ferrite
(50). On the other hand, the change from white phosphorus to red is
accelerated by the addition of a small amount of iodine. Clearly any
theoretical calculation must,if it is to be realistic,take into account
the unavoidable effects of impurities and structural defects.

Structurally, two polymorphic phases differ only in the arrange-
ment of their atoms. The energy difference between two polymorphs is
thus largely concerned with the forces between the same atoms but which
are bound in different configurations. On this basis according to
Burger (47), polymorphic transitions can be divided into four types.
These are: (a) transformations of first co-ordination, (b) transforma-
tions of second co-ordination, (c) transformations involving order-
disorder, and (d) transformations involving a change in the type of
binding. Of these, only (a) and (b) are of immediate relevance to
this thesis.

(a)    Transformations of First Co-ordination

These transformations involve a structural change in which the
primary co-ordination of some of the atoms changes. One way of
achieving this is by disrupting all the bonds and reconstructing another
altogether different structure. Such a process would involve a very
drastic change and would have a very large energy barrier. A

reconstructive transformation of this type would obviously be very
sluggish, and no symmetry relationship would necessarily exist between
the polymorphs.

Another way in which a transformation of first co-ordination
may be effected in some relatively simple structures is by a differ-
ential dilation of the whole structure.  This involves a homogeneous
distortion in which the structure expands along an axis of symmetry
(which would be preserved) and contracts at right angles to it.


(b)    Transformations of Second Co-ordination

In these transformations the nearest neighbour configuration
remains intact, but the arrangement of the non-nearest neighbours alters,
i.e. the difference in the polymorphs arises from the way in which the
identical first co-ordination units are linked.  Since the most
important contribution to the energy of a crystal is from the first
co-ordination bonds, a transformation of this type is expected to
involve a relatively small change in the co-ordination energy.  However,
the ways in which the actual transformation occurs may differ and as a
result of transformation of this type may be sluggish or fast.  One way
in which such a transformation may be achieved is by disrupting all the
bonds (including the first co-ordination bonds) and re-establishing
them in another structure in such a way that the net change is in the
configuration of the non-nearest neighbours.  In such a transformation
the energy barrier would be of the order of the first co-ordination and
hence the transformation would be sluggish with no necessary symmetry
relationship between the polymorphs.

Another way in which a transformation of second co-ordination
may be effected is by distorting the structure into another having a

different non-nearest neighbour arrangement. Such a "distortional" or "displacive" transformation would have a relatively small energy barrier and would tend to be rather fast.


## 5.15    Polymorphism in the II-VI compounds

Many of the II-VI compounds such as CdS, CdSe, ZnS, ZnSe etc. can crystallize in the zincblende and the wurtzite structure, depending on the manner in which they are produced. There is also a third poly-morphic modification, with the rocksalt-type of structure, which so far has only been produced under very high pressures.

With the four compounds listed above it appears that in CdS and CdSe the dominant structure at room temperature is hexagonal wurtzite, whereas in ZnS and ZnSe, it is the cubic zincblende. The zincblende and the wurtzite forms appear in the first and the second groups of these compounds as metastable states. From this the question arises as to whether these metastable modifications are really metastable in the entire temperature range (from O K to the melting point) or is it that there is a definite temperature range in which the metastable form of any of these compounds could exist as a stable phase. Towards this end the available information concerning CdS and ZnS (as representing the Cd and the Zn group) is considered here.

CdS    Generally, CdS crystals produced from the vapour phase (including the various chemical transport methods), and from the melt, are hexagonal. The zincblende modification has only been produced at relatively low temperatures by chemical precipitation methods (51-55) and then in the form of very small particles (with an average diameter of a fraction of a micron). Ulrich et al (52) succeeded in transforming their zincblende samples into hexagonal by annealing at a temperature between 700 and 800$^{\circ}$C,

while Rittner et al (54) achieved the same result by annealing their

samples at 500°C. Ahlburg et al (55) found that satisfactory phase

transformation of their samples occurred at a temperature between 400

and 450°C in agreement with the temperature of 450°C found by Lind and

Bube (56). As far as is known there is no report of any hexagonal CdS

having been transformed into cubic as a result of annealing. It is

suggested, however, that the zincblende form is the stable modification

at temperatures below 20°C (54,55). If this is the case, then there is

no chance of converting hexagonal CdS into the zincblende form by

changing the temperature only, since at low temperatures the transforma-

tion rate can be expected to be almost infinitesimal.

Phase transformation of CdS (CdSe and CdTe) under high pressure

was first reported by Edwards et al (57) who investigated the shift

of the absorption edge of wurtzite samples with pressure. At a

pressure of about 27000 kg/cm$^2$ a discontinuity in the shift of the

absorption edge of CdS with pressure occurred, and from this and sub-

sequent work (58) it was suggested that the wurtzite structure had been

transformed into zincblende at high pressures. However, Rooymans (59,60)

and Kabalkina et al (61) investigated the structures of their samples

at high pressures using X-ray techniques and found that a phase transition

did occur at high pressures, but the structure obtained was not of zinc-

blende type but that of rocksalt. In essence a transition involving

wurtzite $\longrightarrow$ rocksalt under high pressures is more likely because of

the increased co-ordination (from four in the tetrahedral bonding to six

in the octahedral) than the transformation wurtzite $\longrightarrow$ zincblende, in

which the two structures of CdS have nearly the same density.

Edwards et al had also observed that on removing the high

pressure, reverse phase transformation occurred at about 10 K bars, but

the absorption edge did not return to its original position when the excess pressure had been removed, even after several days. However, they paid insufficient attention to the phenomenon. Manca et al (62) on the other hand, carried out similar experiments and spectroscopically determined the absorption spectra of their CdS sample before and after a pressure cycle. From their measurements of the positions of the absorption edges they showed unambiguously that the absorption edge after a pressure cycle corresponded to that of a zincblende structure. Moreover, X-ray investigations (59-61) are in agreement with this interpretation. The picture that emerges is therefore as follows. In CdS (CdSe and CdTe) phase transformation to the rocksalt-type of structure occurs at high pressures. On reducing the pressure the rocksalt structure starts transforming into zincblende at a pressure of approximately 10 kbars, and disappears at a pressure of 1 bar. The structure obtained at the end is mainly of zincblende with a small admixture of wurtzite.

ZnS    Phase transformation of zincblende ZnS into wurtzite was first reported by Allen et al (63) at a temperature of about $1100^{\circ}$C. From a series of experiments with naturally occurring samples of wurtzite and zincblende ZnS, Allen et al determined a transition temperature of $1020 \pm 5^{\circ}$C. Furthermore, they investigated the effect of impurities such as Fe on the transition temperature and found that the presence of Fe increased the transition temperature. Addamingo and Aven (64) produced hexagonal ZnS crystals from the melt, and in contrast with the reported temperature of $1020 \pm 5^{\circ}$C, obtained a transition temperature of $1150^{\circ}$C in a series of eight samples they investigated. Impurity analysis of these samples showed them to be of very much higher purity than the naturally occurring ZnS minerals used by Allen et al.

Addamingo et al therefore suggested that the reason for the difference

between their transition temperature and that reported by Allen et al,

is to be found mainly in the higher purity of their samples.  Kremheller

(65) on the other hand, working with vapour grown samples observed con-

version of zincblende ZnS into wurtzite at 975$^{\circ}$C in the presence of

chlorides, but no transformation even at 1170$^{\circ}$C, in the absence of

chlorides.  Furthermore, in wurtzite crystals Kremheller observed the

appearance of zincblende phase at 1130$^{\circ}$C about 110$^{\circ}$C above the transition

temperature reported by Allen et al.  The effect of pressure on the

absorption edge of ZnS (and ZnSe) was first investigated by Edwards et al

(57,58).  In contrast with results obtained for CdS, no discontinuity

in the shift of the absorption edge with pressure could be seen in the

pressure range investigated.  Samara and Drickamer (66), however,

investigated the effect of pressure on the resistivity and found that

the resistivity of cubic ZnS samples dropped sharply by more than 6

orders of magnitude in ZnS at a pressure of about 240 kbars.  This

sharp drop in the resistivity was taken to be a sign of transformation

to a different phase (from zincblende);  either to a conducting liquid

state or a metallic state.  The possibility of ZnS transforming to the

liquid state at 240 kbars was rejected because of the appearance of the

sample when the pressure had been removed.  The observation of a sharp

drop in resistivity in ZnS (and ZnSe) has been confirmed by a number of

other investigators (67,68) but as yet no explanation of the suggested

metallic state has been given.  However, Smith et al (69,70) in 1965

investigated the structure of the high pressure phase using X-ray

techniques and from the X-ray diffraction lines obtained confirmation

that a phase transformation does occur at high pressures, but they

assert that the high pressure phase has a rocksalt-type of structure.

The diffraction lines obtained by Smith et al for samples at high pressures were very weak, which was attributed to the non-ideal conditions of the sample and the experiment.

One report which does contain a rather surprising result is due to Cline et al (71). There it is stated that hexagonal ZnS transformed into zincblende under pressure. No experimental detail or evidence is given to illustrate or support this claim. Nor is there any reference to any exact pressure at which this transformation is supposed to have occurred, apart from the mention of a pressure range from 0-45 kbars. This result is surprising since the wurtzite form of ZnS is denser than the zincblende (72), and generally with increasing pressure a given structure is transformed into a denser one. Similarly Van Weiringen (73) interpretation of the ESR spectrum of ZnS:Mn samples obtained when the sample was under a high pressure, is very questionable.

## 5.16 Polytypism

The stacking of Zn-S double layers (denoted by A, B, C) in hexagonal ZnS along the C-axis has the sequence

$$AB\ AB\ AB \longrightarrow C\text{-axis}$$

and in the zinceblende structure the sequence can be written as

$$ABC\ ABC\ ABC \longrightarrow [111]$$
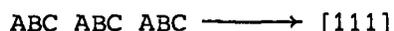
These two structures, with identity periods of 2 and 3, are the two simplest and most common close-packing structures. However, the identity period need not necessarily stop at 3 layers. In ZnS, for instance, a possible six-layered structure is

$$|\ ABCACB\ |\ ABCACB\ |\ .$$
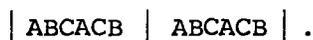
To such a relatively long-period structure the name polytype has been given.

Superficially, polytypism can be regarded as a one-dimensional kind of polymorphism which may occur in some close-packed and layered structures. In these structures geometrically the first co-ordination of some atoms (or ions) can be satisfied in more than one way (for instance equivalent in cubic and hexagonal close packing), with the result that the various modifications, have the same nearest neighbour relationship but differ in the second and/or higher co-ordinations. In polytypism, the various polytypes of a substance differ in structure only along the stacking axis, with the consequence that the unit cell dimensions are constant in two directions (in the stacking plane), but have different heights (the height is an integral multiple of the unit cell). For instance, in ZnS the height of the unit cell in the 2H polytype is 6.246 $\overset{o}{A}$ and that in the 10 H polytype is 31.20 $\overset{o}{A}$.

Though polytypism may be looked upon as a one-dimensional kind of polymorphism, in many respects it is entirely different. For instance, the polymorphic modifications of a compound normally form under different conditions of temperature and pressure, with each modification having its own range of thermodynamical stability and in many respects its own properties, i.e. the polymorphs are distinct phases which obey thermodynamical rules. With polytypism, in the case of SiC for instance, all the modification, except the cubic and the 2H modification, appear to form under the same conditions of temperature and pressure (74,75), and the different polytypes do not undergo transitions from one into another at any temperature or pressure (76). Similarly in ZnS the polytypes cannot be changed from one into another.

Generally the structure of two polytypes of a substance differ from each other because of the different ordered periodic stacking faults in them. The energy of a stacking fault is, however, very small as it produces a difference in higher co-ordinations only. Consequently, the

difference in the internal energy of two polytypes is expected to be very small.

The II-VI compounds mentioned on page 137 can be produced in either of the two common close-packed structures; cubic zincblende or hexagonal wurtzite. Because of this, at first sight, one may expect polytypism to be widespread amongst them. However, with the exception of ZnS, polytypism seems to be toally absent in the other compounds mentioned. It must be remembered that though, in principle, these compounds can be produced in either of the two structures, with the exception of ZnS (and to a lesser extent ZnSe) usually one of the two structures cannot be produced as readily as the other.

Stacking faults and polytypism in ZnS crystals grown under known conditions were first extensively studied by Strock and Brophy (77). Since then more than 150 new polytypes have been observed and studied (78,79). Amongst the theories put forward to explain polytypism in ZnS (80,81) the recent one due to Alexander et al (79) seems to be most satisfactory. To review it briefly it is, however, necessary to mention the prevalent crystal growth theory first.

The theory of the growth of a perfect crystal (from the vapour phase) at low supersaturation predicts a negligibly small growth rate. This has been generally found to be in disagreement with the experimental observations on real crystals. In 1949 Frank (82) suggested that any theory of crystal growth must take into account the fact that real crystals are not ideally perfect as had been assumed in the theory; they contain point defects, dislocations, stacking faults etc. In 1951 he put forward a theory of crystal growth for real crystals involving screw dislocations (83). According to this theory, in the early stages of crystal growth a screw dislocation emerges on the surface of a

crystallite and provides it with a step necessary for crystal growth. This step (due to the screw dislocation) is self-perpetuating, i.e. when one or more layers of atoms (or ions) have been laid down on the crystal surface, the step still remains. The difference between this theory and the earlier nucleation theory for the growth of a perfect crystal is that in the latter, nucleation has to provide a step on the crystal surface which then extends all the way across the crystal surface thereby completing a new layer. After this, nucleation again has to provide another step; this way the crystal grows layer by layer. In Frank's theory on the other hand, once a step has been created by the screw dislocation, it advances by rotating round the dislocation point without having to stop. Frank's theory thus offers a realistic mechanism for crystal growth at low supersaturation, and evidence for the existence of screw dislocations has been obtained from the observed growth spiral patterns on some surfaces of crystals. As to the origin of the screw dislocation, no definite information is available: it may be due, for example, to misalignment of crystallites on the substrate, or to the buckling followed by slip of a very tiny platelet, or due to an inhomogeneous distribution of impurities.

To explain the formation of polytypes several theories have been put forward from time to time. These include theories in which poly- typism was suggested to be related to the impurity content of the crystal (84-86), and theories in which some direct relationship was suggested between polytypism and the rate of crystal growth (87). However, the theories which are prevalent today can be divided into two main groups; statistical theories, and theories based on dislocations.

The statistical theories (88-90) attempt to describe the long- range order in polytypes in terms of thermodynamical considerations.

However, as far as ZnS is concerned, the observed experimental
evidence is in total disagreement with these theories. According to
the theories, each polytype should have a distinct temperature range
of stability. In ZnS more than 150 polytypes have been observed which,
on the basis of the statistical ideas, would mean more than 150
distinct temperature ranges of stability. Similarly the suggestion
put forward by Gobrech et al (91) that some polytypes of ZnS are very
likely to be stable modifications of the compound, is unrealistic,
since a stable modification of a compound should undergo reversible
phase transformations with temperature, and Gobrecht et al certainly
did not observe this in their samples. Finally, in ZnS samples only
structurally related polytypes are found to occur (79) and the statisti-
cal theories cannot explain this at all.

The formation of polytypes by means of dislocations was first
suggested by Frank (92) following the success of his screw-dislocation
theory of crystal growth. According to Frank polytypes grow by means
of a screw dislocation with a large Burgers vector, or else around a
cluster of similar screw dislocations. This suggestion received
experimental support from the observation of growth spirals on the
(000.1) faces of polytypic SiC crystals. Thus in Frank's theory the
formation of a polytypic structure is regarded as a purely growth
phenomenon, and it follows therefore that such a structure has no
themodynamic stability, in contrast with the statistical theories in
which only thermodynamic considerations are regarded as being responsible.
Thus in Frank's theory screw dislocations of different Burger's vectors
create different polytypes in a substance, and when the Burgers vector
is an integral multiple of the height of the parent unit cell, then the
resulting structure will evidently be the same as the basic structure.

To explain polytypism in ZnS satisfactorily, it has been suggested by Alexander et al (79) that the formation of a polytypic structure occurs not during crystal growth, but subsequently, during the cooling down process. It is proposed that in ZnS, hexagonal 2H needles grow around a screw dislocation with a Burgers vector (along the C-axis) which is a multiple of the parent unit cell. The crystal can, therefore, be looked upon as consisting of a set of interleaved helicoidal (00.1) surfaces. If during the cooling down process a stacking fault is created in a region, then with the possible help of thermal fluctuations and mechanical stress, it may expand along the appropriate spiral surface throughout the crystal thus producing a polytypic structure. In support of this theory it is pointed out that it can explain the occurrence of related polytypes in ZnS samples more satisfactorily, and that experiments (43) show that slight heating (to, say 400$^{o}$C) of a hexagonal 2H ZnS crystal produces stacking faults, and that stacking disorders appear even at room temperature as a result of moderate mechanical stresses (94).

From the dislocation theories of polytypism mentioned above, it is very difficult to explain the absence of polytypism in the other II-VI compounds (bearing in mind the fact that in ZnS polytypism seems to be very common). In Frank's theory of formation of polytypes, it is the length of the Burgers vector which is regarded as being responsible. On this basis why should the screw dislocation responsible for crystal growth have a variety of Burgers vectors only in ZnS and not in the other II-VI compounds also? Similarly, in the theory put forward by Alexander et al, why should stacking faults occur during cooling down process only in ZnS, and not, for instance, in CdS as well. The dislocation theories cannot answer this. One suspects that thermodynamic considerations have to be invoked. It could be that a complete

understanding of polytypism needs a theory involving dislocations as well as thermodynamical considerations.

## 5.17   Phase Transformation in ZnSe

ZnSe powder (Derby Luminescence Electronic Grade) was used as the starting material to grow crystals at approximately $1300^{\circ}C$ in a horizontal furnace employing the method described in Chapter 2.  To incorporate manganese in the crystals, elemental  manganese was added to the charge.  Generally each crystal-growth run yielded a boule, some 5 cm long with a diameter of approximately 1 cm which consisted of a number of single crystals.  These crystals were very carefully separated from one another using a minimum of force because there is evidence that mechanical force can start a phase transformation in ZnS (94).  Examination of the single crystals under the polarising microscope indicated that twinning was not particularly common;  out of 18 samples twinning bands could be seen in only 5.  The ESR spectrum of the $Mn^{2+}$ ion in the crystals produced by this method showed that they had a mixed cubic-hexagonal structure with the hexagonal proportion probably no larger than a few percent.  No attempt was made to determine the hexagonal proportion exactly, because it is not known whether the solubility of Mn in the two phases is the same or not.  For instance, Schneider et al (26) in their investigation of the cubic-hexagonal admixture in ZnS obtained different answers for the hexagonal proportion from their analysis of the ESR spectra of the $Mn^{2+}$ and $Fe^{3+}$ ions. Similarly results obtained by Aven et al show discrepancies in the ratio of the cubic-hexagonal admixture in ZnS:Mn between the results obtained from X-ray measurements and those using ESR of the $Mn^{2+}$ ion.

In the ZnSe:Mn samples investigated here no relationship could
be found between the hexagonal proportion and the size of the sample,
or its position in the boule.  On the whole the hexagonal proportion
did not vary much from sample to sample, especially when compared with
the range of variation usually observed in the flow crystals.

In view of the fact that the hexagonal phase can be annealed out
very readily from flow crystals, a comprehensive programme of annealing
was undertaken to investigate the phase transformation in our samples.
Initially samples were annealed at 700°C in vacuum for 10 hours, but
no detectable change in the structure could be observed.  As a result
the annealing time was gradually increased to three weeks, but again
with no detectable change.  The annealing temperature was then increased
in steps of 50°C to 750°C, 800°C etc. to 1050°C.  Each annealing run
lasted for three weeks.  Only annealing at 1050°C produced any alteration
to the ESR spectrum of the $Mn^{2+}$ ion in the sample.  This change indicated
a cubic ⟶ hexagonal phase transformation.  Figures (5.7) and  (5.23)
illustrate the ESR of the $Mn^{2+}$ ion in a sample before and after annealing
at 1050°C for three weeks.  Altogether 10 samples were annealed and
similar results were obtained.  The results show that:

a.   The hexagonal component could not be annealed out, i.e. no

hexagonal ⟶ cubic phase transformation was observed.

b.   The cubic ⟶ hexagonal transformation occurred systematically

in all samples annealed at 1050°C.

c.   Compared with reported data, the phase transformation which took

place was found to be very slow, as can be seen from Figures (5.7)

and (5.23).

In addition to the samples grown at high temperature, ZnSe:Mn
crystals were also grown at 850°C using the iodine-transport method which

M = 5/2

5351    5190    5029

M = 1/2

X11

3571    3356    3140 (gauss)

M = -3/2

1693    1518    1343

M = 3/2

4414    4248    4082

M = -1/2

2635    2464    2292
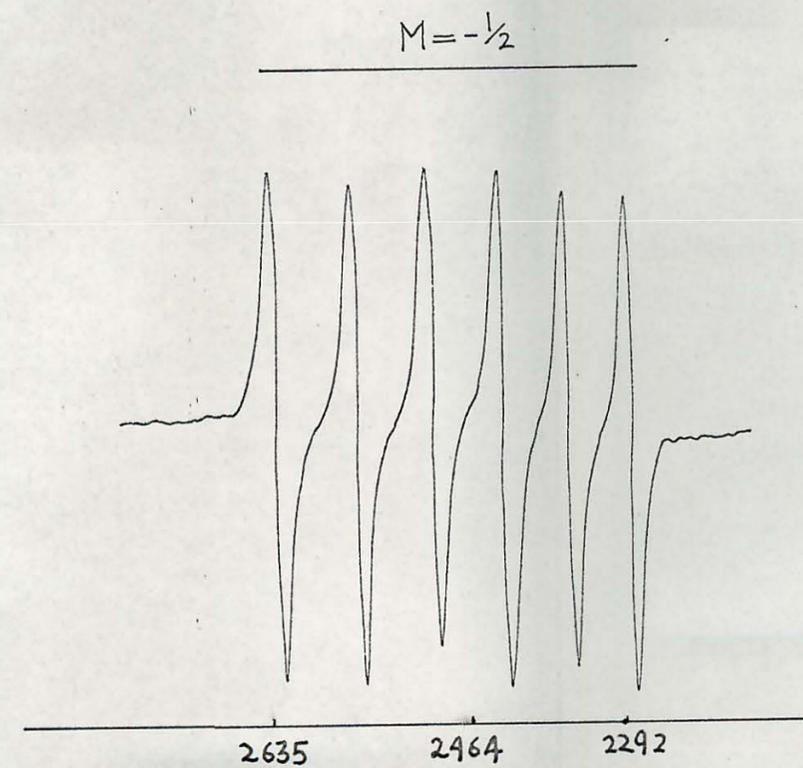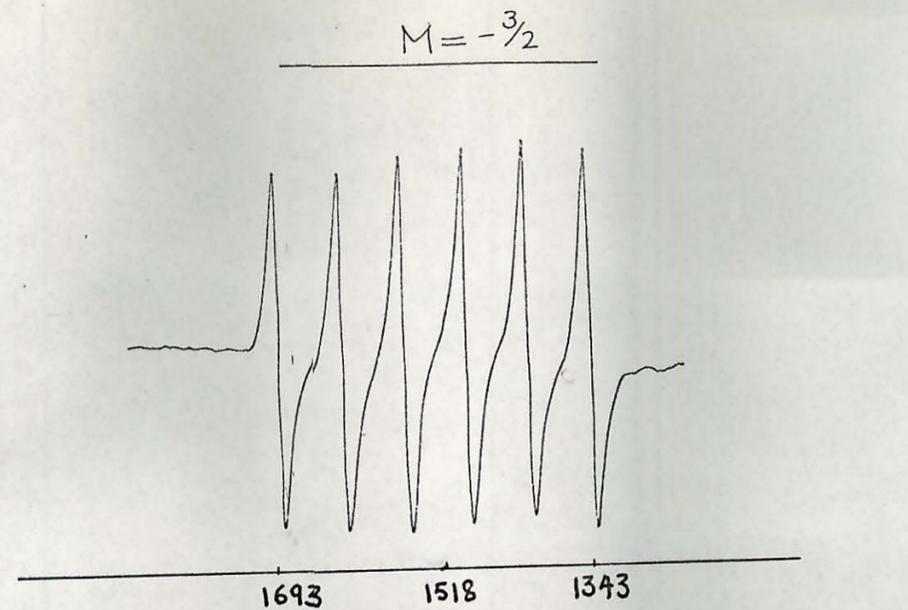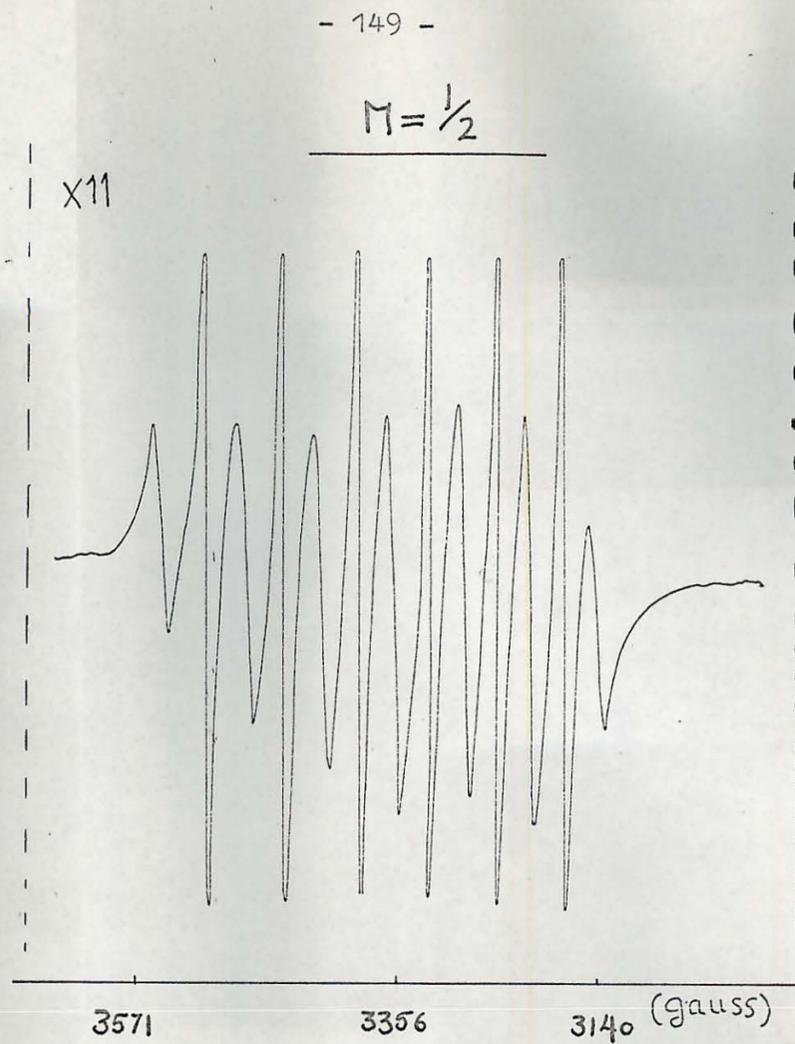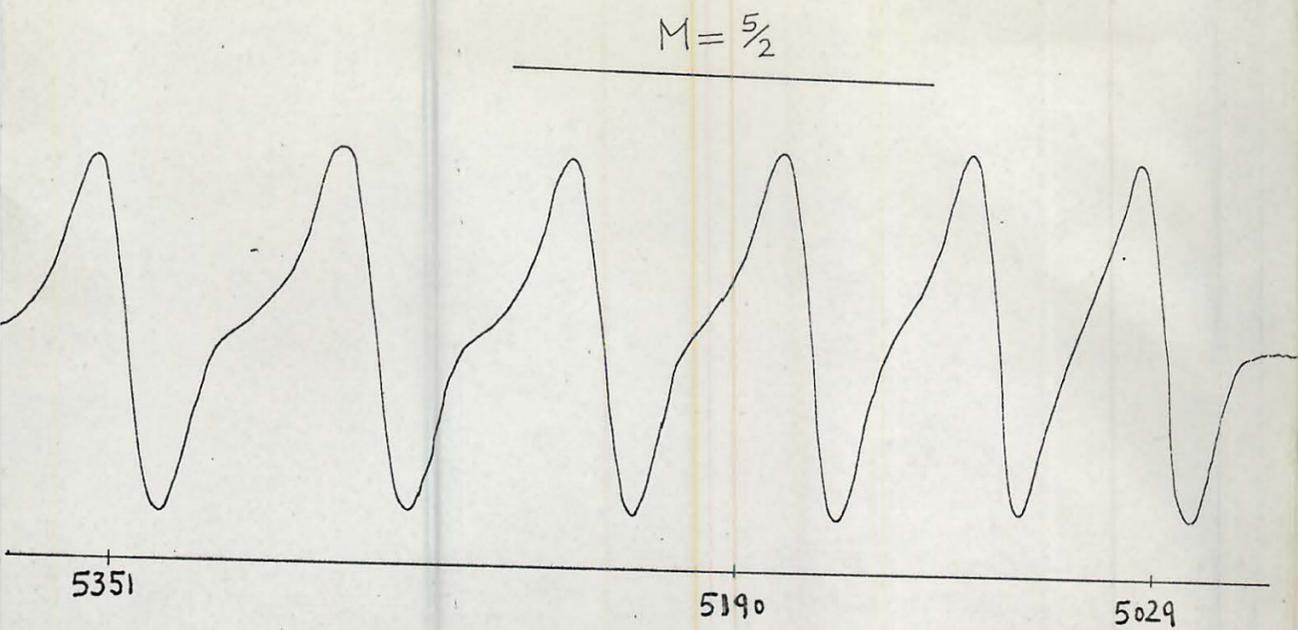
Fig.(5.23) Electron spin resonance of $Mn^{2+}$ in a cubic-hexagonal
ZnSe crystal [ as in Fig.(5.7)] after annealing at 1050C .
Notice the increase in the intensity of the Mn hyperfine
lines in hexagonal ZnSe.

was described in Chapter 2.  The aim in this case was to produce samples
which were entirely cubic, so that the cubic ⟶ hexagonal phase transition
could be investigated in samples with no hexagonal component.

The starting material for these crystals was ZnSe (Derby) powder
which had been baked and sublimed in a stream of high purity argon in
order to reduce the impurity content of the powder.  It is important to
note that no iodine transport of the charge took place when unprocessed
(Derby) ZnSe powder was used as a starting material.

The crystals obtained by this method were of millimetre dimensions
with a body colour lighter than those grown at $1300^{O}C$.  Furthermore the
majority of them had well defined (111) or (110) faces.

The ESR spectrum of the $Mn^{2+}$ ion in these crystals showed that
all of them had a cubic structure.  However, the solubility of Mn in
these crystals was found to be smaller than in those produced at $1300^{O}C$.
This was discussed previously in Section  5.12.

To investigate the possibility of cubic ⟶ hexagonal phase trans-
formation occurring in these crystals, three of them were annealed at
$1050^{O}C$ for three weeks.  However, the ESR measurements indicated no change
in the structure.  A fourth sample annealed at $1100^{O}C$ for three weeks,
was found to have broken up in a number of pieces in the furnace.  The
ESR spectrum of the $Mn^{2+}$ ion indicated a cubic structure in the broken
up pieces.  In view of these results, the conclusion arrived at is that
the cubic ⟶ hexagonal phase transition does not occur in samples
produced by the iodine-transport method.  It is important to remember
that the starting material used in this process was pre-sublimed ZnSe.

Before attempting to explain the observed results, it is relevant
to consider briefly the observations of other authors.

Pashkin et al (96) annealed mixed cubic ⟶ hexagonal samples of ZnSe (which had been produced by the flow-method) at $900^{\circ}C$ in vacuum for 40 hours. Examination under the polarizing microscope showed that the hexagonal phase had disappeared. Williams et al (97) bombarded very thin hexagonal crystals (produced by the flow-method) with 75 KeV $Mn^{2+}$ ions and after annealing at $500^{\circ}C$ in vacuum for about six hours obtained a complete hexagonal ⟶ cubic phase transformation. Similarly, Hartman (98) annealed very small, fine hexagonal and mixed hexagonal ⟶ cubic samples under vacuum and obtained a hexagonal ⟶ cubic phase transformation at temperatures ranging from $400^{\circ}C$ to $800^{\circ}C$. According to Hartman an annealing time of ten hours at $450^{\circ}C$ changes the hexagonal structure of a small sample completely. Also of great significance is his observation that annealing in an atmosphere of HCl can half the time required for the hexagonal ⟶ cubic transition. The factor responsible for the enhanced rate of transition in this case seems to be chlorine since he observed no change in the rate of the hexagonal ⟶ cubic phase transition when samples were annealed in atmospheres of hydrogen, nitro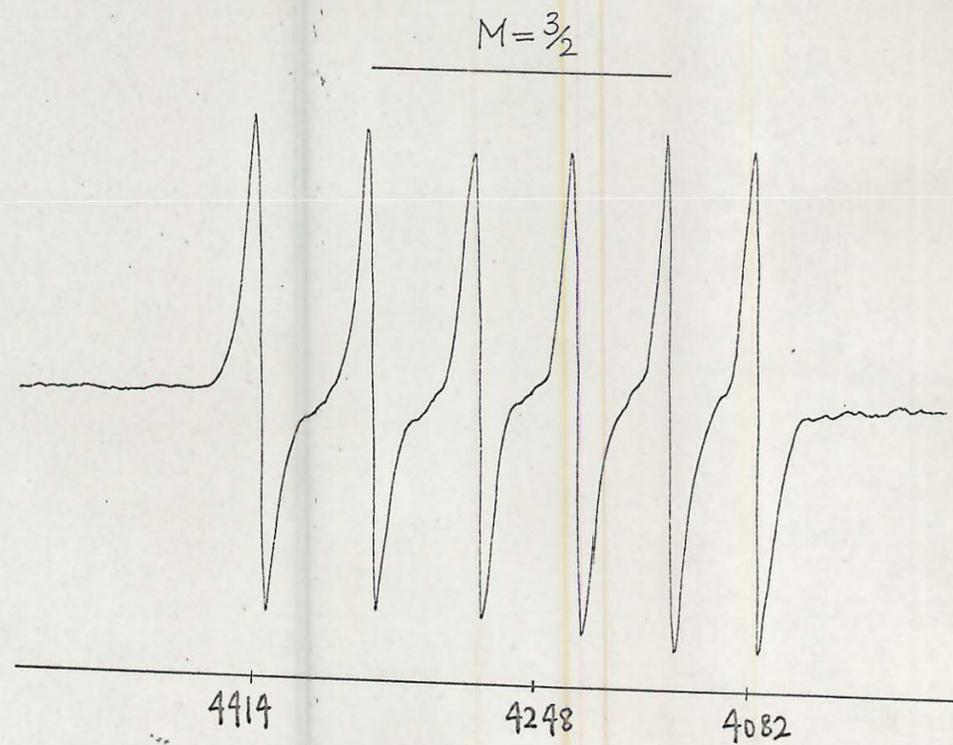gen etc. This result is rather surprising since Hartman had previously, in agreement with the published data of Kallerman (99), found that annealing in an atmosphere of chlorine slowed the hexagonal ⟶ cubic phase transition in ZnS. Considering the similarities between ZnS and ZnSe, one might have expected the effect of annealing in an atmosphere of chlorine to have been more or less the same instead of opposite.

Hartman explained this difference in behaviour between ZnS and ZnSe by suggesting that the hexagonal phase of ZnSe, unlike that of ZnS, is metastable and that it is this metastability which is responsible for the different annealing results. Furthermore, Hartman annealed some

cubic ZnSe crystals at different temperatures in an effort to achieve

cubic ⟶ hexagonal phase transition, but reports that at no temperature

was such a transition obtained.  These results obviously support his

suggestion that the hexagonal phase of ZnSe is metastable.  However, the

hexagonal phase in ZnSe does occur and that Hartman's explanation of its

occurrence in his flow-type samples is that an enhanced rate of nucleation

and fast crystal growth are responsible.  In support of this suggestion

he states that hexagonal and mixed cubic-hexagonal samples were found in

the crystal growth tube whenever the nucleation and growth rates were

high.

Thus from the work of Pashkin and Hartman it can be inferred that

the hexagonal phase in ZnSe flow crystals has its origin in thermodynamical

causes which can be annealed out very readily.

The relationship between structural stability and the electro-

negativity difference between ions forming a compound and the ionicity,

was investigated in 1967 by Caveney (100).  Caveney maintains that, as

the effective charge of the group II ion of the II-VI compound increases

the stable structure changes from cubic to hexagonal.  Using empirical

formulae of Sache (101) Caveney calculated the following quantities, an

effective charge $q_v$, a term defined as the crystalline ionicity $\lambda$ , and

the stacking fault energy $\gamma$ .  From the variation of $\lambda$ with $\gamma$ , Caveney

concluded that the stable structure for a compound with $\lambda$ < 0.64 is

cubic, and for a compound with $\lambda$ > 0.64 is hexagonal.  In the case of the

III-V compounds Caveney's conclusion is obeyed without exception, but with

the II-VI compounds there are irregularities.  Table (II) lists the values

of  $\Delta x$ (electronegativity difference according to Caveney) and those of

$\lambda$  for some of the II-VI compounds.  Thus MgTe with $\lambda$ < 0.64 should have

a cubic structure, but in practice the stable structure is found to be

hexagonal.  Caveney explained such an irregularity by suggesting that,

Table II

| Compound | $\Delta x$ | $\lambda$ |
|----------|------|------|
| MgTe | 0.9 | 0.48 |
| ZnTe | 0.5 | 0.50 |
| HgTe | 0.2 | 0.50 |
| CdTe | 0.4 | 0.54 |
| HgSe | 0.5 | 0.57 |
| ZnSe | 0.8 | 0.63 |
| HgS | 0.6 | 0.63 |
| CdSe | 0.7 | 0.65 |
| CdS | 0.9 | 0.77 |
| ZnO | 1.9 | 0.8 |

for instance, in the case of MgTe, the high value of $\Delta x$ (difference in electronegativity of Mg and Te) stabilizes the hexagonal phase.

With ZnSe the calculated value of $\lambda$ is 0.63, i.e. very close to the limiting value of 0.64. At the same time the calculated value of $\Delta x = 0.8$ is relatively large and comparable to those of compounds with the hexagonal structure, e.g. for ZnS $\Delta$ is 0.9, for CdS it is 0.8 and for CdSe it is 0.7. Thus from Caveney's analysis it follows that ZnSe should crystallize with a cubic structure, but structurally it is very close to the border line separating the cubic from the hexagonal structure. At the same time the value of $\Delta x$ is high, and because of this the difference in the free energies of the two phases is probably not very large. As a result factors that affect the relative free energy of the two phases may produce and stabilize the hexagonal phase. One such factor could be the presence of a suitable impurity. There is a considerable amount of experimental evidence that some impurities can affect the relative free energy of two phases of a solid significantly.

In an ideal solid, nucleation of a new phase occurs as a result of local energy fluctuations and also as a result of configurational fluctuations which may momentarily approximate an embyronic atomic configuration characteristic of another phase. For example, in very pure metals it is believed that there is a definite probability of formation of embryonic nucleation of another phase as a result of configurational fluctuations (102). In real solids, structural defects and impurities may not only modify the fluctuations mentioned above, but also they may in their own right, affect the relative free energy and the nucleation process. Thus, singularities in the structure may distort the lattice and the resulting strain energy may be sufficient to affect the relative free energy and enhance the probability of nucleation of another phase.

Furthermore, structural singularities may bring about changes in the local atomic bindings and amplitudes of vibrations. Dislocation and grain boundaries should also provide favoured sites for the nucleation of certain phases, because these defects can affect the interfacial energy and tension between two solid phases. Such factors as atomic or ionic size mismatch and variation of impurity concentration within the solid may also play important roles in nucleation. Furthermore, if an impurity in a solid forms a separate phase of its own, the actual structure of the impurity phase may be of great significance to the nucleation of another phase. Let us consider the formation of a new phase $\beta$ in a solid whose structure is denoted by $\alpha$. If the solid contains an impurity which precipitates with a configuration of its own (denoted by I), then the net free energy of formation of unit area interface between $\beta$ and impurity in $\alpha$ is

$$W = \delta_{\beta I} - \delta_{\alpha I} \qquad\qquad ---(36)$$

where $\delta_{\beta I}$ and $\delta_{\alpha I}$ are the $\beta$-impurity and $\alpha$-impurity interfacial tensions. The impurity surface would provide preferred nucleation sites for $\beta$ if $W < \delta_{\alpha\beta}$ (where $\delta_{\alpha\beta}$ is the interfacial tension between the $\alpha$ and $\beta$ phases of the solid). Theoretical treatment of strain energy and interfacial energy in phase transformations indicates that the effectiveness of the impurity in nucleating $\beta$ should depend significantly on the relationship between the structure of the impurity phase, that of $\alpha$ and $\beta$; in other words, the most effective impurity should be that whose structure permits the best molecular fit across impurity interface. W would tend to be small if the interfacial "disregistry" is small.

No exact information is available concerning the impurity content of the Derby Luminescent (Electronic Grade) ZnSe powder used as the starting material. However, X-ray powder photographs taken in the

Department (103) indicated that it contained approximately 5% by weight

of ZnO. Furthermore, ESR investigation of the powder at 77 K indicated

that it contained a very small amount of Mn (as $Mn^{2+}$) impurity.

In the light of the experimental data on phase transformations in

ZnSe mentioned earlier, and the above discussion on nucleation, it is

suggested that the experimental results obtained can best be explained

by postulating that the ZnO present in the charge precipitated and

formed a configuration of its own and in so doing affected the relative

free energy of the cubic and hexagonal phases in ZnSe and that it

initiated nucleation of the hexagonal phase.

It is important to state at the outset that ZnO, which is a member

of the II-VI group of compounds, crystallizes with a hexagonal structure

The ESR of the $Mn^{2+}$ ion in ZnO has been investigated comprehensively by

Schneider et al (104) and their results show an ESR absorption spectrum

similar to that of hexagonal ZnS and ZnSe, but with parameters which

are obviously different. In principle the hexagonal surface of ZnO in

cubic ZnSe should provide very suitable nucleation sites for the

hexagonal phase of ZnSe. Using the expression $(36)$ the net free

energy of formation of unit area of interface between ZnO and hexagonal

ZnSe in cubic ZnSe can be written as

$$\omega = \delta_{oh} - \delta_{oc} \qquad ---(37)$$

where $\delta_{oh}$ is the ZnO-(hexagonal ZnSe) interfacial tension, $\delta_{oc}$ is the

ZnO-(cubic ZnSe) interfacial tension and $\delta_{ch}$ the cubic-hexagonal ZnSe

interfacial tension. The condition for nucleation (and stabilization

of hexagonal ZnSe by ZnO) would be that $\omega$ should become negative. This

would occur if $\delta_{oc} > \delta_{oh}$, a condition which is very reasonable if the

general interfacial disregistry between the hexagonal and cubic structure

(of ZnSe) is taken into consideration.

As mentioned before, the hexagonal proportion in the mixed cubic-hexagonal samples investigated did not vary very much from sample to sample, irrespective of which part of the main boule the sample came from. This is consistent with an impurity having nucleated the hexagonal phase. If the hexagonal phase owed its origin to thermo-dynamical causes, say, a very much greater variation in the proportion of the hexagonal component would have occurred. Such a large variation does indeed occur in the flow crystals; in a typical flow run, samples can be found with structures ranging from totally cubic to totally hexagonal.

In general a solid state phase transformation does not start homogeneously throughout the solid. Initially embryonic nuclei of the new phase are formed at suitable sites and after an incubation period they grow to become distinct domains of a new phase. These domains then propagate at the interfaces at the expense of the old phase. Thus the rate of phase transformation is determined by the rate of nucleation and the rate at which growth occurs at the interfaces.

In the case of our cubic-hexagonal ZnSe samples, it is suggested that nucleation of the hexagonal phase would have occurred at the sites provided by ZnO. It follows then that the nucleation rate would have depended on the surface area of ZnO. Therefore, initially the nucleation rate would have increased reaching a maximum as more and more sites are taken up, then gradually decreased, finally reaching zero as all the suitable sites are occupied. From then on the rate of phase transforma-tion would have depended on the rate of growth at the interfaces. In the case of our cubic-hexagonal samples the rate of growth at the inter-faces would be complex if only because the hexagonal phase in ZnSe seems to be basically metastable and because it is the presence of ZnO which stabilizes this phase. For instance, it is not clear over what

distance the relative free energy of the cubic and hexagonal phases would be affected by a given amount of ZnO, localized at a point In such a situation, one possibility is that initially the growth rate at the interfaces would be reasonably rapid then would decrease and finally come to a halt when the interfaces were at such a distance from the ZnO that the oxide nucleus could not affect the relative free energy of the two phases in favour of the hexagonal phase. Such a situation could explain the following experimental observations:-

(a)   The Consistently low hexagonal proportions in all the samples

  as grown

This can occur when the hexagonal phase is impurity-controlled and the impurity concentration is not sufficiently large to produce completely hexagonal structure.

(b)   The hexagonal phase could not be annealed out

In contrast with the results obtained by Pashkin and Hartman, the hexagonal $\longrightarrow$ cubic transition could not be achieved in our samples despite the suggestion that the hexagonal phase is metastable. This indicates that the hexagonal phase in our samples had a different origin from that which produces the hexagonal phase in the flow-crystals. Again this is consistent with the postulated hypothesis.

(c)   The cubic $\longrightarrow$ hexagonal phase transition occurred consistently

  in all samples annealed at $1050^{\circ}C$

As mentioned before, Hartman in his investigation could not achieve the cubic $\longrightarrow$ hexagonal phase transition because, as he stated, the hexagonal phase in ZnSe is metastable. Hartman in his investigation used flow-type crystals which can be relatively free from impurities. No cubic $\longrightarrow$ hexagonal phase transition was observed in

our samples prepared by the iodine-transport method which agrees with

Hartman's data.  The controlling feature here was that the starting

material for the iodine transport method was ZnSe (Derby) powder which

had been baked and sublimed in a stream of argon and was, therefore,

of high purity. These results once again suggest that the hexagonal

phase in the samples prepared at 1300°C was produced by an impurity.

(d)    The very slow rate of the cubic ──➤ hexagonal phase transition

       with annealing

Generally when a solid phase transformation occurs for thermo-
dynamical reasons, the nucleation rate and the subsequent self-sustaining

growth rate are fairly fast.  According to Hartman an annealing time of

10 hours is quite sufficient to produce a complete hexagonal ──➤ cubic

phase transition in a small ZnSe sample at 450°C.  Yet in the ten samples

annealed at 1050°C for three weeks, the small hexagonal proportion in

each sample could only be doubled or at most trebled (as can be seen from

Figures (5.7)   and (5.23) .  This is a very slow rate of transition

especially when compared with that in ZnS, or the hexagonal ──➤ cubic

transition in ZnSe.  Usually in a solid the presence of a small amount

of a phase enhances the phase transition towards that phase at the

transition temperature, because the initial problem of nucleation is more

or less by-passed.

The conclusion that can be drawn from the annealing results is that

the cubic ──➤ hexagonal transition observed was not one involving two

basically stable phases of a solid, but one involving a stable phase

(cubic) to a metastable (hexagonal) phase which had been stabilized by

an impurity.

Phase transformations controlled by impurities in metals and alloys

have been the subject of many investigations.  However, not a great

quantity of work has been done on the II-VI compounds. The effect of

chlorine on the phase transformation in ZnS and ZnSe has already been

mentioned. Another investigation which is of direct relevance is that

of Aven et al (95) who found that copper and silver could bring about

a hexagonal ———→ cubic phase transformation in ZnS. In a series of

experiments Aven et al added different amounts of copper to a charge of

ZnS: Mn and produced a range of samples with different concentrations

of copper. Using the ESR spectrum of the $Mn^{2+}$ ion to monitor the

structure of their samples, they found that the basic structure in the

absence of copper impurity was hexagonal. However, in samples with

increasing copper concentrations the structure gradually changed to

mixed hexagonal-cubic with the cubic proportion directly dependent on

the copper concentration. According to Aven et al, the presence of

$7.5 \times 10^{-4}$ atomic fraction of copper in the ZnS produces a completely

cubic ZnS after firing at $1100^{\circ}C$. The mechanism envisaged by Aven et al

to explain this observation is that "uncompensated" Cu in ZnS

precipitates on cooling to form cuprous sulphide. This then brings

about nucleation of the cubic phase in hexagonal ZnS. As the nucleation

depends on cuprous sulphide, it follows that the cubic proportion in a

given sample depends on the amount of copper added. Aven et al also

found that silver produced a similar effect whereas aluminium tended

to produce the opposite result.

The investigations of Aven et al are in agreement with the explan-

ation suggested here for the results obtained with ZnSe. ZnO has been

suggested to be the impurity responsible because it is known that it

was present in the Derby ZnSe powder in measurable quantities (∿5% by

weight) and that its hexagonal structure can provide very good inter-

facial "registry" with the hexagonal phase of ZnSe. However, there is

no structure (or component) in the measured ESR spectra which can be attributed to the $Mn^{2+}$ ion in ZnO. The probable reason for this is that the ZnO precipitates in each sample were at random orientations and as such only the six central hyperfine components of the $Mn^{2+}$ ion which are not angularly dependent could have been obtained. In the ESR spectra recorded, these central hyperfine components would fall close to those of the $Mn^{2+}$ ion in cubic and hexagonal ZnSe, and as can be seen from Figures (5.7) and (5.23) would not have been resolved. Also it must be noted that Aven et al in discussing their ESR spectra of the $Mn^{2+}$ ion in ZnS:Cu do not attribute any feature or component to precipitated cuprous sulphide.

By comparing the hexagonal components of the ESR spectra of Figures (5.7) and (5.23), it can be seen that there is an approximately three-fold increase in the hexagonal proportion when the crystals are annealed at $1050^{\circ}C$ for three weeks. This was the maximum increase obtained with annealing; the minimum was an increase by approximately a factor of two. In the light of the explanation suggested this increase probably represents growth of the hexagonal phase at the cubic-hexagonal interfaces without any significant new nucleation. Most probably the majority of the suitable nucleation sites were taken up shortly after the precipitation of ZnO.

In conclusion, therefore, the results suggest an impurity was responsible for the nucleation and stabilization of the metastable hexagonal phase in ZnSe. Furthermore, the impurity was probably ZnO, but no direct evidence to this effect has been obtained. The only way to test this suggestion would be to prepare a series of ZnSe:Mn samples at $1300^{\circ}C$ with different ZnO concentrations to see if there was any correlation between the hexagonal proportions of the samples and their ZnO concentrations.

CHAPTER   6

ELECTRON SPIN RESONANCE OF SOME IMPURITIES IN ZnSe

6.1     Electron Spin Resonance of Chromium in ZnSe

Trapping Centre due to Chromium

The free chromium atom has the electronic configuration $3d^5 4s$.

In the II-VI compounds experimental data indicate that chromium can

enter the lattice substitutionally for the divalent cations, so that

in the absence of any charge unbalance it will be in the charge state

$Cr^{2+}$ with the electronic configuration $3d^4$. Moreover, the indications

are that $Cr^{2+}$ can accept a free electron to become $Cr^+$ with the

captured electron joining the 3d shell so the $Cr^+$ has the configuration

$3d^5$. As was mentioned in Section 5.1   an ion with such a configuration

has a half filled shell and by Hund's rule the ground state is 6S.

Because of the spherical symmetry of such a state, in principle, no

interaction with the crystal field should take place. Also since the

magnetic field at the centre of the ion is zero, there should not be

any interaction with the magnetic moment of the nucleus either. Yet

the ESR of $Cr^+$ in the II-VI compounds shows fine and hyperfine structures.

For a discussion of the possible processes leading to crystal field

splitting and hyperfine interaction involving an ion with the $3d^5$

electronic configuration the reader should consult Section 5.1.

Of the two chromium charge states, $Cr^{2+}$ and $Cr^+$ , $Cr^{2+}$ has a

very short relaxation time and as a result its ESR can be only observed

at temperatures below 1.4 K under ideal conditions. Investigations

carried out by Moriagi (1) show that in CdS the orbital degeneracy of

$Cr^{2+}$ is lifted by the impurity ion being displaced from the ideal Cd

site in accordance with the Jahn-Teller rule. With very careful measure-

ments Moriagi was able to determine the exact magnitude of the

displacement.

In contrast with $Cr^{2+}$, $Cr^+$ has a long relaxation time so that its ESR can be observed even at room temperature. Furthermore, the intensity of the ESR signal can be enhanced by irradiating the sample with light with photon energy corresponding to the band gap, or light that releases free electrons into the conduction band from localized impurity defect levels. The electron released into the conduction band is then captured by $Cr^{2+}$ to produce $Cr^+$ which enhances the ESR signal. As the intensity of the signal decays very slowly after the cessation of optical excitation, the depth of the $Cr^{2+}$ trapping level below the conduction band must be rather deep. The signal can, however, be quenched very easily by irradiating the sample with infra-red radiation which enables the captured electrons to escape from the trapping centres. Thus by determining the wavelength of the infra-red radiation (of the longest wavelength) that quenches the ESR signal, one has a direct method of estimating the depth of the trapping level below the edge of the conduction band.

To produce ZnSe:Cr single crystals for ESR investigations, metallic chromium (0.01% by weight) was added to ZnSe powder (Derby Luminescent) and the charge was pulled very slowly through a temperature gradient in a horizontal furnace with a maximum temperature of $1350^{\circ}$C. At the end of the run it was found that no transport of charge had taken place. The resulting sintered material was pulled through the furnace a second time, but with no effect. A similar result was also obtained when metallic chromium was replaced with chromium selenide. Attempts were also made to grow ZnSe:Cr single crystals using the iodine transport method at $850^{\circ}$C, but again no transport of charge took place. Considering the success normally achieved with these two methods of crystal growth, a good deal of investigation is needed to find out why chromium prevents transport of the charge.

Using a sintered ZnSe:Cr sample, no ESR signal could be detected at 4.2 K or temperatures above from $Cr^{2+}$.

Figure (6.1) illustrates the ESR of $Cr^+$ at 77 K, while Figure (6.2) illustrates the signal observed with the sample under UV. excitation from a high pressure 250 W Hg lamp. The g-value determined is 2.001 ± 0.001 which compares very well with 2.0016 found by Title (2) in a ZnSe:Cr single crystal at 77 K. The crystal used by Title in his investigation had been produced from the melt at $1500^{\circ}C$ in a graphite crucible. It is interesting to note that according to Title's investigations, chromium from the graphite crucible was found to be present in all ZnSe crystals produced from the melt.

As was mentioned before, $Cr^+$ has a spin S = 5/2 which should lead to five fine structure lines in its ESR spectrum. Of these lines, apart from that due to the central transition 1/2 ⟷ -1/2, the rest are angular dependent and have transition probabilities which are very much smaller than that of the central transition. As a result in a powder, or sintered sample, it may not be possible to resolve them. Furthermore, hyperfine interaction may occur with the nuclear magnetic moment of $Cr^{53}$ (9.5%) which has a nuclear spin I = 3/2. To resolve the hyperfine structure best, Title found that the most favourable orientation was in a direction where the five fine-structure lines coincided.

In incorporating chromium in the ZnSe lattice, it is important to note that chromium with an ionic radius of about 0.96 A in a cation site in place of zinc (which has an ionic radius of 0.74 A) would require the lattice to undergo a local expansion. Because of its large ionic radius the charge on the chromium ion may overlap with the charge on the neighbouring ions. Also interaction may occur

(a)

(b)
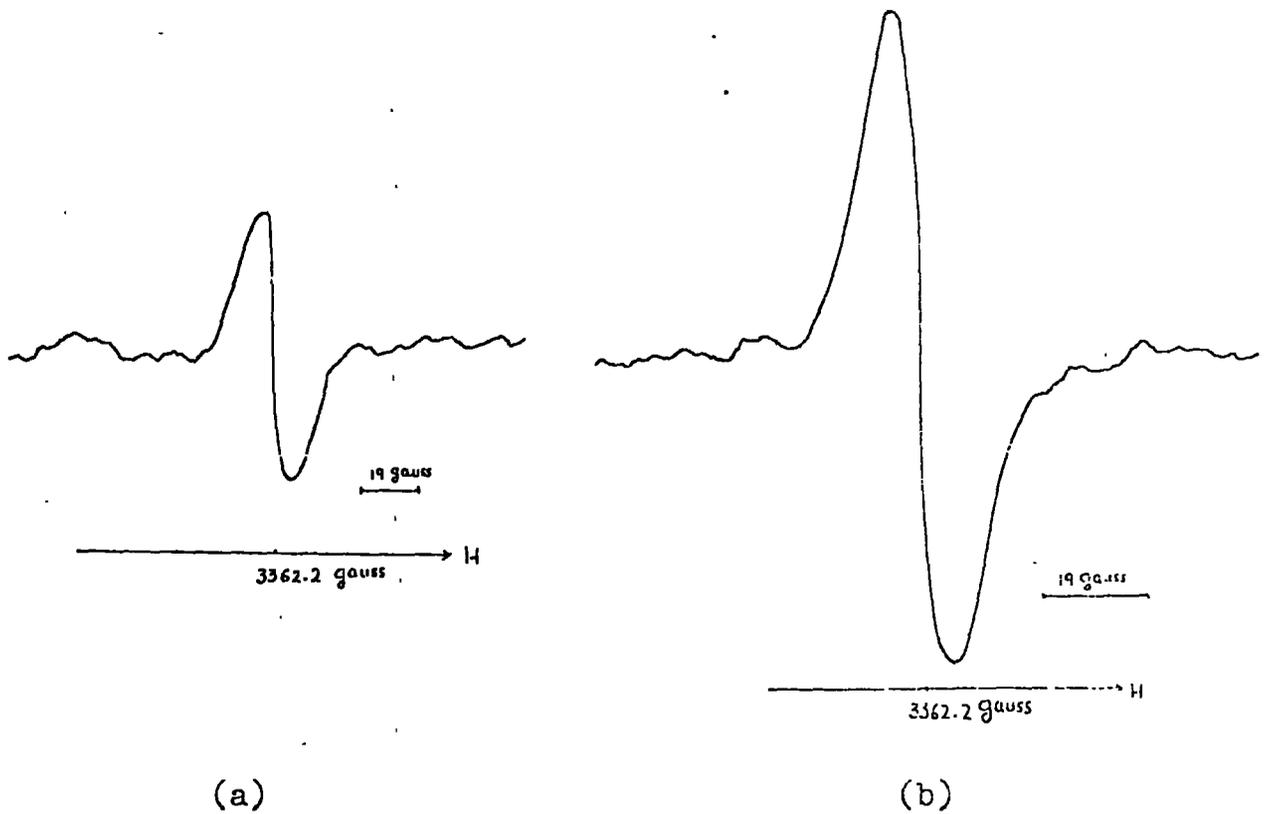
Fig.(6.1)   Electron spin resonance of $Cr^{+1}$ in ZnSe at 77K.

(a) Sample in the dark.

(b) Sample under u.v. excitation.

between the 3d electrons of $Cr^+$ and the magnetic moment of the $Zn^{67}$ nucleus which may occupy any of the twelve equivalent cation sites nearest to chromium.

In the ESR spectrum of Figure (6.1) no hyperfine or super-hyperfine structure (as was found by Title) could be resolved. The relatively broad line is due mainly to the central transition $1/2 \longleftrightarrow -1/2$ with the other structures not resolved. The reason for this is mainly to be found in the sintered, polycrystalline, quality of the sample.

Though Title investigated the ESR of $Cr^+$ in ZnSe, he however, made no attempt to determine the depth of the trapping level below the edge of the conduction band. As can be seen from Figures (6.1) and (6.2), the intensity of the ESR signal at 77 K could be enhanced more than two-fold by irradiating the sample with UV radiation. Also, as was mentioned before, a very straightforward method of determining the depth of the trapping level below the conduction band is from infra-red quenching experiment. In our case this had to be abandoned due to the lack of a suitable monochromator. An alternative method is to measure the decay of the photo-induced ESR signal at a number of temperatures. Figure (6.3) illustrates the variation of the decay time with temperature for the temperature range 250-293 K. The decay time of the photo-induced ESR signal was determined in this temperature range for two reasons. Firstly, in the Dewar cryostats used for cooling the sample, there was no facility for controlling the temperature of the sample. Measurements as a function of temperature could, therefore, only be made as the sample warmed up. At very low temperatures the rate at which ·the temperature of the sample·increased was too fast for the relatively long decay time to be determined with any degree of accuracy. However, between 250 K and room temperature (with the cryostat well

lagged) the rate at which the temperature of the sample increased

was sufficiently slow to permit measurement of the rapidly decreasing

decay time.   The second reason is associated with the variation of

the decay-time with temperature.

Determination of trapping levels in the II-VI compounds using

electrical methods has been discussed by a number of authors (see for

instance Cowell and Woods (3),  Nicholas and Woods (4)).  Similarly

Curie (5) has reviewed a number of theories concerned with trapping

levels as applied to luminescence and phosphorescence.  Generally in

phosphorescence it is found that the emission decay-time (after the

cessation of optical excitation) $\tau$ varies with temperature as

$$\log_e \tau \;=\; \frac{E_t}{kT} \;-\; \log_e \; S \qquad\qquad ---(38)$$

where $E_t$ is the trap depth below the conduction band and S usually a

constant depending on the sample.  In the case of the decay of the photo-

induced ESR signal (say, due to $Cr^+$) the situation is in a sense

similar to that of phosphorescence.  Whereas in phosphorescence the

intensity of emission (after the cessation of optical excitation)

depends on the number of electrons being released from the trapping

centres, in the case of photo-induced ESR of $Cr^+$, the intensity of

the signal would depend on the number of electrons still trapped.

Nevertheless, the variation of the decay-time with temperature would

still be of the same form as (38 ).  Such an exponential variation

of the decay-time with temperature was investigated for $Cr^+$ in ZnS (6)

and was found to be valid for temperatures above approximately 250 K.

Thus according to the expression (38), if the decay-time varies with

temperature exponentially, a plot of $\log_e \tau$ against $1/kT$ should give a

straight line with a gradient which is a measure of the depth of the
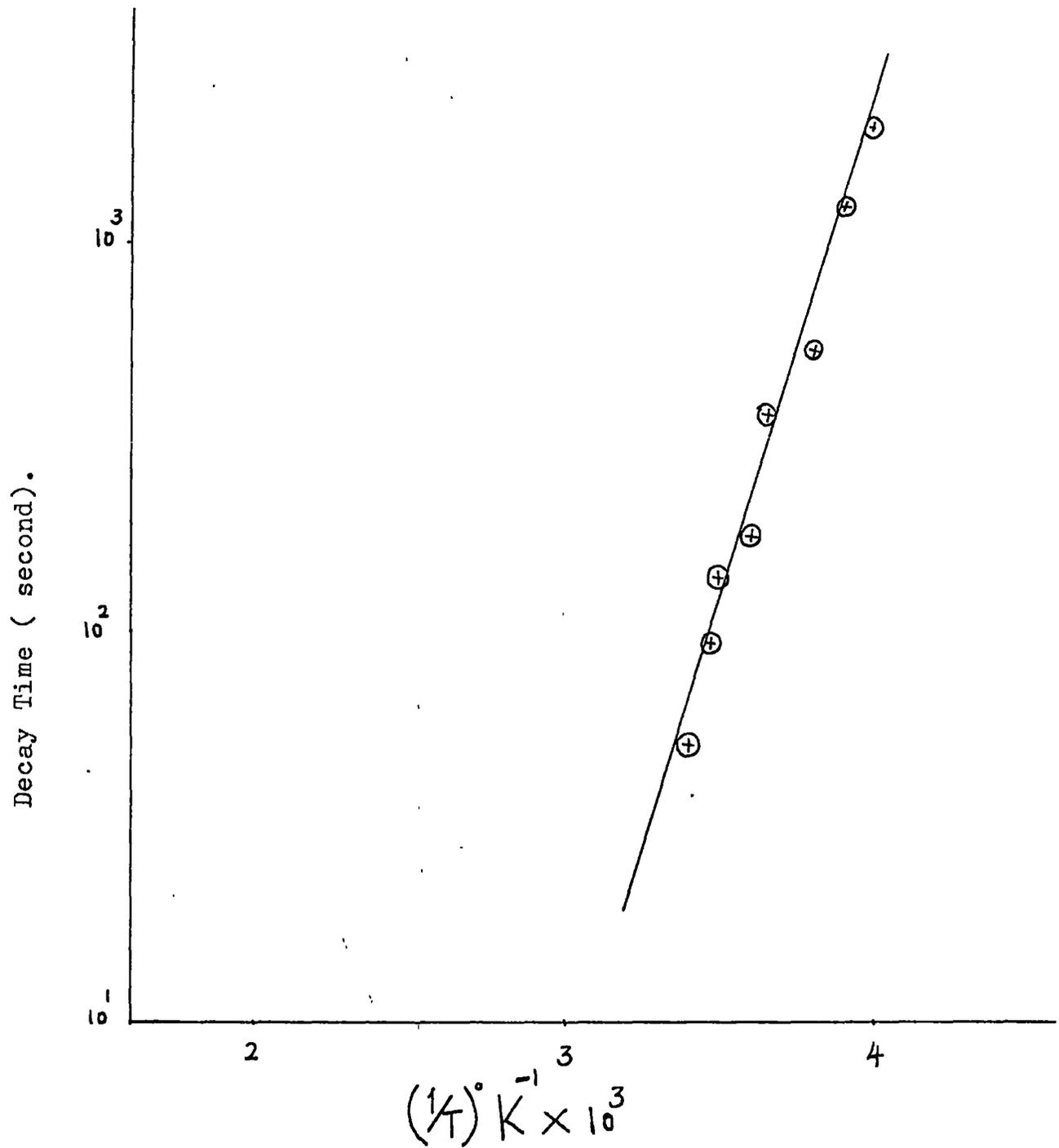
Fig.(6.3) Exponential variation of decay time with temperature.

trapping level below the conduction band. Experimental data illustrated in Figure (6.3) confirm such a variation for the temperature range 250-293 K. From Figure (6.3) a value of 0.51 eV was determined for the depth of the trapping level below the conduction band. In measuring the decay-time at any particular temperature, it is important to avoid the cumulative effect of previous UV irradiation. This was achieved by quenching with infra-red light before applying UV radiation.

From an exponential variation of the decay-time with temperature, of the type shown in Figure (6.3), it is not possible to determine whether the recombination process is monomolecular or bimolecular. It is of interest to note that according to a simple trapping model, theoretical calculations anticipate the decay-time to vary with temperature exponentially for both monomolecular and bimolecular recombination (6).

In ZnSe:Cr there is no reported value for the depth of the trapping level due to chromium with which the value of 0.51 eV could be compared. In ZnS:Cr there have been several investigations and the consensus of the recent results is that the trapping level associated with chromium lies 0.76-0.78 eV below the conduction band.

## 6.2 Electron Spin Resonance of Donor Electrons in ZnSe

ZnSe samples doped with such donor-type impurities as I, Cl, Al and In were subjected to ESR investigations in order to study the role of these impurities. In particular it was necessary to determine whether the self-activated centre which consists of a cation vacancy associated with a donor impurity, could be detected in the doped and undoped samples. As is explained in Chapter 7 no spin resonance associated with the self-activated centre could be detected in any sample. In the samples doped with donor impurities, however, spin

resonance characteristic of electrons in a shallow donor band was observed.

Electron spin resonance of unpaired donor electrons was first observed in silicon doped with such donor-type impurities as phosphorus and arsenic. At concentrations of about $10^{15}$-$10^{16}$ per $cm^3$, the spectrum in each case consisted of a number of hyperfine lines (two from the $P^{31}$ nuclei and four from the $As^{75}$) with an almost isotropic and identical g-value. As the concentration of the donors was increased a dramatic change in the spin resonance spectra was noticed. For instance in the phosphorus-doped samples the two hyperfine lines collapsed into a single featureless line at a concentration of $10^{18}$ per $cm^3$, while at intermediate concentrations there appeared in addition to the two hyperfine lines, a number of very weak and poorly resolved subsidiary peaks. These results were interpreted in the light of the ideas of Kohn and Luttinger (7) and Luttinger and Kohn (8) who used a hydrogen-like model for the unpaired (bound) donor electron. From this model it follows that the donor electron moves in an orbit of large radius (with the radius depending on the dielectric constant of the material and the electron effective mass) and that its electron spin resonance properties are determined by the shape of the conduction band and the dielectric constant of the host lattice. At low temperatures when the donors are not ionized, if their concentration is sufficiently low to prevent overlap of their wave functions each unpaired donor electron would show hyperfine structures arising from interaction with the spin of its nucleus. As the concentration is increased the wave-functions gradually overlap and additional weak hyperfine lines appear in the spectrum. These are associated with pairs or small groups of donors. As the concentration is increased further, the orbitals begin to overlap until eventually they coalesce so that the donor electrons

can no longer be considered as being localized, i.e. they become mobile

in the donor band, and the hyperfine interaction with the spins of the

nuclei is averaged out. At this critical concentration (and concentra-

tions above) a single featureless ESR line would be observed. In the

case of phosphorus-doped silicon, ESR of localized donor electrons was

observed by Feher ( 9 ) at a concentration of about $10^{15}$ per $cm^3$,

while at concentrations of $10^{18}$ per $cm^{\cdot3}$ the spectrum was characteristic

of electrons mobile in the donor band. At intermediate concentrations

of $10^{16}$ and $10^{17}$ per $cm^3$, the spectra corresponded to pairs or clusters

of donors.

In the II-VI compounds prior to 1963 a number of almost iso-

tropic ESR lines had been observed with g-values that varied from com-

pound to compound, but which were always smaller than that of the free

electron spin. As these lines had no hyperfine structure their

identification was a matter of speculation. However, following their

ESR study of an iodine-doped ZnS sample, Muller and Schneider ( 10 )

suggested that these lines were due to donor electrons mobile in

shallow donor bands as in Si and Ge. Using this suggestion Muller and

Schneider were able to account satisfactorily for a number of features

of these lines. Furthermore, following the calculations of Hudson (11)

they determined a concentration of about $10^{17}$ per $cm^3$ as that at which

the overlap of donor electron orbitals would be expected to occur in

the II-VI compounds. From this it follows that since the reported

observations of donor resonance in the II-VI compounds had been for

donor concentrations exceeding $10^{17}$ per $cm^3$, it is not very surprising

that the spectra had consisted of featureless lines. Thus to observe

the ESR of localised donor electrons in the II-VI compounds the donor

concentration (and those of unwanted impurities) must be at least one
or two orders of magnitude below $10^{17}$.

An experimental result that strongly supports the explanation
put forward by Muller and Schneider comes from their investigation of
donor spin resonance in Zn(S:Se):I samples. In 1967 Muller and Schneider
(12) studied the resonance of iodine donors in a series of ZnS:I,
Zn(S:Se):I and ZnSe:I samples and found that the g-values of the donor
electrons shifted uniformly and continuously from 1.882 in ZnS:I to
1.14 in ZnSe:I, with intermediate values in Zn(S:Se):I samples. This
continuous and uniform shift of the g-value indicated that the spin
resonance originated from mobile donor electrons. This is because a
paramagnetic electron cannot reflect lattice fluctuations, if it is in
a highly delocalized orbit, when its g-value would be averaged to a
mean and isotropic value.

Though ESR of localized donors in Si and Ge was reported in
1959, such a report for the II-VI compounds is still awaited. The main
reason for this has been the difficulty of producing material of suf-
ficient purity, i.e. a purity corresponding to those of Si and Ge
available in 1959.

Figure (6.4) illustrates the spin resonance absorption line
of a ZnSe crystal, grown from a charge containing 1000 p.p.m. Al. This
crystal had been produced at $1150^{\circ}C$ in a vertical furnace employing the
technique described by Burr and Woods (13). The signal was observed
while the sample was irradiated with UV light and decayed fairly quickly
when the optical excitation was removed. Investigation of the g-value
and the shape of the resonance line in the different crystallographic
directions showed it to be isotropic with a g-value of $1.18 \pm 0.02$.
These results and the fact that no such resonance line could be found
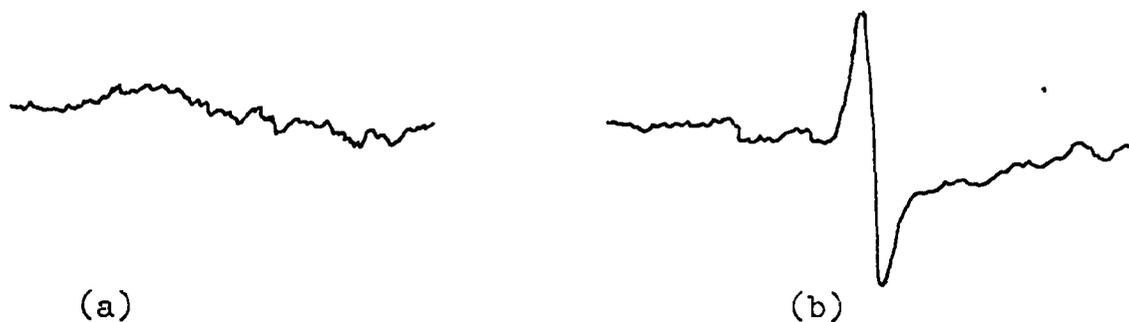
Fig.(6.4) Electron spin resonance of Al donor electrons in ZnSe .
(a) Sample in the dark.
(b) Sample under U.V. excitation.
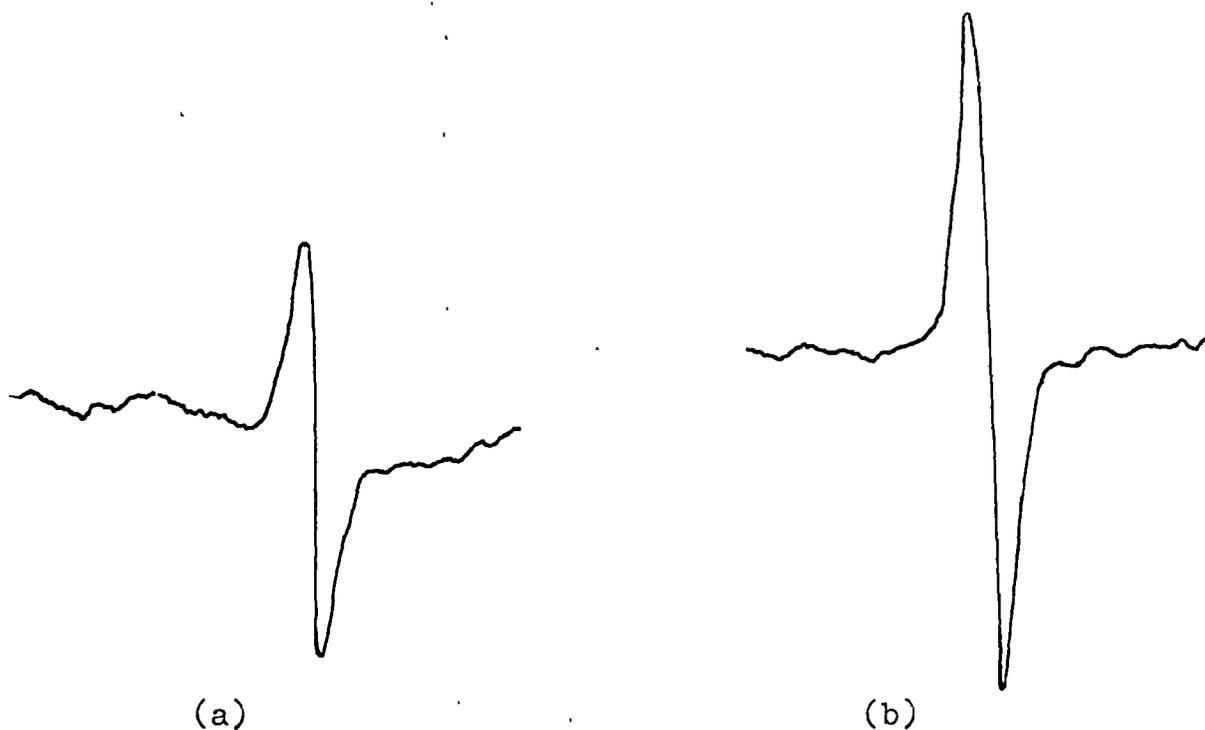


Fig.(6.5) Electron spin resonance of Al donor electrons after
annealing the sample in molten zinc.
(a) Sample in the dark.
(b) Sample under U.V. excitation

in undoped samples produced in a similar manner, lead to the conclusion that the resonance line originated from Al donor electrons probably in a donor band. Next the sample was annealed in molten Zn at $850^\circ$C for three days and Figure (6.5) illustrates the spin resonance observed after such treatment. Now, the same resonance line appeared in the dark and its intensity was enhanced under U.V. excitation. Generally the effect of annealing in molten Zn is to increase the dark conductivity some 4 or 5 orders of magnitude by removing some impurities (particularly the acceptor-type) and probably affecting the native defects. In the absence of detailed information about the impurities and distribution of native defects in the sample, it is not possible to account precisely for the appearance of the donor resonance line in the dark after annealing in molten Zn. However, one possibility could be connected with the way in which the donors in ZnSe are compensated; for instance it could be that in the as-grown sample a very large number of donors are not in the paramagnetic state because of the auto-compensation mechanism involving the acceptors, and that after annealing their magnetic status changes as a result of some acceptor impurities having been removed or as a result of a redistribution of the native defect complexes. Very little is known about the configuration of the defect-impurity complex responsible for the compensation in the II-VI compounds, hence detailed optical, electrical and spin resonance investigations would be required to understand this.

Electron spin resonance due to Al donors was also detected in a sample doped with Al by diffusion. Polycrytalline ZnSe produced at $1150^\circ$C in the vertical furnace showed no spin resonance signal due to donors either in the dark or under optical excitation at 77 K. Two such samples were then annealed at $850^\circ$C, one in Zn and the other one

in Zn to which 1% Al by weight had been added.  Electron spin resonance

of both samples after annealing indicated no change in the spin resonance

of the sample annealed in Zn, but the characteristic donor spin resonance

appeared in the sample annealed in Zn to which Al had been added.  This

spin resonance signal corresponded to that obtained in ZnSe:Al after

it had been annealed in Zn, i.e. the signal appeared in the dark.  This

diffusion of Al into ZnSe at $850^{\circ}$C should be contrasted with the

behaviour of Mn which as explained in Section 5.12 was found not to

diffuse into ZnSe at $850^{\circ}$C in the presence of molten Zn.

Of all the donor-doped ZnSe samples investigated (i.e. ZnSe

doped with I, Cl, Al and In), the spin resonance of Al donor electrons

could be detected most easily and uniformly in ZnSe:Al samples.  For

instance in ZnSe samples produced at $850^{\circ}$C in the presence of iodine,

no donor spin resonance line could be detected in the dark or under

optical excitation.  However, a spin resonance line did appear under

U.V. excitation after the sample had been annealed in molten Zn.  It

is very difficult to account for this behaviour not having detailed and

precise knowledge of the impurities in the sample.  In polycrystalline

ZnSe (flow-type) doped with In, a spin resonance signal due to In donor

electrons under optical excitation could only be detected in one sample

out of the five samples investigated.  Similar variable results were

also obtained in flow-type crystals doped with ZnCl, whereas in flow-

type polycrystalline samples doped with Al, the donor spin resonance

line under optical excitation could be detected in all samples investi-

gated.  From these results it appears that Al is the least difficult

of the donors to incorporate in ZnSe.

Table III gives the g-values and the bandwidths of the donor

electron spin resonance lines in the ZnSe samples investigated.  The

## Table III

The g-value of some donor electrons in ZnSe.

| | |
|---|---|
| ZnSe:Al | $1.18 \pm 0.02$ |
| ZnSe:In | $1.18 \pm 0.02$ |
| ZnSe:I | $1.17 \pm 0.02$ |
| ZnSe:Cl | $1.17 \pm 0.02$ |

g-values should be compared with the value of 1.144 $\pm$ 0.01 determined by Muller and Schneider in ZnSe:I, and 1.46 as calculated theoretically by Cardona (14). Also if the wavefunctions of the mobile electrons in the shallow donor band are taken to be the same as that of the free electrons in the conduction band, the g-value according to Roth (15) would be

$$g = 2\left[1 - \left(\frac{m}{m^*} - 1\right)\frac{\lambda}{3E_g + 2\lambda}\right] \qquad ---(39)$$

where $\lambda$ is the spin orbit splitting of the valence band, $m^*$ the effective mass in the conduction band and $E_g$ the band gap. Taking a value of 0.17 for $\frac{m^*}{m}$ as determined by Marple (16), the g-value of the donor electrons according to Roth's formula would be 1.54. It is interesting that this value and that calculated by Cardona is larger than the values found experimentally.

CHAPTER 7


PHOTOLUMINESCENCE IN ZnSe:Mn

Mn as an activator has received a great deal of attention

firstly because of its ability to produce luminescence in a wide

variety of crystal lattices and secondly because of the technological

importance of the class of phosphors activated by Mn. The emission

peaks in these phosphors range from yellow in zinc fluoride, orange

in ZnS, to green and red in zinc silicate. From some of the earliest

studies of phosphors the emission from compounds containing Mn has

been attributed to internal transitions within the Mn itself. This

came about not only because of the ease with which Mn activates a

large number of compounds, but also because optical absorption experi-

ments (1) have shown that the present of Mn in a compound gives rise

to a series of discrete absorption bands (in the visible and U.V.

region of the spectrum) which were later shown to be the excitation

bands for the luminescence. Furthermore, Klick et al (2) associated

these absorption bands with the energy levels of the $Mn^{2+}$ ion.

In general when an emission band is associated with an internal

transition within an ion, the spectral location of the emission band

would depend on the amount of perturbation received by the emitting

centre from the particular lattice. The greater part of this perturba-

tion is due to the nearest neighbour atoms (or ions). Klasens et al (3)

investigated this effect by studying the displacement of the emission

band due to Mn in compounds of the type $ABF_2$:Mn where the $Mn^{2+}$ ion was

co-ordinated by fluorine ions as nearest neighbours. The distance

between the $Mn^{2+}$ ion and fluorine neighbours was varied by using Li,

Na, K etc. as A ion and Zn, Cd, Mg and Sr as B ions. The general result

obtained was that as the space available to the $Mn^{2+}$ ion increased the

emission band was displaced to shorter wavelengths, i.e. the greater

the Mn-fluorine ion distance, the more the state of the free ion was

approached. Basically when Mn enters a compound, e.g. ZnSe, the two

4s electrons are stripped off leaving the electrons in the 3d shell

exposed. As was mentioned in Section 5.1  this shell is not well

shielded so that the detailed absorption and emission properties of

the $Mn^{2+}$ ion are determined by the surroudings in which the ion is

co-ordinated. In zinc silicate when the Mn concentration is of the

order of a few per cent a green emission band is observed. At very

high Mn concentrations (approaching 20%) no emission band is observed

at room temperature, but at 77 K a red band appears in addition to

the green band. Incorporation of beryllium even at low Mn concentrations

promotes the development of the red band. In zinc germanate, which is

structurally similar to zinc silicate, a green band only is observed

even at high Mn concentrations. However, the addition of beryllium

again produces a red band in addition to the green band. To account

for these effects two explanations have been proposed, one based on

cluster theory and the other on the co-ordination theory. According

to Kroger et al (4) the different emission bands correspond to different

clusters of the $Mn^{2+}$ ions. The green band is thought to be due to

isolated $Mn^{2+}$ ions and the red band due to pairs of ions in close

proximity. According to this hypothesis it is postulated that the

intensity of the red emission band increases with concentration since,

assuming random distribution, the relative number of the Mn clusters

increases with increasing Mn concentration. The effect of beryllium

is accounted for by suggesting that the $Mn^{2+}$ ions tend to cluster

preferentially around beryllium which in zinc silicate - Mn leads to

a reduction in the strain energy due to size mismatch.

In contrast, according to the co-ordination theory (5), the green emission band arises from the $Mn^{2+}$ ion (which substitutionally replaces Zn) being surrounded by four oxygen ions, whereas the red emission band is produced when the $Mn^{2+}$ ion is co-ordinated by six oxygens. Co-ordination of Mn by six oxygen ions is thought to occur when Mn at high concentrations takes up interstitial sites. The effect of beryllium is explained by suggesting that beryllium forces the $Mn^{2+}$ ions into interstitial positions and the reasons for this are to be found in the size mismatch between the Zn, Mn and Be ions. Optical and ESR experiments carried out to test these two theories tend to support the co-ordination theory (6), which reinforces what was stated before; namely, that the detailed optical etc. properties of the $Mn^{2+}$ ion in a lattice depend on the surroundings in which the ion is co-ordinated.

As was mentioned in Section 5.1 the electrons in the outermost shell of free $Mn^{2+}$ ion have the configuration $3d^5$, with a ground state, in which according to Hund's rule, electron spins are all aligned in the same direction and which is an orbital singlet or S-state. In the immediate low lying excited states one of the electron spins is reversed to give rise to the series of energy levels 4G, 4P, 4D, 4F. When the ion is placed in a crystal field of cubic symmetry, the first excited state 4G splits into three terms $^4T_1$, $^4T_2$, ($^4E$, $^4A_1$), with the ground state remaining practically unaffected. Of particular interest is the metastable term $^4T_1$, since the Mn emission band in many compounds is believed to be due to $^4T_1 \longrightarrow {}^6A_1$ transition. (For a discussion of the splitting of the excited states of the $Mn^{2+}$ ion in crystal fields of cubic and hexagonal symmetries the reader should consult Orgel (7), Tanabe and Sugano (8) and McClure (9)). However, transitions to the

metastable state $^4T_1$ are nominally forbidden by parity and spin considerations, but occur only because of coupling with lattice vibrations and spin-orbit effects. Van Vleck (10) made a theoretical investigation of the optical absorption processes of transition metals when placed in crystal fields of octahedral symmetry and found that it was necessary to include the vibrations of the co-ordinating ligands in the wave functions in order to obtain transition probabilities sufficiently high for the optical absorption process to take place. Generally the allowed  forbidden nature of a transition may be judged from the decay time of luminescence which is of the order of $10^{-8}$ sec. when the transition is allowed. In the case of the $Mn^{2+}$ ion the decay time is observed to be very much longer. For instance, in ZnS:Mn, the decay time is of the order of $10^{-3}$ sec., and in $Zn_2SiO_4$:Mn it is $10^{-2}$ sec. (11), which again suggests that the luminescence is due to a nominally forbidden transition. It must be pointed out that since the Mn transition occurs within the ion, the decay time is expected to be more or less independent of temperature and that any change that may occur in the spectral location of the emission band with temperature must be very small.

In the II-VI compounds ZnS:Mn was one of the earliest phosphors whose absorption and emission properties were investigated. Studying the absorption spectrum of ZnS:Mn containing about 2% Mn Kroger (1) obtained a series of discrete absorption bands which have been shown to correspond to the various excited states of $Mn^{2+}$. Of great interest also was the observation that unlike the luminescence due to such activators as Cu, Ag or Au, the emission associated with Mn (under excitation with 3650 A radiation) was not accompanied with photoconductivity or charge transport. Furthermore the width of the Mn

emission band was narrower than that of other activators, while its peak shifted very little with temperature. More detailed and recent studies of the Mn absorption bands in ZnS (i.e. those of Langer and Ibuki (12)) at low temperatures have revealed fine structures due to phonon coupling which indicates that the electron transition within the Mn ion is coupled to lattice vibrations. Although Mn in ZnS has been the subject of many investigations, there is as yet no certainty about the position of the $Mn^{2+}$ ion ground state relative to the energy bands of the host lattice. The reason for this has been the difficulty in devising an experiment to give unambiguous information about the energetic position of the $Mn^{2+}$ ion ground state relative to the conduction or the valence bands. Using theoretical calculations and experimental data Allen (13) has suggested that the ground state lies approximately 0.1 eV above the valence band. Gurmlich et al (14) however, have estimated the ground state to be approximately 6 eV below the top of the valence band. Recent experimental results of Langer et al (15) using photoelectron spectroscopy put the ground state at approximately 3 eV below the top of the valence band.

Mn in the other II-VI compounds has not received the same degree of attention as in ZnS. However, because of the possibility of fabricating suitable electroluminescent devices, in recent years attempts have been made to investigate the properties of Mn in ZnSe and in the other II-VI compounds.

In ZnSe Langer et al (16) studied the optical properties of the $Mn^{2+}$ ions in samples grown from the melt, and at 4.2 K observed three absorption bands corresponding in order of increasing energy to the transitions $^5A_1 \longrightarrow ^4T_1$, $^6A_1 \longrightarrow ^4T_2$ and $^6A_1 \longrightarrow ^4A_1$, $^4E$.

Phonon structures were observed in two of these bands, but not in the energetically lowest $^6A_1 \longrightarrow {}^4T_1$ band because of its small absorption coefficient. Furthermore from their data Langer and Richter concluded that the Mn emission band due to the $^4T_1 \longrightarrow {}^6A_1$ transition has a peak at approximately 5815 A in ZnSe. In contrast with this conclusion, Apperson et al (17) investigated the photo-luminescence and photoconductivity of a number of ZnSe:Mn samples and stated that the Mn emission band in ZnSe lies at approximately 6350 A at room temperature. Also Asano et al (18) from their investi-gations of photoluminescence suggest that the Mn emission band in ZnSe has its peak at 6400 A at 80 K.

In the previous page reference was made to the position of the $Mn^{2+}$ ion ground state relative to the valence band in ZnS. In ZnSe:Mn the available information is due to Braun et al (19) who carried out photocapacitance measurements and from their data concluded that the ground state of $Mn^{2+}$ ions lies 0.6 eV above the valence band.

Figure (7.1) illustrates the emission spectrum of a ZnSe:Mn sample under excitation with U.V. radiation of 3650 A. This sample was produced at $1300°C$ from ZnSe powder (supplied by Derby Luminescent Ltd.) to which 0.4% Mn by weight in the metallic form was added. Figure (7.1) should be contrasted with Figure (7.2) which shows the luminescence of a crystal produced under identical conditions but without adding any Mn impurity. Comparing Figures (7.1) and (7.2) it can be seen that there is no difference in the emission spectra of the two samples under U.V. excitation. Figure (7.3) illustrates the emission spectrum of a ZnSe:Mn sample (with Mn concentrations of 0.4%) produced by the iodine transport method at $850°C$. As explained in Chapter 2 the charge used to produce crystals at $850°C$ by the
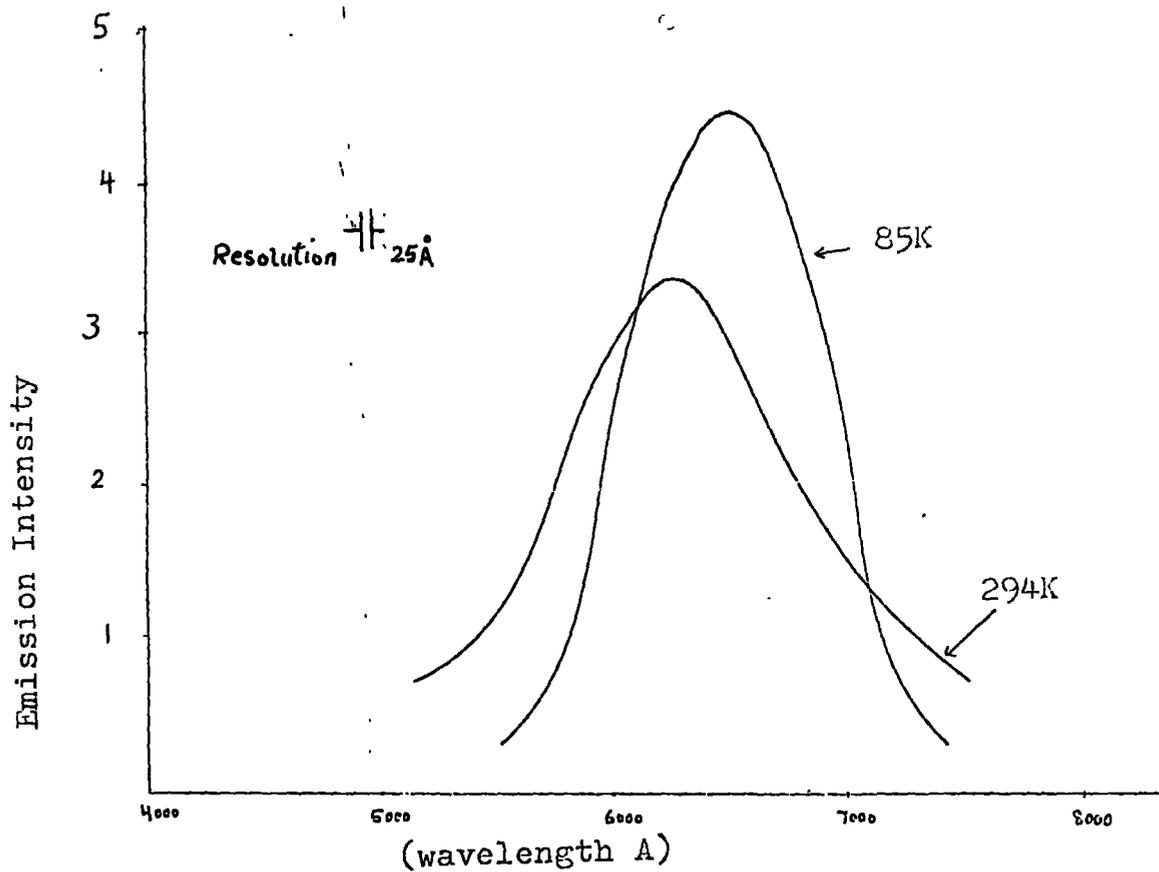
Fig.(7.1)  Emission spectrum of a ZnSe:Mn crystal ( produced
at 1300C) under U.V. excitation.
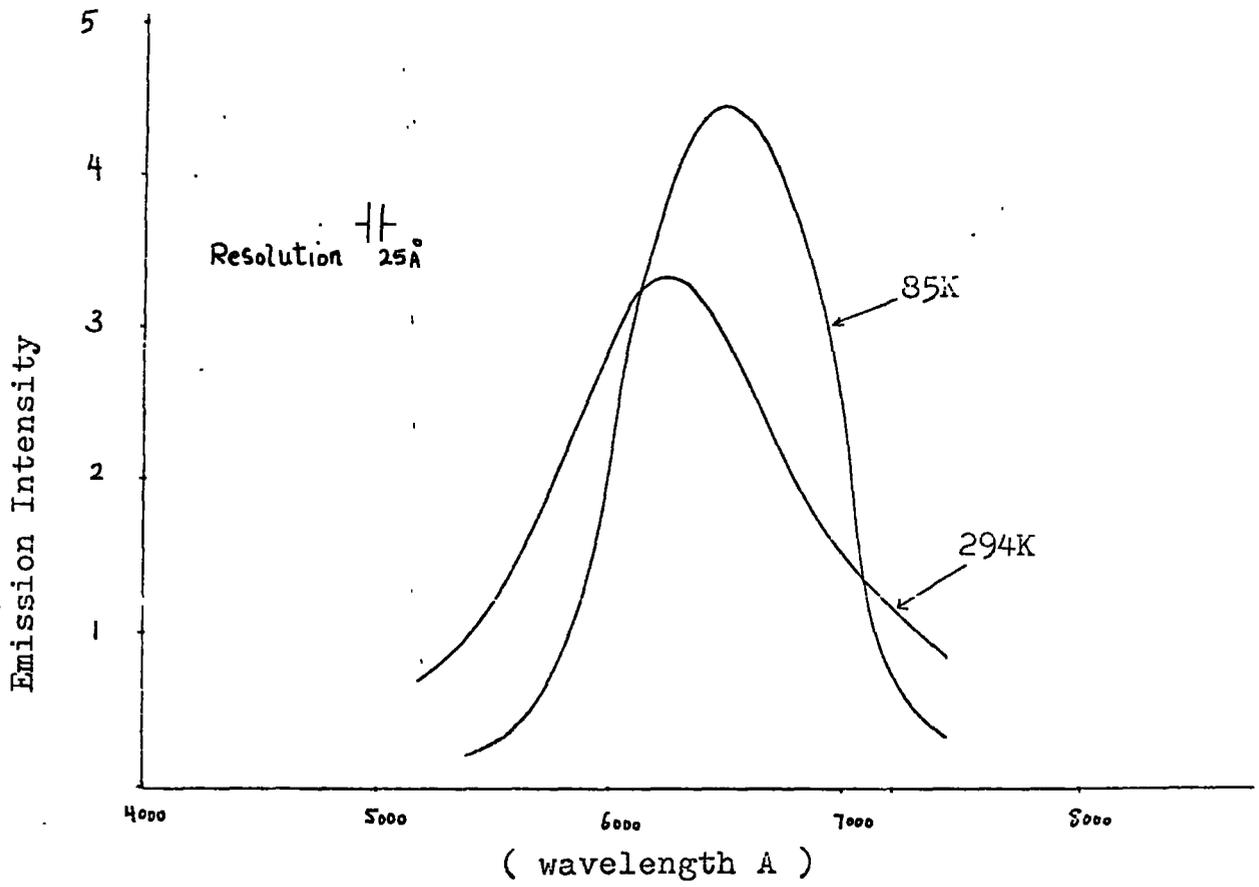
Fig.(7.2) Emission spectrum of a ZnSe crystal ( produced at 1300C) under U.V. excitation .
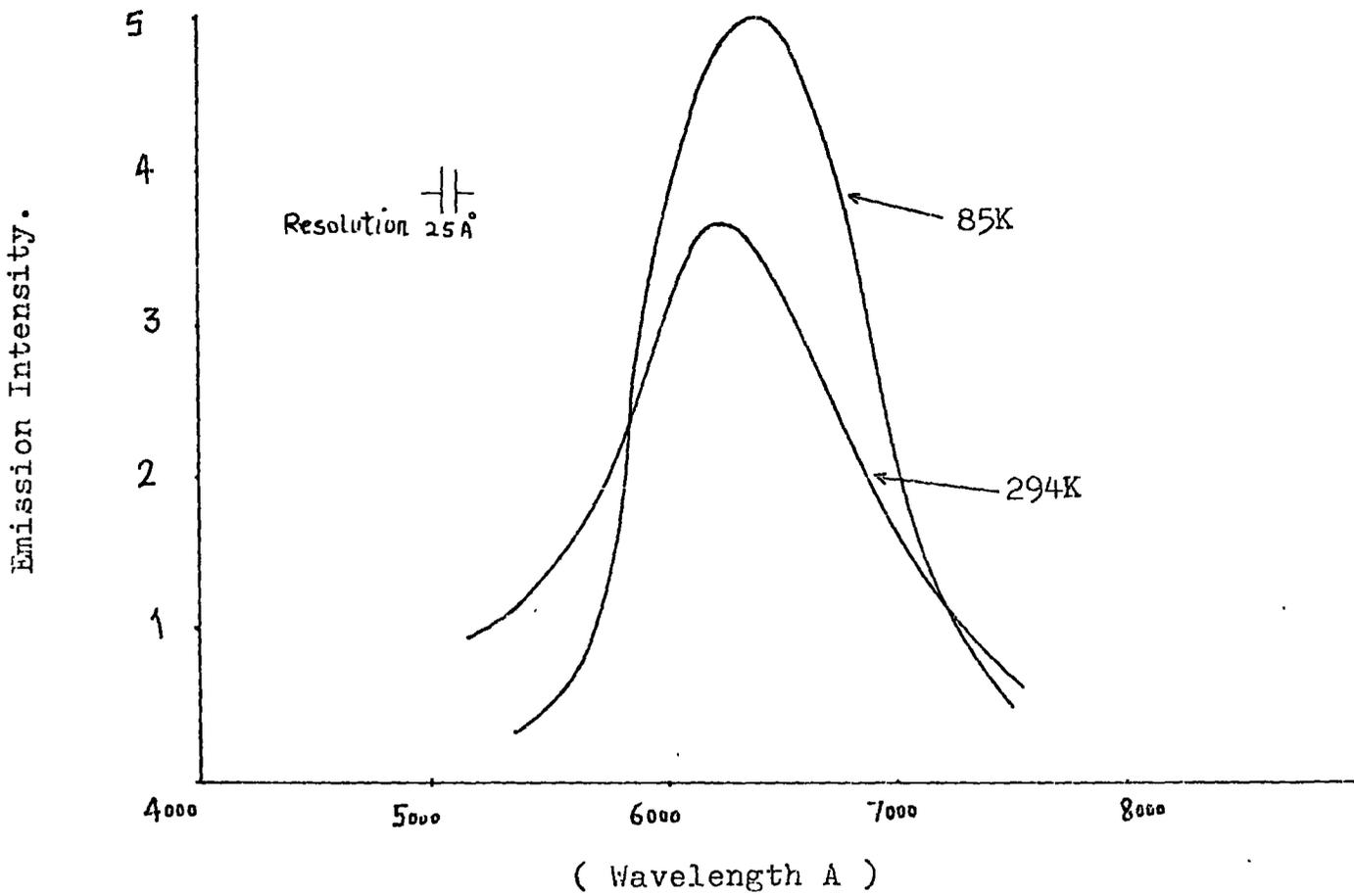
Fig. (7.3) Emission spectrum of a ZnSe:Mn crystal
( produced at 850C ) under U.V. excitation.

iodine transport method was ZnSe powder (Derby Luminescent) which had previously been sublimed in a stream of argon gas to remove the volatile impurities. In Figure (7.3) the emission peaks at 292 K and 80 K are at approximately 6400 A and 6270 A. These should be compared with emission peaks of approximately 6500 A and 6280 obtained for the sample produced at $1300^{O}C$ and illustrated in Figure (7.1). However, it must be borne in mind that the sample produced at $850^{O}C$ by the iodine transport method contained a high concentration of I. In addition the emission spectrum shown in Figure (7.3) was compared with the spectrum of a sample produced at $850^{O}C$ without any Mn, and the spectra of a number of samples containing different concentrations of Mn, but no significant difference in the emission spectra could be detected.

Since no emission band characteristic of the $Mn^{2+}$ ion in ZnSe:Mn could be identified in crystals prepared at $1300^{O}C$ and $850^{O}C$, a series of Zn(S:Se):Mn solid solution samples with an Mn concentration of 1% was prepared, so that the characteristic Mn emission band in Zns could be monitored as Se replaced S in Zn(S:Se):Mn. To avoid having solid solution samples of mixed hexagonal-cubic structure the solid solutions were prepared at $980^{O}C$, a temperature well below the hexagonal ZnS transition temperature which is approximately $1050^{O}C$. Generally Mn can be incorporated into ZnS very readily and its characteristic emission band with its peak at 5800 A (at room temperature) under U.V. excitation with a wavelength of 3650 A can be detected unambiguously. Figure (7.4) illustrates the result obtained as Se replaced S in Zn(S:Se):Mn. At no composition of Zn(S:Se):Mn could any shift be detected in the spectral location of the Mn characteristic emission band in ZnS. Instead as can be seen in Figure (7.4), the intensity
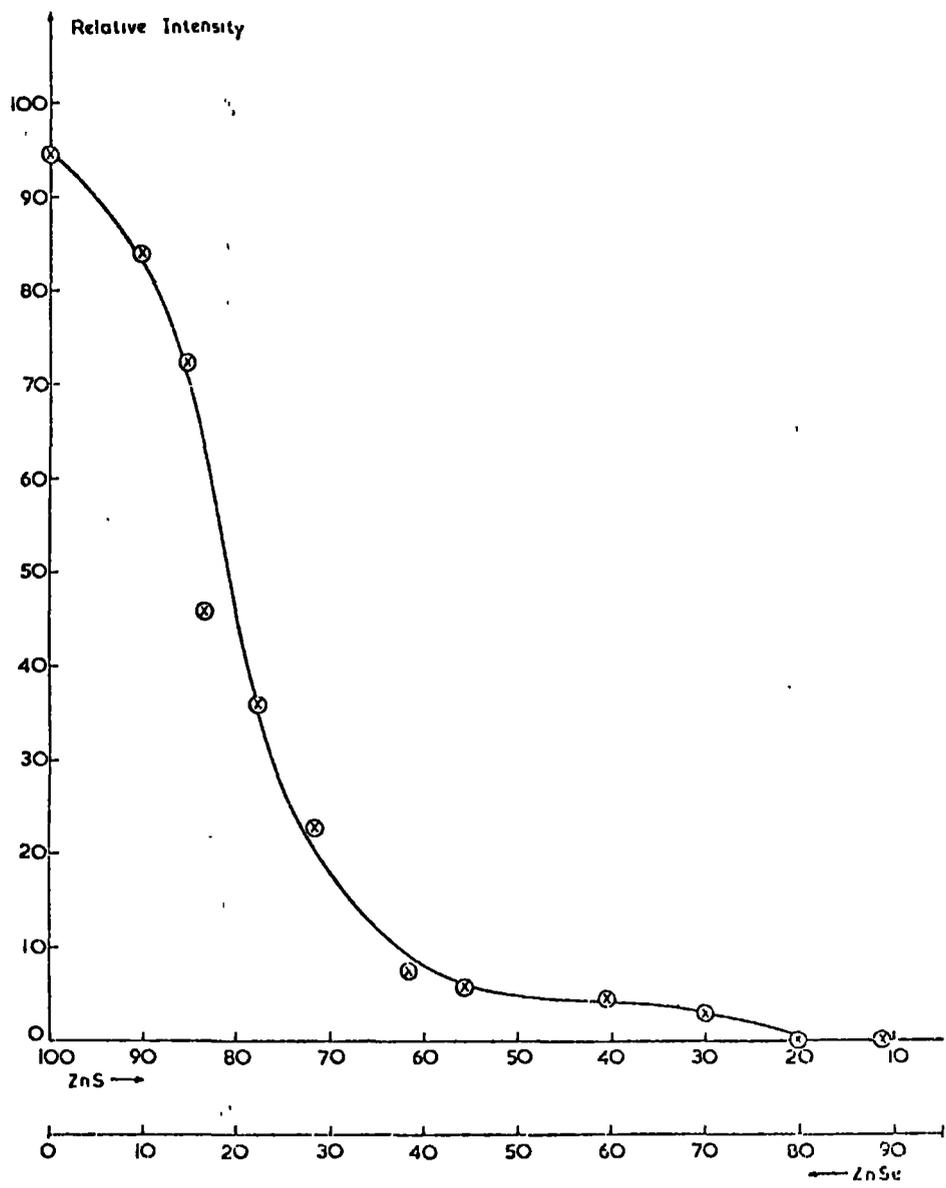
Fig.(7.4)   Luminescence of Mn-doped Zn(S,Se) powder phosphors
            underU.V. excitation at 300K. The variation in
            ZnS and ZnSe is by weight.

of this band decreased rather sharply as Se replaced S. A similar result

was also obtained at 85 K. ESR investigations of the Zn(S:Se):Mn samples

were carried out to see if information could be obtained concerning the

manner in which Se replaced S in Zn(S:Se), and also to see if reasons

could be found for the quenching of the Mn emission band as Se replaced

S. However, with an Mn concentration of 1% in the samples, dipole-dipole

interactions arising from the $Mn^{2+}$ ions being too close to each other,

produced a single featureless broad line in all the samples, which

yielded no information. To overcome this effect of dipole-dipole broad-

ening a new series of Zn(S:Se)Mn solid solution samples with an Mn concen-

tration of 0.2% was prepared. Again the Mn characteristic emission band

at 5800 A was monitored as Se replaced S in Zn(S:Se), and as before a

variation in the intensity of the emission band was observed very similar

to that illustrated in Figure (7.4), without any shift in the spectral

location. ESR absorption spectra of these samples were recorded at room

temperature and at 77 K. Each spectrum was, however, found to consist of

six relatives broad lines in principle corresponding to central transi-

tions $M_{\frac{1}{2}} \longrightarrow M_{-\frac{1}{2}}$ (see Section 5.6 ). To obtain information regarding

the manner in which Se replaces S in Zn(S:Se), it would be necessary to

resolve these lines. The ESR spectrometer used proved, however, of

insufficient sensitivity and resolving power for this purpose. In principle

as a $Se^{-2}$ ion replaces one of the four $S^{-2}$ ions which surround the $Mn^{2+}$

ion tetrahedrally there would be a change in the symmetry of the crystal

field in the vicinity of the $Mn^{2+}$ ion. This change would affect some of

the energy states of the $Mn^{2+}$ ion, which in turn would be reflected in

the ESR absorption spectrum. In this connection it is relevant to

consider briefly the conclusions reached by Asano et al (18) who

studied the ESR spectra and the emission band of the $Mn^{2+}$ ion in

Zn(S:Se) as the composition was altered. According to Asano et al,

when the ZnSe fraction in Zn(S:Se)Mn is below approximately 60 mole%

none of the four $S^{-2}$ ions surrounding the $Mn^{2+}$ ion is replaced by $Se^{-2}$

and the crystal field is quasi-cubic. When the fraction of ZnSe is

between 60 and 90 mole% some of the $S^{-2}$ ions are replaced and the

crystal field appears to be non-cubic. However, the crystal field

again appears to become quasi-cubic when the ZnSe fraction is above

90 mole% implying that all the $S^{-2}$ ions have been replaced by $Se^{-2}$.

Parallel with the ESR investigations Asano et al also studied the Mn

emission band as the Zn(S:Se) composition was altered. From their

data they maintained that the Mn emission band in ZnS at 5800 A (at

room temperature) remains unchanged for Zn(S:Se) compositions below

about 60 mole% ZnSe, then it shifts rapidly to a much broader band

with a peak at 6400 A for compositions with higher fractions of ZnSe.

According to Asano et al this band at 6400 A excited with U.V.

radiation of 3650 A is the characteristic Mn emission band in ZnSe.

To account for it being broader than the emission band in ZnS:Mn,

Asano et al suggest splitting of the sub-levels of the orbital multiplets

between the excited states of the $Mn^{2+}$ ion.

Generally in ZnS:Mn as $Se^{-2}$ replaces the $S^{-2}$ ions that surround

the $Mn^{2+}$ ion, more lattice space becomes available to the $Mn^{2+}$ ion,

and it follows that in accordance with the findings of Klasens et al

discussed on page 177 , the Mn emission band at 5800 A should shift to

shorter wavelengths. At the same time since ZnSe is more covalently

bonded than ZnS, there would be a tendency for the characteristic Mn

emission band to shift towards the longer wavelengths. These two

counteracting effects may cancel each other out or one of them may

dominate the other to a small extent. In any case it is principally

within the context of these two counteracting effects that any shift

in the spectral location of the Mn emission band from 5800 A must

be explained.

As discussed above, as Se replaces S, there should in principle,

be a gradual shift in the spectral location of the 5800 A emission band.

The fact that only a decrease in the intensity of this emission band

was observed as the composition Zn(S:Se) was altered tends to suggest

that as soon as one of the four $S^{-2}$ ions surrounding Mn was removed

(or replaced) the emission from that $Mn^{2+}$ ion ceased. From the experi-

mental results this appears to be the case, otherwise, a shift in the

spectral location would have been observed. From this it follows that

Figure (7.4) also represents the relative probability of finding four

S ions surrounding a. $Mn^{2+}$ ion as the composition Zn(S:Se):Mn is

altered. (In stating this the effect of the third nearest neighbour

shell of S or Se ions surrounding the Mn is neglected, since the con-

tribution of the third nearest neighbour shell to the crystal field

in the vicinity of the $Mn^{2+}$ ion is very small compared with the contri-

bution of the first and the second shell). This should be contrasted

with the conclusion of Asano et al mentioned in the previous page

regarding the manner in which $S^{-2}$ ions were replaced in their Zn(S:Se)

solid solution samples. It is interesting to compare Figure (7.4) with

Figure (7.5) which illustrates the theoretically calculated results

of Schneider et al (20) showing the statistical (relative) probability

of finding four $S^{-2}$ ions in the first shell around a four-fold co-

ordinated metal ion (e.g. Mn) as the composition Zn(S:Se) is altered.

There is good agreement between Figure (7.4) and the theoretically

calculated relative probabilities of Figure (7.5). It is, however,

important to note that Schneider et al calculated the data of

Figure (7.5) on the assumption that the distribution of $S^{-2}$ and $Se^{-2}$

ions in Zn(S:Se) is governed by the laws of statistics, without any
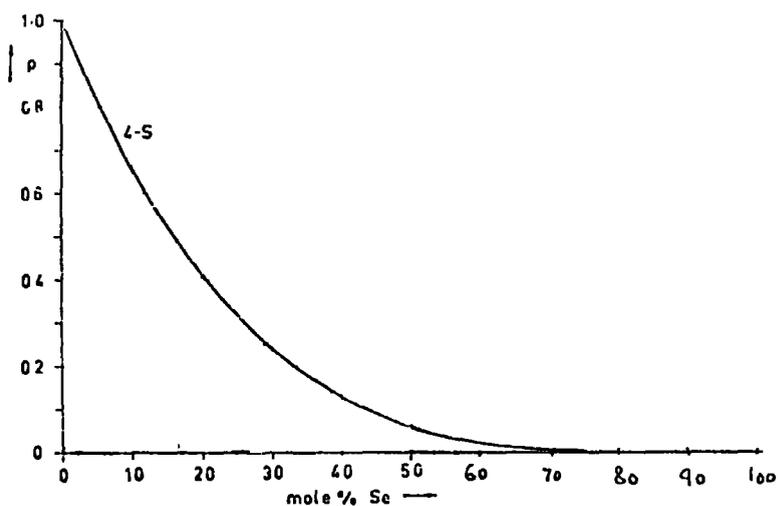
Fig.(7.5) Statistical probability of finding in the first shell around a fourfold co-ordinated metal ion four sulphur ions in Zn(S,Se).

preference that S or Se may have for co-ordination with a metal impurity ion such as Mn.

As mentioned before, no information could be obtained from the ESR investigations concerning the quenching of the Mn emission as $S^{-2}$ ions were replaced by $Se^{-2}$ in Zn(S:Se) solid solutions. Basically in Mn photoluminescence occurs as a result of direct absorption of optical energy by the ion itself. This results in electrons being raised to the excited states with subsequent emission of optical energy when the electrons return to the ground state. Poisoning or quenching of luminescence may occur if the $Mn^{2+}$ ions are prevented from absorbing optical energy or if their efficiency is greatly affected. In our case when the intensity of the $Mn^{2+}$ emission band decreased as ZnSe is incorporated in ZnS:Mn, one may assume that incorporation of ZnSe produced killer centres. Killer centres may operate, for instance, by absorbing the exciting radiation to such an extent that the density of optical excitation left becomes insufficient for a reasonable number of the $Mn^{2+}$ ions to produce a detectable level of emission, or alternatively the killer centres may interact with the $Mn^{2+}$ ions directly or indirectly to prevent them from absorbing a sufficient level of optical energy, or to affect favourably the non-radiative processes within the $Mn^{2+}$ ions, or to dissipate the energy absorbed by the $Mn^{2+}$ ions through a non-radiative transfer process from the activator (Mn) to a killer centre. There is also another possibility, and that is if the radiation emitted by the $Mn^{2+}$ ions is very efficiently absorbed by other centres (killer) in the sample so that no radiation can actually escape from the sample. In our case since the experimental samples were very thin, this last possibility is probably very unlikely. Apart from this it is not possible to say which of the above possible processes may have been responsible for

the poisoning of the Mn emission in our samples. Nor is it possible to consider the identity of the killer centres, which may have been simple, or complex native defects or very small traces of impurities. What is, however, very clear is that the concentration of the killer centres depended on the amount of ZnSe incorporated in ZnS:Mn.

Poisoning of phosphors by traces of impurities is well known (21). In ZnS:Mn Bube et al (22) investigated the poisoning of the Mn emission band by traces of Fe, Ni and Co impurities. In general it was found that very small traces of these impurities affected the emission band. For instance addition of 0.0003% of Ni to ZnS:Mn (Mn concentration 1%) reduced the intensity of the Mn emission band to 40% of that of an unpoisoned sample. From their investigations Bube et al concluded that the principal poisoning mechanism was inter- action between the impurities and the $Mn^{2+}$ ions. However, Bube et al from their investigations could not elaborate on the actual nature of the interaction between the poison centres and the $Mn^{2+}$ ions.

Apart from killer centres poisoning the Mn emission band, there is also the possibility of the emission band being quenched by a high density of free carriers. Thus in a recent investigation Jones and Woods (23) found that the characteristic Mn emission band in ZnSe:Mn (see below) disappeared if the sample was heated in molten zinc at $850^{\circ}C$ for one week. Since one very well known effect of heating a sample in molten zinc is to increase the conductivity by removing some of the acceptor-like compensating centres, Jones and Woods suggest that the characteristic Mn emission band in ZnSe cannot be produced in the presence of a high concentration of free electrons because Auger processes quench the emission.

Since the completion of the experimental investigations by the author, a paper published recently by Jones and Woods (23) goes a long way to remove the ambiguities associated with the $Mn^{2+}$ ion emission band in ZnSe. Briefly, Jones and Woods carried out systematic experiments to determine the excitation bands of the $Mn^{2+}$ ion in ZnSe. Then irradiation in one of the excitation bands with a peak at 5370 A, corresponding to the $^6A_1 \longrightarrow ^4T_1$ transition was used to monitor the emission. An emission band was then observed at 5900 A (at room temperature) which showed all the characteristics of an internal transition within an ion. Further investigations confirmed that this was indeed the $Mn^{2+}$ emission band in ZnSe, i.e. the band width, temperature variation etc., were found to be very similar to the characteristic Mn emission band in ZnS. Moreover, Jones and Woods found that excitation with U.V. radiation with wavelength 3650 A pro- duced much broader emission bands with maxima in the range 6200-6400 A depending on the sample. These bands were found to mask the Mn emission band completely. Thus from the work of Jones and Woods it appears that to observe the Mn emission band unambiguously, excitation must·be with light of wavelength 5370 A, and not with U.V. radiation with $\lambda$ = 3650 A.

The origin of the emission bands occurring in the range 6100-6500 A in ZnSe observed by the author and other investigators is not known with certainty. Two possible emission bands have been considered;  one the self-activated band, and the other the low-energy Cu band.

Of the variety of defects that may be introduced in the II-VI compounds during the firing process, cations and/or anion vacancies almost always unavoidably come into existence. In ZnS the cation vacancy has been thought for a long time to be associated with an emission

band centred at about 4560 $\overset{o}{A}$, the so called self-activated emission

band.  Originally Kroger and Vink (24) suggested that the centre

responsible consisted of a Zn vacancy and a neighbouring $S^{-2}$ ion

that had lost one of its electrons.  Magnetic susceptibility experi-

ments, however, indicated that the self-activated centre was diamagnetic

(25) whereas the model proposed by Kroger and Vink was paramagnetic.

Another model suggested by Prener and Williams (26) regarded the

self-activated centre as consisting of a Zn vacancy with which a charge

compensating donor (e.g. Cl, Br, Al etc.) was associated at the

nearest neighbour site in the lattice.  This model was supported by

various luminescence experiments (27), and furthermore, ESR studies

provided unambiguous identification of the centre in agreement with

the model proposed.  For a discussion of this centre, and the fact

that there are basically two self-activated centres depending on

whether Cl, Br, I or Al, Ga are used as the associated donors, the

reader should consult Section  4.9 .  Here suffice it to say that in

cubic ZnS the self-activated emission band ranges from 4560 A in ZnS:Cl

to 4700 A in ZnS:Al and ZnS:Ga at room temperature.

To study the effect on the self-activated band of ZnS of

replacing S by Se, Leverenz (28) and Lehmann (29) monitored the S.A.

band in a series of Zn(S:Se):Br solid solution samples.  They found

that initially the gradual replacement of S by Se produced a green

band in addition to the S.A. blue emission band of ZnS.  This green

emission band became of equal intensity to the S.A. blue band when

the ZnSe fraction in Zn(S:Se) was about 5%.  As the ZnSe fraction was

gradually increased, the intensity of the blue band decreased and also

the peak of the green band shifted towards the red part of the spectrum.

This continued with increased ZnSe fraction until the S.A. blue band

could no longer be detected.  At that composition the green emission

band had moved to the red part of the spectrum with its peak at
6200-6250 A at 77 K.

In parallel with the investigation of luminescence in our
samples, ESR studies were also carried out under U.V. excitation to
see if the self-activated centre could be detected in any of them.  Of
the 17 different samples investigated at 77 K, in none could an ESR
signal characteristic of the self-activated centres be detected.  Nor
was there any such signal in the seven samples investigated at
temperatures down to 4.2 K.  This is rather surprising since most of
these samples were doped with such donors as Al, Cl and I, and in
almost all of them there was an emission band in the 6200-6450 A
region.  However, in samples doped with donors, apart from that doped
with I, an ESR signal characteristic of free electrons was detected
(see Section 6.2 ).  Since the S.A. centre becomes paramagnetic under
U.V. excitation, the level of the optical energy that samples in the
microwave cavity received was investigated in a darkened laboratory.
This was found to be satisfactory in the sense that luminescence from
samples in the microwave cavity could be observed with the naked eye.
It therefore follows that if self-activated centres had existed in
the samples investigated, its ESR absorption should have been detected.
This remark also applies to the basic  ZnSe powder (supplied by
Derby Luminescent Ltd) which under U.V. excitation produced an emission
band at approximately  6250 A at room temperature (ESR studies of this
powder indicated traces of Mn impurity).

Since NaCl, a well known flux, has been used to produce the
self-activated centres in ZnS (30), ZnSe:NaCl samples were made by
firing ZnSe and NaCl at $1000^{o}$C for two hours.  The object of this was
to produce S.A. centres so that their characteristic emission band
and ESR spectra could be investigated.  Optical investigation of a

sample doped with 0.5% NaCl showed a very sharp decrease in the intensity of the emission band at 6250 A compared with an undoped sample. This emission band was not observed when the concentration of NaCl in the phosphor slurry was increased to 0.7%. ESR investigation of these samples at temperatures as low as 4.2 K failed to show any sign of the self-activated centres.

In ZnSe the only report of the ESR of the self-activated centres is due to Holton et al (31) who investigated the emission bands in ZnSe doped with Al, Cl and Br. They report the ESR of the self-activated centres in ZnSe:Al only. The emission bands which Holton et al consider to be due to the self-activated centres in ZnSe:Al and ZnSe:Cl are respectively at 6410 A and 6250 A at 4.2 K.

From the ESR results obtained it appears that the emission bands in the samples investigated were not due to the self-activated centres. In the ZnSe powder, for instance, if the self-activated centres had been responsible for the emission band at 6250 A, there seems no reason why the emission should cease when NaCl was incorporated in the powder. This should be contrasted with ZnS, in which Kassi et al (32) in their investigations (ESR and luminescence) of the self-activated centres doped ZnS with NaCl in order to produce the self-activated centres. Of course NaCl has been used as a flux in the II-VI phosphors for a very long time.

In the absence of more definite information about the impurities in the ZnSe powder, it is very difficult to account for the quenching effect of NaCl or to explain why it failed to produce the self-activated centres as it should have done.

One impurity that may be responsible for the emission bands in ZnSe in the red part of the spectrum, is copper. However, the copper emission bands in ZnSe have not been studied extensively.

In contrast, copper activated ZnS is one of the most investigated
phosphors, as addition of copper to ZnS produces a number of emission
bands in the visible and the infra-red parts of the spectrum. For
a review of these emission bands and some of the models suggested to
account for them the reader should consult Curie and Prener (33).
In particular one of the two main emission bands in the visible part
of the spectrum (i.e. a band at about 5230 A) may be of relevance to
the red emission bands observed in ZnSe. In ZnS all the available
evidence indicates that the green copper band is formed as a result
of the association of copper with a coactivator, e.g. a halogen or
a trivalent element (Al, Ga, In). Of all the models put forward to
explain the green emission, the one which seems to be most satisfactory
is that of William and Prener of associated donor-acceptor centres.
According to this the green emission band occurs when there is a
transition from a donor level (co-activator) to the copper (acceptor)
level. This idea is supported by the experimental work of Kroger
et al (34) who showed that the green emission has a maximum (compared
with the copper blue) when the ratio of copper to co-activator concen-
trations are close to unity.

Klasens (35), Morehead (36) and Lehmann (37) investigated the
spectral shift of the two copper bands in ZnS as Se replaces S in a
series of Zn(S:Se):Cu:Cl solid solutions. Lehmann found that replace-
ment of about 1% of ZnS by ZnSe caused a decrease in the intensity of
the two copper emission bands of ZnS and the appearance of two new
bands of lower photon energies. Further increase of the ZnSe fraction
in Zn(S:Se) produced a comparatively slow shift of these new bands
towards lower energies to finish at 5300 A (green) and 6360 A (red)
in ZnSe at 77 K.

Though the two main copper emission bands in ZnS have been extensively studied, nevertheless there is a slight uncertainty about the spectral position of their peaks. Generally it has been found that the maxima of the peaks may vary from sample to sample over a small range (37).

In our work on ZnSe the starting powder used was found to contain oxygen and traces of Mn. Of the other impurities no information is available, but it seems likely that the powder contained copper and probably some other impurities. If this is correct, then copper in conjunction with donor-type impurities would have produced red emission bands. In this connection it is significant to note that in ZnS:Cu incorporation of oxygen produces the copper green emission band (38). It is very probable that in ZnSe:Cu incorporation of oxygen would produce a red emission band by a similar process.

Since the red copper emission band in ZnSe is probably due to donor-acceptor pairs, i.e. a transition from a donor level to the copper acceptor level above the valence band, depending on the donor depth below the conduction band, the emission band may vary from sample to sample. Unfortunately since the copper ion has a very short relaxation time, its ESR can only be observed at temperatures below 1.2 K. With the cryostat system employed on our ESR spectrometer, it was not possible to achieve such low temperatures. As a result no direct (ESR) evidence can be presented to demonstrate the existence of copper in our samples, although it seems very probable that at least some of the emission bands observed were due to copper-donor pairs.

To understand fully some of the results presented in this chapter, e.g. quenching of the emission band at 6250 A when NaCl was incorporated, quenching of the Mn emission band when ZnSe was added to ZnS:Mn, ZnSe of very much higher purity than that supplied by the Derby Luminescent Ltd. is required. With such material the effect of incorporating controlled impurities may be understood in time.

## NOTE ADDED AFTER TYPING

Concerning the disappearance of the Mn emission band in ZnS:Mn when S was replaced by Se in Zn(S,Se):Mn (see Figure (7.4) , the following possibility must also be considered. In ZnS ($E_g$ = 3.8 eV) U.V. radiation $\lambda$ = 3650 Å , $h\nu$ = 3.4 eV excites the $Mn^{2+}$ ion to produce the characteristic emission band without producing free carriers. However, as the composition of Zn(S,Se):Mn changes by increasing the Se/S ratio, the energy band gap narrows from 3.8 eV in ZnS to a value depending on the Se/S ratio in the Zn(S,Se). In the II-VI compounds assuming a predominantly ionic chemical binding, the conduction band is formed approximately by the cations and the valence band by the anions. It follows that a variation in the ratio Se/S in Zn(S,Se) would produce a change mainly in the valence band while the conduction band remains approximately unaltered. When the energy band gap of the Zn(S,Se):Mn composition approaches, say, 3.4 eV the incident U.V. radiation would produce free carriers as well as exciting the $Mn^{2+}$ ion. Depending on the density of free electrons created, there exists the possibility of free electrons interacting with the excited $Mn^{2+}$ ions in a type of Auger process so as to prevent radiative transition to the ground state. As a result the characteristic Mn emission band may not manifest itself. Such a possibility was recently considered by Jones and Woods ( 24 ) in order to explain the quenching of the Mn band in ZnSe:Mn when the sample had been annealed in molten Zn. In support of such a possibility it is important to bear in mind the result of the spin-lattice relaxation time study of Schneider et al ( 40 ) as mentioned in Section 5.11 . Schneider et al found that the relaxation time $t_1$ of Mn in ZnS decreased rather strongly when the sample was irradiated with U.V. light. Since the effect of U.V. radiation would have been

to create free carriers (as well as exciting the $Mn^{2+}$ ions), Schneider
et al interpreted their results in terms of free electrons shortening
the relaxation time. They, however, made no attempt to obtain a
qualitative relationship between the decrease in $t_1$ and the intensity
of U.V. radiation used. It is important to state that, although a
decrease in $t_1$ was observed with the sample under optical excitation,
no change could be detected in the spin resonance spectrum of the $Mn^{2+}$
ion.

## CHAPTER 8

### SUMMARY, CONCLUSIONS AND SUGGESTIONS FOR FUTURE WORK

The aim of the research work reported in this thesis has been to apply ESR techniques to study (doped and undoped) ZnSe bearing in mind the long-term objective; the need for suitably doped electro-luminescent material.

At the start ZnSe crystals were produced by sublimation at $1300^{\circ}$C using ZnSe powder acquired from Derby Luminescent Ltd. With the exception of Cr, no difficulty was experienced in producing doped crystals by adding the dopant to the charge. Addition of 0.01% Cr, however, prevented charge transport down the temperature gradient and a sintered mass of charge material resulted. This sintered material was pulled through the temperature gradient a second time but with no improvement. Except for the difficulty with Cr, this method of producing ZnSe crystals with the charge at $1350^{\circ}$C, on the whole yielded reasonably large single crystals (of about 4 millimeter dimensions). The crystals had a deep red body colour and luminesced in an emission·band at about 6500 A under U.V. excitation at room temperature.

Examination of the spin resonance spectrum of the $Mn^{2+}$ ion in these crystals indicated that they had a mixed cubic-hexagonal structure. A comprehensive programme of annealing was undertaken to see if the hexagonal phase could be converted into cubic, as is usually observed and reported in the flow crystals, but with no result. Instead it was found that annealing at $1050^{\circ}$C increased the hexagonal proportion in each sample, i.e. the cubic ⟶ hexagonal phase transition occurred. To investigate this further, attempts were made to produce (cubic) ZnSe crystals at low temperatures employing the iodine transport technique. With the Derby ZnSe powder no charge transport could be achieved.

However, crystals were grown successfully at 850°C when pre-sublimed

ZnSe material was used. On the whole crystals obtained at 850°C were

smaller than those produced by sublimation at 1300°C. They had an

orange-red body colour and luminesced in an emission band at about 6400Å

under U.V. excitation at room temperature. Addition of Mn to the charge

slightly retarded the charge transport down the temperature gradient.

From the spin resonance of the $Mn^{2+}$ ion in these crystals it

was concluded that they had a cubic structure. Since a cubic ⟶

hexagonal phase transition had occurred at 1050°C (in crystals produced

at 1300°C) similar annealing treatments were also carried out with the

crystals grown at 850°C., However, no cubic ⟶ hexagonal phase

transition could be achieved in these. From the facts that in flow

crystals annealing has so far produced only a hexagonal ⟶ cubic

phase transition, and that the cubic ⟶ hexagonal phase transition

observed in crystals produced at 1300°C is slow, it is concluded that

the hexagonal phase in ZnSe is metastable, and that it had occurred in

crystals produced at 1300°C, not for thermodynamic reasons, but because

of presence of an impurity. Examination of the Derby ZnSe powder by

X-ray techniques indicated that it contained a measurable quantity

of ZnO. Considering the fact that ZnO crystallizes with a hexagonal

structure, it is suggested that the presence of ZnO in the starting

material produced the hexagonal phase in ZnSe crystals grown at 1300°C.

The phase transition results, and the relevant discussions in general,

in the II-VI compounds and in ZnSe are presented in Section 5.14 - 5.17.

While Sections 5.7 and 5.9 contain the electron spin resonance of $Mn^{2+}$

ion in cubic ZnSe and in ZnSe crystals with a cubic-hexagonal structure.

To compare the solubility of Mn in crystals produced at different

temperatures, slices were cut from crystals produced at 1300°C, and

after polishing they were examined under a polarizing microscope. Small

regions exhibiting no birefringence were considered to be cubic, and small samples were made of them. They were then subjected to X-ray and spin resonance investigation to confirm their structure. Those that were cubic were used to study Mn solubility in crystals produced at 850°C and at 1300°C. Comparing the spin resonance of the $Mn^{2+}$ ion in different crystals, it was found that Mn has a larger solubility in crystals produced at 1300°C. For instance in crystals produced at 850°C with a Mn concentration of 0.1% the $Mn^{2+}$ ions were found to be close enough to each other to produce dipole-dipole interaction which resulted in a distorted spin resonance spectrum. On the other hand in crystals produced at 1300°C with a Mn concentration of 0.4% no dipole-dipole interaction could be detected in the spin resonance of the $Mn^{2+}$ ion.

ZnSe crystals were also produced at 1100°C in a vertical furnace (by another member of the research group). Considerable difficulty was experienced in introducing Mn into crystals grown in this way. Spin resonance investigations indicated that when Mn was added to the charge, a negligible amount of it was incorporated in the resultant crystals. Furthermore, what little Mn had been incorporated, was found to be con-centrated in a few points in each sample, so that the weak spin resonance signal showed strong dipole-dipole interaction. A much better result was eventually obtained when Mn as $MnCl_2$ was added to the Zn reservoir. On the whole crystals produced at 1300 and 850°C were of very much better quality than the crystals produced at 1100°C. For instance in these latter crystals twinning was found to be very common. The electron spin resonance of $Mn^{2+}$ ions in a twinned crystal is described in Section 5.8. Generally in a cubic crystal twinning produces a stacking fault (with hexagonal packing) which may affect the spin resonance of the $Mn^{2+}$ ion. In our case with our spectrometer and samples it was

not possible to investigate this.

Attempts were made to dope ZnSe crystals with Mn by diffusion at $950^{\circ}$C but with no success. Similarly no diffusion of Mn into ZnSe took place when the sample was heated in molten Zn at $850^{\circ}$C to which Mn had been added. From these experiments it is concluded that ZnSe cannot be doped with Mn by diffusion. It is important to note that Mn has a larger ionic radius than Zn and that incorporation of Mn at a Zn site would require the lattice to undergo a local expansion. ZnSe:Mn crystals were also annealed in molten Zn as part of a programme to study the effect of annealing in Zn and Se. Spin resonance results indicated that annealing ZnSe:Mn in molten Zn removes some of the Mn impurity. Since the completion of this research work, atomic absorption spectroscopy carried out for Jones and Woods has indicated that annealing in molten Zn has no effect on Mn. This result is rather surprising, because incorporation of Mn in ZnSe results in the lattice becoming slightly strained. At $850^{\circ}$C in molten Zn it is very probable that the lattice would tend to eject Mn so that the strained regions could return to normal. It is also important to bear in mind that as-grown ZnSe crystals usually have large densities of vacancies and that these vacancies should help the Mn to diffuse out. In the crystals produced at $850^{\circ}$C, the spin resonance results show that at a Mn concentration of 0.1% the Mn ions were aggregating close to each other to produce dipole-dipole interaction. This certainly is not a high concentration. Even assuming the Mn solubility in the crystals produced at $1300^{\circ}$C to be ten times larger, this still is not a high concentration. It therefore follows that Mn does not have a high solubility in ZnSe; probably its solubility is lower than that in molten Zn at $850^{\circ}$C.

In Chapter 7 the efforts made to identify the Mn emission band in ZnSe were described. In the light of the results published by

Jones and Woods it is now clear that to observe the characteristic Mn
emission band unambiguously the excitation should be with wavelengths
lying within the 5370 A excitation band.  If U.V. radiation is used,
a broad emission band may mask the narrower Mn band completely.

In Chapter 7 also an explanation was given for the quenching of
the Mn emission band in Zn(S,Se):Mn as Se replaced S.  The explanation
was based on impurity killer centres.  Another possible explanation is
that of free electrons (created by the U.V. radiation) de-exciting
the Mn centres, since in ZnSe with its band gap of 2.7 eV, U.V. radiation
of wavelength 3260 A can create a relatively high density of free
carriers.

No conclusive explanation was, however, offered for the emission
band observed in Mn-doped and undoped ZnSe samples.  Spin resonance
experiments carried out to look for the self-activated centres in
ZnSe gave negative results, even in samples doped with such donors as
Cl, I and Al.  Instead the spin resonance of mobile donor electrons was
detected.  In Section 6.2 where the spin resonance investigations of
a number of samples doped with donor impurities are discussed, it was
concluded that the resonance signal due to Al could be detected more
readily and consistently than that of any other donor impurity.  Further-
more experiments carried out to determine if ZnSe could be doped with
Al by diffusion indicated that unlike Mn, Al does diffuse into ZnSe.
One very interesting feature in the samples doped with donors was that
(with the exception of I-doped samples) the spin resonance signal due
to mobile donor electrons could be detected in the dark, only after the
samples had been annealed in molten Zn (a process which usually increases
the conductivity).

In Section 6.1 the spin resonance investigation  of Cr doped ZnSe
was described.  Attempts were made to produce single crystals of ZnSe

doped with Cr, but with the high temperature sublimation method as well as the low temperature iodine method, addition of Cr was found to prevent charge transport completely. As a result sintered (polycrystalline) samples had to be used. From the spin resonance results the trapping centre associated with Cr in ZnSe was found to lie 0.51 eV below the edge of the conduction band. This is the first report of the energy depth of this trapping centre in ZnSe.

### Suggestions for Future Work

To extend the work reported in this thesis an important requirement would be ZnSe starting material of very much better purity than that obtainable from Derby Luminescents Ltd. In this connection the work started in the department to produce ZnSe from high purity elements (Zn and Se) should in time make a significant contribution. With the high purity material crystals should be produced at $1300^{\circ}$C (with and without ZnO to test the explanation offered in Section 5.17 for the occurrence of the hexagonal phase in crystals produced at $1300^{\circ}$C. Attempts should also be made to produce crystals at $850^{\circ}$C by the iodine transport method again with and without ZnO to determine if oxygen is the agent that prevents charge transport. This is stated as, at the moment, it is not possible to explain why no charge transport took place when the Derby ZnSe was used as the starting material in the iodine transport method.

The study of the solubility of Mn in crystals produced at different temperatures should be extended by finding the critical concentrations at which aggregating Mn ions produce a dipole-dipole interaction. Needless to say such a study should also include crystals produced at $1100^{\circ}$C.

The effect of annealing ZnSe:Mn crystals in molten Zn needs more comprehensive investigations. Spin resonance studies and atomic

absorption spectroscopy should be carried on the same sample (if possible) so that the present disagreement could be resolved. This is very important as at the moment annealing in molten Zn is the only way of reducing the resistivity of the as-grown samples, and also Mn is required as the emission centre for electroluminescent devices.

The effect of Cr in preventing charge transport should be studied with high purity ZnSe material to see if it is the interaction of Cr with ZnSe that disrupts charge transport or interaction of Cr with some other impurity (as possibly existed in the Derby ZnSe powder).

Efforts should be made to create the self-activated centre for spin resonance and optical studies and to find out under what circumstances donor impurities associate with native defects to form the self-activated centre, and under what circumstances they do not, i.e. in the samples investigated donor impurities were found (e.g. Al), but not the self-activated centres.

In the iodine-doped samples no spin resonance signal from the donor electrons could be detected in the dark or under optical excitation in the as-grown samples. Yet after annealing in molten Zn such a signal appeared (only) under optical excitation. This is rather odd compared with crystals containing other donor impurities, and should be studied further, preferably in conjunction with optical and transport investigations.

The possibility of free carriers de-exciting the Mn centres needs comprehensive investigation. A quantitative relationship between the density of free carriers and any accompanying decrease in the relaxation time, $\tau_1$, can be obtained by measuring $\tau_1$ with the sample receiving different intensities of U.V. radiation (this can be done by modifying the existing spectrometer with electronic apparatus already present in the department). This coupled with transport measurements (on the same

sample in darkness and under U.V. excitation) would relate the decrease

in the relaxation time to carrier density and mobility.  Such combined

investigations would go a long way to clarifying the various issues.

REFERENCES   -   CHAPTER 2

(1)    R. Frerichs  Phys. Rev.  72,  594,  1947

(2)    J.M. Stanley  J. Chem. Phys.  24,  1279,  1956

(3)    Park and Chan  J. Appl. Phys.  36,  800,  1965

(4)    Fitzgerald, Mannami, Pogson and Yoffe  J. Appl. Phys.  38, 3303, 1967

(5)    Dean and Merz  Phys. Rev.,  178,  1310,  1969

(6)    Pashinkin, Tishchenko, Korneeva and Royzhenko   Kristallographiya
       5,  261,  1960

(7)    H. Hartmann    Kristall and Technik,  5,  527,  1970

(8)    D.C. Reynolds and S.J. Czyzak  Phys. Rev.  79,  543,  1950

(9)    W.W. Piper and S.J. Polich  J. Appl. Phys.  32,  1278,  1961

(10)   L. Clarke and J. Woods  Brit. J. Appl. Phys.  17,  319,  1966

(11)   L. Clarke and J. Woods  J. Cryst. Growth,  3,  127,  1968

(12)   M. Aven et al  J. Appl. Phys.  32,  2261,  1961

(13)   K. Burr and J. Woods  J. Mat. Sci.  6,  1007,  1971

(14)   Y. Tswyimoto et al   Jap. J. Appl. Phys.  5,  636,  1966

(15)   R.S. Title   Phys. Rev.  133,  A1613,  1964

(16)   R. Nische   J. Phys. Chem. Solids,  17,  163,  1960

REFERENCES - CHAPTER 3

(1)    L. Pauling    The Nature of the Chemical Bond , Connell U.P, 1939

(2)    R.H. Bube    Photoconductivity in Solids,  John Wiley & Son N.Y.,  1960

(3)    B. Segall    Phys. Rev.  105,  108,  1957

(4)    J.L. Birman    Phys. Rev.  109,  810,  1958

(5)    F.E. Williams    Theorie des Centres Luminogenes dutype donneur-
       accepteur Associes,  17,  671,  1956

(6)    M. Balkanski,  Proprietes Optiques des Semi-conducteurs  2,  79,
       1959,  Faculte des Science Paris

(7)    D. Curie    Luminescence in Crystals,  P.111,  Methuen,  1963

(8)    L. Pauling,  The Nature of the Chemical Bond,  P.6,  34  Cornell U.P.
       1945

(9)    B.D. Saksena    Phys. Rev.  81,  1012,  1951

(10)   L. Pauling    The Nature of the Chemical Bond P.178,  Cornell U.P.
       1945

(11)   C.A. Coulson, L.B. Redei and D. Stocker    Proc. Roy. Soc. (Lond.)
       270,  352,  1962

(12)   J.C. Phillips    Rev. Mod. Physics,  42,  317,  1970

(13)   R.M. Martin    Phys. Rev.  B1,  4005,  1970

(14)   R.M. Martin    Sol. Stat. Comm.  8,  799,  1970

(15)   D.L. Camphaussen    Phys. Rev. Letts.  26,  184,  1971

(16)   J.P. Walter    Phys. Rev. Letts.  26,  17,  1971

(17)   J.S. Van Wieringen,    Discussions Faraday Soc.  19,  118,  1955

(18)   O.N. Matamura    J. Phys. Soc. Japan,  14,  108,  1959

(19)   Fidone and Stevens    Proc. Phys. Soc.  73,  116,  1959

(20)   F. Herman    J. Electronics  1,  103,  1955

(21)   R.H. Parmenter    Phys. Rev.  100,  573,  1955

(22)   G. Dressenhaus    Phys. Rev.  100,  580,  1955

(23)   J.P. Walter and M.L. Cohen    Phys. Rev.  183,  763,  1969

(24)   D.J. Stukeel et al    Phys. Rev.  179,  740,  1969

(25)   J.P. Walter et al    Phys. Rev.  B1,  2661,  1970

(26)     Y. Petroff, M. Balkanski, J.P. Walter and M.L. Cohen,   Sol. Stat.
         Comm.  7,  459,  1969

(27)     M.L. Cohen and T.K. Bergstresser   Phys. Rev. 141,  789,  1966

(28)     M. Aven, D.T.F. Marple and B. Segal   J. App. Phys. Supp.  32,
         2251,  1961

(29)     D.C. Reynolds et al   J. App. Phys. 32,   2250,  1961

(30)     Aven and Segall   Phys. Rev. 130,  81,  1963

(31)     C.E. Hite, D.T.F. Marple, M. Aven and B. Segal   Phys. Rev.
         156,  850,  1967

(32)     M. Cardona   J. Appl. Phys.  32,  2151,  1961

(33)     M. Balkanski   J. Phys. Chem. Solids,  27,  299,  1966

(34)     D.T.F. Marple   J. Appl. Phys.  35,  1879,  1964

(35)     J.L. Burman   Phys. Rev.  115,  1493,  1959

                      Phys. Rev.  109,  810,  1958

(36)     M. Cardona   Phys. Rev.  129,  1068,  1963

(37)     M. Cardona and G. Harbeke   Phys. Rev.  137,  A1467,  1965

(38)     W.Y. Liang and D. Yoffe   Proc. R. Soc.  A300,  326,  1967

(39)     Y.S. Park and F.L. Chan   J. Appl. Phys.  36,  800,  1965

(40)     Aven, Marple and Segal   J. Appl. Phys. Supp. 32,  2261,  1961

(41)     R.L. Bower and G.D. Mahan   Phys. Rev.  185,  1073,  1969

(42)     R.H. Bube   Phys. Rev.  110,  1040,  1958

(43)     Aven and Halstead   Phys. Rev.  137,  A228,  1965

(44)     G.B. Stringfellow and R.H. Bube   Phys. Rev.  171,  903,  1968

(45)     H.H. Woodbury and M. Aven   7th Int. Conf. Phys. Semicond.  P.179
         Paris  1964

(46)     Y. Fukuda and M. Fukai   J. Phys. Soc. Japan  23,  902,  1967

(47)     M. Aven    J. Appl. Phys.  42,  1204,  1971

(48)     M.R. Lorenz and H.H. Woodbury   Phys. Rev. Lett.  10,  215,  1963

(49)     Lorenz, Segall and Woodbury   Phys. Rev.  134,  A752,  1964

REFERENCES - CHAPTER 4

(1)    J. Becquerel   Z. Physik  58,  205,  1929

(2)    H.A. Bethe  Ann. Phys. LPZ,  3,  133,  1929

(3)    H.A. Kramer   Proc. Acad. Sci. Amst.  33,  959,  1930

(4)    J.H. Van Vleck    Electric and Magnetic Susceptibility  Oxford U.P.
       1932

(5)(6) J.H. Van Vleck    J. Chem. Phys.  3,  807,  1935
                         J. Chem.Phys.  7,  61,  1939
                         J. Chem.Phys.  7,  72,  1939
                         Phys. Rev.  57,  426,  1940
                         Phys. Rev.  71,  413,  1947

(7)    C.J. Gorter   Phys. Rev. 42,  437,  1932

(8)    G.E. Pake   Paramagnetic Resonance  P.56,  W.A. Benjamin Inc.  1962

(9)    A.A. Abragam and B. Bleaney    Electronic Paramagnetic Resonance of
       Transition Ions   P.590,  Oxford U.P.  1970

(10)   M. Tinkham    Group Theory and Quantum Mechanics  McGraw-Hill  1964

(11)   C.M. Herzfeld and P.H. Meiyer    Solid Stat. Phys. 12,  1,  1961

(12)   J.S. Griffith    The Theory of Transition Metal Ions  P.330
       Cambridge U.P.  1961

(13)   K.W. Stevens    Proc. Phys. Soc. A65,  209,  1952

(14)   W. Low    Sol. Stat. Phys. Suppl.  2,  39,  1960

(15)   B. Bleaney and K.W. Stevens    Rept. Prog. Phys.  16,  108,  1953

(16)   K.W. Stevens    Magnetism I,  Ed. G.T. Rado and H. Suhl    Academic
       Press  1963

(17)   J.R. Brailsford    Ph.D. Thesis  Durham University  1967

(18)   R.S. Title  Phys. and Chem. of II-VI Compounds  P.267,  Ed.
       M. Aven and J.S. Prener,  North Holland Pub. Co.  1967

(19)   G.D. Watkin    Bull. Am. Phys. Soc.  14,  312,  1969

(20)   F. Kroger and    Vink,  J. Chem. Phys. 22,  250,  1954

(21)   R. Bowgers and N.T. Melamed    Phys. Rev.  99,  1781,  1955

(22)   J.C. Prener and F.E. Williams    J. Chem. Phys.  25,  361,  1956

(23)   J.S. Prener and J. Weil   J. Electrochem. Soc. 106, 409, 1959

(24)   P.H. Kasi and Y. Otomo   Phys. Rev. Lett, 7, 17, 1961

(25)   J. Schneider, W.C. Holten, T.L. Estle and R. Rauber   Phys. Letts.
       5, 312, 1963

(26)   S. Shivnoya, T. Koda, K. Era and H. Fujiward   J. Phys. Soc.
       Japan 18 Suppl. II, 299, 1963

(27)   J. Diekeman, S.H. De Bruin, C.Z. Van Dooran and J.H. Haanstra
       Phys. Res. Rept. 19, 311, 1964

(28)   S.H. De Bruin , J. Dieleman and C.Z. Can Doorn   Acta. Phys.
       Polon. 26, 579, 1964

(29)   R.S. Title   Phys. and Chem. of II-VI Compounds P.299
             Ed. M. Aven and J.S. Prener,   North Holland Pub. Co.   1967

(30)   W.C. Holton, M. de Wit,  R.K. Watts, T.L. Estle and J. Schneider
             J. Phys. Chem. Sol. 30, 963, 1969

(31)   I. Broser and H. Maier   J. Phys. Soc. Japan, 21,  Suppl. 254, 1966

(32)   I.,Broser, H. Maier and H.J. Schulz,  Phys. Rev. 140, A2135, 1965

(33)   R.K. Watts,' Phys. Rev. 188, 568, 1969

(34)   K. Morigaki   J. Phys. Soc. Japan 19,  1240

(35)   R.S. Title, B.L. Crowden and J.W. Mago  in  II-VI Semiconducting
             Compounds,  P.1367,  Ed. D.G. Thomas, Benjamin N.Y. 1967
       J. Schneider,  Ibid.  P.40
       W.C. Holton, M. deWit, T.L. Estle, B. Dischler and J. Schneider
             Phys. Rev. 169, 359, 1968
       R.C. Kemp,  J. Phys. (Sol. Stat. Phys.) 2, 1416, 1969

(36)   R.C. Kemp,  Phys. Stat. Sol. 42, 795, 1970

(37)   R.K. Watts,  Phys. Rev. 2, 1239, 1970

(38)   K. Sugibuche and Y. Mita,  Phys. Rev. 147, 355, 1966

(39)   K. Suto and M. Aoki,  J. Phys. Soc. Japan, 26, 287, 1969

(40)   J.S. Van Weiringen, Dis. Faraday Soc. 19, 118, 1955

(41)   M. Aven and J.A. Parodi, J. Phys. Chem. Sol. 13, 56, 1960

(42)   J. Schneider, S.R. Sircar and A. Rauber, Z. Naturforschg, 18a,
       980, 1963

## REFERENCES - CHAPTER 5

(1)   J.H. Van Vleck and W.G. Penny,  Phil. Mag. 17, 961, 1934

(2)   A.A. Abragam and M.H.L. Price,  Proc. Phys. Soc. A, 63, 409, 1951

(3)   M.H.L. Price,  Phys. Rev. 80, 1107, 1950

(4)   H. Watanabe,  Prog. Theoretical Phys. (Kyoto) 18, 405, 1957

(5)   G.D. Watkin,  Phys. Rev. 113, 79, 1959

(6)   E. Low,  Sol. Stat. Phys. Suppl. 2, 120, 1960

(7)   H.J.D. Powell, J.R. Gabriel and A.F. Jognston,  Phys. Rev. Lett. 5, 145, 1960

(8)   J.R. Gabriel, D.F. Johnston and H.J.D. Powell,  Proc. Roy. Soc. (Lond.) A264, 503, 1961

(9)   J. Kondo,  Prog. Theoret. Phys. (Kyoto), 23, 106, 1960
                                                    28, 1026, 1962

(10)  A.S. Chakraverti,  J. Chem. Phys. 39, 1004, 1963

(11)  R.R. Sharma, T.P. Das and R. Orbach,  Phys. Rev. 149, 257, 1966

(12)  R.R. Sharma, T.P. Das and R. Orbach,  Phys. Rev. 171, 378, 1968

(13)  J. Schneider, S.R. Sircar and A. Rauber,  Z. Naturforschg. 18a, 980, 1963

(14)  A.A. Abragam,  Phys. Rev. 79, 534, 1950

(15)  J.H. Wood and G.W. Pratt Jr.,  Phys. Rev. 107, 995, 1957

(16)  V. Heine,  Phys. Rev. 107, 1002, 1957

(17)  A.J. Freeman and R.E. Watson,  Phys. Rev. 123, 2027, 1961

(18)  R.E. Watson and A.J. Freeman,  Phys. Rev. 156, 251, 1967

(19)  J.S. Van Wieringen,  Discussions Faraday Soc. 19, 118, 1955

(20)  O.N. Matamura,  J. Phys. Soc. Japan, 14, 108, 1959

(21)  F.L. Chan and Y.S. Park,  Bull. Am. Phys. Soc. (2), 9, 296, 1964

(22)  D. Curie,  Luminescence in Crystals,  Methuen, 1963

(23)  S.P. Keffer and A.M. Portis,  J. Chem. Phys. 27, 675, 1957

(24)  R.L. Kronig and C.J. Bouwkamp,  Physica 6, 290, 1939

(25)  J. Schneider and S.R. Sircar,  Z. Naturforschg, 17a, 570, 1962

(26)     L. Matarrese and C. Kikuchi,  J. Phys. Chem. Sol.  1,  117,  1956

(27)     G.D. Watkins,  Bull. Amer. Phys. Soc.  2,  345,  1957
         W. Low,  Phys. Rev.  105,  793,  1957
         R.S. Title,  Phys. Rev.  131,  2503,  1963

(28)     R.S. Title,  Phys. Rev.  131,  2503,  1963

(29A)    A.A. Abragam and B. Bleaney,  Electron Paramagnetic Resonance
         of Transition Ions,  Oxford U.P.  1970

(29B)    G.H. Azarbayeyani,  Rpt. No. 04385-2-F of the Office of Res.
         Admins.  The University of Michigan,  Ann Arbor

(29C)    H. Watanabe,  Prog. Theoret. Phys. (Kyoto),  18,  405,  1957

(29D)    I. Fidone and K.W.H. Stevens,  Proc. Phys. Soc. (Lond.)  73,
         116,  1959

(29E)    L. Pauling,  The Nature of the Chemical Bond,  Cornell U.P.  1959

(29F)    E. Simanek and K.A.Muller,  J. Phys. Chem. Solids,  31,  1027,  1970

(30)     I.Z. Waller,  Z. Physik,  79,  370,  1932

(31)     R. de L. Kronig,  Physica  6,  33,  1939

(32)     K.W.H. Stevens,  Repts. on Prog. in Physics,  30,  189,  1967

(33)     J.H. Van Vleck,  Phys. Rev.  74,  1168,  1948

(34)     C. Kittle and E. Abrahams,  Phys. Rev.  90,  238,  1958

(35)     P.A.M. Dirac,  The Principles of Quantum Mechanics,  Oxford U.P.  1935

(36)     M.H. Pryce and K.W.H. Stevens,  Proc. Phys. Soc.  A63,  36,  1950

(37)     D.S. McClure,  J. Chem. Phys.  39,  2850,  1963

(38)     F.A. Krogen and P. Zalm,  J. Electrochem. Soc.  98,  177,  1951

(39)     J.H. Schulman,  J. Appl. Phys.  17,  902,  1947

(40)     J. Lambe and C. Kikuchi,  Phys. Rev.  119,  1256,  1960

(41)     D. Turnbull,  Am. Soc. for Metals,  121,  144,  1955

(42)     D. Turnbull,  Acta,  Met.  3,  55,  1955

(43)     D. Turnbull,  Sol. Stat. Phys.  3,  226,  1956

(44)     J.H. Holloman,  Am. Soc. for Metals,  116,  161,  1950

(45)     M.A. Melvin and M. Avrami,  J. Chem. Phys.  7,  1103,  1939
                                    J. Chem. Phys.  8,  212,  1940
                                    J. Chem. Phys.  9,  177,  1941

(46)    D. Turnbull,  J. Chem. Phys.  18,  198,  1950

(47)    M.J. Burger,  Phase Transformation in Solids  P.183,
            John Wiley,  1951

(48)    M.C. Bloom and M.J. Buerger,  Z. Krist (A),  96,  363,  1937

(49)    J.H. Becker,  Bull. Am. Phys. Soc.  11,  1,  1954

(50)    M. Andre and G. Chaudron,  Com. Rend. Acad. Sci. Paris,  201,
            191,  1935

(51)    Bohm and Niclassen,  Z. Anurg. W. Allgem. Chem.  122, 7,  1923

(52)    F. Urbrick and W. Zachariasen,  Z. Krist.  63,  260,  1925

(53)    W.O. Milligan,  J. Phys. Chem.  38,  797,  1934

(54)    E.S. Rittner and J.H. Schulman,  J. Phys. Chem.  47,  537,  1943

(55)    H. Ahlburg and R. Caines,  J. Chem. Phys.  36,  185,  1962

(56)    E.L. Lind and R.H. Bube,  J. Chem. Phys.  37,  2499,  1962

(57)    A.L. Edwards, T.E.S. Pykhouse and H.G.Drickamer, J. Phys. Chem.
            Sol.  11,  140,  1959

(58)    A.L. Edwards and H.G. Drickamer,  Phys. Rev.  122,  1149,  1961

(59)    C.J.H. Rooymans,  J. Inorg. Nucl. Chem.  25,  253,  1963

(60)    C.J.H. Rooymans,  Phys. Letts.  4,  186,  1963

(61)    S.S. Kabalkina and  Z.V. Troitskaya,  Dokaldy 8,  800,  1964

(62)    P. Manca  and F. Raga,  Nature  200,  874 ,  1963

(63)    E.T. Allen and J.L. Crenshaw,  Am. J. Sci.  (4),  34,  348,  1912

(64)    A. Addamingo and M. Aven,  J. Appl. Phys.  31,  36,  1960

(65)    A. Kremheller,  J. Electrochem. Soc.  107,  422,  1960

(66)    G.A. Samara and H.G. Drichamer,  J. Phys. Chem. Sol.  23,  457,  1962

(67)    A. Jayaraman and G.C. Kennedy,   Phys. Rev. 130,  2278,  1963

(68)    C. Burnet and H.G. Drichamer,  J. Phys. Chem. Sol.  23,  451,  1962

(69)    P.L. Smith and J.E. Martin,  Phys. Lett.  19,  541,  1965

(70)    J.E. Martin and P.L. Smith,  Brit. J. Appl. Phys.  16,  495,  1965

(71)    C.F. Cline and D.R. Stephens,  J. Appl. Phys.  36,  2869,  1965

(72)    C.J.M. Rooymans,  Structural Investigations of some Oxides etc. at
            High Pressures.  Ph.D. Thesis, University of Amsterdam,  1967

(73)   J.S. Van Weiringen,  Physica  19,  397,  1953

(74)   P. Krishna and A.R. Verma,  Proc. Roy. Soc. (Lond.)  A272,  490,  1963

(75)   P. Krishna and A.R. Verma,  Acra. Xtal,  17,  51,  1964

(76)   A. Hayashi,  J. Mineral Soc. Japan,  4,  363,  1960

(77)   L.W. Strock and V.A. Brophy,  Amer. Min.  40,  92,  1952

(78)   S. Mardix, E. Alexander, O. Brafman and T. Steinberger,  Acta
       Crystallogr.  22,  808,  1967

(79)   E. Alexander, Z.H. Kalman, S. Mardix and I.T. Steinberger,
       Philosophical Mag.  21,  1237,  1970

(80)   H. Muller,  Neues. Jahrb. Mineral.  84,  43,  1952

(81)   F.G. Smith,  Am. Mineralogist  40,  658,  1955

(82)   F.C. Frank,  Discussion of Faraday Soc.  5,  48,  1949

(83)   F.C. Frank,  Phil. Mag.  42,  1014,  1951

(84)   G.S. Zhdanov and Z.V. Minervina,  J. Phys. USSR,  9,  244,  1945

(85)   G.S. Zhanov and Z.V. Minervina,  Acta Physico Chim. USSR,  20,
       386,  1945

(86)   D. Lundquist,  Acra Chem. Scand.  2,  177,  1948          .

(87)   G. Hagg and E. Hermanson,  Arkiv Kemi Mineral,  Geol.  17B,  10, 1943

(88)   H. Jagodzinski,  Acta Crystal.  7,  300,  1954

(89)   H. Jagodzinski,  Acta Crystal.  3,  49,  1954

(90)   C.J. Schneer,  Acta Cryst.  8,  279,  1955

(91)   H. Gobrecht,  Internationales Lumineszenz Symposium, Munchen
       P.407,  1965

(92)   F.C. Frank,  Phil. Mag.  42,  1014,  1951

(93)   H. Hartman,  Kristall. Tech.  1,  27,  1966

(94)   S. Mardix and I.I. Steinberger,  Israel J. Chem.  3,  243,  1966

(95)   M. Aven and J.A. Parodi,  J. Phys. Chem. Sol.  13,  56,  1960

(96)   Pashnikin,  Tishschenko, Korneeva and Kiyzkenko,  Kristalografiga
       5,  261,  1960

(97)   P.M. Williams and A.D. Yoffe,  Philos. Mag.  25,  247,  1972

(98)     H. Hartmann,  Kristall. and Technik.  5,  527,  1970

(99)     E.W. Kellerman,  Phil. Trans. Roy. Soc. (Lond.)  Ser. A.,
         238,  513,  1940

(100)    R.J. Caveney,  Philos. Mag.  149,  943,  1968

(101)    J.P. Suchet,  Chemical Physics of Semiconductors,  Van Nostrand 1965

(102)    R. Smoluchowski,  P.149,  Phase Transformations in Solids,
         John Wiley  1951

(103)    Prog. Report Feb. 1970,  Agreement No. AT/2051/08/RL
         Dept. Applied Physics, University of Durham

(104)    J. Schneider and R. Sircar,  Z. Naturforschg,  17a,  651,  1962

## REFERENCES - CHAPTER 6

(1)     K. Moriagi,  J. Phys. Soc. Japan  18,  733,  1963

        J. Phys. Soc. Japan  19,  187,  1964

(2)     R.S. Title,  Phys. Rev.  133,  A1613,  1964

(3)     T.A.T. Cowell and J. Woods,  B.J.A.P.  15,  783,  1964

(4)     K.H. Nicholas and J. Woods,  Brit. J. Appl. Phys.  18,  1045,  1967

(5)     D. Curie,  Lummescence in Crystals  P.147,  Methuen  1963

(6)     T. Taki and H. Bo,  J. Phys. Soc. Japan  25,  1324,  1968

(7)     W. Kohn and J.M. Luttinger,  Phys. Rev.  98,  915,  1955

(8)     J.M. Luttinger and W. Kohn,  Phys. Rev.  97,  869,  1955

(9)     G. Feher,  Phys. Rev.  114,  1219,  1959

(10)    K. Muller and J. Schneider,  Physics Letts.  4,  288,  1963

(11)    A.R. Hutson,  Phys. Rev.  4,  505,  1960

(12)    K. Muller and J. Schneider,  J. Phys. Chem. Solids,  29,  451,  1968

(13)    K. Burr and J. Woods,  J. Mat. Sci.  6,  1007,  1971

(14)    M. Cardona,  J. Phys. Chem. Solid,  24,  1543,  1963

(15)    L.M. Roth,  Phys. Rev. 118,  1534,  1960

(16)    D.T.F. Marple,  J. Appl. Phys.  35,  1879,  1964

REFERENCES - CHAPTER 7

(1)     F.A. Kroger,  Some Aspects of the Luminescence of Solids  P.57
         Elsevier Amsterdam  1948

(2)     C.C. Klick and J.H. Schulman,  J. Opt. Soc. Amer.  42,  910,  1952

(3)     H.A. Klasens,  Philips Res. Reports  8,  441,  1953

(4)     F.A. Kroger and P. Zalm,  J. Electrochem. Soc.  98,  177,  1951

(5)     J.H. Schulman,  J. Appl. Phys.  17,  902,  1947

(6)     H.W. Leverenz and D.O. North,  Phys. Rev.  85,  930,  1952
         G.E. Spencer et al,  J. Chem. Phys.  20,  1177,  1952

(7)     L.E. Orgel,  J. Chem. Phys.  23,  1004,  1955

(8)     Y. Tanabe and S. Sugano,  J. Phys. Soc. Japan,  9,  753,  1954

(9)     D.C. McClure,  Sol. Stat. Phys.  9,  400,  1959

(10)    J.H. Van Vleck,  Electric and Magnetic Susceptibilities,
         Oxford U.P.  1932

(11)    D. Curie,  Luminescence in Crystals,  P.123,  Methuen & Co.  1963

(12)    D.W. Langer and S. Ibuki,  Phys. Rev.  138,  809,  1965

(13)    J.W. Allen,  Proc. Seventh Int. Conf. Physics of Semiconductors,
         P.781,  Dunod, Paris

(14)    H.E. Gumlich, R.L. Pfrogner, J.C. Shaffer and F.E. Williams,
         J. Chem. Phys.  44,  3929,  1966

(15)    D.W. Langer, J.C. Helmer and N.H. Weichet,  J. Luminescence  1,
         341,  1970

(16)    D.W. Langer and H.J. Richter,  Phys. Rev.  146,  554,  1966

(17)    J. Apperson, Y. Vorobiov and G.F. Garlick,  Brit. J. Appl. Phys.
         18,  389,  1967

(18)    S. Assano, N. Yamashita, M. Oishi and K. Amori,  J. Phys. Soc.
         Japan,  24,  1302,  1968

(19)    S. Assano, Y, Nakav and K. Omori,  J. Phys. Soc. Japan  20,  1120,  1964

(19)    S. Braun, H.G. Grimmeiss and W.J. Allen,  Phys. Stat. Sol. a,  14,
         527,  1972

(20)    V.J. Schneider, S.R. Sircar and A. Rauber,  Z. Naturforschg  18a,
         980,  1963

(21)  D. Curie,  Luminescence in Crystals  P.220,  Methuen  1963

(22)  R.H. Bube, S. Larch and R.E. Shrader,  Phys. Rev.  92,  1135,  1953

(23)  G. Jones and J. Woods,  J. Phys. D.  6,  1640,  1973

(24)  F.A. Kroger and H.J. Vink,  J. Chem. Phys.  22,  250,  1954

(25)  R. Bowers and N.T. Melamed,  Phys. Rev. 99,  1781,  1955

(26)  J.S. Prener and F.E. Williams,  J. Chem. Phys.  25,  361,  1956

(27)  J.S. Prener and D.J. Weil,  J. Electrochem. Soc.  106,  409,  1959

(28)  H.W. Leverenz,  An Introduction to Luminescence of Solids,
       John Wiley & Son,  1950

(29)  W. Lehmann,  J. Electrochem. Soc.  114,  83,  1967

(30)  P.H. Kasi and Y. Otomo,  Phys. Rev. Letts.  7,  17,  1961

(31)  W.C. Holton,  M. de Wit and T.L. Estle  Phys. and Chemistry of II-VI
       Compounds,  P.304,  Ed. M. Aven & J.S. Prener, North Holland
                                    Pub. Co.  1967
(32)  P.H. Kasi and Y. Otomo,  J. Chem. Phys.  37,  1263,  1962

(33)  D. Curie and J.S. Prener,  Phys. and Chemistry of II-VI Compounds.
       P.436.  Ed.  M. Aven and J.S. Prener, North Holland Pub. Co. 1967

(34)  F.A. Kroger and J. Dikhoff,  Physica 16,  297,  1950

(35)  H.A. Klasens,  J. Electrochem. Soc.  100,  72,  1953

(36)  F.F. Morehead,  J. Phys. Chem. Sol.  24,  37,  1963

(37)  W. Lehmann,  J. Electrochem Soc. 113,  449,  1966

(38)  D. Curie,  Luminescence in Crystals, P.117,  Methuen 1963.